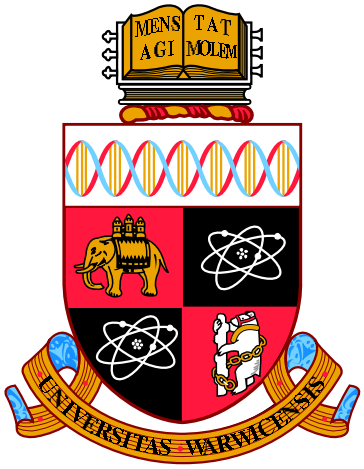

Predicting QRS and PR interval prolongations in humans using nonclinical data

by

Linnéa Bergenholm

Thesis

Submitted to the University of Warwick

for the degree of

Doctor of Philosophy

School of Engineering

February 2017

Contents

List of Tables

List of Figures

Acknowledgements

In the years spent working on this PhD thesis, I am fortunate to have had wonderful people around me to push me forward.

I would like to thank my university supervisors Dr Michael Chappell and Dr Neil Evans for giving me the opportunity to study for this PhD, for generously sharing your ideas and support and for all opportunities to learn and develop at courses, conferences and work-shops.

My industry supervisors at AstraZeneca, Dr Joanna Parkinson and Teresa Collins, for generously sharing your expertise, pushing me to develop and learn to see the industry perspective, for your endless support and valuable advice through these years and for your friendship.

My husband and best friend David Bergenholm for staying by my side when my choices have taken me to work and study across the world, for your optimism, support and love and for (repeatedly) teaching me to unwind and remember what really matters.

The ESR crew: Elin Boger, Magnus Trägårdh, Robert Andersson and David Janzén for laughs, discussions, friendship and uncountable flights together. Without you this would never have been the same!

The Biomedical Superheroes for taking us all in when we stormed the office in 2013, for all the amazing parties, excursions and food tastings.

My growing family for making the world smaller by always being there: on Skype, visiting me wherever I am and trusting me to come home. I love you all.

AstraZeneca for providing the data required for these analysis, and for all the wonderful people I have gotten to know within Discovery Safety, Safety and ADME Translational Sciences and the CVMD and RIA M&S groups.

I would also like to thank the European Union for funding this project.

Formal acknowledgements:

This project was funded through the Marie Curie FP7 People ITN European Industrial Doctorate (EID) project No.316736, IMPACT (Innovative Modelling for Pharmacological Advances through Collaborative Training).

AZD8683 and AZD9164 are the result of a collaboration between AstraZeneca and Pulmagen Therapeutics Limited (formerly Argenta Discovery Limited).

Declarations

I hereby declare that except where specific reference is made to the work of others, the contents of this dissertation are original and have not been submitted in whole or in part for consideration for any other degree or qualification in this, or any other university. This dissertation is my own work and contains nothing which is the outcome of work done in collaboration with others, except as specified in the text and Acknowledgements. This dissertation contains fewer than 65,000 words including appendices, bibliography, footnotes, tables and equations and has fewer than 150 figures.

This thesis is submitted to the University of Warwick in support of my application for the degree of Doctor of Philosophy. It has been composed by myself and has not been submitted in any previous application for any degree.

The work presented (including data generated and data analysis) was carried out by the author except in the cases outlined below:

- All nonclinical and clinical studies were conducted prior to the work performed in this thesis and not by the author. This work was focused on data analysis and not the generation of new data.
- The structural identifiability analyses presented in chapter 3 were performed by the Early Stage Researcher David Janzén.

Parts of this thesis have been published by the author:

- Section 2.3.3 contains material originating from a review publication [1] conducted in collaboration with the supervisor and AstraZeneca employee Teresa Collins.

- Chapter 3 is an extended version of an accepted publication [2]. The work was performed in collaboration with the Early Stage Researcher David Janzén. The practical identifiability analyses and the case study were conducted primarily by the author of this thesis, while the structural identifiability analyses were performed primarily by David Janzén.
- Chapter 4 presents the data analysed in the accepted publication [3] and a manuscript under revision [4].
- Chapter 5 presents the methods and modelling results for the in-house data, all extended from an accepted publication [3] and a manuscript under revision [4].
- Chapter 6 presents the collection and modelling of literature data, all extended from a manuscript currently under revision [4].
- Chapter 7 presents an extended version of the results and discussion of the translational analyses from a manuscript currently under revision [4].

List of publications including submitted papers:

- Collins, T. A., Bergenholm, L., Abdulla, T., Yates, J. W. T., Evans, N., Chappell, M. J., & Mettetal, J. T. (2015). Modeling and Simulation Approaches for Cardiovascular Function and Their Role in Safety Assessment. CPT: Pharmacometrics & Systems Pharmacology, 4 (March), 1-14. [1]
- Bergenholm, L., Collins, T., Evans, N. D., Chappell, M. J., & Parkinson, J. (2016). PKPD modelling of PR and QRS intervals in conscious dogs using standard safety pharmacology data. Journal of Pharmacological and Toxicological Methods, 79, 34-44. [3]
- Janzén, D.L.I., Bergenholm, L., Jirstrand, M., Parkinson, J., Yates, J., Evans, N.D., & Chappell, M.J. Parameter identifiability of fundamental pharmacodynamic models. [2]
- Bergenholm, L., Parkinson, J., Mettetal, J., Evans, N. D., Chappell, M. J., & Collins, T. Predicting QRS and PR interval prolongations in humans using

nonclinical data. *Under review.* [4]

Selection of conference presentations/posters presented by the thesis author:

- Predicting QRS widenings in humans using nonclinical data. QSP-UK, Surrey, UK, September 2016. *(oral presentation)*
- Population PKPD modelling of QRS and PR intervals in conscious dogs. PK-UK, Chester, UK, October 2015. *(poster presentation)*
- Population PKPD modelling of QRS and PR intervals in conscious dogs. PAGE, Hersonissos, Crete, Greece, June 2015. *(poster presentation)*
- Poster: Translation from pre-clinical to clinical effects of a drug that prolongs the QRS complex. PK-UK, Bath, UK, November 2014. *(poster presentation)*
- Translating pre-clinical cardiovascular biomarkers to clinical effects: Preliminary results for a drug that prolongs the QRS complex. 7th Noordwijkerhout Symposium on Pharmacokinetics, Pharmacodynamics and Systems Pharmacology, Leiden, The Netherlands, April 2014. *(poster presentation)*
- Assessing cardiovascular safety beyond QT. PK-UK, Harrogate, UK, November 2013. *(poster presentation)*

Abstract

Risk of cardiac conduction slowing (QRS/PR interval prolongations in monitored electrocardiograms) is assessed in nonclinical studies, where the current AstraZeneca strategy involves ensuring high margins to *in vitro* effects and statistical tests to identify *in vivo* effects. This thesis aims to improve QRS/PR risk assessment using pharmacokinetic-pharmacodynamic modelling for describing QRS/PR effects and evaluating translation to human effects.

Data for six compounds were collected from the literature and previously performed *in vitro* (sodium/calcium channel), *in vivo* (guinea pig/dog) and clinical AstraZeneca studies. Mathematical models were developed and evaluated to describe and compare effects across compounds and species.

Key results were that proportional drug effect models often suffice for small QRS/PR changes (up to 20%), while larger effects require nonlinear models. Heart-rate correction and circadian rhythm models reduced residuals primarily for describing baseline PR intervals, with highest impact in humans followed by dogs and guinea pigs. Meaningful (10%) human QRS/PR changes correlated to low levels of sodium channel block (3-7%) and calcium channel binding (13-21%) and to small effects in guinea pigs and dogs (QRS 2.3-4.6% and PR 2.3-10%). This suggests that worst case human effects can be predicted by assuming four times greater effects at the same concentration from dog/guinea pig.

Small changes *in vitro* and *in vivo* consistently translate to meaningful PR/QRS changes in humans across compounds. Accurate characterisation of concentration-effect relationships therefore require a model-based approach. Although the presented work is limited by the small number of investigated compounds, it provides a starting point for predicting human risk using routine QRS/PR data to improve the safety of new drugs.

Abbreviations

ADME	absorption, distribution, metabolism and elimination (of drug)
AIC	Akaike criterion
AV node	atrio-ventricular node
AP	action potential
BP	blood pressure
BSV	between-subject variability
Cav1.2	an L-type calcium channel
COPD	chronic obstructive pulmonary disease
CV	cardiovascular
ECG	electrocardiogram
EM	expectation maximisaton
FTIM	first time in human
IOV	inter-occasion variability
JT interval	duration from the start of the J wave to the end of the T wave in the ECG
hCav1.2	human Cav1.2
hERG	the potassium channel encoded by the human ether-a-go-go related gene
hNav1.5	human Nav1.5
HR	heart rate
MCMC	Markov chain Monte Carlo
ML	maximum likelihood
M3 receptor	muscarinic receptor M3
M&S	modelling and simulation
Nav1.5	a cardiac sodium channel
PB-PK	physiologically-based pharmacokinetics
PD	pharmacodynamics
PK	pharmacokinetics
PPB	plasma protein binding
PQ/PR interval	duration from the start of the P wave to the end of the Q or R wave in the ECG

QRS complex	duration from the start of the Q wave to the end of the S wave in the ECG
QT interval	duration from the start of the Q wave to the end of the T wave in the ECG
QTc interval	heart rate corrected QT interval
rCav1.2	rat Cav1.2
RR interval	duration between to R waves (heart beat duration)
RUV	residual unexplained variability
SA node	sino-atrial node
SAEM	stochastic approximation expectation maximisation
TdP	torsades des pointes
t-QT study	thorough QT study
WBC	white blood cell
-2LL	-2 loglikelihood

Chapter 1

Introduction

Adverse cardiovascular (CV) effects caused by abnormal function of the heart are a major cause of the withdrawal of marketed small molecule drugs and of late stage attrition in drug development [5, 6]. Important biomarkers for heart function include the duration of key intervals monitored in the electrocardiogram (ECG), such as the QT, QRS and PR intervals. Most known is the prolongation of the heart-rate corrected QT (QTc) interval, corresponding to delayed ventricular repolarisation. Nonclinical and clinical observations have linked QTc prolongation to inhibition of the human potassium channel encoded by the ether-a-go-go-related gene (hERG) and to risk of the potentially lethal arrhythmia Torsades des Pointes (TdP) [7, 8]. Numerous investigations provide insights for identifying and predicting risk of QTc prolongation in the clinic [9, 10, 11, 12, 13, 14]. However, much less is known of the nonclinical to clinical translation of conduction liabilities manifested in the ECG as QRS and PR prolongations [15]. QRS widening is linked to sudden cardiac death in healthy males [16] and PR prolongations are associated with increased risk of atrial fibrillations and death in risk populations [17]. Identifying QRS/PR risks of drug candidates already in nonclinical studies is therefore vital for the progression of safe compounds into first clinical trials.

As most quantitative investigations prior to this work had focused on QTc„ QRS and PR intervals were selected as the focus for this thesis. Established modelling and simulation (M&S) methods allows the identification, quantification and prediction of nonclinical and clinical QTc effects [1, 10, 14] and similar models and methods may be useful also for QRS and PR. Applying M&S methods to QTc has been shown to improve the power to detect and quantify small effects in simulated pre-clinical studies [18]. Furthermore, incorporation of factors predictive of baseline effects such as sex, age, heart rate corrections and circadian rhythms has been shown to reduce unexplained residual variability and improve the estimation of drug effects [10, 14]. In addition to improved sensitivity to detect risks, M&S has been used to investigate the relative sensitivity of nonclinical assays compared to the clinic, pro-

viding information on the translational relationship and allowing quantitative risk assessment and prediction to humans. For example, investigations into the dog to human translation of clinical QTc effects have suggested that 2-8 ms QTc change in dogs translate to 10 ms change in humans [12]. Similar M&S analyses could provide a framework for improved identification, prediction and mitigation of risks related to changes in QRS/PR durations.

Nonclinical CV safety assays for detection of conduction slowing include molecular-, cell- and tissue-based *in vitro* assays and *in vivo* telemetry studies. Functional ion channel inhibition assays and binding assays are used to assess the potency to inhibit or bind to cardiac ion channels *in vitro*, and are typically conducted in early discovery phases. The major ion channels studied to assess risk of conduction slowing are the sodium (Nav1.5) and L-type calcium (Cav1.2) channels. Drug-induced QRS widening is primarily linked to Nav1.5 inhibition, and recent studies suggest that QRS widening may occur already at exposures corresponding to low inhibitions *in vitro*. A margin of 30-100-fold between potency to human Nav1.5 (hNav1.5) and maximum free (unbound) plasma concentrations have been suggested to reduce risk of QRS widening in the clinic [19]. Another study found that <10% block of hNav1.5 may lead to QRS widening in humans [20]. The primary mechanism for drug-induced PR prolongation is AV block through Cav1.2 inhibition [15], however, safety margins for Cav1.2 were not identified in the literature. Early CV safety assessment could thus be improved by increased quantitative understanding of the *in vitro* to clinical translation of QRS and PR prolongations.

In vivo investigations of drug-induced effects on ECG intervals are typically conducted in anaesthetised and/or conscious rats, guinea pigs and dogs [21, 22, 23]. At AstraZeneca, CV safety rodent animal studies are typically conducted at the lead optimisation phase, providing the first data on CV effects in complete systems. For the development of small molecule drugs, the lead optimisation stage involves the optimisation of lead compound series, and the final compound is yet to be selected. CV safety information is therefore available at a time of (relatively) low accumulated cost and high chemical choice. CV safety studies in dogs or non-human primates are conducted following candidate selection, and are required for all compounds prior to first time in human (FTIM) studies, primarily to evaluate potential effects on QTc [24]. While QTc modelling is routinely conducted at AstraZeneca, allowing quantitative risk assessment, effects on QRS and PR intervals are primarily evaluated by point-wise statistical tests. As QRS and PR effects similar to QTc may be smaller in dogs compared to humans, safety risks may not be detected as effectively as possible in the nonclinical and clinical studies. Also, this method does not allow for quantitative comparisons between candidates and to competitors nor clear evaluations of the therapeutic window. Improved methods for analysing the nonclinical and clinical data may thus improve risk assessment, reduce unnecessary animal usage and risk

to humans and increase efficiency in drug discovery and development.

1.1 Aims and objectives

Ultimately, the goal within safety pharmacology is to mitigate safety risks as early in drug discovery and development as possible in order to reduce risk of exposing volunteers and patients to unsafe drugs and to spare animal lives. A new modelling framework for quantifying and predicting drug-induced QRS and PR effects in humans may lead to earlier identification of conduction liabilities, and consequently to reduced risk to humans and to more efficient drug discovery and development. The aim of this thesis is therefore to increase the understanding of how drug-induced cardiac conduction slowing in humans, reflected by QRS and PR prolongations in monitored ECGs, may be predicted and mitigated using nonclinical *in vitro* and *in vivo* data, with the following objectives:

1. Apply and develop models to quantify QRS and PR intervals monitored in nonclinical species and in humans at baseline conditions and during drug treatment.

2. Investigate the translation between nonclinical *in vitro* and *in vivo* effects and clinical QRS and PR prolongations.

3. Develop a model framework to quantitatively predict QRS and PR prolongations in humans using nonclinical data, that can be adopted by the pharmaceutical industry to improve safety assessment.

1.2 Thesis outline

This thesis will present novel methods for prediction of QRS and PR effects in humans using nonclinical *in vitro* and *in vivo* data, where the resulting predictions can help inform and improve decisions for compound selection, progression and development. The work is divided into separate chapters as detailed below:

- Chapter 2 provides relevant background information regarding M&S techniques within pharmacology, a brief discussion of the mechanisms of cardiac electrophysiology relevant to this work and a review of current M&S approaches used within CV safety assessment.

- Chapter 3 presents work performed related to parameter identifiability of a set of pharmacodynamic models. Several of these models were later applied in

this thesis.

- Chapter 4 presents the compounds that were investigated in this thesis and the studies from which data were collected. These studies include nonclinical assays previously performed or outsourced by AstraZeneca, a clinical Phase I study performed by AstraZeneca and published studies identified from literature searches.

- Chapter 5 presents the development of mathematical models using the collected in-house data for each investigated compound and species, including guinea pigs, dogs and humans. These models were developed with the higher purpose of performing translational analyses, but the results also provides useful information on appropriate models for characterising these effects in animals and humans.

- Chapter 6 presents the development of mathematical models for the clinical effects observed in the collected literature data. These models were developed with the higher purpose of performing translational analyses.

- Chapter 7 presents translational analyses performed using the models developed in Chapters 5 and 6, but also using additional mechanistic methods. Investigations into the translations were conducted between *in vitro*, *in vivo* and clinical effects. This chapter also presents how the results of these analyses can be used to predict effects in humans using the nonclinical data.

- Chapter 8 concludes the work conducted for this thesis and addresses how far the aims and objectives of this thesis have been met. In addition, future work to further advance nonclinical risk assessment of cardac conduction are suggested.

Chapter 2

Background

2.1 Introduction

This chapter aims to provide background information of relevance to this thesis. It comprises a brief overview of M&S methodologies within pharmacology, a brief discussion of the mechanisms of cardiac electrophysiology and a review of the M&S approaches that are currently used within CV safety assessment.

2.2 Modelling & simulation within pharmacology

Many different types of data are collected during drug discovery (nonclinical phase) and development (clinical phase), and integration and understanding of these data is key to making the right decisions at any stage of this process [25, 26, 27]. Applying M&S can impact both drug discovery and development. For example, M&S is in drug development used to quantify and explain sources of variability, inform study design, make comparisons to competitor compounds, refine dosing schedules and to predict effects in untested populations, such as paediatrics [28]. In drug discovery, M&S can impact target validation through improved understanding of the hypothesised biological mechanism of action, predict exposure and effect in healthy volunteers or patients and optimise experimental design both for further nonclinical studies and FTIM [28, 29]. Also, M&S can in drug discovery be an integrated part of the design-make-test cycle, where modelling results can be used to compare effects of candidate compounds. These effects can be both desired (efficacy) and unwanted (off-target, potentially toxic), thereby quantifying the therapeutic index of the compounds (the margin between efficacy and toxicity). M&S can thus, in addition to improving integration of efficacy data, inform and improve the identification, evaluation, prediction and mitigation of safety liabilities [1]. QRS and PR prolongations, which are the topic of this work, are for non-arrhythmic indications typically undesired off-target effects that should be mitigated.

2.2.1 Pharmacokinetic and pharmacodynamic modelling

M&S approaches within pharmacology are traditionally centred around pharmacokinetic (PK) and pharmacodynamic (PD) modelling. PKPD modelling allows the integration of data across subjects, doses and time points, as well as the capture of delayed effects, effects in noisy data and baseline variations over time; all of which would be more difficult to analyse through the application of standard statistical approaches.

2.2.1.1 Modelling the pharmacokinetics

The pharmacokinetics of a drug describe the processes that govern drug exposure, such as drug absorption, distribution, metabolism and excretion (ADME), and pharmacokinetic models aim to quantitatively link dose administration to drug exposure (concentration in whole blood or plasma). Drug concentrations at the site of action would be preferred as these are likely to more accurately predict drug effects, however, plasma concentrations are typically used as a substitute for effect site concentrations as these are more readily obtained. PK data typically consist of plasma concentrations measured at specific time points following the administration of one or several doses.

Empirical PK models may consist of a series of exponentials, consistent with the number of linear phases visible when plotting the observed concentration data over time on a logarithmic scale. Though useful for interpolation, the parameters of these models are difficult to interpret physiologically. Through re-parameterisation, these models can also be described by compartmental models. Compartmental models are simple models incorporating the concepts of drug absorption, distribution and elimination where features of the model, such as number of compartments or non-linear terms, tend to be driven by the experimental data. Typically, first-order rate constants define the exchange of drug between well-mixed compartments representing different regions of the body where the drug equilibrates at different rates. An example of a linear two-compartment model with first order absorption is provided in Figure 2.1.

In this example, c_1 is the plasma drug concentration (which is typically observed), a_0, a_1 and a_2 the amounts of drug in the gut, central and peripheral compartments (where the peripheral compartment represents slowly equilibrating tissues), f the oral bioavailability, V the volume of distribution of the central compartment, k_a the rate-constant for first-order absorption of drug from the gut to the central compartment, k_e the rate constant for first order elimination of drug from the central compartment and k_{12} and k_{21} controls the distribution to the peripheral compartment. Experimental plasma concentration data typically support the fitting of 1-3 compartments. Also, it is not uncommon to see non-linear absorption

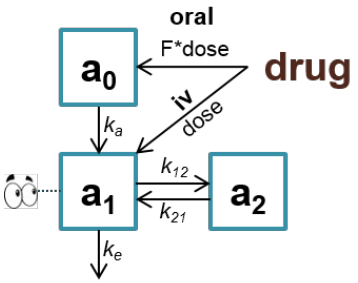

Corresponding system equations:

$$\begin{aligned} \dot{a_0} &= -k_a * a_0 \\ \dot{a_1} &= k_a * f * a_0 - (k_{12} + k_e) * a_1 + k_{21} * a_2 \\ \dot{a_2} &= k_{12} * a_1 - k_{21} * a_2 \end{aligned} \tag{2.1}$$

with observations

$$y = c_1 = a_1/V$$

Figure 2.1 Example of a 2 comparment PK model with iv and oral administration

or elimination rates, typically visible upon dosing with a large range of doses. The plasma concentrations seldom match the concentrations where the pharmacological effects occur, as this is often in target tissues and may also be inside cells. However, although imperfect, plasma concentrations are extremely important biomarkers for pharmacological and toxicological effects.

While the compartments of data-driven PK models are abstract and rarely represent specific parts of the body, physiology-based (PB) PK models connect compartments to specific tissues, incorporating physiological properties such as tissue volumes and blood flow rates as well as drug-specific parameters such as partition fractions [30]. Such models are more complex to parameterise, and are therefore more costly to develop. PB-PK models have improved predictions of drug disposition between species as individual parameters can often be scaled using physiological values specific to each species [31].

2.2.1.2 Modelling the pharmacodynamics

While the pharmacokinetics of a drug in simple terms describes the link between dose and plasma concentrations, the pharmacodynamics is concerned with the effects the drug has on the body. This includes both desired and unwanted effects, where the measured effects may be sensitive biomarkers or clinical outcomes. Clinical outcomes are direct measures of the effects of drug treatment, such as the cure of disease, adverse events or survival, and can therefore take a long time to manifest. Biomarkers are directly or indirectly linked to drug concentrations and/or the clinical outcome, and may be biochemical measurements such as levels of specific proteins or chemicals, or physiological measurements such as heart rate or blood pressure. A useful classification of biomarkers, separating biomarkers into intermediary steps which may be incorporated into mathematical models, is described in [32] and shown in Figure 2.2. Biomarkers are often used as surrogates for clinical outcomes as the

readout typically is faster, allowing shorter and more efficient assays and trials.

Figure 2.2 Biomarker classification based on their relation to clinical effects of drugs. Adapted from [32].

The processes from drug exposure to physiological effects, such as changes in biomarkers, can be described by pharmacodynamic (PD) models. Empirical PD models aim to describe the data without including details of the processes leading to the effects, thus limiting the number of assumptions required when developing the model. A strictly empirical model may be any mathematical function, however, it is common to use descriptive models derived from receptor theory. Many pharmacological and toxicological effects occur after interaction between a drug molecule and a receptor, and these effects tend to saturate at high drug concentrations. This is often modelled with the E_{max} model given by

$$E = \frac{E_{max} C^{\gamma}}{EC_{50}^{\gamma} + C^{\gamma}} \tag{2.2}$$

where E is the pharmacological effect, E_{max} the maximal effect, EC_{50} the concentration at half-maximum effect and γ a shape parameter determining how steep the curvature is (Hill factor). The shape of this model is illustrated in Figure 2.3, where E_{max} reflects the efficacy of the drug while EC_{50} reflects its potency.

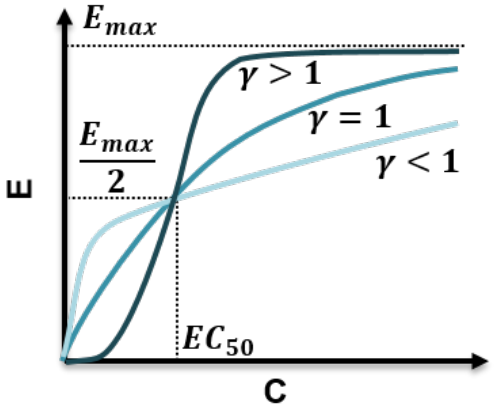

Figure 2.3 Shape of the E_{max} model curve, illustrating the influence of each parameter.

At low concentrations, the concentration term in the denominator becomes negligible and therefore the model can be approximated by the power model, given

by

$$E = \frac{E_{max}C^{\gamma}}{EC_{50}^{\gamma}} = a * C^{\gamma} \tag{2.3}$$

where a is the ratio of E_{max}/EC_{50}^{γ}. Furthermore, when γ equals 1, the effect is at low concentrations proportional to E_{max}/EC_{50}, resulting in the proportional model given by

$$E = \frac{E_{max}C}{EC_{50}} = slopeC \tag{2.4}$$

where *slope* is the proportional drug effect. Proportional and power models are commonly used to describe small effects. These alternative concentration-driven PD models can be tested to see which best describes the observed data.

2.2.1.3 Accounting for time delays

Time delays may be present between plasma concentrations and observed effects. These may be identified in hysteresis plots of concentrations plotted against response, showing the timing of the observations as illustrated in Figure 2.4.

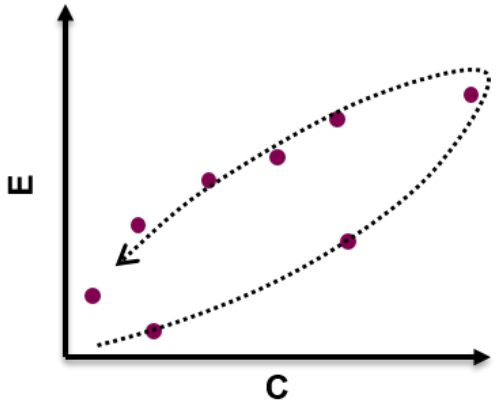

Figure 2.4 Time delays between plasma and effect can be visualised in a hysteresis plot. In this example, the purple dots are observations and the black line reflect the order of data collection. At similar drug concentrations, the effect appear to be greater when measured at late time points compared to early time points.

Short time delays that are assumed to arise from a delay in distribution to the target tissues may be modelled with an effect compartment model [33]. This model assumes that the effect occurs at a hypothetical "effect site". The distributional delay between the plasma concentrations C_c and the concentrations at the "effect site" C_e is given by

$$(dC_e)/dt = k_{e0}(C_c - C_e) \tag{2.5}$$

where k_{e0} governs the distribution rate. Importantly, plasma concentrations are typically assumed to be unaffected.

Pharmacodynamic models may also incorporate assumptions of the mechanisms of drug action. If the kinetics of dissociation from the receptor is the rate-limiting step, the system can for example be modelled applying a receptor model according to

$$\begin{aligned} \dot{RC} &= k_{on} \cdot (R_{tot} - RC) \cdot C - k_{off} \cdot RC \\ E &= k_e \cdot RC \end{aligned} \tag{2.6}$$

where RC is the drug-receptor complex, R_{tot} the total receptor concentration, C the drug concentration at the effect site, k_{on} and k_{off} the rates of binding and dissociation of the drug-receptor complex and k_e the proportional effect elicited by the receptor-bound drug. This model relates to the $\mathrm{E_{max}}$ model by $EC_{50} = k_{off}/k_{on}$ and $E_{max} = R_{tot} \cdot k_e$. Contrary to the receptor model, the $\mathrm{E_{max}}$ model assumes rapid receptor binding kinetics compared to the time scale on which data are collected. In this model, the relationship between drug-receptor complex and pharmacological effect is assumed to be proportional. Alternative models may easily be applied to describe this relationship.

Pharmacological responses may also be slow due to the processes that occur between receptor binding and response. A drug may act by increasing the production or elimination rate of the target protein, or cascades of events may occur that eventually lead to the pharmacological effect. Such slow processes in the signal transduction can sometimes be modelled using indirect response (turnover) models [34]. For these models, the response is assumed to be defined by a differential equation given by

$$\dot{E} = k_{in} - k_{out} \cdot E \tag{2.7}$$

where k_{in} is the zero-order (constant) rate of production of response, k_{out} is the first order rate of loss of response and the baseline level of response is the fraction k_{in}/k_{out}. Concentration-driven drug effect models may be added to the rate parameters defining enhanced or inhibited rates dependent on drug concentration by for example proportional or $\mathrm{E_{max}}$ type equations [34]. An example of a turnover model where the drug enhances the production of response is given by

$$\dot{E} = k_{in}(1 + \frac{E_{max}C}{EC_{50} + C}) - k_{out} \cdot E \tag{2.8}$$

where E_{max} and EC_{50} describe the drug-induced effect on k_{in}. Series of turnover models may also be used based on known mechanisms (and measured data or known rate parameters) for signal transductions with several steps.

The benefit of including mechanistic understanding when developing models

is the distinction between parameters of different type, such as species-, disease- or compound-specific, enabling the improved integration of information from different sources, such as *in silico*, *in vitro* and *in vivo* studies or knowledge. Importantly, these approaches allow continuous refinement of hypotheses as more data become available.

2.2.1.4 Operational model of pharmacological agonism

The relationship between the concentration of the drug-receptor complex and the pharmacological response may be assumed to saturate with the bound receptor to a physiological maximum of response. This is assumed in the operational model of pharmacological action [35] given by

$$E = \frac{E_m \cdot RC^n}{RC_{50}^n + RC^n} = \frac{E_m \frac{R_{tot}C}{K_d+C}^n}{RC_{50}^n + \frac{R_{tot}C}{K_d+C}^n} = \frac{E_m(R_{tot}C)^n}{(K_d+C)^n RC_{50}^n + (R_{tot}C)^n}, \tag{2.9}$$

so, if $\tau = R_{tot}/EC_{50}$, then

$$E = \frac{E_m(\tau C)^n}{(K_d+C)^n + (\tau C)^n} \tag{2.10}$$

where E_m is the maximum response possible in the system, τ the transducer ratio, n describes the sigmoidicity of the relationship between the drug-receptor complex and the response and K_d the equilibrium constant for drug binding to the receptor. The transducer ratio τ is the fraction of the total receptor concentration R_{tot} divided by the concentration of RC that induces a half-maximum response. As such, τ is a measure of the efficiency of the transduction from receptor binding to pharmacological effect. For translational modelling, receptor models such as the operational model separate the drug-specific parameters (K_d) from the system-specific parameters (E_m, τ, n) [9]. With some assumptions, for example that the modelled mechanism is the sole mechanism of the effect and that the concentrations in the *in vitro* and *in vivo* settings are equivalent, the drug-specific parameters may be estimated *in vitro*. Also, the system-specific parameters are (in theory) the same for drugs that act by the same mechanism. This may potentially be used to predict responses between species or for new compounds, once the system properties are known and K_d has been generated.

Through pharmacodynamic (PD) models, the concepts and processes of the pharmacokinetics and pharmacodynamics of a drug can be combined and studied in an integrated way, quantifying individual processes from dose administration through exposure to physiological effects.

2.2.2 Non-linear mixed effects modelling

An important aspect of modelling physiological processes is to understand and quantify variability. The same dose may result in different exposure if given to different subjects, or even to the same subject twice. Similarly, the same exposure may lead to different pharmacodynamic effects for different subjects. This occurs as a result of differences in the processes involved, absorption rates may change after a meal, and the density of metabolising enzymes may differ between subjects. Quantifying and understanding the sources of variability is important to improve drug efficacy and reduce the risk of unwanted effects.

Simple approaches that have been used to model changes in a population rather than in an individual include estimating parameter values to averaged data, pooling the data and treating them as if measured in a single individual (naive pooled approach) and modelling each individual separately and averaging the estimated parameters (two-stage approach) [28]. However, these methods have been shown to potentially lead to biased results [36] (Table 2.1). Also, none of these approaches takes prior assumptions about the variability into account. A better approach is to incorporate the assumption of variability directly into the model definitions, adopting a mixed effects approach [37]. Mixed effects models comprise of fixed effects, defined by a deterministic model structure, and random effects, defined by statistical models allowing parameter values to vary in a population following pre-defined distributions. In some cases the two-stage approach gives similar results as a mixed effects approach, e.g. when modelling a small number of individuals with rich data for each individual.

Table 2.1 Benefits and limitations of different approaches to deal with population data.

Approach	+	−
Average data		Can result in biased structure and estimates
Naive pooled	Easy to implement	No measure of variability between subjects
	Quick first estimates	Difficult to deal with missing data or varied sample sizes
Two-stage	Easy measure of variability between subjects	Requires rich data for each subject
		Difficult to deal with missing data or varied sample sizes
		Variability may be overestimated
Mixed effects	Can quantify different sources of variability	Requires specialised software
	Reduces residual variability	Time intensive
	All data used simultaneously	
	Sparse or missing data can be informed by remaining subjects	

In mixed effects models, the fixed effects describe the trends in the population through a set of "population" parameters, which correspond to the average parameter values (such as E_{max} or EC_{50}) in the investigated population. The random effects contain information on different types of variability in the population, such as between-subject variability (BSV) or inter-occasion variability (IOV) in the parameter values and residual unexplained variability (RUV). The RUV describes the variance between the observed data and individual model predictions, and may include for example measurement error, within-subject variability and model misspecification error. Quantifying known sources of variability using BSV and IOV reduces the RUV, which is typically required. A general mixed effects model including BSV and RUV is given by

$$y_{ij} = f\left(\theta_i, x_{ij}\right) + \epsilon_{ij}, \qquad \epsilon_{ij} \sim N\left(0, \sigma^2\right) \tag{2.11}$$

$$\theta_i = \theta + \eta_i, \qquad \eta_i \sim N\left(0, \omega^2\right) \tag{2.12}$$

where y_{ij} is the j^{th} observation for subject i, f represents the structural model with independent variables x_{ij} and parameter vector θ_i for subject i, and residual variability ϵ_{ij}. The parameter vector for subject i (θ_i) relates to the population parameter vector θ by η_i. ϵ_{ij} and η_i are assumed to be normally distributed with mean 0 and standard deviations σ and ω, respectively. This implies that θ_i is normally distributed with mean θ and standard deviation ω. Normal distributions may be appropriate for parameters which can take positive and negative values. Instead, log-normal distributions are often selected to describe variability of rate parameters, as these often are assumed to be non-negative, and is given by

$$\theta_i = \theta + e^{\eta_i}, \qquad \eta_i \sim N\left(0, \omega^2\right) \tag{2.13}$$

where η_i is normally distributed with mean 0 and standard deviation ω. The distribution for the RUV is in the example above assumed to be normally distributed and additive. Other commonly applied RUV models are the proportional and combined error models. The combined error model comprise both an additive and a proportional part. It is given by

$$y = f + (a + b\,|f|)e \tag{2.14}$$

where y is the observation, f the model function value, a the additive error, b the proportional error and e are normally distributed random variables with mean 0 and variance 1. For an additive error model, b is assumed to be 0, while for a proportional error model, a is assumed to be 0.

2.2.2.1 Estimating parameter values for mixed effects models

Parameters values of mixed effects models may be estimated using for example parametric maximum likelihood (ML) approaches (implemented in NONMEM [38], Phoenix [39] and Monolix [40]) or Bayesian methods (implemented in WinBUGS [41]). The ML approach involves estimating the parameters values that maximise the log of the likelihood of the observed data (given the model structure). Calculating this likelihood analytically is highly complicated even for simple mixed effects models, and the parameter estimation is therefore accomplished by numerical methods [42].

Monolix 4.3.2 was used through-out this thesis for estimating the parameter values of mixed effects models. The ML approach implemented in Monolix is stochastic approximation expectation maximisation (SAEM) [43, 44]. This approach is based on the expectation maximisation (EM) method [45], which can be used to find ML estimates for the parameters θ of a model when the data are incomplete. This is the case for mixed effects models, as the complete data consist of both the observations for each individual subject y (known) and the individual parameter values ψ (unknown). The EM method iteratively updates estimates for the unknown data and the parameter values to arrive at the ML estimator by separating each iteration k into two steps; the expectation step where the function for the loglikelihood of the complete data is created using the current estimate of the parameters (θ_k), and the maximisation step where this function is maximised with respect to θ to update the estimate of θ (θ_{k+1}). The EM method requires that the expectation of the loglikelihood is created in closed form, which limits its use to estimate parameters of mixed effects models as these rarely can be solved analytically. In the SAEM method, the expectation step is therefore replaced by two steps in order to solve the system numerically, namely simulation and stochastic approximation. Each iteration (k) in the SAEM algorithm thus consists of three steps:

1. Simulation: A Markov Chain Monte Carlo (MCMC) procedure using the Hastings-Metropolis algorithm is used to generate a sequence of random samples for the individual parameters ψ (ψ_k) given the current approximation of θ (θ_k). To improve convergance, more than one Markov Chain can be run.

2. Stochastic approximation: The approximation of the complete data likelihood is updated using ψ_k and (with a reducing step-size when the number of iterations increases) the expectation from the previous iteration.

3. Maximisation step: The estimation of θ is updated by maximising the approximated complete data likelihood, resulting in the updated parameters θ_{k+1}.

This method was first implemented in Monolix, and has later been implemented in other software, including NONMEM and Matlab. In addition to the

estimated parameter values for the fixed effects and variance components of the models, Monolix produces an estimate of the covariance matrices for the parameters and estimates for the individual parameter values. The covariance matrices are estimated by approximating the Fisher information matrix either by a linearisation or a stochastic approximation approach. Also, the likelihood of the data given the parameter values is approximated either by a Monte Carlo approach (importance sampling) or by linearisation and is used to calculate summary statistics such as minus twice the log of the likelihood (-2LL) and the Akaike information criterion (AIC [46]), given by

$$AIC = -2LL + 2P \tag{2.15}$$

where P is the total number of parameters that are estimated. The AIC thus adds a penalty to increasing the number of parameters.

2.3 Assessing cardiovascular (side) effects

The heart is the pump driving the CV system, supplying tissues with blood containing oxygen and vital nutrients while removing carbon dioxide and waste products. This is accomplished by two loops of vasculature (arteries, veins, capillaries) joined at the heart. The pulmonary circulation ensures the replenishment of oxygen while the systemic circulation distributes oxygen to all cells in the body. The CV system is essential for the survival of each cell and ultimately the organism. CV function is controlled by the nervous and the endocrine systems to maintain homeostasis and respond to stimuli, such as the increased oxygen need during exercise or changed blood pressure caused by laying down. Side effects of drugs on the CV system may cause long-term damage, potentially putting the patient at greater risk of mortality and morbidity. Minimising drug-induced CV side effects is therefore essential for the development of safe drugs.

2.3.1 Cardiac electrophysiology

The heart is divided into four chambers: The two right chambers pump blood through the lungs while the two left chambers pump blood through the remaining tissues. Blood is first loaded into the atria, which contract to load the ventricles, followed by ventricular contraction to pump the blood around the body. The human heart beats at a rate of about 60 bpm at rest, and the duration between the initiation of each heart beat is thus around 1 s. These regular contractions are controlled by electrical signals called action potentials (AP). Each heart beat is initiated at the sino-atrial (SA) node, followed by propagation of the AP across the cardiac tissues to ensure that different parts of the heart contract in a coordinated fashion

and in the correct order. This AP propagation can be monitored using the ECG, which measures the electrical stimulation across the body surface (Figure 2.5). The standard 12-lead ECG is constructed from 10 electrodes placed across the subject's body, where 12 angles (leads) are measured simultaneously and combined to form the standard ECG. Following initiation of the heart beat at the SA node, the AP propagates through the atrial tissue. The PR (or PQ) interval corresponds to the series of events from depolarisation and activation of the atria, leading to contraction of the atrial tissue, through the atrio-ventricular (AV) node, the His-Purkinje system and the bundle branches and ends when the AP has reached the Purkinje fibres. PR intervals are often monitored due to the large R wave being a more robust measure compared to the smaller Q wave, although PQ intervals more accurately reflect atrial depolarisation and conduction through the AV node as PR intervals also include a short initial part of the ventricular depolarisation (QR). After reaching the Purkinje fibres, ventricular depolarisation follows as the AP conducts through the ventricular tissues, giving rise to the QRS complex in the ECG. Finally, the ventricles relax in the repolarisation phase, with the QT interval representing the duration of the full ventricular action potential.

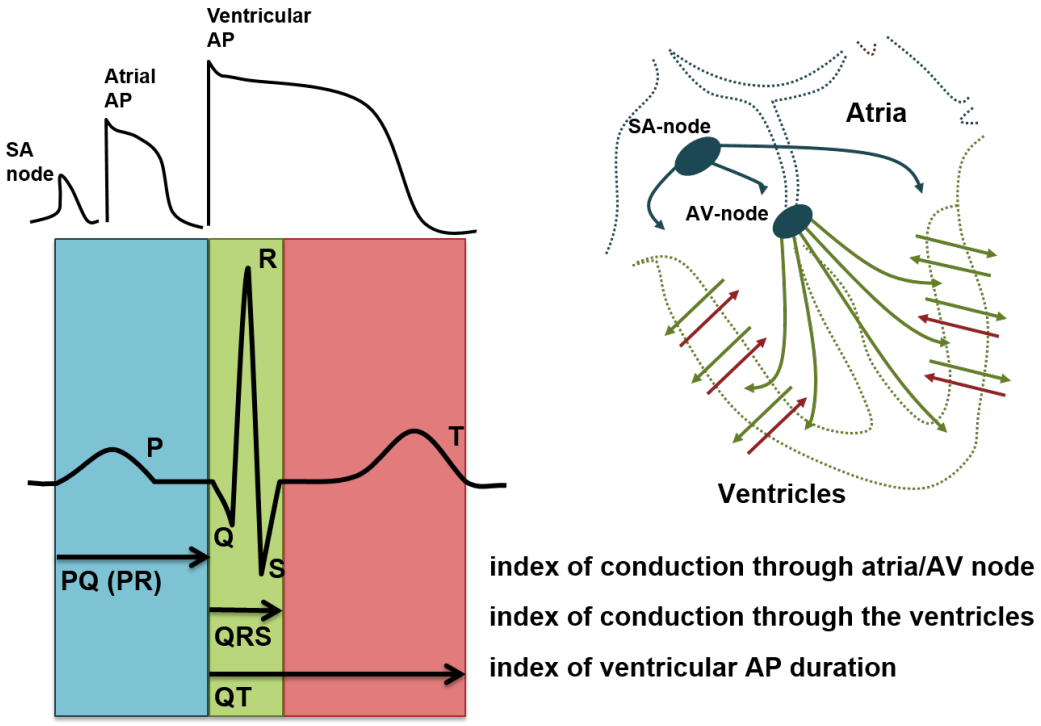

Figure 2.5 The ECG of normal sinus rhythm, highlighing the basic electrophysiology of a heart beat. Initial activation of the sino-atrial (SA) node is followed by atrial depolarisation and contraction, and conduction to the atrio-ventricular (AV) node. From the AV-node, the action potential conducts through the Purkinje fibres to the ventricles, followed by ventricular depolarisation and contraction. Finally, the ventricles relax in the repolarisation phase.

In the contractile cells of the heart (myocytes), the AP is controlled by ion fluxes through membrane channels (Figure 2.6). Many different ion channels are involved in the AP, and their prevalences vary between different parts of the cardiac tissues (myocardium) to ensure optimal CV function, such as maintaining the delay between atrial and ventricular contraction. This delay ensures the proper filling of the ventricles and in turn a high cardiac output.

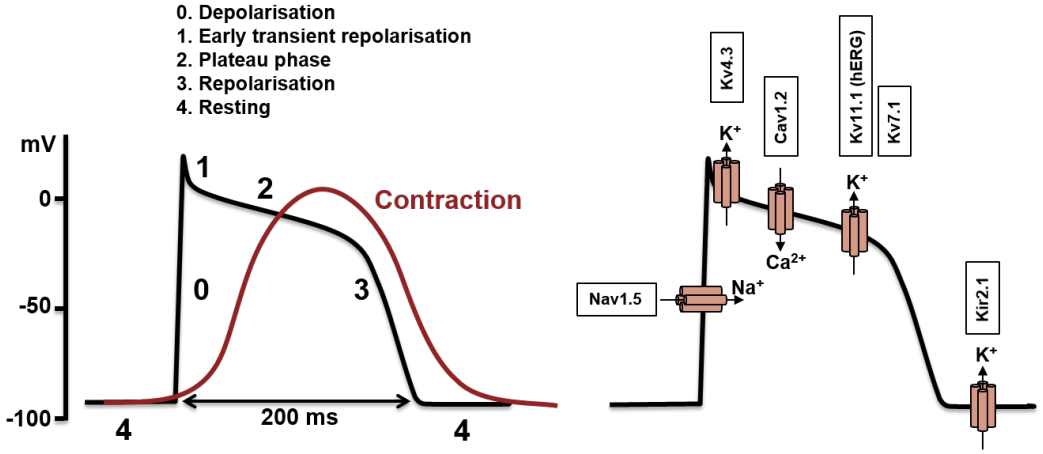

Figure 2.6 Opening and closing of ion channels in the myocyte membrane control the different phases of the cardiac action potential [47]. Phase 0: Depolarisation by rapid inward INa current through the Nav1.5 channel. Phase 1: Early repolarisation through transient outward IK current through the Kv4.3 channel. Phase 2: Plateau phase by balanced inward ICa current through the Cav1.2 channel and outward IK current through the Kv11.1 (hERG) and Kv7.1 channels. Phase 3: Dominance of the repolarisation due to closing of the hCav1.2 channels. Phase 4: Maintained resting potential due to outward IK current through the Kir2.1 channel.

2.3.2 Biomarkers for cardiovascular safety

The importance of CV safety assessment is highlighted in a recent study, implicating CV complications as the leading cause of drug withdrawals from the EU market between 2002 and 2011 [48]. CV risks of potential new drugs are routinely assessed in drug discovery and development, aiming to identify CV risks early in order to minimise risks to volunteers and patients and to avoid costly late-stage drug attrition. A panel of functional biomarkers is tested in clinical and nonclinical assays, and typically includes heart rate (HR) and blood pressure (BP), ECG, indices of cardiac contractility and, in nonclinical studies, structural damage by histopathological changes of the heart and/or vessels (Figure 2.7).

The ECG is investigated by visual assessment and/or automated software to find signs of arrhythmias and irregularities, to assess the amplitudes of peaks and to identify changes in the durations of the intervals between specific peaks. Key intervals are QT, PR and QRS, which, as described previously, correspond

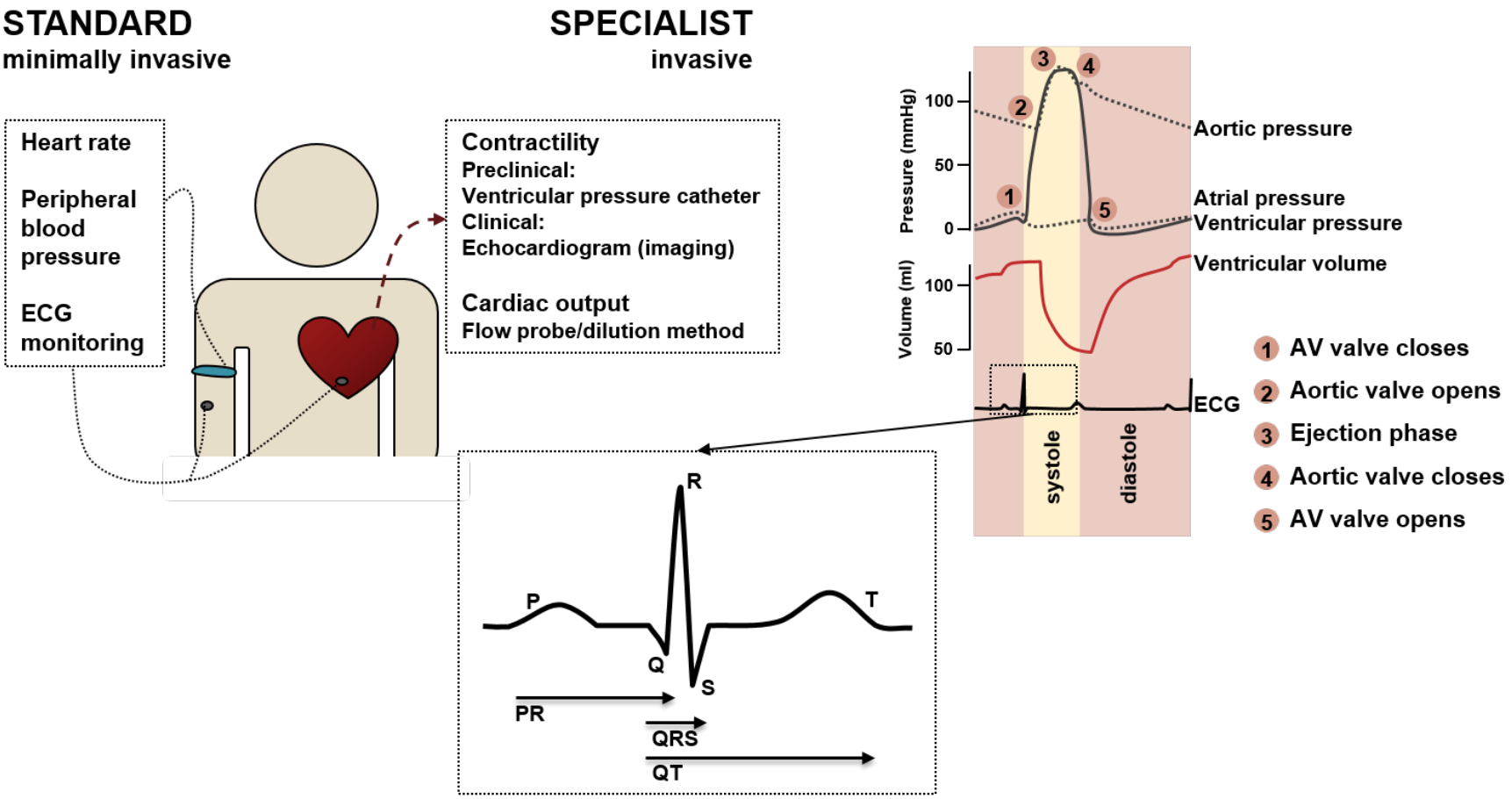

Figure 2.7 Standard minimally invasive and invasive CV measurements that can be obtained from a whole body system. The Wiggers diagram (top right) show the dynamics of some measurable variables, including atrial and ventricular pressure as well as ventricular volume. Also, a standard 12-lead ECG curve is shown, and the main intervals (QT, QRS and PR) indicated. Figure from [1].

to different and specific events in the heart beat. Changes in the durations of these intervals indicate undesired side effects for most new drugs, with the possible exception of antiarrhythmic drugs.

As was mentioned in the introduction, the most known safety risk is prolongation of the QTc interval, to which abundant observations have linked inhibition of the hERG channel and risk of the potentially lethal arrhythmia Torsades des Pointes (TdP) [7, 8]. QTc liabilities are regulated in the specific ICH guidelines for pre-clinical (S7B, [24]) and clinical (E14, [49]) development, and QTc is the only ECG biomarker for which a clear regulatory threshold of concern for clinical use has been established. This threshold is stated in the E14 guidelines, where the upper bound of the 95 % confidence interval around the mean QTc effect should be <10 ms for all time points, measured in a thorough QT/QTc (TQT) study [49]. Since the update of the E14 guidelines in December 2015, QTc effects may also be investigated by PK-PD or PD modelling of other clinical data, where the upper bound of the 90% confidence interval should be <10 ms at the highest clinically relevant exposure [50].

The focus of this thesis is however not QTc, but QRS and PR prolongations, reflecting drug-induced slowing of cardiac conduction. Prolonged QRS and PR intervals are linked to increased mortality and morbidity in cardiac risk populations [15]. PR interval prolongations are primarily caused by delays in conduction through the AV node and are associated with increased risk of atrial fibrillations and death in risk populations [17]. Widening of the QRS complex represents slowed conduction through the ventricles and is linked to sudden cardiac death in healthy males [16]. Early identification of these cardiac conduction liabilities is therefore vital for effective nonclinical CV safety assessment. Contrary to QTc, QRS and PR intervals are only regulated by the general requirement to evaluate undesirable pharmacodynamic effects in the general *in vivo* safety pharmacology guidelines (ICH S7A [51]). Also, no regulatory thresholds for acceptable levels of effects in clinical studies have been established.

2.3.2.1 Nonclinical studies to assess conduction liabilities

Identification and mitigation of cardiac conduction liabilities is at AstraZeneca performed using multiple nonclinical *in vitro* and *in vivo* assays (Figure 2.8). *In vitro* assays primarily involve assessing the interaction of compounds with the cardiac ion channels that are known to control the heart beat, where conduction slowing is primarily studied by assessing effects on the sodium (Nav1.5) and L-type calcium (Cav1.2) channels. Inhibition of Nav1.5 leads to reduced Na^+ influx which slows ventricular depolarisation, causing widening of the QRS complex (Figure 2.9) and/or prolongation of the PR interval (reviewed in [19, 52]). In early discovery phases such as the lead generation and lead optimisation phases, automated or conventional func-

tional human Nav1.5 (hNav1.5) whole-cell voltage clamp assays are typically used to identify compounds that inhibit hNav1.5 and reduce the Na^+ flux *in vitro*. Safety margins of 30-100 fold between predicted maximal exposures in humans (predicted C_{max}) and IC_{50} measured *in vitro* have been suggested for hNav1.5-QRS based on collected information of *in vitro* potencies and clinical findings [19].

Potential mechanisms for PR prolongations are more complex, as the PR interval represents action potential propagation through the atria, the AV node, the His-Purkinje system and the bundle branches to reach the Purkinje fibres. The major mechanism for drug-induced PR prolongation is AV block through inhibition of the cardiac L-type calcium (Cav1.2) channel (reviewed in [15], Figure 2.9). Cav1.2 is activated following the fast Na^+ depolarisation, initiating an influx of Ca^{2+} that in turn triggers the release of intra-cellular Ca^{2+} deposits, provoking myocyte contraction. Cav1.2 inactivates slowly and counter-acts repolarisation of the myocytes through continued influx of Ca^{2+}, and is thus also vital for maintaining the plateau in the ventricular myocyte action potential influencing the QT interval. Functional human Cav1.2 (hCav1.2) assays may be used to detect potential conduction liabilities [53]. However, both conventional and automated functional hCav1.2 assays have been shown to correlate poorly [54] to an *in vitro* contractility assay using dog myocytes [55], showing low sensitivity with many false negative responders. Alternatively, radioligand binding to rat Cav1.2 (rCav1.2) may be used to detect compounds that bind to Cav1.2. Two binding sites predictive of cardiac contractility have been identified, namely the verapamil and diltiazem sites [54]. In addition to hCav1.2 inhibition, rCav1.2 binding to these sites is therefore typically analysed at AstraZeneca. In addition, PR prolongation may be caused by hNav1.5 inhibition e.g. through reduced conduction through the His-Purkinje system [56]. Contrary to hERG and hNav1.5, safety margins have not to the authors knowledge been suggested for hCav1.2 inhibition or rCav1.2 binding.

In vivo investigations of drug-induced effects on ECG intervals may be conducted in anaesthetised and/or conscious rats, guinea pigs and dogs [21, 22, 23]. Rodent animal studies are typically conducted early, at the lead optimisation phase, providing the first data on cardiovascular effects in complete systems at a time of (relatively) low cost and high chemical choice. Animal studies in dogs, or sometimes minipigs or non-human primates, are conducted during pre-clinical development to confirm the safety of compounds before first time in man (FTIM) studies as part of regulatory requirements. Both conscious and unconscious animal telemetry studies are used, as conscious animal studies enable long term safety assessment, while unconscious (open chest) animal studies enable measurement of additional variables, reduce noise and allow for higher doses. ECGs are typically generated using automatic systems for calculating the durations of the intervals, often followed by manual checks at pre-defined time-points around which data are averaged to reduce noise

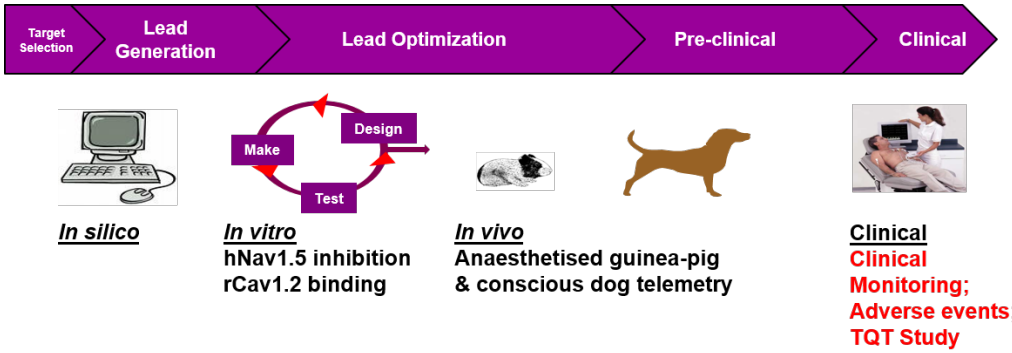

Figure 2.8 Assays for cardiac conduction risk assessment at AstraZeneca. Cardiac conduction risk is mitigated during lead generation/optimisation by *in vitro* assays, primarily assessing effects on Nav1.5 and Cav1.2. During lead optimisation, rodent *in vivo* studies are conducted to assess cardiac safety, including QRS/PR interval prolongations in monitored ECGs. Cardiac safety, including QRS/PR changes, is also evaluated in a large animal telemetry study during pre-clinical development, and prior to human testing.

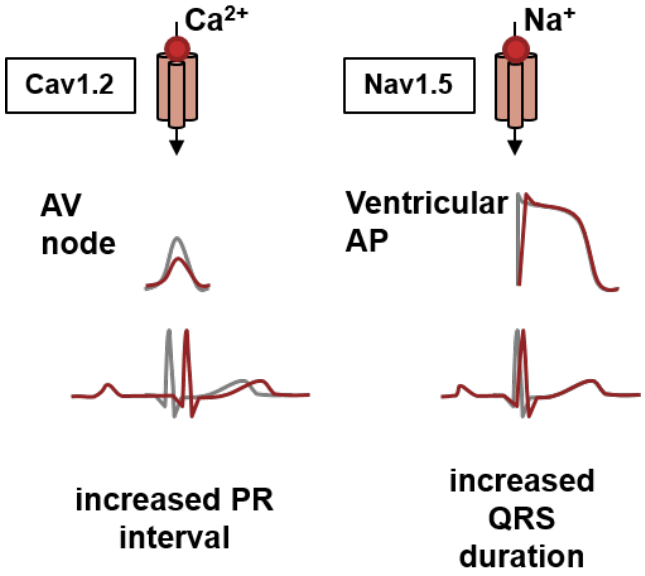

Figure 2.9 The ECG informs on electrophysiological changes in heart function as changes in ion fluxes cause predictable changed in the ECG. Inhibition of the Cav1.2 calcium channel slows down conduction through the AV node, leading to prolonged PR interval. Inhibition of the Nav1.5 sodium channel leads to reduced rate of depolarisation across the myocyte membrane, causing widening of the QRS complex. Figure by Matt Skinner, AstraZeneca.

and extracted for analysis. Any drug-induced effects on QRS and PR intervals are typically identified by statistical tests, e.g. pair-wise comparison to the vehicle group at each time point and evaluated considering additional information, such as drug exposure and time point of the identified effects.

2.3.3 Modelling & simulation for cardiovascular risk assessment

The following section describes the history and current status for a selection of modelling approaches to assess CV safety in drug discovery and development, partly published previously in Collins, Bergenholm et al. 2015 [1].

2.3.3.1 PKPD modelling of QTc, QRS and PR

PKPD modeling of QT prolongation began in the late 1970s and is arguably the most characterized of all PK-ECG relationships, with numerous published models in pre-clinical species and human [1]. Currently, PKPD modeling of clinical or non-clinical data is routinely modeled using population (mixed effects) approaches rather than individual or pooled datasets [57, 58], typically with direct models or fast equilibrating effect compartments. The following factors have been identified as important considerations in the modelling of QT [10, 14], and could also remain relevant for QRS and/or PR intervals:

1. Heart rate correction, preferably individual specific in humans and animals [59, 60].
2. Variability of the baseline including between subject variability, inter-occasion variability and within-subject variability (e.g. a circadian rhythm modelled using single or multiple cosine functions).
3. Subject demographic information such as age, sex.
4. Genetics.
5. Environmental or other factors such as obesity, physical activity, electrolyte levels, blood pressure, blood glucose and alcoholism.

Modelling baseline variability of intervals in the ECG

QT interval duration is strongly dependent on HR and the use of correction methods aim to remove the influence of heart rate, providing a more stable measure: QTc. HR correction formulas include linear, fixed exponential (Bazett, QTcB, Fridericia, QTcF) and individual exponential (exponents estimated to data, QTcI). QTcI and QTcF has been shown to perform best in humans, while QTcI performed best in pre-clinical species including dogs, guinea pigs and cynomolgus monkeys [59]. In addition to QT, QRS and PQ intervals have been shown to correlate to RR intervals in a subject-specific manner [61], with PQ showing primarily positive correlations and QRS small positive or negative correlations. Correcting to RR intervals may therefore reduce variability also for modelling of QRS and PR intervals. Cosine functions [62] have been used to account for within-subject variability in baseline due to homeostatic mechanisms, external factors or circadian rhythms (regular diurnal fluctuations), either using typically single or where necessary multiple cosine functions [12, 58, 63]. While early models were primarily developed by individual or

pooled data modelling, population models are commonly applied today (reviewed in [1]). Inter-individual variability is often included both for baseline and drug effect parameters. This reflects the availability of high quality, rich ECG data combined with more readily available software to conduct these analyses.

Modelling drug-induced effects on intervals in the ECG

Both empirical and systems level models have been used to investigate and predict drug-induced ECG (primarily QT) effects. Empirical models that have been used include both proportional and E_{max} models (Equations 2.2 and 2.4). In many cases, proportional models described the drug effect adequately [1]. While it is expected that drug effects will eventually saturate with exposure, proportional models may be more prevalent for ECG changes, as maximal effects are often not achieved in safety studies where doses are selected based on margins to the therapeutic exposure and not to characterise full concentration-response relationships. Studies can also be halted before reaching a maximum level due to lack of tolerability at these exposures. However, E_{max} models can sometimes be fitted when the effects of anti-arrhythmic compounds with intended effects on the ECG are evaluated. Once in the clinic, concentrations required to reach maximal effect are less often reached for these same reasons, leading to even fewer saturable models being observed. Where E_{max} models have been utilised for clinical QTc changes, the maximal activity level appears to be compound-specific rather than reaching a system specific or physiological upper limit [1].

It is very common to observe a delay between blood or plasma drug concentrations and CV effect, resulting in hysteresis observable in a concentration-effect plot. This time delay is often short, and of the order of minutes. Under these circumstances, an effect compartment model (Equation 2.5) is often applied to describe the delay between the measured plasma concentrations and the distribution of drug to the effect site [62]. Almost half of the ECG models reviewed in [1] included a time delay, primarily using the effect compartment model and where the estimated time delays rarely exceeded 30 minutes. The use of indirect response models (Equation 2.8) which describe the physiological turnover of the response parameter in terms of synthesis and degradation is uncommon for ECG intervals. One potential reason for this is that the effect of the drug on ion channel activity is expected to be rapid once the compound has reached the myocytes, not requiring a turnover process to have an effect. Although PK-PD modelling examples of intervals other than QT are limited, it appears most other endpoints are typically treated similarly to QT. The concentration-QRS relationship of a number of compounds has been investigated in dogs [57] using a population approach, and this enabled comparison across compounds and investigation of therapeutic window. The data were modelled as percent change from baseline and the size of the estimated E_{max} for QRS change

varied from 8 to 57 %.

2.3.4 Approaches to predict CV effects in humans

Methods to translate and predict CV risk in humans that incorporate different levels of mechanistic insight are used and continously developed. Depending on the questions asked, the current level of understanding of the system and the available data, translational approaches involving models including different levels of detail may be optimal. Three broad categories for modelling physiological systems to describe pharmacodynamics can be defined:

1. Top-down (data-driven) models: Empirical models used to describe and quantify data may be used to investigate translations by comparing effects between species.
2. Systems pharmacology "middle-out" models: Systems-based models incorporating physiological processes and mechanism of action at targets may potentially be used to predict effects in new species.
3. Mechanistic or systems biology models: Detailed models that combine knowledge of the system from cellular targets to their impact at a cellular, tissue or whole body level may potentially be used in combination with for example *in vitro* data to predict effects in humans.

2.3.4.1 Empirical (top-down) translational approaches

In order to predict human effects from animal data, some assumptions must be made considering the effect of the drug in humans compared to animals. Using PKPD modelling, data can be integrated across subjects, doses and time points in order to achieve good estimates of the effect in animals and humans, to be applied to investigate empirical relationships between drug effects across species (Figure 2.10). The most simple translational model would assume that the effect in the animal species and humans are the same (either the absolute or relative effect compared to baseline). Estimated drug effects from PKPD modelling can then be applied to generate human predictions using predicted human drug concentrations. However, the assumption of equal responses between animals and humans at the same drug concentrations may not be ideal as animals and humans have different physiology.

Where simple physiological determinants control the drug effects, allometric scaling may be used to quantify differences between animals and humans. Allometric scaling may be used when the effects can be assumed to depend on a physiological measure such as body mass, heart rate etc. The allometric relationship can for example be given by

$$Y = a * M^b \tag{2.16}$$

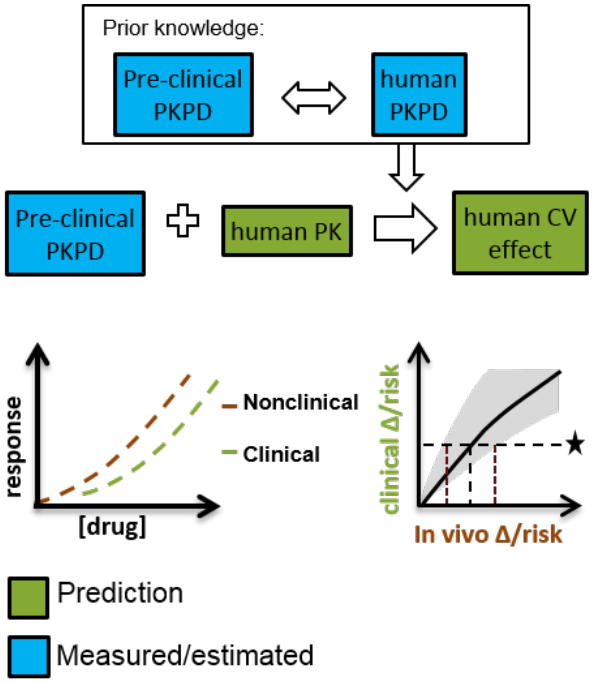

Figure 2.10 Comparative assessment between species using descriptive PK-PD modelling and simulation to identify predictive *in vitro*/*in vivo* assays and quantify empirical translational relationships. Figure adapted from [1].

which implies that

$$\log Y = b \log M + \log a \tag{2.17}$$

where Y is the physiological parameter of interest, M is the body mass and a defines the origin and b the slope of the logarithmic relationship. For example, while organ weights scale proportionally to body mass, many biological rates (e.g. HR, breath frequency) scale with $b \approx -0.25$ and volume-rates (e.g. cardiac output, ventilation) scale with $b \approx 0.75$ [64]. Allometric relationships can also be used to extrapolate to drug properties in humans through regression of a and b from data in multiple nonclinical species.

Another method for translation using PK-PD models is by identifying inter-species transducer functions using species-specific dose-response curves. This concept is used in [12], where the translation from a pre-clinical species to man is found using a three-step process (Figure 2.11). First, species-specific PK models are developed and time-matched exposure data points for the response data extracted. Second, a model for the response is identified and fitted for both species, and the species-specific dose response curves estimated. Finally, the response in humans is plotted as a function of the response in the nonclinical species at matched unbound drug concentrations. Within safety pharmacology, this approach can be used to define nonclinical thresholds of effects, compare translational relationships between

compounds and to compare the relative sensitivity of different models to humans. This method was used to compare QTc prolongations in dogs and humans for four different drugs [12], and suggested that average QTc prolongations of 2-8 ms (≈ 1-3%) in dogs compare to 10 ms (≈ 2.8%) in humans. However, prior to the work presented in this thesis, the translational relationship and relative sensitivity of drug-induced PR and QRS prolongations in animals and humans were not known.

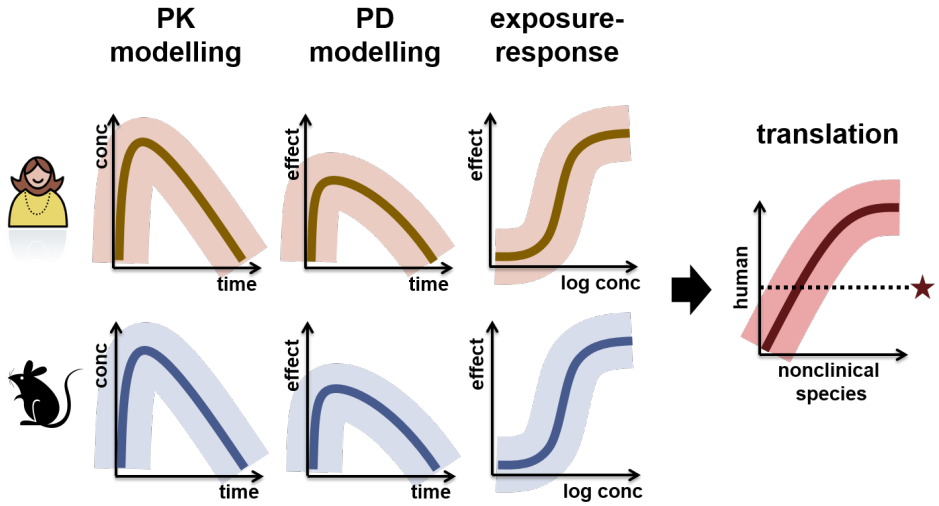

Figure 2.11 Translational modelling to find the translational relationship between pre-clinical species and man. A possible goal may be to define how a safety margin in man translates to pre-clinical results.

QTc risk has also been assessed by the probability of QTc prolongation as a function of plasma concentration [13]. Here the probability of QTc prolongation was assessed using Bayesian modelling. The posterior distribution of QTc changes was used to create a cumulative probability of QTc change above 10 ms (Figure 2.12). Such probability curves were derived for three different compounds and for both dogs and humans. It was found that the slope of the drug effect was smaller in dogs compared to humans for the investigated compounds, and also that the probability of a 10 ms increase in humans occurred at lower exposure levels compared to dogs. In this example, the drug-induced effects in dogs were found to be 0.5-1.5 ms at concentrations where the effect in humans were 10 ms. This relationship indicates an even lower sensitivity in dogs compared humans when contrasted to the results in [12].

An important limitation is that these models do not inherently take into account underlying physiological differences across species, such as ion channel expression levels and heart structure and size. This limits the possibility of using these empirical modelling methods to understand the mechanisms behind the reduced sensitivity in animals compared to humans.

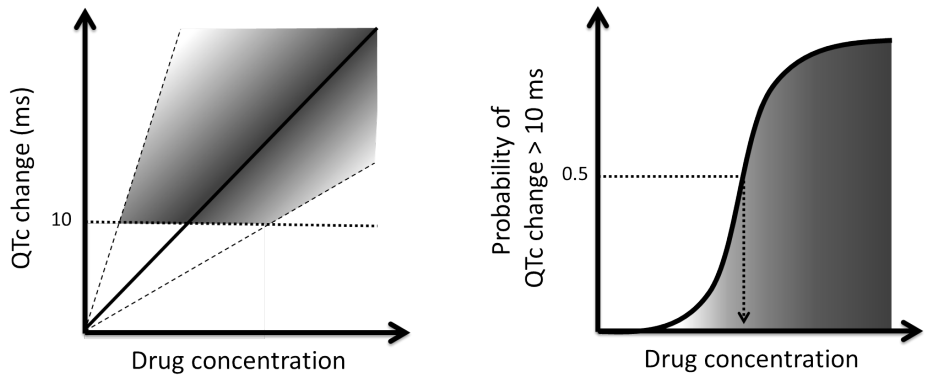

Figure 2.12 Using the posterior distribution of QTc effects to find the probability of QTc change above 10 ms for different concentrations. Adapted from [63]. It may be possible to relate the predicted QTc distribution in dog to that in man to find the translation.

2.3.4.2 Bottom-up systems pharmacology modelling

Drug-induced effects on cardiac ion channels have been modelled to predict morphology changes in the AP or ECG in detailed, "bottom-up" mechanistic models (Figure 2.13). Whilst models to translate a single *in vitro* experiment to *in vivo* change are standard in integrated pre-clinical risk assessment [9], these *in silico* predictions allow assessment of the combined effects on multiple molecular targets. These models represent the relevant electrophysiological aspects of the cellular system: transmembrane conductance, ion channels and their inhibition by drugs, as well as other pumps/exchangers and intracellular ion concentrations, and integrate the influence of these factors over time on cellular ion concentrations. Drug effects are modelled by altering the ion conductance term which represents the gating (open/closed etc.) of the relevant ion channel.

Cellular cardiac AP models have been developed for different species including humans [65, 66], dogs [67] and guinea pigs [68]. Such cardiac AP models have been applied to predict the effects of anti-arrhythmic drugs that alter ion channel activities [69, 70, 71] and better describe the effects of multiple ion channel inhibition rather than focusing purely on potency values. Mirams et al. [70] showed that a human AP model could be trained to classify TdP risk based on predicted therapeutic maximal concentrations (predicted C_{max}) and Nav1.5, Cav1.2 and Kv4.3 channel IC_{50} values with markedly improved accuracy compared to safety margins between hERG IC_{50} and therapeutic C_{max} alone. A recent comparison of the predicted effect of ion channel block in AP models from humans and nonclinical species highlights the importance of cautious extrapolation between species [72]. For example, a 70% block of the hERG ion channel resulted in an 80% AP prolongation in humans, but only a 30% and 20% change in dogs and guinea pigs respectively. So, detailed species-specific models may better explain and predict differences in the sensitivity

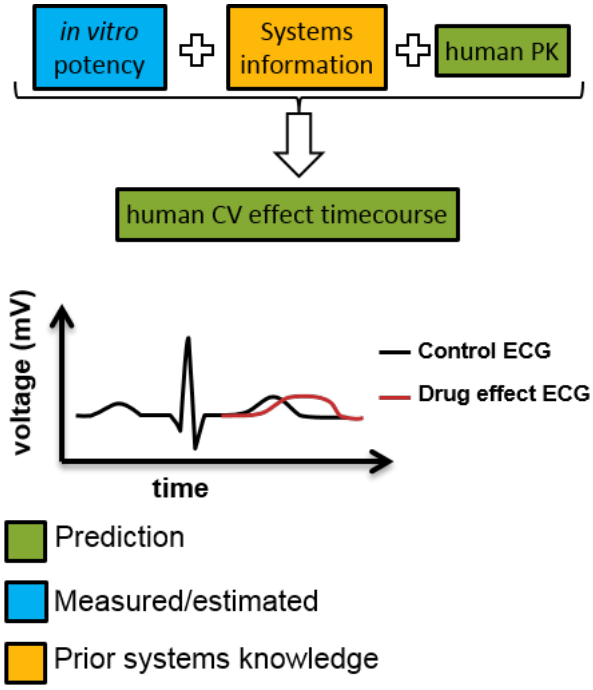

Figure 2.13 Bottom-up systems pharmacology approach using *in vitro* potency to predict clinical effects based on mechanistic knowledge. Figure adapted from [1].

to drugs between species.

While these ion flux models can capture information relating to the membrane potential in a single cell, the resulting ECG measurements are at the tissue/whole body level (Figure 2.14) and depend in part on the spatial orientation of myocytes in the heart and the AP propagation in tissue. Models of cardiac tissue have therefore been constructed to describe the propagation of the AP in 1, 2 and 3 dimensions [73] by linking multiple cellular models in a spatially relevant way. These tissue models have been used to study the effects of single and multiple ion channel blockade on Purkinje fibres [74]. At the whole heart level, cardiac structure and electrophysiology have been integrated with whole body geometry to translate ion channel effects through the simulation of cardiac AP propagation to calculate 12-lead ECG and QRS widening and QT prolongation as measured in the torso [75]. Similarly, 12-lead ECGs derived from simulated body surface potentials have been used to compare the two QTc-prolonging drugs cisapride (pro-arrhythmic) and amiodarone (anti-arrhythmic) [76], identifying the effect AP conduction of amiodarone alone as the mechanism behind the drug being anti- rather than pro-arrhythmic. However, with increasing model complexity, it becomes more difficult to evaluate if the model structure correctly describes the system, is structurally and practically identifiable and also that fixed parameters are correct.

The usefulness of mechanistic *in silico* models in drug discovery and development needs to be further demonstrated, as a recent study investigated the ability

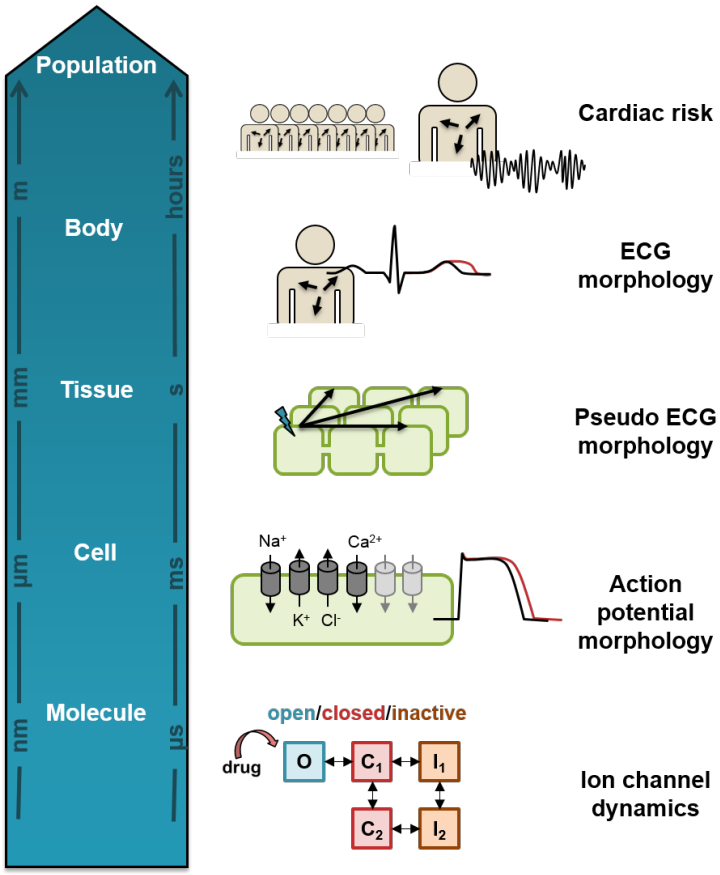

Figure 2.14 Spatial and temporal scales at which ECG systems models operate. At each level, different assumptions and variabilities need to be addressed, to meet the ultimate goal of predicting cardiovascular liabilities in patient populations. Figure adapted from [1].

of AP models to predict the QT change in TQT studies and showed that the models in general under-predicted the TQT outcome [77]. However, evaluating a 10- to 100-fold therapeutic window led to much improved predictions, suggesting that something related to tissue or cellular concentrations may be missing in the systems models. One tool built specifically to do this is the Cardiac Safety Simulator (Certara), a commercially available tool designed to increase the ability of non-modellers to test the effect of ion channel activity on the ECG incorporating population variability on both exposure (through SimCYP, Certara) and ECG prediction. As a test of predictivity of the simulator, the QTc effects of 6 anti-psychotic drugs [78] were investigated using the Cardiac Safety Simulator showing good agreement between predicted and observed mean QTc change, though the predictions did not account for all of the observed variability. Also, PK and PD effects of combination treatment with doinperidone and ketoconazole were predicted from *in vitro* data using *in silico* models [79]. To date, this approach has been used to demonstrate translation largely for ion channel inhibition and QTc effects [78, 79].

2.3.4.3 Middle-out systems pharmacology modelling

The final type of approach represents a middle-out [80] approach which attempts to combine the best properties of the purely descriptive top-down and reductionist bottom-up approaches (Figure 2.15). For example, comprehensive *in vivo* systems pharmacology models are in existence for CV system behaviour, particularly for haemodynamics [81, 82, 83] but these have so far only been implemented in a single species making translational predictions from pre-clinical species to human difficult. We do not have feedback from the clinic yet to understand how successful human predictions have been and there are no reports of cross-species comparisons with these models. Alternatively, simplified model structures can be applied that capture the relevant process governing information flow without over-parameterisation [57, 84]. Models of cardiovascular function with similar structure, but with species specific parameters could allow for further refinement of the predictive power of these approaches. In these approaches, substituting human physiological parameters into the preclinical model is a key part of the translation. For example, when HR changes have been translated from dogs to humans using a PKPD approach [84], the sensitivity to drug in addition to a baseline typical for humans were applied. In another example where BP was translated using an indirect response model, human baselines and rates of turnover (k_{out}) for SBP and DBP were obtained from the literature and combined with a PK prediction and the drug sensitivity obtained in dog to successfully predict the effects in first-time-in-human studies [57].

Mechanistic models may be used to quantify the relationship between *in vitro* data and the physiological response in the clinic using the operational model of pharmacological action (Equation 2.10). This has been done for hERG-QTc, where the authors in [9] estimated that only 10% hERG inhibition induced by the selective hERG blocker dofetilide translates to 20 ms (95% confidence interval 12-32 ms) QTc prolongation in humans. Mechanistic PD models can also be used to distinguish between different mechanisms for the drug effect. As an example, a mechanistic model of drug effects on blood pressure (BP) has been used for this purpose. The fundamental relationships between mean arterial pressure (MAP), total peripheral resistance (TPR) and cardiac output (CO) were used for the development of the structural model [82] given by

$$\begin{aligned} \frac{d}{dt}CO &= k_{in\_CO} * (1 - f_1 * MAP) - k_{out\_CO} * CO \\ \frac{d}{dt}TPR &= k_{in\_TPR} * (1 - f_2 * MAP) - k_{out\_TPR} * TPR \\ MAP &= CO * TPR + \sum_{n=1}^{10} A_n * \cos\left(n * (t + \tau)\frac{2\pi}{24}\right). \end{aligned} \tag{2.18}$$

where TPR and CO are modelled using two linked turnover equations with "pro-

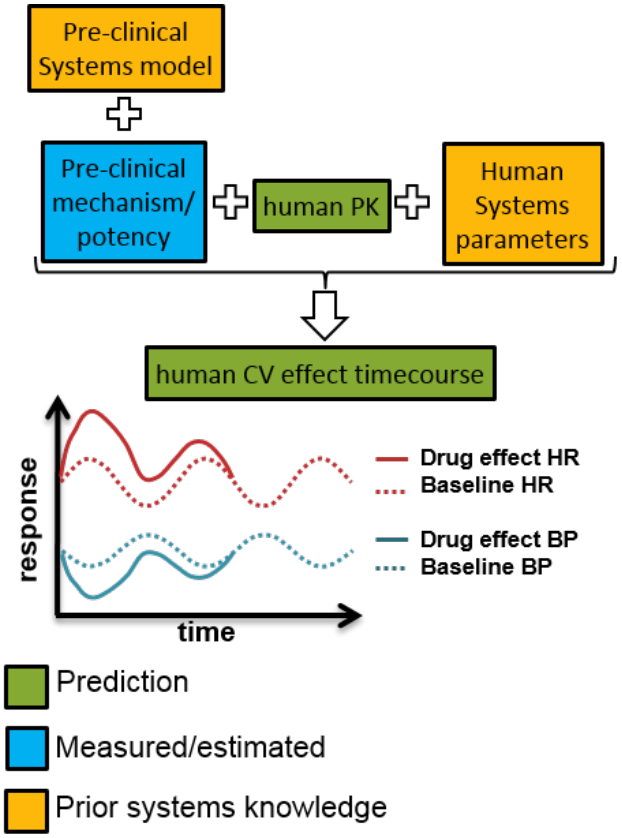

Figure 2.15 Systems pharmacology approach to predict clinical effects based on systems knowledge and *in vitro*/*in vivo* data. Figure from [1].

duction rates" k_{in_CO} and k_{in_TPR} and negative feedback parameters f_1 and f_2 by the *MAP*. The *MAP* in turn depends on *CO* and *TPR* and also incorporates circadian variations modelled with a set of up to 10 cosine functions selected if inclusion significantly improved fit to data. System-specific parameters such as production rates, feedback strengths and circadian effects were estimated by challenging the model with six compounds that affect either TPR or CO by different (established) mechanisms. Several biomarkers were measured to collect data to populate and parameterise the model, including HR, MAP, CO, stroke volume (SV) and TPR. Drug exposure was not measured, and therefore modelled using PK models from the literature. In theory, the developed model may be used to predict the mechanism(s) of novel drugs affecting BP.

Importantly, model selection must be based on the type of questions to be addressed, available resources, system knowledge and available data. A systems approach may be preferable for translational purposes, but requires understanding of the drug effect mechanism and important processes in the system. When a drug effect mechanism is understood and well characterised, systems translational models

can be adopted to generate robust predictions, while less understood mechanisms are more challenging and simpler approaches may be preferred.

2.4 Summary

Current methodologies and best practices for assessing CV risk in drug discovery and development are most advanced for the prediction and translation of QTc. For other ECG parameters such as the QRS and PR intervals, little is known of the translation from pre-clinical ion channel blockade or *in vivo* ECG changes to the clinic. M&S methods and techniques to predict clinical QTc interval changes range from empirical cross-species scaling to highly detailed multi-level models describing cardiac function starting at the ion channel level controlling the cellular AP, propagation of the AP in different cardiac tissues and through the torso to predict the 12-lead ECG response. These methods may also be useful for describing and predicting effects on other ECG intervals.

This chapter identifies a gap in the current strategies for assessing cardiac safety, as the quantitative translations from nonclinical to clinical effects of biomarkers for cardiac conduction slowing were largely unknown at the time of initiating this work. In addition, despite the wealth of published examples of PKPD modelling of drug-induced prolongations of the QT interval, few publications were identified where drug-induced QRS and PR interval effects were described using PKPD models. The aims of this thesis are therefore to address this gap by developing models to quantify QRS and PR intervals monitored in nonclinical species and in humans, and to investigate the translation between nonclinical and clinical effects. Relevant background information for performing these tasks has also been presented.

Chapter 3

Parameter identifiability

3.1 Introduction

This chapter introduces the concepts of structural and practical identifiability and investigating parameter identifiability of commonly applied pharmacodynamic models. Some models were applied in further chapters of this thesis, and the results of these investigations are therefore of high relevance to this thesis. The work presented in this chapter was performed in collaboration with Early Stage Researcher David Janzén, and is based on a journal publication (Janzén and Bergenholm et al. [2]).

3.2 Structural and practical identifiability

M&S within pharmacology often involves the estimation of model parameter values using experimental and/or literature data. The model with the estimated parameter values may be used to predict new data and scenarios such as outcomes across different populations or with new dosing schedules. Such predictions may not always be valid: In particular, the estimated parameters may not be possible to identify. Within the concept of parameter identifiability, there are two distinct types: **structural identifiability** [85] and **practical identifiability** [86].

Structural identifiability concerns the inherent identifiability of the parameters in a model given its structure and observed outputs [85]. If a model is structurally identifiable, it means that all parameters can *in theory* be identified, given perfect (e.g. noise free, continuous) data. However, an unidentifiable model has at least one parameter that can take any value without changing the model output (albeit with possible readjustment of remaining parameters). A well-known structurally unidentifiable problem is the linear model commonly used for estimating bioavailability F and volume of distribution V from plasma concentrations measured after oral drug administration. The most simple case is the one compartment PK model with first order absorption, where the plasma drug concentration C following a single

dose is defined according to

$$C(t) = \frac{F \cdot DOSE \cdot k_a}{V\left(k_a - k_e\right)} \left(e^{-k_e \cdot t} - e^{-k_a \cdot t}\right) \tag{3.1}$$

where F is the bioavailability of the drug, $DOSE$ is the orally administered dose, V is the volume of distribution, k_a is the rate of absorption and k_e is the rate of elimination. It has been shown that only the fraction $\frac{F}{V}$ can be identified, and any estimate of F will therefore inversely correlate to V and both values will be biologically meaningless [87]. Importantly, predictions of $C(t)$ are still valid as these depend on the identifiable fraction $\frac{F}{V}$.

Practical identifiability is a measure of the amount of information contained in the experimental data and how this information is translated to parameter uncertainty and subsequent prediction uncertainty. Practical identifiability is analysed by, for example, assessing standard errors and correlation matrices.

The structural identifiability of a model is preferably analysed prior to parameter estimation, ensuring that any uncertainty in the estimated parameters is related to the quality of the data and how well the model can describe them (Figure 3.1). However, parameter identifiability is unfortunately often only investigated and considered at the level of practical identifiability using more simple measurements such as standard errors or correlation matrices rather than more sophisticated approaches such as the profile likelihood approach [86].

This is problematic for several reasons. The primary reason is that it cannot be guaranteed that the estimated parameter values are uniquely determined by just looking at the estimation results. In addition, if the structural identifiability of a model is unknown, it means that the source of uncertainty in the parameter estimates may be either due to the experimental data, the model structure, or both (Figure 3.1). Thus, increasing the quality of the data may or may not improve the precision of the parameter estimates. On the contary, if structural identifiability analysis has concluded that the model is identifiable, the uncertainty in the model parameters is directly linked to the quality of the data and how well the model can describe them. In this scenario, the uncertainty of the model parameters can be improved by increasing the quality of the data. However, there will always be uncertainties in the parameter estimates, even if the model is structurally identifiable and the quality and quantity of the experimental data are relatively high. An approach to further strengthen the plausibility of the model predictions under such conditions is to divide the experimental data into two parts: data used for parameter estimation and data used for model validation, i.e. by estimating the unknown parameters using a subset of the experimental data and using the resulting estimates to predict the validation data.

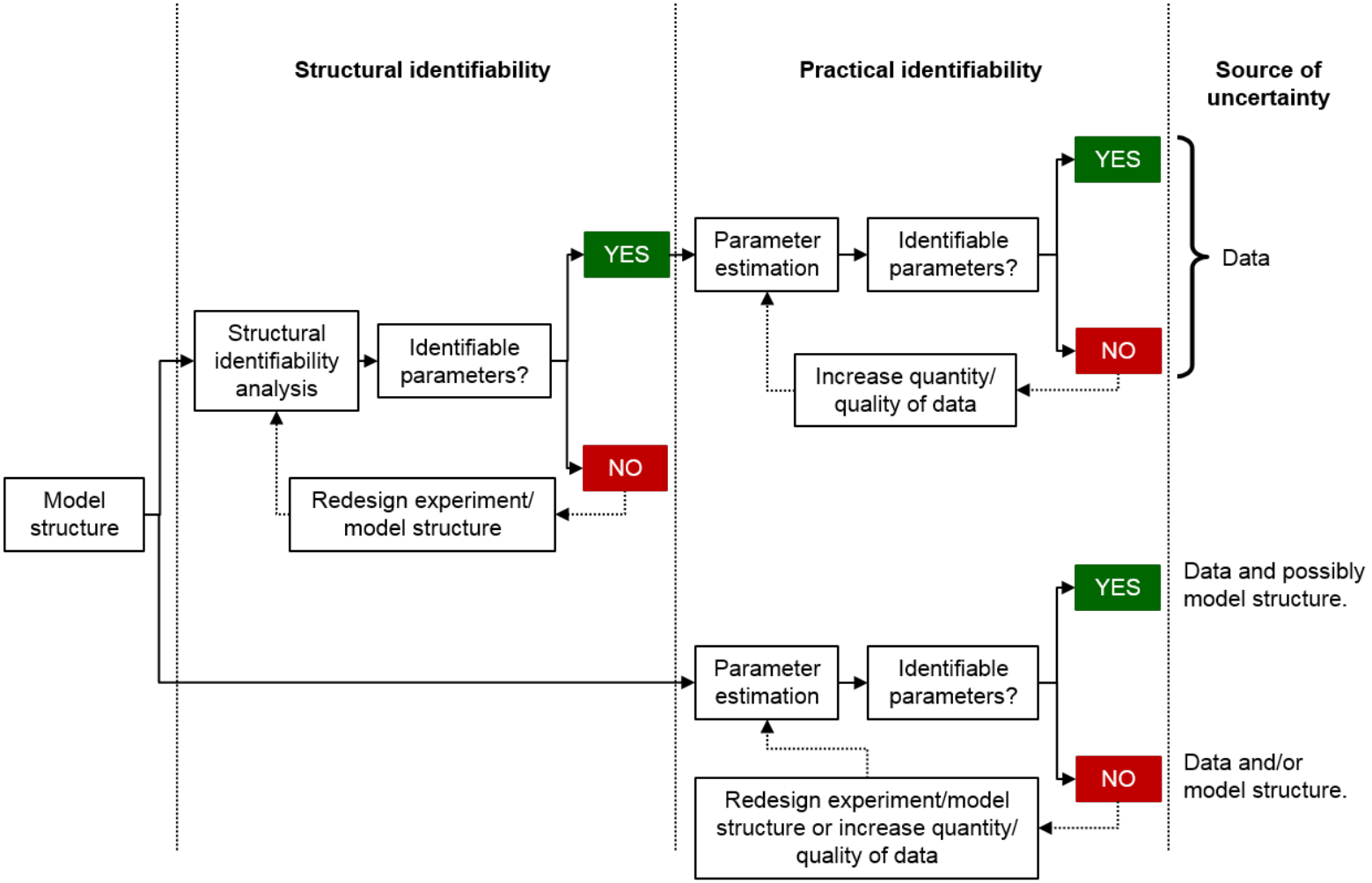

Figure 3.1 Schematic comparing the model development process including or excluding a structural identifiability analysis. If the structural identifiability of a model is known, the standard errors in the parameter estimates reflect the uncertainty in the data and and how well the model can describe them. However, if the structural identifiability is unknown, the standard errors in the parameter estimates may reflect both issues with the model structure and the data. Figure from [2].

The difference between structural and practical identifiability and the importance of proper analyses are highlighted in Figure 3.2. The parameters of an unidentifiable and a reparameterised version of a model (Model 5, presented later) was estimated in three separate runs. Parameters in the unidentifiable version of the model were estimated in two different runs using different initial estimates. For the third parameter estimation run, the model was reparameterised following insights from the structural identifiability analysis.

Investigating the estimated parameters shows that standard errors of unidentifiable parameters differ significantly between the two estimation runs, and are larger than the standard error of the product of the parameters. For one of the estimation runs the magnitude of the standard errors (37.6 and 33.7 %) did not clearly indicate a structural identifiability problem. In the second estimation run the standard errors are much higher (163 and 154 %) and did indicate a structural identifiability problem. However, for both estimation runs the estimated correlations between R_{tot} and k_e were close to -1 (-0.9 and -0.99), indicating a potential structural identifiability problem. Analysing the models using the profile likelihood approach [86] would also potentially indicate a problem with structural and practical identifiability.

Although estimation of an unidentifiable model in theory should lead to infinitely large uncertainty for the structurally unidentifiable parameters due to a flat likelihood function in the directions representing those parameters, this did not happen in practice. The reason why this did not happen can be explained by measurement and numerical noise. In real-world problems, the likelihood function is never completely flat which introduces false local minima where the optimisation routine may become "stuck" depending on the initial guesses used for the model parameters and the optimisation algorithm itself. This example shows the potential danger of using practical identifiability analysis as a tool to deduce structural identifiability.

3.2.1 Structural identifiability of 16 pharmacodynamic models

Commonly used PD models such as the effect compartment model, indirect response models and drug-receptor binding models were described in Section 2.2.1.2. However, despite frequent use, relatively few PD models have been analysed from a structural identifiability perspective. An example of a published structural identifiability analysis is for an approximation of the receptor binding model. Receptor binding often occurs over very fast timescales relative to the PK, and sometimes also with respect to the effects elicited by the receptor once bound. In such cases, the receptor binding model may be approximated by a quasi- or pseudo-steady state approximation. When using such an approximation, it has been shown that

A. Structural identifiability analysis

Input: C
Output: E
Initial conditions: $R(0) = R_{tot}$, $RC(0) = 0$
Parameters: k_{on}, k_{off}, k_e

$$C + R \underset{k_{off}}{\overset{k_{on}}{\rightleftharpoons}} RC \xrightarrow{k_e} E$$

Identifiable parameters: k_{on}, k_{off}
Unidentifiable parameters: k_e, R_{tot}
Identifiable combinations: $k_e * R_{tot}$

B. Estimation of structurally unidentifiable (SU) models

1. SU model

	Start	Estimate	RSE	Residuals
R_{tot}	10	11.9	37.6	7.66
k_e	10	16.4	33.7	
k_{on}	1	3.71	22.3	
k_{off}	1	4.85	22.5	

2. SU model (different start guess)

	Start	Estimate	RSE	Residuals
R_{tot}	100	87	163	7.66
k_e	1	2.17	154	
k_{on}	1	3.45	22.9	
k_{off}	1	4.76	22.8	

3. Reparameterised model (R_{tot} = 100)

	Start	Estimate	RSE	Residuals
k_e	1	2.03	15.8	7.67
k_{on}	1	3.61	22.6	
k_{off}	1	4.86	22.9	

Figure 3.2 **A.** Results of the structural identifiability analysis of Model 5. **A.** Optimisation results following estimation of unidentifiable and identifiable versions of Model 5 using example data. Figure from [2].

the individual on and off rates of drug binding to the receptor cannot be uniquely identified [88]. Another example is the target-mediated drug disposition model [89] applicable to the modelling of biologics, which has been shown to be structurally identifiable [90]. However, the identifiability of the effect compartment model and the operational model have, to the author's knowledge, not previously been analysed. Furthermore, mixed effects ("population") models are often used to account for and quantify known sources of variability in data sets, such as between-subject variability (BSV). Such models are combined structural and statistical models, with additional statistical parameters describing the variance of a postulated distribution of the model parameter values across e.g. subjects. The structural identifiability of mixed effects models describing BSV has not been investigated previously.

The parameter identifiability was investigated in [2] for 16 commonly applied PD models comprising combinations of sub-models representing different potential delays, including receptor binding, distribution through a hypothetical effect compartment and direct or indirect transduction (see Figure 3.3 and Table 3.1). Details of the methods applied for the structural identifiability analyses are described elsewhere [2], as these analyses were not performed by the author of this thesis and therefore are outside the scope of this work. Briefly, the input-output approach [91] was applied, allowing to distinguish globally identifiable, locally identifiable and unidentifiable models. This approach involves step-wise derivation of the model written in state-space form and substitution of all state variables on order to identify if all parameters have a single, finite or infinite number of solutions. By definition, a model is structurally globally identifiable only if all parameters are structrually globally identifiable.

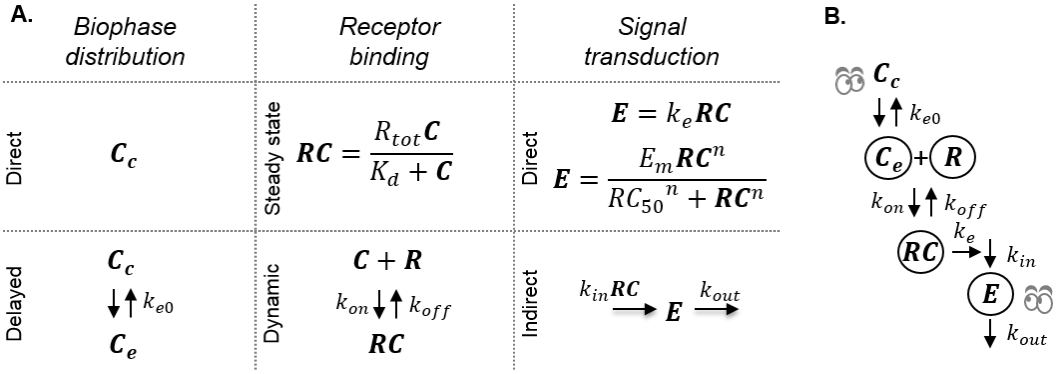

Figure 3.3 Schematic of the investigated pharmacodynamic models. **A.** The 16 investigated models are constructed by combining the following submodels: Direct or delayed biophase concentration through distribution to a hypothetical effect compartment, dynamic or direct receptor binding using the steady-state approximation and direct proportional or sigmoid signal transduction or delayed signal transduction applying a turnover model. **B.** Example of a full model where all three processes are assumed to be dynamic and cause delay between plasma concentration and drug effect. Figure from [2].

Table 3.1 Summary of the 16 PD fixed effects and mixed effects models for which the structural identifiability was investigated. Adapted from [2].

				Fixed effects models	Mixed effects models	
N	Model equations	I/O	ICs	Fixed effect parameters	Fixed effect parameters[a]	Random effect parameters[b]
1	$E = k_e \frac{R_{tot}C_p}{K_d+C}$	C_p/E		R_{tot}, k_e, K_d	k_e, K_d	η_{ke}, η_{Kd}
2	$E = \frac{E_m(R_{tot}C_p)^n}{(K_d+C_p)^n RC_{50}^n+(R_{tot}C_p)^n}$	C_p/E		$R_{tot}, E_m, RC_{50}, n, K_d$	E_m, RC_{50}, n, K_d	$\eta_{Em}, \eta_{RC50}, \eta_n, \eta_{Kd}$
3	$\dot{E} = k_{in}(1 + k_e \frac{R_{tot}C_p}{K_d+C_p}) - k_{out}E$	C_p/E	$E(0) = k_{out}/k_{in}$	$R_{tot}, k_{in}, k_{out}, k_e, K_d$	$k_{in}, k_{out}, k_e, K_d$	$\eta_{kin}, \eta_{kout}, \eta_{ke}, \eta_{Kd}$
4	$\dot{E} = k_{in} - k_{out}(1 + k_e \frac{R_{tot}C_p}{K_d+C_p})E$	C_p/E	$E(0) = k_{out}/k_{in}$	$R_{tot}, k_{in}, k_{out}, k_e, K_d$	$k_{in}, k_{out}, k_e, K_d$	$\eta_{kin}, \eta_{kout}, \eta_{ke}, \eta_{Kd}$
5	$\dot{RC} = k_{on}(R_{tot} - RC)C_p - k_{off}RC$ $E = k_eRC$	C_p/E	$RC(0) = 0$	$R_{tot}, k_{on}, k_{off}, k_e$	k_{on}, k_{off}, k_e	$\eta_{kon}, \eta_{koff}, \eta_{ke}$
6	$\dot{RC} = k_{on}(R_{tot} - RC)C_p - k_{off}RC$ $E = \frac{E_m RC^n}{RC_{50}^n+RC^n}$	C_p/E	$RC(0) = 0$	$R_{tot}, k_{on}, k_{off}, E_m,$ RC_{50}, n	$k_{on}, k_{off}, E_m,$ RC_{50}, n	$\eta_{kon}, \eta_{koff}, \eta_{Em},$ η_{RC50}, η_n
7	$\dot{RC} = k_{on}(R_{tot} - RC)C_p - k_{off}RC$ $\dot{E} = k_{in}(1 + k_eRC) - k_{out}E$	C_p/E	$RC(0) = 0$ $E(0) = k_{out}/k_{in}$	$R_{tot}, k_{on}, k_{off}, k_{in},$ k_{out}, k_e	$k_{on}, k_{off}, k_{in},$ k_{out}, k_e	$\eta_{kon}, \eta_{koff}, \eta_{kin},$ η_{kout}, η_{ke}
8	$\dot{RC} = k_{on}(R_{tot} - RC)C_p - k_{off}RC$ $\dot{E} = k_{in} - k_{out}(1 + k_eRC)E$	C_p/E	$RC(0) = 0$ $E(0) = k_{out}/k_{in}$	$R_{tot}, k_{on}, k_{off}, k_{in},$ k_{out}, k_e	$k_{on}, k_{off}, k_{in},$ k_{out}, k_e	$\eta_{kon}, \eta_{koff}, \eta_{kin},$ η_{kout}, η_{ke}
9	$\dot{C}_e = k_{e0} * (C_p - C_e)$ $E = k_e \frac{R_{tot}C_e}{K_d+C_e}$	C_p/E	$C_e(0) = 0$	$k_{e0}, R_{tot}, k_e, K_d$	k_{e0}, k_e, K_d	$\eta_{ke0}, \eta_{ke}, \eta_{Kd}$
10	$\dot{C}_e = k_{e0} * (C_p - C_e)$ $E = \frac{E_m(R_{tot}C_e)^n}{(K_d+C_e)^n RC_{50}^n+(R_{tot}C_e)^n}$	C_p/E	$C_e(0) = 0$	$k_{e0}, R_{tot}, E_m, K_d,$ RC_{50}, n	$k_{e0}, E_m, K_d,$ RC_{50}, n	$\eta_{ke0}, \eta_{Em}, \eta_{Kd},$ η_{RC50}, η_n
11	$\dot{C}_e = k_{e0} * (C_p - C_e)$ $\dot{E} = k_{in}(1 + k_e \frac{R_{tot}C_e}{K_d+C_e}) - k_{out}E$	C_p/E	$C_e(0) = 0$ $E(0) = k_{out}/k_{in}$	$k_{e0}, R_{tot}, k_{in}, K_d,$ k_{out}, k_e	$k_{e0}, k_{in}, K_d,$ k_{out}, k_e	$\eta_{ke0}, \eta_{kin}, \eta_{Kd},$ η_{kout}, η_{ke}
12	$\dot{C}_e = k_{e0} * (C_p - C_e)$ $\dot{E} = k_{in} - k_{out}(1 + k_e \frac{R_{tot}C_e}{K_d+C})E$	C_p/E	$C_e(0) = 0$ $E(0) = k_{out}/k_{in}$	$k_{e0}, R_{tot}, k_{in}, K_{,}d$ k_{out}, k_e	$k_{e0}, k_{in}, K_d,$ k_{out}, k_e	$\eta_{ke0}, \eta_{kin}, \eta_{Kd},$ η_{kout}, η_{ke}
13	$\dot{C}_e = k_{e0} * (C_p - C_e)$ $\dot{RC} = k_{on}(R_{tot} - RC)C_e - k_{off}RC$ $E = k_eRC$	C_p/E	$C_e(0) = 0$ $RC(0) = 0$	$k_{e0}, R_{tot}, k_{on}, k_{off}, k_e$	$k_{e0}, k_{on}, k_{off}, k_e$	$\eta_{ke0}, \eta_{kon}, \eta_{koff}, \eta_{ke}$
14	$\dot{C}_e = k_{e0} * (C_p - C_e)$ $\dot{RC} = k_{on}(R_{tot} - RC)C_e - k_{off}RC$ $E = \frac{E_m RC^n}{RC_{50}^n+RC^n}$	C_p/E	$C_e(0) = 0$ $RC(0) = 0$	$k_{e0}, R_{tot}, RC_{50}, k_{on}, k_{off},$ E_m, n	$k_{e0}, RC_{50}, k_{on}, k_{off},$ E_m, n	$\eta_{ke0}, \eta_{RC50}, \eta_{kon}, \eta_{koff},$ η_{Em}, η_n
15	$\dot{C}_e = k_{e0} * (C_p - C_e)$ $\dot{RC} = k_{on}(R_{tot} - RC)C_e - k_{off}RC$ $\dot{E} = k_{in}(1 + k_eRC) - k_{out}E$	C_p/E	$C_e(0) = 0$ $RC(0) = 0$ $E(0) = k_{out}/k_{in}$	$k_{e0}, R_{tot}, k_{on}, k_{off}, k_{in},$ k_{out}, k_e	$k_{e0}, k_{on}, k_{off}, k_{in},$ k_{out}, k_e	$\eta_{ke0}, \eta_{kon}, \eta_{koff}, \eta_{kin},$ η_{kout}, η_{ke}
16	$\dot{C}_e = k_{e0} * (C_p - C_e)$ $\dot{RC} = k_{on}(R_{tot} - RC)C_e - k_{off}RC$ $\dot{E} = k_{in} - k_{out}(1 + k_eRC)E$	C_p/E	$C_e(0) = 0$ $RC(0) = 0$ $E(0) = k_{out}/k_{in}$	$k_{e0}, R_{tot}, k_{on}, k_{off}, k_{in},$ k_{out}, k_e	$k_{e0}, k_{on}, k_{off}, k_{in},$ k_{out}, k_e	$\eta_{ke0}, \eta_{kon}, \eta_{koff}, \eta_{kin},$ η_{kout}, η_{ke}

N: Model number. I/O: Inputs/outputs. ICs: Initial conditions. [a]R_{tot} was fixed at 100. [b]Assuming a diagonal covariance matrix $\boldsymbol{\Omega}$ with lognormal random effects.

Both fixed-effects and mixed-effects versions of each model were analysed from a structural identifiability perspective, and the results are presented in Table 3.2. The results of the structural identifiability analysis showed that all of the fixed effects versions of the models were in their original parameterisation structurally unidentifiable. For all of the models, the source of the unidentifiability problem was the parameters R_{tot} and either RC_{50} (Models 2, 6, 10, 14) or k_e (remaining models) (see Table 3.2). The analysis showed that these parameters are unidentifiable and therefore any numerical estimates of them are effectively meaningless from a biological perspective. Furthermore, it was shown that even though R_{tot} and k_e or RC_{50} are unidentifiable, the product $R_{tot}k_e$ and fraction R_{tot}/RC_{50} are globally identifiable. The remaining parameters in the analysed models were all shown to be globally identifiable. Therefore, three methods may be applied to ensure structurally globally identifiable models: *1)* A reparameterisation of the model could be performed, e.g. defining a new parameter as $R_{tot}k_e$, representing the effect when all targets are bound, and R_{tot}/RC_{50}, representing the transducer ratio, to replace the unidentifiable parameters. *2)* R_{tot} or *3)* k_e and RC_{50} may be fixed to known or assumed numerical values. However, the latter two affects the units and interpretation of the non-fixed parameter. For example, R_{tot} may be fixed at 100 %, resulting in changed units for k_e to units per percent bound receptor.

For the mixed effects versions of the models, it is discussed in [92] that if the structural model is structurally globally identifiable, and if the statistical sub-model is structurally globally identifiable, then it follows that the mixed-effects model is also structurally globally identifiable. The statistical sub-model for the random effects considered in this paper takes the form of a structurally globally identifiable lognormal distribution. Therefore, the mixed-effects versions of the models in Table 3.1 are structurally globally identifiable following the suggested reparameterisation or by fixing of R_{tot} or k_e and RC_{50}.

3.2.2 Simulation study to investigate practical identifiability

Once the structural identifiability of the postulated model has been determined, parameter estimation can be performed. As with the structural identifiability example, Model 13 (Table 3.1) was selected for the simulation study to investigate the influence of varying data quality on the practical identifiability of the parameters. This model includes two different sources of delay, one from distribution to the effect site, where the rate is controlled by the parameter k_{e0}, and also through slow receptor dynamics, where the off-rate is controlled by the parameter k_{off}. The possibility to distinguish the two different delays in practice under varying data quality was investigated in a simulation study. R_{tot} was fixed to 1 following the results of the

Table 3.2 Results of the structural identifiability analysis of the mixed-effects models 1-16 in Table 3.1. Structurally identifiable and unidentifiable parameters and a suggested reparameterisation are provided for the corresponding fixed effects models. Random effects were evaluated for the reparameterised models Adapted from [2].

Model description		Structural identifiability results		
		Fixed effects		Random effects[a]
N	Distr. | Binding | Transd.	SU parameters	SI parameters & combinations	SI parameters
1	Direct | SS | Linear	R_{tot}, k_e	$R_{tot}k_e, K_d$	η_{ke}, η_{Kd}
2	Direct | SS | Sigmoid	R_{tot}, RC_{50}	$R_{tot}/RC_{50}, k_e, K_d, n$	$\eta_{RC50}, \eta_{ke}, \eta_{Kd}, \eta_n$
3	Direct | SS | Indirect	R_{tot}, k_e	$R_{tot}k_e, k_{in}, k_{out}, K_d$	$\eta_{kin}, \eta_{kout}, \eta_{ke}, \eta_{Kd}$
4	Direct | SS | Indirect	R_{tot}, k_e	$R_{tot}k_e, k_{in}, k_{out}, K_d$	$\eta_{kin}, \eta_{kout}, \eta_{ke}, \eta_{Kd}$
5	Direct | Dynamic | Linear	R_{tot}, k_e	$R_{tot}k_e, k_{on}, k_{off}$	$\eta_{Rtot/RC50}, \eta_{kon}, \eta_{koff}, \eta_{Em}$
6	Direct | Dynamic | Sigmoid	R_{tot}, RC_{50}	$R_{tot}/RC_{50}, k_{on}, k_{off}, E_m, n$	$\eta_{RC50}, \eta_{kon}, \eta_{koff}, \eta_{Em}, \eta_n$
7	Direct | Dynamic | Indirect	R_{tot}, k_e	$R_{tot}k_e, k_{on}, k_{off}, k_{in}, k_{out}$	$\eta_{kon}, \eta_{koff}, \eta_{kin}, \eta_{kout}, \eta_{ke}$
8	Direct | Dynamic | Indirect	R_{tot}, k_e	$R_{tot}k_e, k_{on}, k_{off}, k_{in}, k_{out}$	$\eta_{kon}, \eta_{koff}, \eta_{kin}, \eta_{kout}, \eta_{ke}$
9	Delay | SS | Linear	R_{tot}, k_e	$R_{tot}k_e, k_{e0}, K_d$	$\eta_{ke0}, \eta_{ke}, \eta_{Kd}$
10	Delay | SS | Sigmoid	R_{tot}, RC_{50}	$R_{tot}/RC_{50}, k_{e0}, k_{on}, k_{off}, E_m, n$	$\eta_{ke0}, \eta_{RC50}, \eta_{Em}, \eta_n, \eta_{Kd}$
11	Delay | SS | Indirect	R_{tot}, k_e	$R_{tot}k_e, k_{e0}, k_{in}, k_{out}, K_d$	$\eta_{ke0}, \eta_{kin}, \eta_{kout}, \eta_{ke}, \eta_{Kd}$
12	Delay | SS | Indirect	R_{tot}, k_e	$R_{tot}k_e, k_{e0}, k_{in}, k_{out}, K_d$	$\eta_{ke0}, \eta_{kin}, \eta_{kout}, \eta_{ke}, \eta_{Kd}$
13	Delay | Dynamic | Linear	R_{tot}, k_e	$R_{tot}k_e, k_{e0}, k_{on}, k_{off}$	$\eta_{ke0}, \eta_{kon}, \eta_{koff}, \eta_{ke}$
14	Delay | Dynamic | Sigmoid	R_{tot}, RC_{50}	$R_{tot}/RC_{50}, k_{e0}, k_{on}, k_{off}, k_{in}, E_m, n$	$\eta_{ke0}, \eta_{RC50}, \eta_{kon}, \eta_{koff}, \eta_{Em}, \eta_n$
15	Delay | Dynamic | Indirect	R_{tot}, k_e	$R_{tot}k_e, k_{e0}, k_{on}, k_{off}, k_{in}, k_{out}$	$\eta_{ke0}, \eta_{kon}, \eta_{koff}, \eta_{kin}, \eta_{kout}, \eta_{ke}$
16	Delay | Dynamic | Indirect	R_{tot}, k_e	$R_{tot}k_e, k_{e0}, k_{on}, k_{off}, k_{in}, k_{out}$	$\eta_{ke0}, \eta_{kon}, \eta_{koff}, \eta_{kin}, \eta_{kout}, \eta_{ke}$

SU: Structurally unidentifiable; SI: Structurally identifiable. [a] R_{tot} was fixed at 100 when analysing the mixed effects models.

structural identifiability analysis to ensure the structural identifiability of the model. True parameter values were assigned to each model parameter: $k_e = 1$, $k_{e0} = 0.2$, $k_{off} = 0.02$ and $k_{on} = 0.05$ amounts per minute. All parameters were assumed to vary between subjects following a log-normal distribution as this ensures positive rates for all subjects, with standard deviation $\sigma = 0.3$ to represent differences in a population. The model is summarised in Figure 3.4A.

The simulation study was performed in MATLAB 2013b (The MathWorks [93]) and Monolix 4.3.2 (Lixoft [40]) as outlined in Figure 3.4 B. 1) PK data were simulated without variability or noise, applying an intravenous bolus dose of 20 mg/kg to a hypothetical typical individual with volume of distribution 1 and rate of elimination 0.2 mg/kg. 2) Model 13 with the selected 'true' parameter values was used to simulate data sets of varying size and quality. Three factors were changed that influence the information available in the data: *i)* different sampling intervals $\Delta t = 1, 2, 5, 10, 15, 20, 25, 30$ minutes. *ii)* different additive noise levels $\sigma = 0.05, 0.15, 0.5$ response units and *iii)* different numbers of subjects $n = 100, 40, 12$. 3) Parameters were estimated using each simulated data set, with the following initial guess selected for the optimisation algorithm: $k_e = 1$, $k_{e0} = 0.1$, $k_{off} = 0.01$ and $k_{on} = 0.01$ units per minute for the structural parameters and 0.3 units per minute for the standard deviations. 4) The ratio between the final parameter estimates and the true parameter values were calculated and compared for the typical parameters to investigate the effects of varying sampling intervals, noise levels and number of subjects on parameter accuracy.

In the simulation study, increasing noise, increasing sampling interval and reducing the number of subjects all led to worse parameter estimation results (Figure 3.4). At the lowest noise level (column a), the model parameters were well estimated up to a sampling interval of $\Delta t = 10$, while increasing the sampling interval above this level led to over- and underestimation of k_e and k_{on} respectively. At the intermediate noise level (column b), similar results were obtained, although problems occured at smaller sampling intervals. At the highest noise level (column c), the parameter estimation was unsuccessful for all estimation runs except for 100 subjects and 1 min sampling interval. The simulation study shows a trend of decreasing accuracy to estimate the true parameters when the amount and quality of the data decreases. Some of the model parameters vary more than others when the data become worse in terms of noise levels, the number of measurements and the number of subjects. For instance, k_{off} was estimated reasonably well, except for the very worst case 3c, while the estimates for k_e and k_{on} are poor in 1a. It can also be seen that the uncertainty in the parameter estimates (standard errors) generally widens with either increased noise, reduced sampling interval or reduced number of number subjects. Interestingly, high precision (small standard errors) is in many

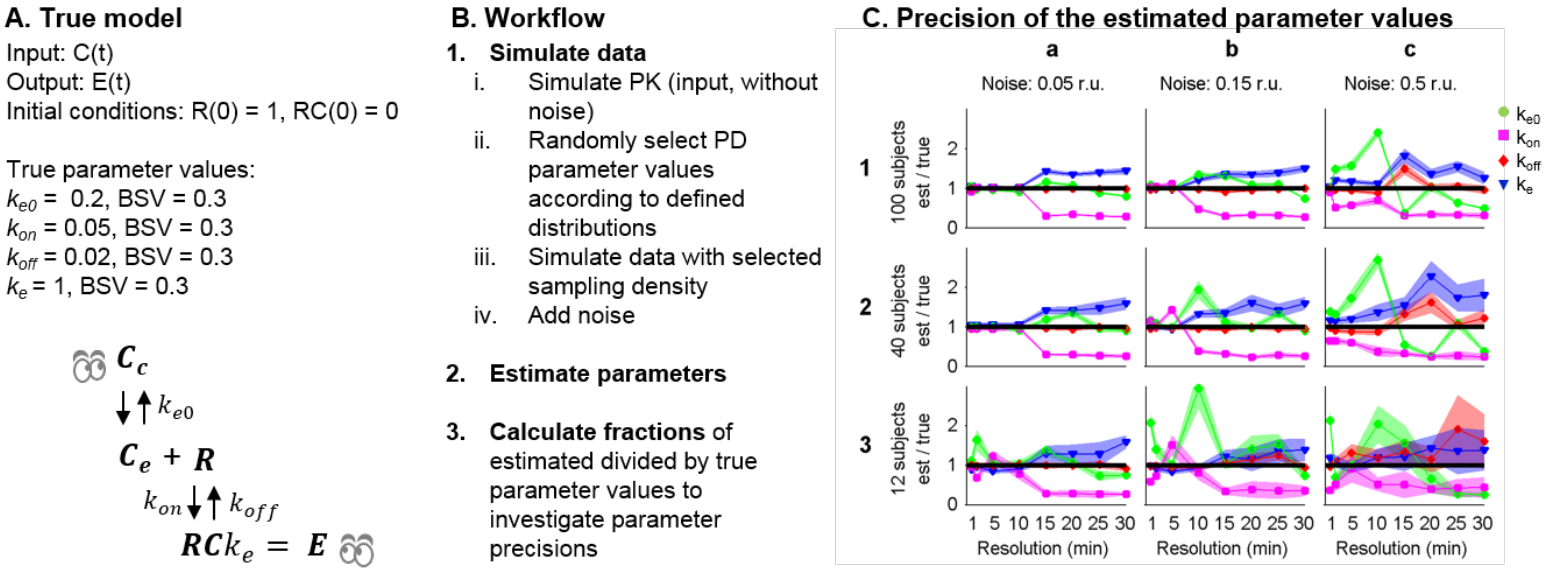

Figure 3.4 A. Model 13 and the selected true parameter values. BSV is between-subject variability. B. Workflow for the simulation study and C. Accuracy of the typical parameter estimates for the combined effect compartment/dynamic receptor model fitted to simulated data. The accuracy of each parameter (y-axis: estimated/true parameter value, line of unity marked by black line) and its uncertainty (normalised standard error, filled lighter area) is given at each data resolution level (x-axis: time between samples increasing from 1, 2, 5, 10, 15, 20, 25 to 30 minutes) for simulated data for 100, 40 and 12 subjects (row 1, 2, 3) adding additive noise with standard deviations 0.05, 0.15 and 0.5 response units (r.u, column a, b, c) respectively. Figure from [2].

optimisations acquired despite low accuracy in the parameter estimates.

3.2.3 Case study

A case study was conducted in order to exemplify the process of model development, including structural identifiability analysis. Side effects of potential new drugs on the heart must be evaluated by monitoring changes in the duration of specific intervals monitored in the electrocardiogram (ECG), such as the QT interval (defined by the Q and T peaks in the ECG) which corresponds to the duration of the ventricular action potential. The main part of the QT interval constitutes the ventricular repolarisation phase, corresponding to the JT interval (defined by the J point and T peak in the ECG), and prolongations are strongly linked to inhibition of the cardiac ion channel hERG [94]. In this example, model 10 (Table 3.1) was applied to link inhibition of the hERG ion channel *in vitro* to prolongation of the JT interval following treatment with the anti-arrhythmic compound and mixed ion channel blocker AZD1305, a proprietary AstraZeneca compound. Model 10 was selected since an identifiable version of this model has been used previously to fit this type of data [9] and following evaluation of additional structures, for example model 2 (without the effect compartment).

Methods. Clinical study and PK and QT interval data are described in [12]. JT intervals were calculated by subtracting QRS from QT. *In vitro* data were acquired from the original data collected by [95]. Methods for PKPD model development are detailed in Chapter 5. Baseline variability of JT intervals was minimised applying a circadian rhythm and RR correction model (Equation 5.5). The PK and PD were modelled sequentially, and Model 10 (Table 3.1) was selected to describe the drug effect. K_d was estimated prior to the PKPD modelling using the I_{max} model, where the inhibition in % is calculated according to

$$I(C) = 100 * C/(IC_{50} + C) \tag{3.2}$$

where IC_{50} corresponds to the drug concentration resulting in 50 % inhibition, substituting K_d in Model 10. Parameter estimations were performed using the stochastic approximation expectation maximisation (SAEM) algorithm as implemented in Monolix 4.3.2 (Lixoft) [40].

Results: The estimated IC_{50} of hERG was 0.37 ± 0.04 μM with between cell variability of 0.19 ± 0.09 μM (Figure 3.5). PK modelling results are described in Chapter 5. Fitting all parameters of the operational model led to high uncertainty and correlation between R_{tot} and RC_{50} (Table 3.3). Structural identifiability analysis of this model showed that only the fraction R_{tot}/RC_{50} is identifiable (see Table 3.2)

and the model was therefore reparameterised with $\tau = R_{tot}/RC_{50}$, resulting in a structurally identifiable model. Estimation of the reduced model resulted in similar parameter values for all of the identifiable parameters, similar goodness of fit values and residuals and good precision in the population estimate of τ (Table 3.3). The fits to the AZD1305 concentration and JT interval data can be seen in Figure 3.6.

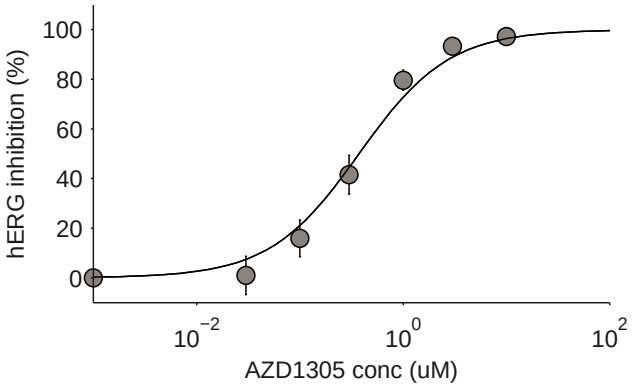

Figure 3.5 hERG inhibition data (markers) and model fit (lines) for AZD1305.

Table 3.3 Estimated parameter values for the original and re-parameterised Model 10 fitted to AZD1305 PK-hERG-JT interval data.

		Unidentifiable model		Identifiable model	
Parameter	Unit	Estimate (SE)	BSV % (SE)	Estimate (SE)	BSV % (SE)
E_m	ms	172 (23.9)	18.7 (9.09)	162 (18.9)	20.6 (7.67)
RC_{50}	μM	0.753 (173)	13.3 (15300)	-	-
n		2.02 (0.24)	35.1 (7.5)	2.1 (0.219)	36.4 (7.69)
R_{tot}	μM	1.1 (252)	13.2 (15400)	-	-
τ		-	-	1.55 (0.163)	15.2 (8.17)
IC_{50}	μM	0.37 (fixed)	0.19 (fixed)	0.37 (fixed)	0.19 (fixed)
k_{e0}	h^{-1}	9.37 (2.96)	125 (24)	9.42 (2.91)	123 (23.4)
Residuals	ms	6.64 (0.155)	-	6.64 (0.155)	-
-2LL		7662		7670	

SE, standard error; BSV, between-subject variability; -2LL, -2 LogLikelihood. Adapted from [2].

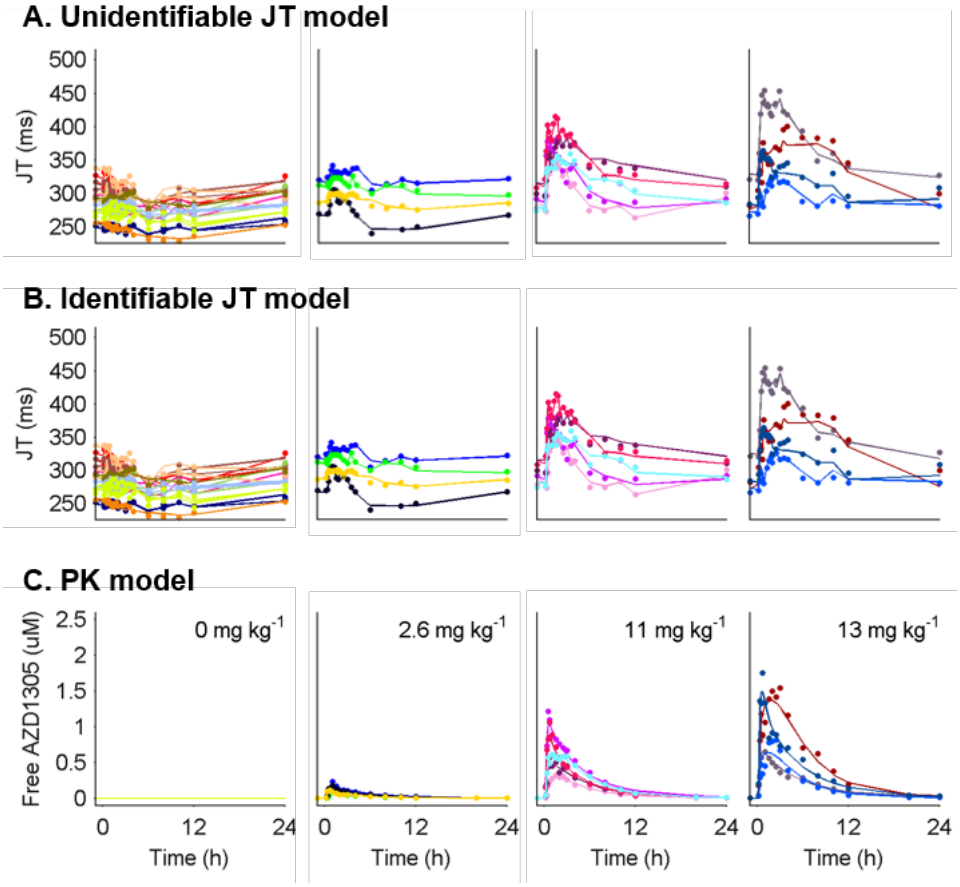

Figure 3.6 PK and JT interval data (markers) and model predictions (lines) for humans treated with placebo and 3 selected doses of AZD1305. A. Model predictions by the unidentifiable JT model. B. Model predictions by the identifiable JT model. C. Individual PK model parameters predicting the PK in each subject were used to drive the PD response. Individual subjects are separated by colour. Figure from [2].

Discussion: Both the full and reparametererised versions of model 10 described the data well. However, standard errors and correlations of R_{tot} and RC_{50} correctly indicated identifiability issues with the former. The estimated parameters were converted to the traditional E_{max} and EC_{50} parameters, which describe the maximal effect and the drug concentration at half-maximum effect respectively. E_{max} and EC_{50} were calculated according to

$$E_{max} = \frac{E_m \tau^n}{1 + \tau^n} \tag{3.3}$$

$$EC_{50} = \frac{IC_{50}}{(2 + \tau^n)^{1/n} - 1} \tag{3.4}$$

and resulted in an estimated E_{max} of 117 ms and 116 ms and EC_{50} of 0.36 and 0.35 μM respectively for the full and reparameterised models. This highlights that identifiable parts of a structurally unidentifiable model are still informative. The estimated E_{max} is similar to that in previous hERG-QT modelling of dofetilide

[9], while the estimated hERG block at 10 ms JT prolongation was slightly higher (18% vs. 9%). This may be caused by AZD1305-induced calcium block [95], as the calcium current depolarises the cardiac cells [47], counter-acting the repolarisation by hERG. The structural identifiability analysis showed that two model parameters could not be estimated. This led to model reduction. Performing this analysis prior to parameter estimation ensures the theoretical possibility of estimating all parameters in the model. Estimating the parameters of the unidentifiable model could have been avoided, reducing the number of iterations in the optimisation. Also, ensuring structural identifiability improves confidence in the biological interpretation of the estimated parameter values.

3.3 Discussion

Unidentifiability issues can cause many different types of problems if not mitigated when models are used to quantify, predict and understand the effects of potential drugs. Most importantly, the biological/physiological interpretations of structurally or practically unidentifiable parameters are not valid. This may lead to wrong conclusions, for example when unknowingly comparing unidentifiable parameters to rate candidate drugs or for comparison with competitors. Also, any predictions based on the profiles of unmeasured states of the system may be meaningless if the parameters directly or indirectly related to those states are unidentifiable. For example, if the effect of interest in a toxicity or efficacy study depends on the concentration in a compartment for which the profile is linked to structurally unidentifiable parameters, it may be impossible to separate the distribution to this compartment and the drug effect. Unidentifiability issues may also cause technical problems, as the parameter estimation step may take a very long time, or fail (crash), if a structurally unidentifiable model is used (depending on what form of optimisation routine is used).

The investigated models (Table 3.1) have been used successfully and repeatedly in practice [96, 97], and the structural identifiability results confirm the general assumption that these models are structurally identifiable. This provides confidence in the theoretical soundness of using these models. For all of the investigated models, the total amount of receptor in the system was fixed (to e.g. 1 or 100%) in order to achieve structural identifiability. This implies that some parameters for the 'signal transduction' are relative. For example, the units of a proportional signal transduction are effect units per fraction bound/inhibited receptor if R_{tot} is fixed to 1. This analysis shows that given sufficient data quality, it is, in theory, possible to distinguish between different sources of delay from the data. Thus, it is possible to differentiate delays that are compound-specific (e.g. distribution, drug-receptor binding kinetics) from delays that are system-specific (e.g. turnover of receptors) to

compare compounds and simulate untested systems.

3.4 Summary

Parameter identifiability should be investigated to ensure both structural and practical identifiability. Concerning structural identifiability, this chapter shows that

- Different initial estimates of the model parameters may lead to different estimates of structurally unidentifiable parameters.
- Large standard errors may indicate that a parameter is structurally (or practically) unidentifiable but **unidentifiable parameters may also appear well-determined**.
- Reparameterising the structurally unidentifiable model to become identifiable leads to similar residuals (and likelihood) and improved parameter precision of the new parameter(s).
- Identifiable parameters can still be well-determined when other parameters are unidentifiable.

A structurally identifiable model is only a prerequisite for successful parameter estimation, and the model parameters may still be difficult to estimate using experimental data. Some considerations for practical identifiability discussed in this chapter were that

- A structurally identifiable model does not guarantee reliable parameter estimates.
- Data must contain information over relevant time scales for the investigated system.
- Noise levels, sampling density and the number of subjects (mixed-effects models) are all important in order to be able to estimate parameters with reasonably high precision.

Chapter 4

Investigated compounds and acquired data

4.1 Introduction

The work in this thesis is based on data acquired from previous in-house or outsourced AstraZeneca studies and collected from published studies. These data were used for the quantitative and translational analyses in Chapters 5-7. The selection of nonclinical assays to investigate was based on previous experience at AstraZeneca, and the availability of in-house data. The primary assays that are conducted to assess cardiac conduction liabilities at AstraZeneca were therefore investigated. These include both *in vitro* and *in vivo* assays. *In vitro* screens of the Nav1.5 and Cav1.2 ion channels were included, and provide early information on the activity of the compound towards the major channels involved in cardiac conduction. The primary *in vivo* models used at AstraZeneca to assess CV safety and ECG effects are the anaesthetised guinea pig and consious dog models. Data from these assays were collected where available for all investigated compounds. Clinical data include in-house Phase I and literature data.

4.2 Investigated compounds

A total of six compounds were investigated in this thesis, and the types of data collected for each compound is summarised in Figure 4.1. Three compounds were proprietary small molecules: AZD1305 [98], AZD8683 [99] and AZD9164 [100]. AZD1305 is an anti-arrhythmic compound previously in development for the treatment of atrial fibrillations, where the development was discontinued due to safety concerns regarding QTc prolongations and TdP risk [101]. AZD1305 is known to have effects on multiple ion channels *in vitro*, including hERG, hNav1.5 and rCav1.2, resulting in prolongations of QTc, QRS and PR observed in dogs and humans.

AZD8683 and AZD9164 are anti-muscarinic compounds which selectively block the human muscarinic acetylcholine receptor 3 (M3 receptor). These anti-muscarinics are the result of a collaboration between AstraZeneca and Pulmagen Therapeutics Limited (formerly Argenta Discovery Limited). AZD8683 and AZD9164 were previously in development for the treatment of chronic obstructive pulmonary disease (COPD), but have been discontinued from development due to unfavourable safety or efficacy (AZD8683) and transient drop in respiratory function in patients (AZD9164). Nonclinical side effects of AZD8683 and AZD9164 indlude effects on rCav1.2 and hCav1.2 *in vitro* resulting in PR prolongations observed in beagle dogs. AZD1305 was manufactured by AstraZeneca, Mölndal, Sweden and AZD8683 and AZD9164 by AstraZeneca, Charnwood, UK.

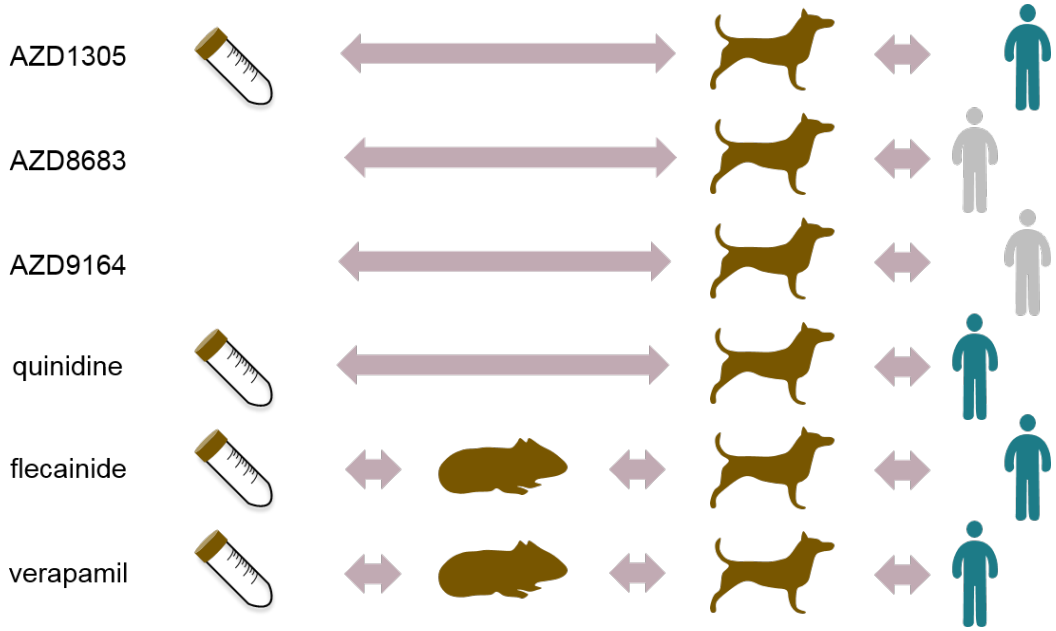

Figure 4.1 Summary of the collected nonclinical and clinical data. *In vitro* data were collected for four compounds, guinea pig data for 2 compounds and dog and human data for all compounds, although only four compounds caused quantifiable changes of QRS or PR in humans (AZD1305, flecainide, quinidine and verapamil).

In addition, three anti-arrhythmic compounds were investigated (flecainide, quinidine and verapamil). Quinidine and flecainide are class 1a and 1c anti-arrhythmics which block hERG, hNav1.5 and to a lesser extent hCav1.2 and bind to rCav1.2 *in vitro*. Both compounds cause QRS widening and QTc prolongation and flecainide also causes PR prolongation. QT prolongation in beagle dogs induced by quinidine has previously been quantified using PKPD modelling [102]. Verapamil is a class 4 anti-arrhythmic which blocks hCav1.2, hERG and hNav1.5 *in vitro* and causes PR prolongation.

4.3 Nonclinical data

This section presents the collected nonclinical data from *in vitro* and *in vivo* studies. These data were acquired from previous AstraZeneca studies including *in vitro* Nav1.5 and Cav1.2 assays and *in vivo* guinea pig and dog assays. These are routine assays at AstraZeneca, conducted at different stages of pre-clinical discovery and development to assess and mitigate the cardiovascular safety of potential new drugs.

4.3.1 *In vitro* ion channel assays

In vitro ion channel assay data provide early information on the risk of cardiac conduction liabilities.

4.3.1.1 Inhibition of hNav1.5

Compound interactions with the Nav1.5 channel had been assessed in cells transfected with human Nav1.5 (hNav1.5) using conventional and automated electrophysiology (Table 4.1). IC_{50} values of the two assays show high correlation [103], and to choose which data to use, the consistency of the assay setup between the evaluated compounds was therefore investigated. The automated electrophysiology IonWorks assay was evaluated consistently at physiological pacing rates for all compounds. However, the conventional electrophysiology assay was performed at different (non-physiological) pacing rates for AZD1305 compared to the remaining compounds. Therefore, the effect parameters (IC_{50}, γ) from the automated assay were chosen to simulate *in vitro* Nav1.5 effects.

Table 4.1 Potency of the investigated compounds to inhibit human Nav1.5 in automated and conventional functional electrophysiology assays. Data generated in-house at AstraZeneca, Alderley Park, UK.

	IonWorks HT[a]		**Conventional**	
Compound	IC_{50} **(μM)**	**Pacing rate**	IC_{50} **(μM)**	**Pacing rate**
AZD1305	34.6	3 Hz	6.4, 1.5[b]	0.2, 10 Hz
AZD8683	>33, >33, 23	3 Hz		
AZD9164	>33	3 Hz		
Flecainide	5.8 (5.7-5.84)	3 Hz	5.5 (4.3-7.0)[a]	3 Hz
Quinidine	8.7 (6.7-11.4)	3 Hz	10.4 (8.3-12.9)[a]	3 Hz
Verapamil	8.9 (7.0-11.3)	3 Hz	4.8 (3.8-6.1)[a]	3 Hz

hNav1.5, human Nav1.5 ion channel; IC_{50}, concentration at half-maximum effect. [a][103]. [b][95].

4.3.1.2 Binding to rCav1.2

Compound interactions with Cav1.2 were studied with automated electrophysiology and radioligand binding to the diltiazem, verapamil and nifedipine sites (Table 4.2). Radioligand binding to the diltiazem site of rat Cav1.2 is the most predictive of contractility in canine myocytes *in vitro* compared to radioligand binding at the verapamil and nifedipine sites and conventional and automated functional hCav1.2 electrophysiology [54]. It is not known why the radioligand binding assay outperformes the functional assay, and as discussed in [54], the converse might be expected to be true. For example, the radioligand assay was performed using rat *brain* Cav1.2 while the functional assay was performed using using human cardiac Cav1.2. Also, a functional assay should theoretically detect the effects from binding to any binding site, while the binding assay is directed at a specific site. All assays were initially explored, however, the estimated parameter for the binding to the diltiazem site (K_i) was chosen to simulate *in vitro* Cav1.2 effects.

Table 4.2 Potency of the investigated compounds to inhibit human Cav1.2 and to bind to three rat Cav1.2 binding sites.

	IonWorks HT	**Radioligand binding**		
	Human Cav1.2	**Rat Cav1.2**		
Compound	IC_{50} **(**μ**M)**	**Verapamil site** K_i **(**μ**M)**	**Nifedipine site** K_i **(**μ**M)**	**Diltiazem site** K_i **(**μ**M)**
AZD1305	>100	39.9	Not active	4.5
AZD8683	1.1			
AZD9164	5.8			
Flecainide	18, >33	14.9	Not active	1.39
Quinidine	>33, 57	5.64	Not active	8.41
Verapamil	2.9 (2.7-3.2)	0.0574	3.63	0.0441

IC_{50}, concentration at half-maximum effect; K_i, dissociation constant. Electrophysiology data were generated in-house at AstraZeneca, Alderley Park, UK and radioligand binding data outsourced to Cerep, France and these have been previously published [54].

4.3.2 *In vivo* guinea pig studies

The anaesthetised guinea pig model is routinely used at AstraZeneca as it provides informative data of CV effects in a complete system [23]. Also, this model may be conducted at the lead generation and optimisation stages, where this information can be utilised for compound selection.

Exposure and telemetry data from anaesthetised guinea pig studies were available for flecainide and verapamil only. Details of the experimental setup for

the guinea pig studies are described in [23]. Exposure and CV biomarkers were investigated in sodium pentobarbitone anaesthetised male guinea pigs using a parallel study design with four animals in each treatment and vehicle group. Baseline variability was minimised by controlled body temperature and respiratory rate. Lead II ECGs were monitored continuously by needle electrodes during a 20 minute stabilisation period followed by an intravenous infusion of three 15-minute ascending doses and a 30-minute washout period. CV measurements were extracted as mean values over 1 minute and exposure collected at 10 time points each. All animal care and experimental procedures had local ethics committee approval and conformed to the UK Animals (Scientific Procedures) Act, 1986. Doses and study designs are summarised in Table 4.3. Example data are provided in Figure 4.2. The three infusion phases are clearly visible in the PK data, while some delays and nonlinearities may be present in the QRS/PR data.

Table 4.3 Summary of the guinea pig studies. Details are found in [23].

Compound	**Flecainide**	**Verapamil**
Animals	Anaesthetised guinea pigs	Anaesthetised guinea pigs
Design	Parallel	Parallel
Dosing	Multiple ascending dose	Multiple ascending dose
n	4 vehicle + 4 treat	4 vehicle + 4 treat
Dose (mg kg^{-1})	iv: 0, 0.3, 1, 3	iv: 0, 0.1, 0.3, 1

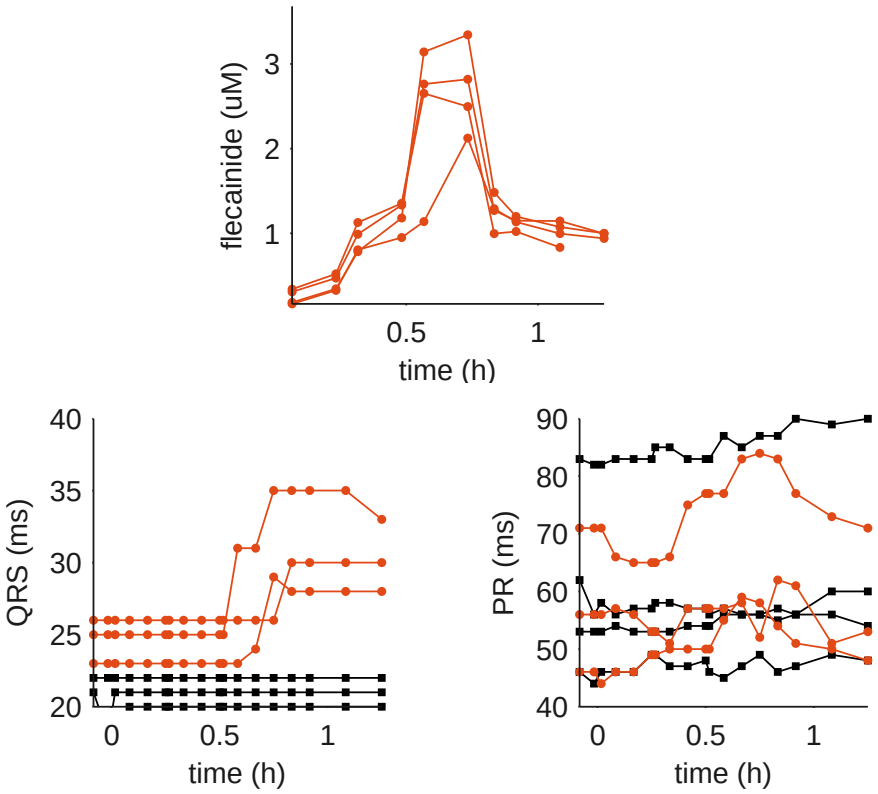

Figure 4.2 Exposure, QRS and PR data following intravenous infusion with three escalating doses of flecainide (orange) and vehicle (black). Exposure, QRS and PR data in individual guinea pigs are provided.

4.3.3 *In vivo* dog studies

A more in-depth analysis of the therapeutic dose range and safety of a compound is required prior to human testing. At AstraZeneca, a conscious beagle dog model is used to assess CV safety (primarily QTc, but also QRS, PR and haemodynamics).

4.3.3.1 Experimental animals and procedures

In vivo studies were carried out in-house at AstraZeneca sites in the UK or Sweden, or out-sourced to Huntingdon Life Sciences Ltd, UK (AZD9164 study). All studies had local ethics committee approval and UK studies were carried out in agreement with the UK Animals (Scientific Procedures) Act 1986. Study designs, experimental procedures and doses are summarised in Table 4.4. Doses were selected based on expected C_{max} at multiples close to and above human therapeutic dose. Human therapeutic routes of administration were used, and effects of AZD1305, flecainide, quinidine and verapamil were therefore orally administered while AZD8683 and AZD9164 were administered through inhalation. Animals were housed individually in pens of at least 2 m^2 during recording days and feeding and in groups of four

or less in larger pens at other times. The pen temperature was kept within 20±5°C. 10/14 hour light/dark cycles were kept in the AZD9164 PK study, and 12/12 hour cycles in all other studies. Dry pellet was offered in the afternoon and consumption recorded after two hours. Water was provided ad libitum and toys offered for environmental enrichment. Example data are provided in Figure 4.3. Three escalating doses were given, the first two by intravenous (iv) infusion and the third by oral administration. Effects are visible in both QRS and PR intervals despite clear between- and within-subject variability.

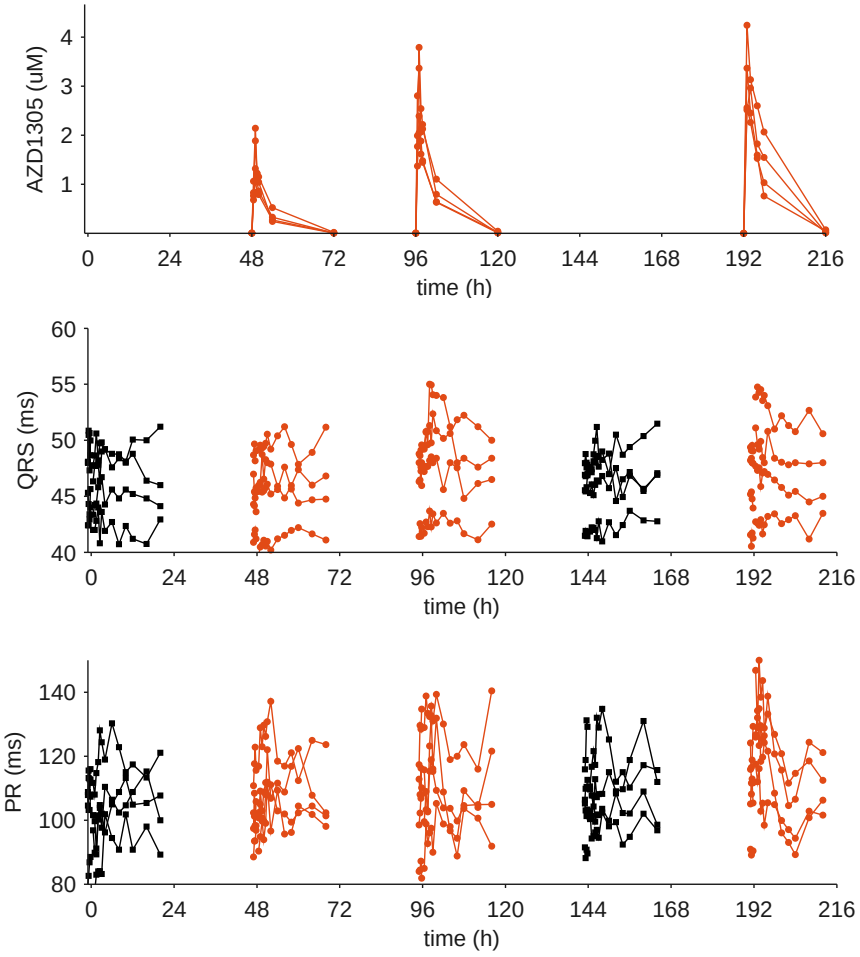

Figure 4.3 Exposure, QRS and PR data following intravenous infusion with vehicle (black) and 2.15 and 4.3 mg kg^{-1} AZD1305 (orange) followed by oral administration of vehicle (black) and 8.7 mg kg^{-1} AZD1305 (orange). Exposure, QRS and PR data in individual dogs are provided. Dots joined by a line represent data from the same animal.

4.3.3.2 Cardiovascular measurements

Cardiac effects were monitored using surgically implanted telemetry devices (DSI® PhysioTel) implanted as previously described [104]. Recordings took place through

Table 4.4 Design of the nonclinical conscious dog studies.

Compound	AZD1305	AZD8683	AZD9164	AZD9164 PK	Flecainide	Quinidine	Verapamil
Design	Cross-over	Cross-over	Cross-over	Parallel	Cross-over		Cross-over
n	4 m	4 m	3 m, 3 f	4 m, 4 f	4 m		4 m
Age (months)	22-31	24-38	Appr. 12-24	9.0-16	19-20		19-25
Weight (kg)	11.2-15	13.9-17.5	10.4-17.1	11.3-17.7	11.2-12.0		14.5-18.3
Dose (mg kg^{-1})	iv: 0, 2.15, 4.3; oral: 0, 8.7	0, 0.02, 0.1, 0.25	0, 0.019, 0.092, 0.22	0, 0.02, 0.1, 0.48	0, 3, 10, 20	0, 10, 25, 50[a]	0, 1, 5, 15
Dose interval	2-5 days	3-4 days	> 5 days	Daily for 7 days	2-5 days	2-5 days	2-5 days
Time of dosing	09:00-09:45	11:00-13:00	Not reported	08:00-14:00	09:30	09:30	09:00
Route	Oral (gavage), iv inf (1 h)	Inh (∼10 min)	Inh (2.5 min)	Inh (4-6 min)	Oral (tablets)	Oral (gavage)	Oral (gavage)
LLQ (nM)	0.2	0.1	0.05	0.1	25	15	2.2
PK sampling	iv: pre-dose, 0.5, 1, 1.5, 2, 6, 24; oral: pre-dose, 1, 2, 4, 6, 24 h	pre-dose, 0, 0.33, 0.67, 2, 4, 8, 24 h a.c.d	pre-dose, a.c.d	pre-dose, 0, 0.33, 0.67, 2, 4, 8, 24 h a.c.d	pre-dose, 1, 2, 4, 24 h	pre-dose, 1, 2, 4, 24 h	pre-dose, 1, 2, 6 and 24 h
ECG sampling	-1, -0.75, -0.5, -0.25, 0.5:0.5:3, 4, 6, 8, 10, 12, 16, 20 h	-0.5[b] h, 5, 20, 40 min, 1:4, 6, 8, 12, 16, 20, 24 h	-70:5:-40, -15, -10, -5, 1:10, 15, 30 min, 1, 2, 3, 5, 8, 12 h	Not collected	-1, -0.75, -0.5, -0.25, 0.5:0.5:3, 4, 6, 8, 10, 12, 16, 20 h	-1[b], 0.5:0.5:3, 4, 6, 8, 10, 12, 16, 20 h	-1, -0.75, -0.5, -0.25, 0.5:0.5:3, 4, 6, 8, 10, 12, 16, 20 h
ECG filtering	Mean of 5 ECG complexes	Mean of 20-60 s	Mean of 1 min	-	Mean of 5 ECG complexes	Mean of 5 ECG complexes	Mean of 5 ECG complexes

Inh, inhalation; iv inf, intravenous infusion.

receivers in telemetry pens and on telemetry tables for the inhalation studies for at least 1h pre-dose to 20-24h post-dose. Inside the telemetry pens, animals were allowed to move freely at all times except during dosing and blood sampling. ECG intervals were acquired and analysed via "Po-Ne-Mah" V4.1 and/or EMKA "ECG Auto" V2.4.0.30 (AZD9164) or the HEM data acquisition system (Notocord Inc.) using Dataquest Open ART software for the telemetry set up and calibration (remaining studies). Lead II ECG (e.g. PR, RR, QRS and QT), body temperature, arterial blood pressure and heart rate (HR) were recorded. PQ intervals were recorded in the AZD8683 study. Automatically marked ECG intervals were manually inspected and corrected at reported time points followed by averaging as indicated in Table 4.4. Intravenous infusion PK data from the AZD1305 study and PK-QRS data from the flecainide/quinidine study have been published elsewhere [12, 22].

4.3.3.3 Bioanalysis

Drug concentrations were measured from 0.5-2 mL blood plasma acquired from the jugular vein. The blood samples were mixed with anticoagulant, centrifuged and blood plasma separated and frozen for storage. Drug concentrations were then quantified with liquid chromatography and tandem mass spectroscopy (LC-MS/MS). Due to sparse sampling in the AZD9164 study, a separate inhalation PK study with similar doses was used to characterise drug disposition and elimination. For all other compounds, PK and PD measurements were taken within the same study.

4.3.3.4 Excluded data

In the PK model development of the verapamil data, all PK data from the 15 mg kg^{-1} dose in dog 2 were excluded. Clear dose-dependent effects in the PD data suggested correct dosing, whilst PK data were approximately tenfold lower than expected considering the exposure in dog 2 following the lower doses as well as following all doses in dogs 1, 3 and 4. Simulated PK data for this dose were used in the PD modelling.

4.4 Clinical data

As AZD8683 and AZD9164 did not cause QRS or PR prolongations in human volunteers, these studies are not presented in this thesis.

4.4.1 Phase I AZD1305 study

A detailed protocol of the clinical phase I AZD1305 study is available in a previous publication of the PK and ECG (QTcF) data from this study [12]. Briefly, 29 healthy male volunteers participated in this randomised, double-blinded and

placebo-controlled study. The study was performed in accordance with the ethical principles of the Declaration of Helsinki and are consistent with the International Conference on Harmonisation (ICH)/Good Clinical Practice. 12-lead standard ECGs were recorded in the supine position (Cardiovit AT-5 recorders, Schiller AG, Baar, Switzerland) and data from Lead II were used in the analysis. Placebo and six oral doses (10-500 mg) and two iv doses (10 and 70 mg) were administered in a scaling dose study design where each subject received two separate doses of placebo or AZD1305. Plasma samples were taken pre-dose and at 14 time points. Lead II ECGs were monitored continuously and extracted at baseline and at 18 specific time points within 24 hours following dose administration. Data are shown in Figures 4.4-4.6.

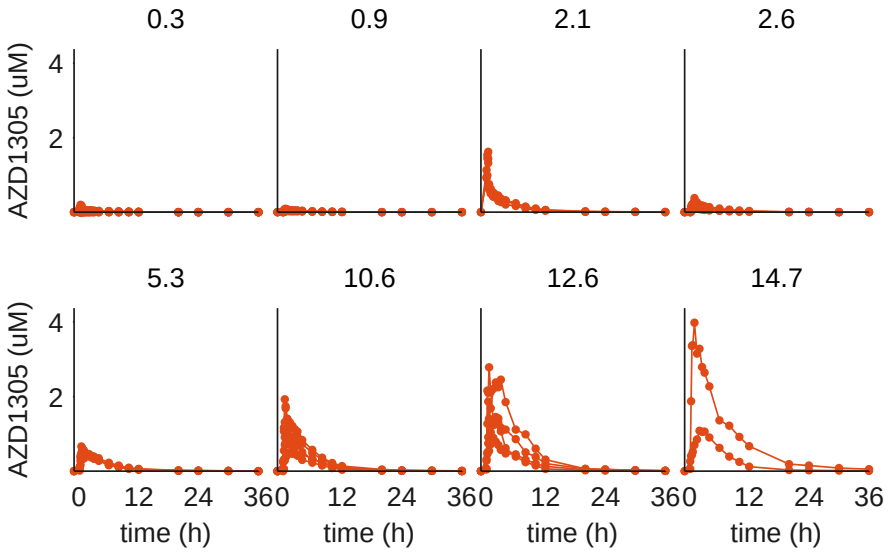

Figure 4.4 Exposure data following intravenous infusion with 10 mg (0.3 mg kg^{-1}) or 70 mg (2.1 mg kg^{-1}) or oral administration of 0.3-14.7 mg kg^{-1} (10-500 mg) AZD1305. Exposure data in individual subjects are provided.

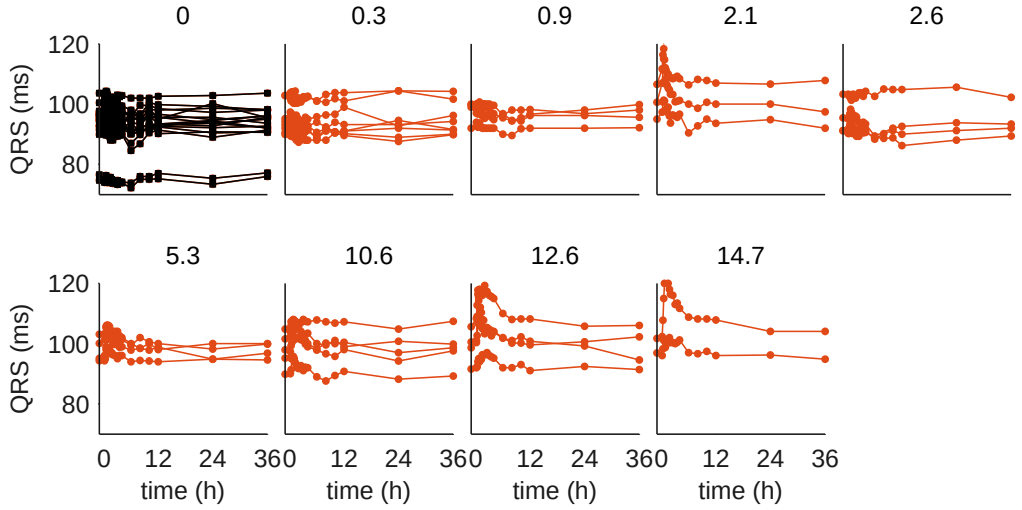

Figure 4.5 QRS data following placebo (black) and intravenous infusion with 10 mg (0.3 mg kg^{-1}) or 70 mg (2.1 mg kg^{-1}) or oral administration of 0.3-14.7 mg kg^{-1} (10-500 mg) AZD1305 (orange). QRS data in individual subjects are provided.

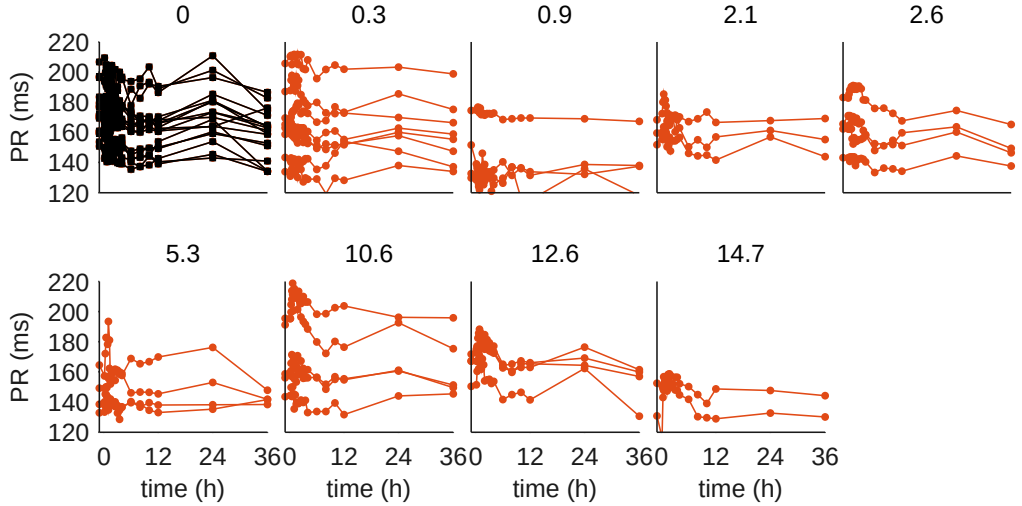

Figure 4.6 PR data following placebo (black) and intravenous infusion with 10 mg (0.3 mg kg^{-1}) or 70 mg (2.1 mg kg^{-1}) or oral administration of 0.3-14.7 mg kg^{-1} (10-500 mg) AZD1305 (orange). PR data in individual subjects are provided.

4.4.2 Literature survey of flecainide, quinidine and verapamil effects

Published studies reporting plasma drug concentrations and associated QRS and/or PR measurements were identified for each compound in separate PUBMED searches. These are described in Chapter 6.

4.4.2.1 Methods for the literature survey

The literature survey was performed in PUBMED using the following search words:

- "drug name" AND (ECG OR electrophysiology OR electrophysiologic OR interval) AND (QRS OR PR OR PQ OR P-R OR P-Q) AND (Humans[Mesh])
- quinidine AND ECG AND (healthy OR volunteer) AND (Humans[Mesh])

Inclusion criteria for the identified publications were the following:

- Study of more than 2 humans (not case studies).
- Plasma concentrations were measured and reported in textual format, tables or figures.
- QRS and/or PR/PQ intervals were measured at sinus rhythm and reported in textual format, tables or figures including change from baseline and/or pre- and post-drug.
- The same type of PK and ECG data were reported. For example, both PK and ECG were maximum values, both were mean values over the treatment time or both were measured at similar time points.

Pairs of plasma concentrations and absolute QRS/PR change from baseline of the same type (e.g. maximum values, mean values or measured at similar time points) were collected or calculated using information published directly in the text, tables and/or figures. Data provided only in figures were converted to numbers through visual assessment or using webplotdigitizer (http://arohatgi.info/WebPlotDigitizer). Average baseline QRS/PR in healthy volunteers were calculated and used to convert the percentage change to absolute change where baselines were not provided. Drug concentrations were converted to free concentrations in μM using in-house *in vitro* plasma protein binding data and the molar mass of each compound. Additional information was collected where available, and included the standard deviations of the concentration and QRS/PR data, time since last dose, the number of subjects, the dose administered, route of administration, dosing history and if the subjects were healthy volunteers or patients.

4.4.2.2 Identified flecainide QRS/PR studies

A Pubmed search was performed on 2015-08-06 and generated a total of 143 published studies of QRS and/or PR effects of flecainide in humans, of which 16 fulfilled the postulated criteria (see Section 4.4.2.1). These are summarised in Table 4.5 and in more detail in Appendix B, Table B.1 and the data are plotted in Figures 4.8 and 4.7.

Table 4.5 Summary of the identified human flecainide studies.

Ref	ECG	Dose	Subjects		Dosing		Data type		
			n	Status	History	Route	PK	ECG	n
[105]	QRS	100-200 mg	24	HV	Both	oral	Mean C_{max}	Mean E_{max}	8
[106]	PR	200 mg	8	HV	Acute	oral	Mean C_{max}	Max E_{mean}	1
[107]	QRS	2 mg/kg	10/12	Both	Acute	iv inf	$C(t)/C_{max}$	$E(t)$	2
[108]	QRS/PR	150 mg	10	HV	Acute	iv inf	$C(t)$	$E(t)$	1
[109]	QRS/PR	2 mg/kg	6	HV	Acute	iv inf	$C(t)$	$E(t)$	1
[110]	QRS/PR	100-200 mg	12	HV	Chronic	oral	Mean C	Mean E	2
[111]	QRS	300 mg	27	Patients	Acute	oral	Fitted C_{max}	E_{reg}	1
[112]	QRS/PR	200-300 mg	13	Patients	Both	oral	Mean C_{max}	Mean E_{max}	2
[113]	QRS/PR	2 mg/kg	93	Patients	Acute	iv inf	$C(t)$	$E(t)$	1
[114]	QRS/PR	2 mg/kg	10	Patients	Acute	iv inf	$C(t)$	$E(t)$	1
[115]	QRS	1.5 mg/kg	11	Patients	Acute	iv inf	$C(t)$	$E(t)$	1
[116]	QRS	2 mg/kg	47	Patients	Acute	iv inf	$C(t)$	$E(t)$	1
[117]	QRS	100-300 mg	9	Patients	Chronic	oral	C_{max}	E_{reg}	1
[118]	QRS	200-400 mg	18	Patients	Chronic	oral	C_{trough}	$E(t)$	1
[119]	QRS/PR	200-600 mg	19	Patients	Chronic	oral	$C(t)$	$E(t)$	2
[120]	QRS/PQ	400 mg	14	Patients	Chronic	oral	$C(t)$	$E(t)$	2

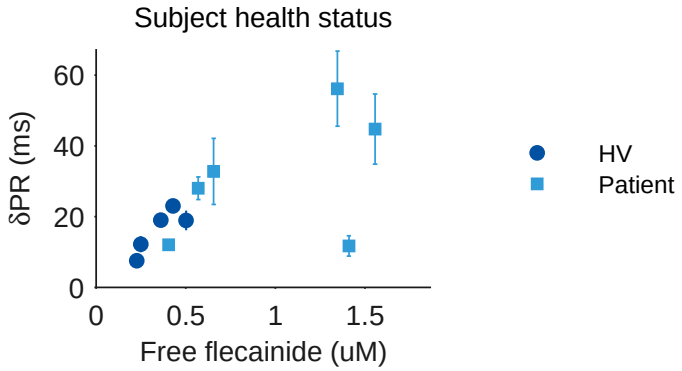

Figure 4.7 PR prolongations in healthy volunteers (HV, circles) and patients (squares) induced by flecainide. Data points represent associated plasma concentration-δPR pairs (1-2 per published study) with standard errors where available.

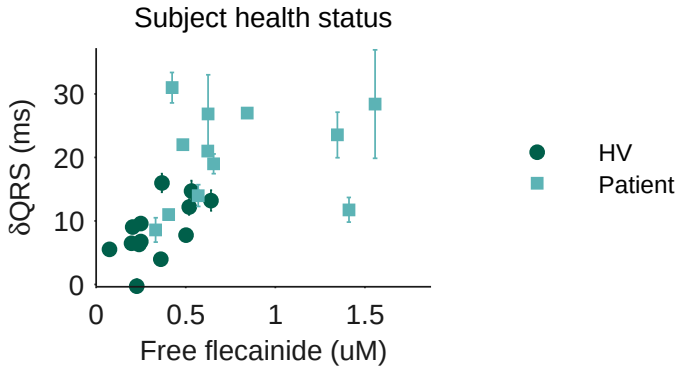

Figure 4.8 QRS widening in healthy volunteers (HV, circles) and patients (squares) induced by flecainide. Data points represent associated plasma concentration-δQRS pairs (1-8 per published study) with standard errors where available.

4.4.2.3 Identified quinidine QRS studies

A Pubmed search was performed on 2015-08-06 and generated a total of 93 published studies of QRS effects of quinidine in humans, of which 15 fulfilled the postulated criteria (see Section 4.4.2.1). These are summarised in Table 4.6 and in more detail in Appendix B, Table B.1 and the data are plotted in Figure 4.9.

Table 4.6 Summary of the identified human quinidine studies.

Ref	ECG	Dose	Subjects		Dosing		Data type		
			n	Status	History	Route	PK	ECG	n
[121]	QRS	3mg/kg	48	HV	Acute	oral	Max C_{mean}	Max E_{mean}	2
[122]	QRS	3.74mg/kg	10	HV	Acute	oral/iv inf	Max C_{mean}	$E(t)$	2
[123]	QRS	100mg	9	HV	Acute	oral	Max C_{mean}	Max E_{mean}	1
[124]	QRS	10mg/kg	8	HV	Acute	iv inf	Max C_{mean}	$E(t)$	1
[125]	QRS	800mg	8	HV	Chronic	oral	Mean C_{max}	Max E_{mean}	1
[126]	QRS	400mg	6	HV	Chronic	oral	Mean C	Mean$E$	1
[127]	QRS	4.4-9.1mg/kg	20	Patients	Acute	iv inf	Mean C_{max}	$E(t)$	1
[128]	QRS	9.1mg/kg	100	Patients	Acute	iv inf	Mean C	Mean E	1
[129]	QRS	1000mg	9	Patients	Chronic	oral	C_{trough}	$E(\approx t)$	1
[130]	QRS	750-2250mg	22	Patients	Chronic	oral	Max C_{mean}	E_{reg}	2
[131]	QRS	800-1600mg	20	Patients	Chronic	oral	C_{trough}	$E(t)$	1
[132]	QRS	Not provided	18	Patients	Chronic	oral	C_{trough}	$E(t)$	1
[133]	QRS	180mg	10	Patients	Chronic	oral	C_{trough}	Mean E	1
[134]	QRS	972mg	10	Patients	Chronic	oral	C_{trough}	Mean E	1
[135]	QRS	Not provided	10	Patients	Chronic	oral	C_{trough}	$E(t)$	1

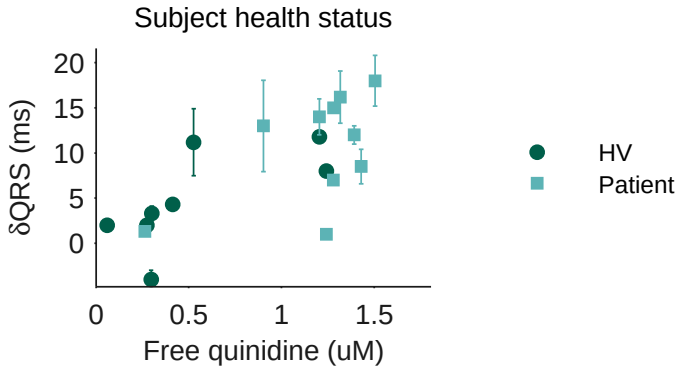

Figure 4.9 QRS widening in healthy volunteers (circles) and patients (squares) induced by quinidine. Data points represent associated plasma concentration-δQRS pairs (1-2 per published study) with standard errors where available.

4.4.2.4 Identified verapamil PR studies

A Pubmed search was performed on 2015-08-06 and generated a total of 159 published studies of PR effects of verapamil in humans, of which 20 fulfilled the postulated criteria (see Section 4.4.2.1). As iv administration of verapamil results in higher potency to induce PR prolongations compared to oral administration [136], only oral administration data were included in the analysis (16 studies). This is primarily due to different first-pass metabolism and potency of the two verapamil enantiomers [137, 138]. The more potent S-enantiomer is subject to higher first-pass metabolism, and therefore the resulting fraction of S-enantiomer in plasma is lower following oral administration compared to iv infusion. The selected studies are summarised in Table 4.7 and in more detail in Appendix B, Table B.1 and the data are plotted in Figure 4.10.

Table 4.7 Summary of the identified human verapamil studies.

Ref	ECG	Dose	Subjects		Dosing		Data type		
			n	Status	History	Route	PK	ECG	n
[139]	PR	240mg	8	HV	Acute	oral	Max C_{mean}	Max E_{mean}	1
[140]	PR	120mg	6	HV	Acute	oral	Max C_{mean}	Max E_{mean}	1
[141]	PR	240mg	8	HV	Acute	oral	Max C_{mean}	Max E_{mean}	1
[142]	PR	80-240mg	16	HV	Acute	oral	Max C_{mean}	Max E_{mean}	4
[106]	PR	120mg	8	HV	Acute	oral	Mean C_{max}	Max E_{mean}	1
[143]	PR	240mg	9	HV	Acute	oral	Mean C_{max}	Mean E_{max}	2
[144]	PR	40mg	6	HV	Acute	oral	Max C_{mean}	Max E_{mean}	1
[145]	PR	80mg	8	HV	Acute	oral	Mean C_{max}	Mean E_{max}	1
[146]	PR	80-160mg	20	HV	Acute	oral	Max C_{mean}	Max E_{mean}	3
[147]	PR	120mg	6	HV	Acute	oral	Mean C_{max}	Max E_{mean}	1
[148]	PR	80mg	9/36	Both	Acute	oral	Mean C_{max}	Mean E_{max}	3
[149]	PR	240mg	8	HV	Chronic	oral	$C(t)$	$E(t)$	2
[150]	PR	240mg	24	HV	Chronic	oral	Max C_{mean}	Max E_{mean}	2
[151]	PR	240mg	26	HV	Chronic	oral	Mean C_{max}	Mean E_{max}	2
[152]	PR	240-480mg	30	Patients	Chronic	oral	Mean C_{max}	Mean E_{max}	8
[153]	PR	480mg	11	Patients	Chronic	oral	$C(t)$	$E(t)$	1

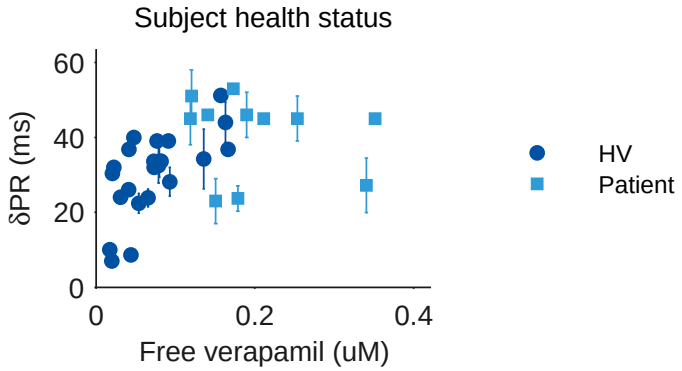

Figure 4.10 PR prolongations in healthy volunteers (circles) and patients (squares) induced by verapamil. Data points represent associated plasma concentration-δPR pairs (1-8 per published study) with standard errors where available.

4.5 Binding to plasma proteins

Free (unbound) plasma concentrations were calculated using *in vitro* estimates of plasma protein binding for each compound in guinea pig, dog and human plasma by a standard equilibrium dialysis method [154] for all compounds except flecainide, where dog plasma protein binding (PPB) was acquired from [21] (Table 4.8).

Table 4.8 Summary of the estimated % unbound drug in plasma for each drug in guinea pig, dog and human plasma.

Compound	AZD1305	Flecainide	Quinidine	Verapamil	AZD8683	AZD9164
Guinea pig		57		19.7		
Dog	50	36.9[a]	6.18	18.9	4.39	12.7
Human	63	62.1	12.2	20.7		

[a] acquired from [21].

4.6 Summary

This chapter presents the nonclinical and clinical data used for the quantitative and translational analyses in Chapters 5, 6 and 7. In chapter 5, the pre-clinical guinea pig and dog data as well as the clinical phase I AZD1305 data are used to develop PKPD models describing QRS and PR intervals at baseline and following drug administration. Following this, chapter 6 presents exposure-effect modelling to quantify the clinical effects on QRS and PR intervals by flecainide, quinidine and verapamil in humans. Finally, the resulting PKPD and exposure-effect models are used together with the *in vitro* data in Chapter 7 to investigate the pre-clinical to clinical translation to predict QRS and PR effects in humans.

Chapter 5

Population PKPD modelling of QRS/PR data in guinea pigs, dogs and humans

5.1 Introduction

As subtle CV effects may cause concern in long term patient use, safety studies aim to detect small changes in often highly variable data. Ethical, practical and economical considerations all underscore the importance of proper workflows and experimental designs that enable maximal information retrieval. PKPD modelling of drug-induced prolongations of QT intervals in animals and humans has been shown to improve both pre-clinical and clinical CV risk assessment, with multiple published examples (reviewed in [155]).

While PKPD modelling of drug-induced QT effects in animals and humans can inform and improve CV risk assessment (reviewed in [155]), examples of published PKPD models describing pharmacological QRS and PR effects are limited [1]. Important factors for predicting baseline QT in humans have been identified, including heart rate, circadian rhythm, sex and age [10]. Incorporating such factors into a model reduces unexplained residual variability and can improve the precision in estimating and predicting drug effects. However, the effects of these factors on QRS and PR intervals are largely unknown. A few PKPD models have been developed to describe drug-induced effects on QRS and PR intervals, including examples in dogs [57, 156, 157] and humans [111, 117, 122]. However, models to describe baseline variability of QRS and PR intervals had not been investigated previously. Therefore, baseline models were adapted from a published QT modelling approach [13, 63], including circadian variations and correction to simultaneous RR intervals, and evaluated to assess their performance in describing the baseline variability of QRS and PR intervals.

This chapter contains descriptions of novel PKPD models developed to describe baseline and drug-induced effects for a selection of compounds on QRS and PR intervals in guinea pigs, dogs and humans (Sections 5.3-5.9). QRS and PR effects in guinea pigs were evaluated for flecainide (section 5.7.2) and verapamil (section 5.9.2), in dogs for AZD1305 (section 5.4.2), AZD8683 (section 5.5.2), AZD9164 (section 5.6.2), flecainide (section 5.7.3), quinidine (section 5.8.2) and verapamil (section 5.9.3) and in humans for AZD1305 (section 5.4.3). The results of the PKPD modelling analyses performed in this chapter were used to define appropriate models for describing QRS and PR intervals in guinea pigs, dogs and humans. PKPD modelling has been shown to considerably improve the power to detect and quantify small effects on QTc in simulated pre-clinical studies [18], and established methods for PKPD modelling of QRS and PR intervals can thus improve cardiac safety assessment with clear impact for compound selection, progression and development decisions.

Methods for modelling QRS and PR intervals were developed by Bergenholm et al. [3], where the effects of four antiarrhythmics (AZD1305, flecainide, quinidine and verapamil) and side effects of two anti-muscarinics (AZD8683 and AZD9164) were investigated using dog telemetry data. PKPD models for QRS and PR effects by flecainide and verapamil in guinea pigs and by AZD1305 in humans were developed using these methods by Bergenholm et al. [**?**].

5.2 PKPD modelling methods

Population PKPD models were developed and evaluated with Monolix 4.3.2, Lixoft, France and MATLAB Release 2013b, The MathWorks, Inc., US. Parameters were estimated using the SAEM algorithm described in Section 2.2.2.1, as implemented in Monolix [44]. Default settings were used for the SAEM algorithm, and standard errors and likelihoods were estimated using linearisation. The mixed effects models were developed using a sequential process, separating the PK and PD parameter estimation steps. Model selection was primarily based on performance statistics using the AIC (Equation 2.15, [46]). The AIC values were used to calculate relative likelihoods of the models according to

$$p = exp((AIC_{min} - AIC)/2) \tag{5.1}$$

where the relative likelihood p of a model compared to a reference model with lower AIC ($\mathrm{AIC_{min}}$) can be estimated [158]. To reduce the risk of over-fitting, a simpler model was selected if it was at least 5 % as likely as the model with the lowest AIC. In addition, precision of parameter estimates, residual plots and visual inspection of the fits to data were considered. When the precision of fixed or random effects

was low (standard errors above 100 %), the random effect for this parameter was removed and the reduced model tested.

5.2.1 Modelling of QRS and PR intervals at baseline

Investigations of different baseline models were conducted to ensure a proper description of QRS and PR interval baselines while modelling the drug effects. Whereas baseline subtraction leads to increased variance in the data, simultaneous fitting of baseline and drug effect parameters can accommodate known sources of variability using "raw" data. Baseline QRS and PR intervals were investigated by fitting vehicle data separately and full data sets to ensure that relevant baseline model structures were used. For dogs, vehicle models were fitted separately both evaluating each study separately and using a merged data set of vehicle data from all studies. Estimated baseline parameters from fitting the vehicle models were used as initial estimates for modelling the full data sets. The performance of two submodels describing baseline variability of QRS and PR intervals was evaluated, namely and individual RR correction model and a single phase cosine model. These submodels were chosen as they have been successfully used to minimise the baseline variabilty of QT intervals [13, 159], and may therefore also be suitable for other ECG intervals. The two submodels were evaluated alone and in combination, resulting in 4 different baseline models: the constant baseline model (Equation 5.2), the circadian rhythm model (Equation 5.3), the RR correction model (Equation 5.4) and the combined model (Equation 5.5), described by

$$ECG = ECG_0 \tag{5.2}$$

$$ECG = ECG_0 \left(1 + A\cos\left(2\pi\frac{(t-\phi)}{24}\right)\right) \tag{5.3}$$

$$ECG = ECG_0 \left(\frac{RR}{RR_{ref}}\right)^{\alpha} \tag{5.4}$$

$$ECG = ECG_0 \left(\left(\frac{RR}{RR_{ref}}\right)^{\alpha} + A\cos\left(2\pi\frac{(t-\phi)}{24}\right)\right) \tag{5.5}$$

where ECG is the duration of the ECG interval (e.g. QRS/PR), ECG_0 is the point baseline, RR_{ref} is the reference RR (or HR), α the exponent of the RR correction function, RR the observed duration between two consecutive R peaks measured simultaneously to QRS/PR and A and ϕ the amplitude and phase shift of the circadian rhythm. The reference RR was varied between the species, and was 250 ms (240bpm) in guinea pigs, 750 ms (80 bpm) in dogs and 1000 ms (60 bpm) in humans [59]. The phase shift ϕ gives identical predictions in 24 h cycles, but was assumed to converge to a local minimum close to the initial condition. Circadian rhythms were not evaluated in guinea pigs due to the short experimental time (2h). The effect

of restraining animals to the inhalation table was also evaluated for AZD8683 and AZD9164 treatment in dogs, as visual assessment of the data suggested that such effects may be present. This was modelled according to

$$ECG = ECG_{baseline} + k_{restraint} * REST \tag{5.6}$$

where $k_{restraint}$ descibes a constant effect of being restrained to the inhalation table. Normal distributions for the between subject variabilities (BSVs) of ECG_0, ϕ and $k_{restraint}$ and log-normal distributions for α and A were assumed for PR intervals while also a normal distribution of α was tested for the QRS intervals.

5.2.2 PK modelling

1-3 compartmental PK models were developed to infer drug concentrations at the full ECG sampling periods. An example two-compartment model is provided in Section 2.2.1.1. Zero-order absorption models and nonlinear bioavailability models were applied where required to fit the data. Data below the limit of quantification (BLQ, 0-33 % excluding pre-dose measurements) for each assay were left-censored with the BLQ value as an upper limit and used in the parameter estimation as implemented in Monolix [160]. A log-normal distribution of the BSVs was assumed for all PK parameters. Residual errors for the PK models were assumed to be mixed additive and proportional (Equation 2.14). The proportional part of the residual error models were estimated from the data or fixed to 10 or 15 %, both in the range of the known analytical variability. Non-linear features and/or inter-occasion variability were applied where required to reach an acceptable fit to individual data.

5.2.3 PKPD modelling

Individually estimated PK parameters were fixed and used as regression variables to drive the response in the PKPD modelling. Predicted plasma concentrations were converted to unbound concentrations through the inclusion of *in vitro* estimated free fractions (1-PPB) as regression variables in the PKPD modelling step. Unbound concentration vs. ECG data were plotted to identify time delays and/or appropriate drug effect model structures. Time delays were modelled with an effect compartment (Equation 2.5) [33], assuming a (distributional) delay between plasma concentration C_c and concentration at a hypothetical "effect site" C_e.

PQ intervals were used for AZD8683 treatment in dogs and AZD1305 treatment in humans as PR intervals were not recorded. PQ intervals are slightly shorter as the QR part (up-rise in the QRS complex) is only included in the PR interval, but both intervals are used to investigate the effects on atrial and AV node conduction. Proportional, power and E_{max} models (Equations 2.2-2.4) were evaluated to describe the drug effects. Normal distributions of the BSVs were assumed for the slope, a and

E_{max} and log-normal distributions for EC_{50} and the exponents. Additive residual errors were assumed for the PD effects (Equation 2.14, b=0).

5.3 Modelling baseline QRS and PR interval variability in dogs

Vehicle data were investigated to identify appropriate baseline models and provide initial parameter estimates in the drug effect modelling step. Four baseline models (Equations 5.2-5.5) were fitted to each vehicle data set separately and to a pooled data set with all vehicle data. Full BSV models were assumed. The percentage likelihood of each baseline model was calculated using Equation 5.1.

5.3.1 Modelling baseline QRS variability of dog data

Assuming a constant baseline (Equation 5.2) with normally distributed BSV resulted in a residual variability of 2.1 ms for the pooled data set, which was reduced to 1.9 ms for the combined model (Equation 5.5). This suggests that little residual variability is explained by the RR correction and circadian rhythm models. The percentage likelihood of each of the four baseline models is summarised in Table 5.1. These likelihoods suggest that RR correction slightly improves the goodness of fit to QRS data in dogs, although constant models perform almost as well with likelihoods of at least 5% compared to the RR correction model for all data sets but one. The circadian rhythm model slightly improved the goodness of fit to QRS intervals in the merged data set, but also here the model with only RR correction was around 5% as likely, suggesting that including circadian rhythms may lead to overfitting. Parameter estimates for the best models were similar between the different data sets (Table 5.2).

Table 5.1 Relative likelihood compared to the model with the lowest AIC (Equation 5.1) of the different QRS baseline models (Equations 5.2-5.5) evaluated using vehicle data sets from each study separately and a pooled data set.

Study	Constant	Circadian rhythm	RR correction	Both
1	**22**	0	100	5
2	**22**	8	100	100
4	0	0	**100**	0
5	**100**	3	14	1
6	**14**	1	100	61
All	0	0	**5**	100

Likelihoods given in %. Vehicle data from telemetry studies investigating AZD1305 (Study=1), AZD8683 (Study=2), flecainide (Study=4), quinidine (Study=5), verapamil (Study=6). Most simple baseline model with likelihood of at least 5% is indicated by bold font for each data set.

Table 5.2 Parameter estimates for the most simple vehicle QRS models with at least 5% relative likelihood compared to the model with the lowest AIC value.

	QRS_0 (ms)		α		Res. (ms)
Study	**Value (SE)**	**BSV % (SE)**	**Value (SE)**	**BSV % (SE)**	**Value (SE)**
1	46 (1)	5.5 (2.0)	-	-	1.2 (0.1)
2	44 (1)	6.1 (2.2)	-	-	1.6 (0.2)
4	53 (1)	5.0 (1.8)	0.012 (0.023)	220 (160)	2.1 (0.2)
5	52 (2)	7.9 (2.8)	-	-	1.3 (0.1)
6	44 (1)	6.0 (2.2)	-	-	2.6 (0.2)
All	47 (1)	9.9 (1.8)	0.038 (0.011)	62 (30)	2.0 (0.1)

BSV is the coefficient of variation, approximated by CV% = SD*100 for log-normal distributions. Vehicle data from telemetry studies investigating AZD1305 (Study=1), AZD8683 (Study=2), flecainide (Study=4), quinidine (Study=5), verapamil (Study=6).

5.3.2 Modelling baseline PR variability of dog data

Assuming a constant baseline (Equation 5.2) with normally distributed BSV resulted in a residual variability of 7.3 ms for the pooled data set, which was reduced to 5.4 ms for the combined model (Equation 5.5). This suggests that some residual variability is explained by the RR correction and/or circadian rhythm models. The percentage likelihood of each of the four baseline models are summarised in Table 5.3. These likelihoods suggest that the goodness of fits are improved by including primarily RR correction, but also circadian rhythms to describe PR intervals in dogs. Parameter

estimates for the best models were similar between the different data sets (Table 5.4).

Table 5.3 Relative likelihood compared to the model with the lowest AIC (Equation 5.1) of the different PR baseline models (Equations 5.2-5.5) evaluated using vehicle data sets from each study separately and a pooled data set.

Study	Constant	Circadian rhythm	RR correction	Both
1	0	0	**100**	37
2	0	0	**100**	61
3	0	0	0	**100**
4	0	1	0	**100**
5	0	**100**	0	37
6	0	0	**100**	2
All	0	0	0	**100**

Likelihoods given in %. Vehicle data from telemetry studies investigating AZD1305 (Study=1), AZD8683 (Study=2), AZD9164 (Study=3), flecainide (Study=4), quinidine (Study=5), verapamil (Study=6). Most simple baseline model with likelihood of at least 5% is indicated by bold font for each data set.

Table 5.4 Parameter estimates for the most simple vehicle PR models with at least 5% relative likelihood compared to the model with the lowest AIC value.

	PR_0 (ms)		A (%)		α		Res. (ms)
Study	**Value**	**BSV %**	**Value**	**BSV %**	**Value**	**BSV %**	**Value**
1	100 (4)	8.4 (3.0)	-	-	0.14 (0.02)	19 (18)	5.5 (0.6)
2[a]	110 (4)	6.3 (2.4)	-	-	0.24 (0.04)	5.6 (46)	6.9 (0.7)
3	91 (3)	8.3 (2.4)	2.8 (0.7)	43 (25)	0.12 (0.02)	25 (18)	3.1 (0.2)
4	95 (3)	6.0 (2.2)	6.0 (1.2)	29 (18)	0.08 (0.05)	110 (53)	3.8 (0.4)
5	94 (3)	6.6 (2.4)	4.9 (1.3)	44 (23)	-	-	3.5 (0.4)
6	110 (6)	10 (3.7)	-	-	0.15 (0.03)	7 (77)	5.9 (0.5)
All	103 (3)	9.9 (1.8)	1.9 (0.6)	93 (26)	0.16 (0.02)	33 (11)	5.4 (0.2)

Data are given as estimated value (SE). BSV is the coefficient of variation, approximated by CV% = SD*100 for log-normal distributions. Vehicle data from telemetry studies investigating AZD1305 (Study=1), AZD8683 (Study=2), AZD9164 (Study=3), flecainide (Study=4), quinidine (Study=5), verapamil (Study=6). [a]PQ intervals.

5.4 Modelling of AZD1305 data

5.4.1 Acquired data

Effects of AZD1305 were available in dogs from an in-house telemetry study and in humans from an in-house Phase I clinical study, as described in Chapter 4. Maximum QRS widenings induced by AZD1305 were 4 ms in dogs and 12 ms in humans, and maximum PR prolongations were 23 ms in dogs and 14 ms in humans (Table 5.5). Similar drug exposures were acquired in dogs and humans, both for total and free drug.

Table 5.5 Summary of the acquired AZD1305 data.

Species	**Dog**	**Human**
n	4	29
Dose	iv: vehicle, 2.15, 4.3; oral: vehicle, 8.7 mg kg^{-1}	iv: placebo, 10, 70; oral: placebo, 10, 30, 90, 180, 360, 430, 500 mg
C_{max} (μM)	3.2 ±0.8	3.4
QRS_0 (ms)	46±3	96.0±6.0
QRS_{max} (ms)	50±5	11.5±12.4 (Δ, n=2)
PR_0 (ms)	108±13	164±19
PR_{max} (ms)	131±15	14.4±12.0 (Δ, n=2)
Free drug (%)	50	63

Data presented as mean±SD. iv, intravenous; QRS_0, QRS at baseline; PR_0, PR at baseline; QRS_{max}, maximal QRS; PR_{max}, maximal PR. Δ, QRS or PR change from baseline for highest dose group.

5.4.2 PKPD modelling in dogs

5.4.2.1 PK modelling

One and two compartment PK models were evaluated following visual inspection of the log-normalised data, and a 2 compartment model selected as this better described the data. Proportional bioavailability for the oral dose and linear elimination were assumed following visual inspection of dose-normalised plasma concentrations. The final PK model well described plasma concentrations following iv and oral AZD1305 treatment (Figure 5.1). BSVs for the rate of elimination and distribution from the peripheral to the central compartment could not be identified (SE >100%), most likely due to the small number of dogs, and these rates were therefore assumed to be the same for all dogs. Estimated parameters are summarised in Table 5.6 and goodness of fit plots are shown in Figure 5.2.

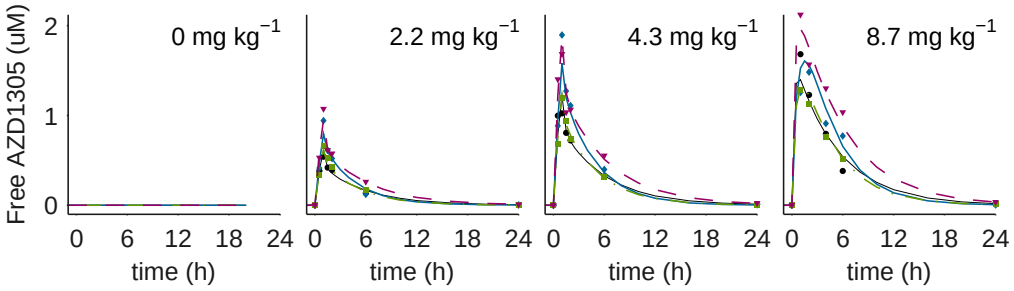

Figure 5.1 Unbound plasma concentration data (markers) and model fits (lines) for dogs treated with AZD1305. Individual dogs are separated by colour and marker type.

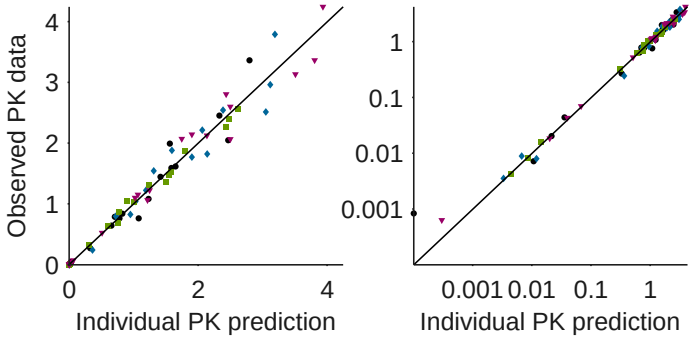

Figure 5.2 Observed data vs. individual model fits of AZD1305 concentrations in linear (left) and log (right) scale with different colour/marker type for each dog.

Table 5.6 Parameter estimates for the dog AZD1305 PK model.

Parameter	Estimate (SE)	BSV % (SE)
k_a (μmol h^{-1})	1.33 (0.21)	24.8 (11)
F	0.796 (0.023)	3.0 (2.4)
V (L kg^{-1})	1.78 (0.18)	20.3 (7.4)
k_{12} (h^{-1})	2.04 (0.05)	-
k_{21} (h^{-1})	1.99 (0.28)	27.4 (9.7)
k (h^{-1})	0.466 (0.009)	-
Additive residuals (μM)	0.00074 (0.00019)	
Proportional residuals	0.132 (0.013)	

BSV is the coefficient of variation, approximated by CV% = ω*100 for log-normal distributions.

5.4.2.2 PK-QRS drug effect modelling

A proportional direct effect model (Equation 2.4) well characterised the AZD1305-induced QRS prolongations (Figure 5.3). Summary statistics for a selection of tested models are provided in Table 5.7. Estimated parameters are summarised in Table

5.8 and goodness of fit plots are shown in Figure 5.4. When evaluating the full data set, similar results were obtained for describing baseline variability compared to the vehicle data set (Section 5.3), where the RR correction model (Equation 5.4), but not the circadian rhythm model (Equation 5.3), slightly improved the goodness of fit to the data. This was mainly driven by a small correlation between QRS and RR in one dog.

Table 5.7 Summary of a selection of the tested dog AZD1305 QRS models.

Model	**Residuals**	**AIC**	**Relative likelihood**	**Comment**
Proportional	1.38	1225	0.0111	
Proportional, RR corr	1.34	1218	0.368	**Selected model**
Proportional, RR corr, circ rhythm	1.32	1220	0.135	No improvement
Proportional, RR corr, effect comp	1.32	1216	1	No improvement

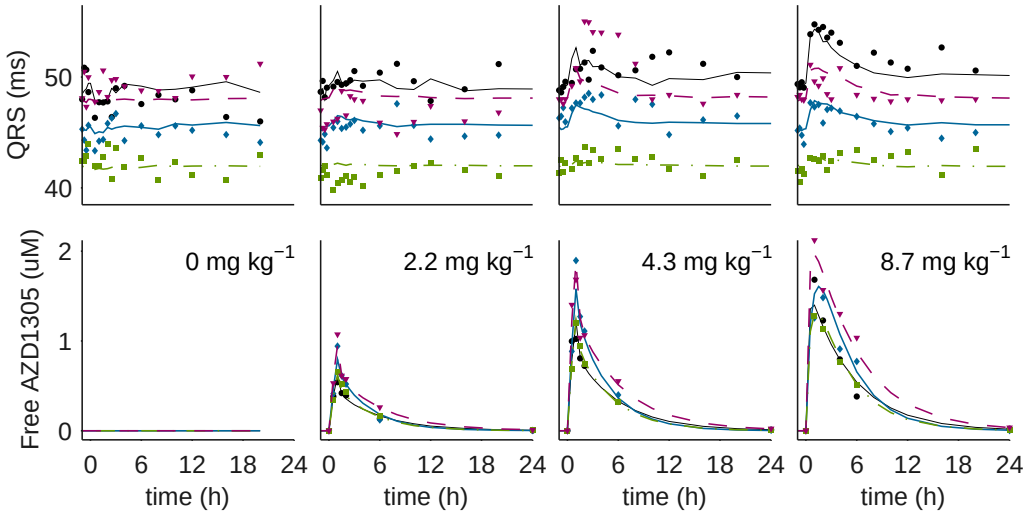

Figure 5.3 Top: QRS interval duration data (markers) and model fits (lines) for dogs treated with AZD1305. Bottom: Individual PK model parameters predicting the PK in each dog were used to drive the PD response. Individual dogs are separated by colour and marker type.

Table 5.8 Parameter estimates for the dog AZD1305 QRS model.

	Estimate (SE)	BSV % (SE)
$\boldsymbol{QRS_0}$ **(ms)**	46.0 (1.4)	5.9 (2.1)
$\boldsymbol{\alpha}$	0.014 (0.008)	79.8 (51.0)
$\boldsymbol{slope_u}$ **(ms** μ**M^{-1})**	1.93 (0.67)	66.2 (25.2)
Additive residuals (ms)	1.34 (0.0524)	

BSV is the coefficient of variation, approximated by CV% = SD*100 for log-normal distributions.

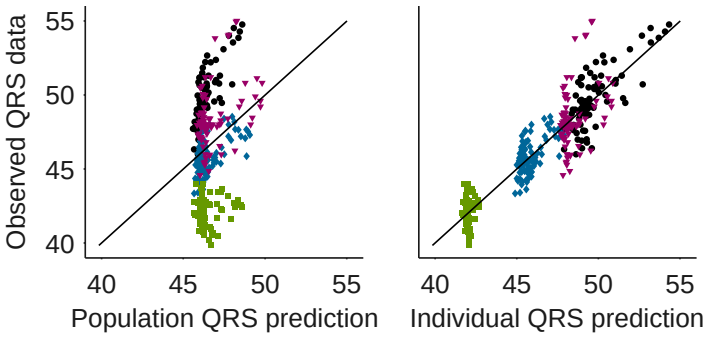

Figure 5.4 Population (left) and individual (right) model fits vs. observed QRS intervals with different colour/marker type for each animal.

5.4.2.3 PK-PR drug effect modelling

A proportional direct effect model (Equation 2.4) well characterised the AZD1305-induced PR prolongations (Figure 5.5). Summary statistics for a selection of tested models are provided in Table 5.9. Estimated parameters are summarised in Table 5.10 and goodness of fit plots are shown in Figure 5.6. When evaluating the full data set, similar results were obtained for describing baseline variability compared to the vehicle data set (Section 5.3), where the RR correction model (Equation 5.4) considerably improved the goodness of fit to the data, and the circadian rhythm model (Equation 5.3) slightly improved the goodness of fit to the data.

Table 5.9 Summary of a selection of the tested dog AZD1305 PR models.

Model	Residuals	AIC	Relative likelihood	Comment
Proportional	7.35	2354	1.6E-28	
Proportional, RR corr	6.05	2233	0.0302	Improved fit
Proportional, RR corr, circadian rhythm	5.87	2228	0.368	Improved fit, high uncertainty BSV(A)
Proportional, RR corr, circ rhythm, no BSV on A	5.86	2226	1	**Selected model**
Proportional, RR corr, circ rhythm, no BSV on A, effect comp	5.86	2229	0.223	No improvement

Table 5.10 Parameter estimates for the dog AZD1305 PR model.

	Estimate (SE)	BSV % (SE)
$\boldsymbol{PR_0}$ **(ms)**	102 (4)	7.95 (2.85)
$\boldsymbol{A}$ **(%)**	2.45 (0.58)	-
$\boldsymbol{\phi}$ **(h)**	4.25 (1.65)	67.4 (31.3)
$\boldsymbol{\alpha}$	0.165 (0.023)	22.4 (11.9)
$\boldsymbol{slope_u}$ **(ms** μ**M^{-1})**	13.8 (1.8)	22.5 (10.0)
Additive residuals (ms)	5.86 (0.23)	

BSV is presented as the coefficient of variation, approximated by CV% = SD*100 for log-normal distributions.

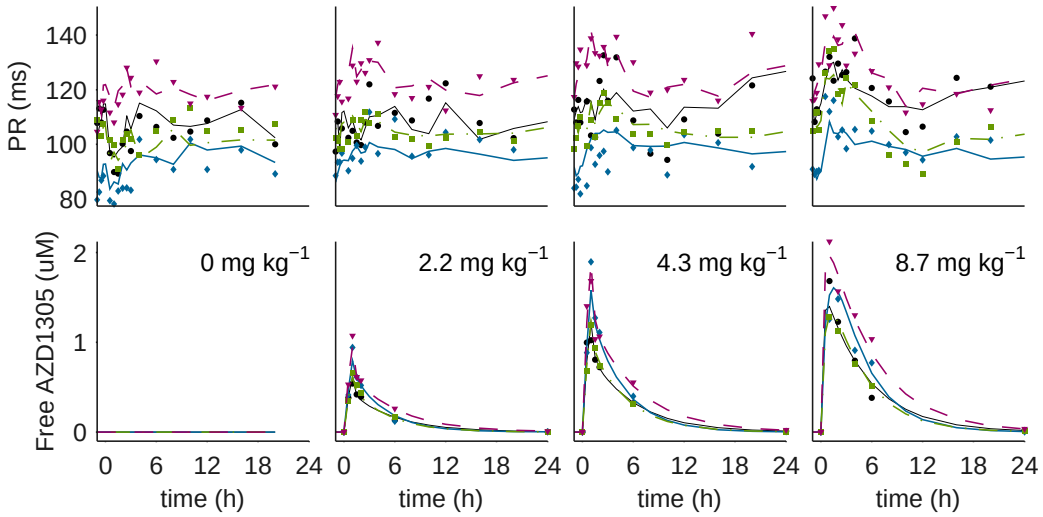

Figure 5.5 Top: PR interval duration data (markers) and model fits (lines) for dogs treated with AZD1305. Bottom: Individual PK model parameters predicting the PK in each dog were used to drive the PD response. Individual dogs are separated by colour and marker type.

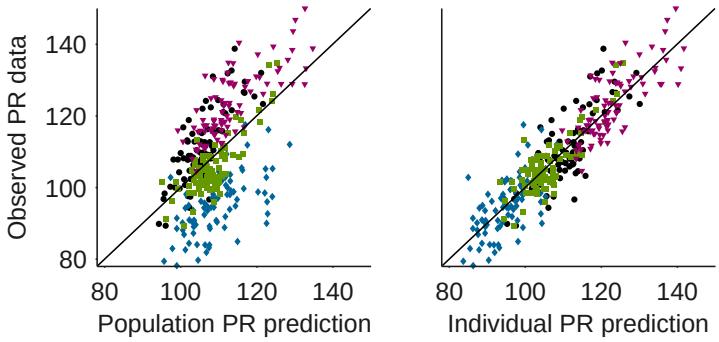

Figure 5.6 Population (left) and individual (right) model fits vs. observed PR intervals with different colour/marker type for each animal.

5.4.3 PKPD modelling in humans

5.4.3.1 PK modelling

Two and three compartment PK models were evaluated following visual inspection of log-normalised plasma concentrations, and a three compartment model was selected as this showed improved goodness of fit to the data. A lag time was included to account for a short delay between administration of the oral dose and the initial increase in plasma concentrations. The oral bioavailability was observed to increase with dose and modelled according to the operational equation

$$F = \frac{F_{max} DOSE}{ED_{50} + DOSE} \tag{5.7}$$

where F is the bioavailability, F_{max} the maximal bioavailability, ED_{50} the dose at half-maximum bioavailability and DOSE is the administered (oral) dose in μmol. Model fits to the data are shown in Figure 5.7. Estimated parameters for the selected PK model are summarised in Table 5.11 and goodness of fit plots are shown in Figure 5.8.

Table 5.11 Parameter estimates for the human AZD1305 PK model.

Parameter	**Estimate (SE)**	**BSV % (SE)**
k_a **(μmol h^{-1})**	1.02 (0.11)	39.7 (7.5)
F_{max}	0.523 (0.064)	31.4 (7.9)
ED_{50} **(μmol)**	1.46 (0.47)	73 (22)
T_{lag} **(h)**	0.172 (0.012)	31.0 (5.1)
V **(L kg^{-1})**	0.712 (0.071)	20.4 (5.9)
k_{12} **(h^{-1})**	4.03 (0.74)	-
k_{21} **(h^{-1})**	1.28 (0.12)	14.4 (6.1)
k_{13} **(h^{-1})**	0.0893 (0.012)	17.8 (12)
k_{31} **(h^{-1})**	0.0472 (0.013)	-
k **(h^{-1})**	0.967 (0.11)	10.1 (4.5)
Additive residuals (μM)	0.0012 (0.0002)	
Proportional residuals	0.147 (0.008)	

BSV is presented as coefficient of variation, approximated by CV% = SD*100 for log-normal distributions.

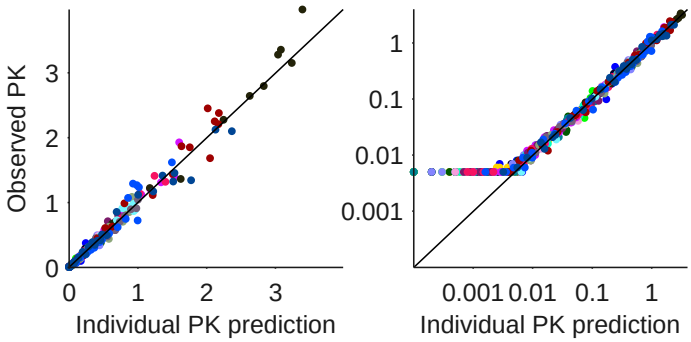

Figure 5.8 Observed data vs. individual model fits of AZD1305 concentration in linear (left) and log (right) scale with a different colour for each subject. Initial horizontal points in the loglog plot are data below the limit of quantification.

5.4.3.2 QRS baseline modelling

Baseline QRS intervals in humans were best described by the combined circadian rhythm/RR correction baseline model (Equation 5.5, AIC -247 for the full data set) and additional inter-occasion variability (IOV) of the point baseline value (AIC -735 for the full data set). Both the estimated correction factor (α) of the QRS-RR

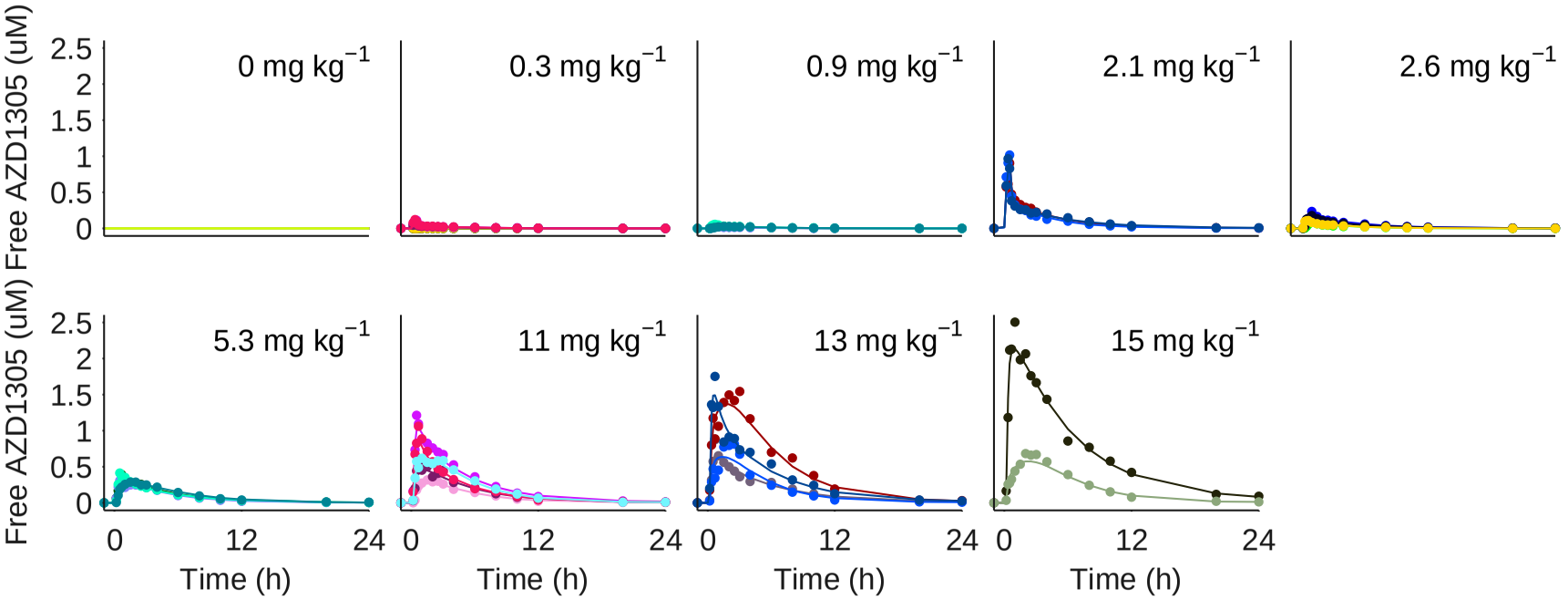

Figure 5.7 Unbound plasma concentration data (markers) and model fits (lines) for humans treated with AZD1305.

relationship and the amplitute of the circadian rhythm were small. However, baseline parameter values were similar when fitting placebo data separately and the full data set (Tables 5.12 and 5.14). As some individuals showed negative correlations between QRS and RR intervals (Figure 5.9), a normally distributed BSV of α was evaluated and improved the goodness of fit. One placebo-treated subject showed consistently lower QRS intervals compared to the remaining subjects, and this difference was not due to shorter RR intervals (Figure 5.9). As this subject had consistently lower QRS intervals at both occasions, it was included in the analysis.

Table 5.12 Parameter estimates for the human baseline QRS model.

	Estimate (SE)	**BSV % (SE)**
$\boldsymbol{QRS_0}$ **(ms)**	93.9 (2.23)	7.5 (1.68)
$\boldsymbol{\alpha}$	0.0463 (0.0276)	159 (47.3)
$\boldsymbol{A}$ **(%)**	1.45 (0.22)	22.9 (21.4)
$\boldsymbol{\phi}$ **(h)**	-7.12 (0.751)	-28.3 (-8.48)
Additive residual (ms)	1.36 (0.0522)	-

BSV and IOV are presented as the coefficient of variation, approximated by CV% = SD*100 for log-normal distributions.

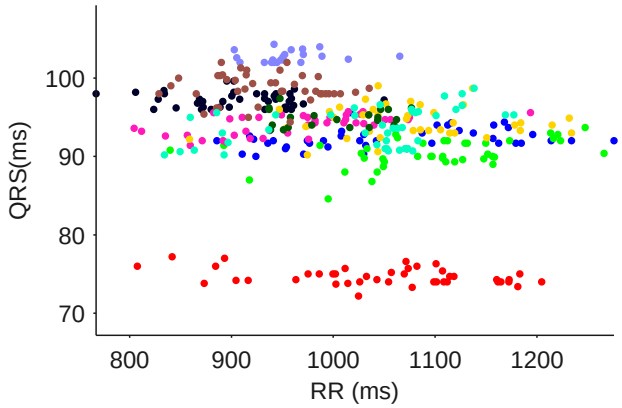

Figure 5.9 QRS duration vs. RR duration for subjects treated with placebo show small but clear individual-specific correlations.

5.4.3.3 PK-QRS drug effect modelling

Proportional and power models (Equations 2.3-2.4) were tested following visual inspection of simulated PK data plotted against QRS intervals. Summary statistics for a selection of tested models are provided in Table 5.13. The power model improved the goodness of fit slightly (AIC -36) with estimated parameters a = 10.1±0.8, b = 0.87±0.08, suggesting an exponentially declining positive drug effect. However, b

was not largely different from 1 and residual unexplained variability was very similar between both models. Also, BSV for both a and b allowed large variability in the drug effect profiles of each subject, potentially leading to overfitting of the data. Therefore, the more simple proportional model was selected. Also, accounting for a short delay using the effect compartment (Equation 2.5) improved the goodness of fit value (ΔAIC = -35). The estimated proportional drug effect was 11.4 $\pm$0.8 ms μM^{-1} unbound AZD1305. The fit to individual data is shown in Figure 5.10, final parameter estimates are summarised in Table 5.14 and goodness of fit plots are shown in Figure 5.11.

Table 5.13 Summary of a selection of the tested human AZD1305 QRS models.

Model	**Residuals**	**AIC**	**Relative likelihood**	**Comment**
Proportional	1.06	3666	4.66E-15	
Proportional, effect comp	1.02	3621	2.75E-05	**Selected model**
Power, effect comp	0.999	3600	1	Improved fit, high freedom with BSV(a) and BSV(b)
Power, effect comp, no BSV(b)	1.01	3616	0.000335	No improvement from proportional when no BSV(b)

All models included IOV on the point baseline and the RR correction and circadian rhythm models to describe the baseline.

Table 5.14 Parameter estimates for the selected human AZD1305 QRS model.

	Estimate (SE)	**BSV % (SE)**	**IOV % (SE)**
$\boldsymbol{QRS_0}$ **(ms)**	96 (1.08)	5.8 (0.838)	2.17 (0.33)
$\boldsymbol{\alpha}$	0.0553 (0.00937)	70 (11.8)	
$\boldsymbol{A}$ **(%)**	1.46 (0.129)	33.1 (8.65)	
$\boldsymbol{\phi}$ **(h)**	-6.46 (0.318)	22.9 (1.94)	
$\boldsymbol{slope_u}$ **(ms** μ**M^{-1})**	11.4 (0.84)	26.1 (1.39)	
$\boldsymbol{ke_0}$ **(h^{-1})**	43.1 (27.1)	203 (13.7)	
Additive residual (ms)	1.02 (0.0241)		

BSV and IOV are presented as the coefficient of variation, approximated by CV% = SD*100 for log-normal distributions.

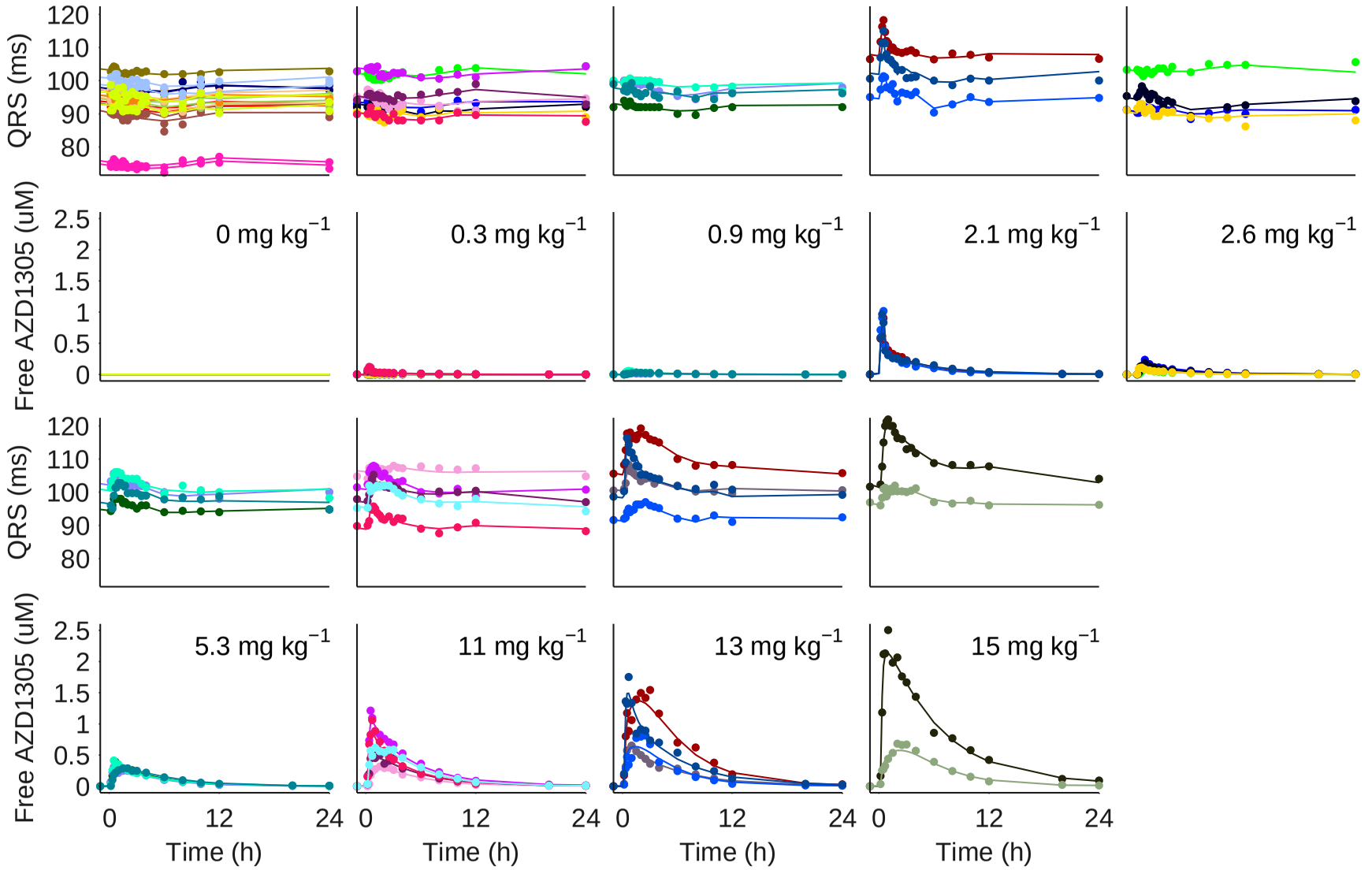

Figure 5.10 Top: QRS interval duration data (markers) and model fits (lines) for humans treated with AZD1305. Bottom: Individual PK model parameters predicting the PK in each subject were used to drive the PD response. Individual subjects are separated by colour.

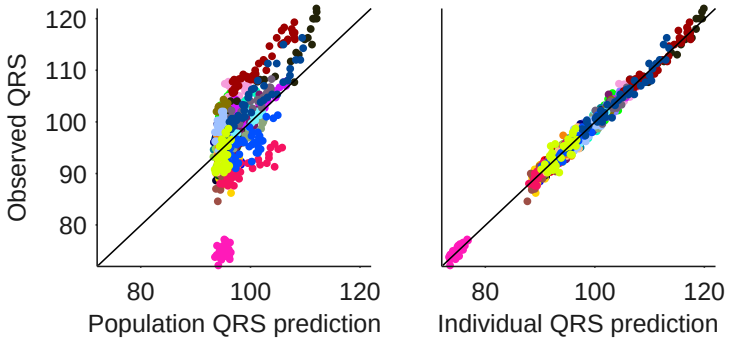

Figure 5.11 Population (left) and individual (right) model fits vs. observed QRS intervals with different colour for each subject.

5.4.3.4 PQ baseline modelling

PQ intervals in humans were best described by the combined circadian rhythm/RR correction baseline model (Equation 5.5, ΔAIC = -511). Both the estimated correction factor (α) of the PQ-RR relationship and the amplitute of the circadian rhythm were similar when fitting placebo data separately and the full data set (Tables 5.15 and 5.17). Goodness of fit was improved using a normal rather than a lognormal distribution of the α parameter across individuals as some individuals showed negative PQ-RR correlations (Figure 5.12).

Table 5.15 Parameter estimates for the human baseline PQ model.

	Estimate (SE)	**BSV % (SE)**
$\boldsymbol{PQ_0}$ **(ms)**	170 (5.94)	11 (2.48)
$\boldsymbol{\alpha}$	0.191 (0.0761)	119 (29.5)
$\boldsymbol{A}$ **(%)**	2.83 (0.528)	50.7 (15.1)
$\boldsymbol{\phi}$ **(h)**	-3.2 (0.905)	-80.8 (-21.8)
Additive residual (ms)	3.57 (0.137)	-

BSV and IOV are presented as the coefficient of variation, approximated by CV% = SD*100 for log-normal distributions.

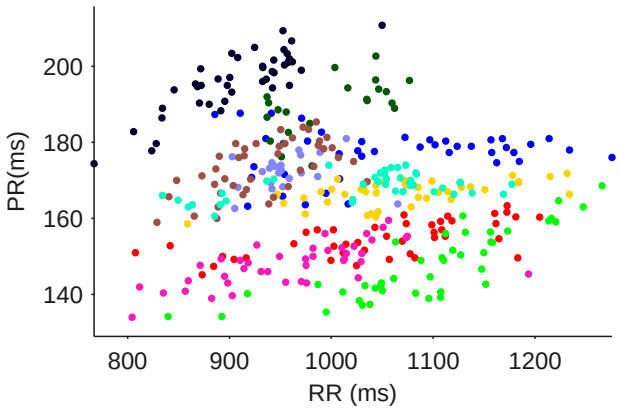

Figure 5.12 PQ duration vs. RR durations for subjects treated with placebo show clear individual-specific correlations.

5.4.3.5 PK-PQ drug effect modelling

Proportional and power models (Equations 2.3-2.4) were tested following visual inspection of simulated PK plotted against PQ intervals. Summary statistics for a selection of tested models are provided in Table 5.16. The power model improved the goodness of fit slightly (ΔAIC = -31) with estimated parameters $a = 18 \pm 3$ and $b = 1.2 \pm 0.2$, suggesting a small exponential increase in the drug effect. However, b was not largely different from 1 and residual unexplained variability was very similar between the proportional and the power model. Also, BSV for both a and b allowed large variability in the drug effect profiles of each subject, potentially leading to overfitting of the data. Therefore, the more simple proportional model was selected. Also, accounting for a short delay using the effect compartment (Equation 2.5) improved the goodness of fit value (ΔAIC = -22). BSV could not be fitted to the rate of distribution to the effect compartment (SE of BSV > 100%) and the BSV of this parameter was therefore removed. The estimated proportional drug effect was 17.0 $\pm$2.6 ms μM^{-1} unbound AZD1305. The fits to individual data are shown in Figure 5.13, final parameter estimates are summarised in Table 5.17 and goodness of fit plots are shown in Figure 5.14.

Table 5.16 Summary of a selection of the tested human AZD1305 PQ models.

Model	Residuals	AIC	Relative likelihood	Comment
Proportional	3.74	6432	1.69E-10	
Proportional, effect comp	3.7	6410	0.0000101	Improved fit, high uncertainty BSV(k_{e0})
Proportional, effect comp, no BSV(k_{e0})	3.7	6406	0.0000749	**Selected model**
Power, effect comp	3.6	6387	1	Improved fit, high freedom with BSV(a) and BSV(b)
Power, effect comp, no BSV(b)	3.69	6405	0.000123	No improvement from proportional when no BSV(b)

All models included IOV on the point baseline and the RR correction and circadian rhythm models to describe the baseline.

Table 5.17 Parameter estimates for the selected human AZD1305 PQ model.

	Estimate (SE)	BSV % (SE)	IOV % (SE)
$\boldsymbol{PQ_0}$ **(ms)**	160 (3.57)	11.7 (1.61)	4.53 (0.70)
$\boldsymbol{A}$ **(%)**	2.77 (0.303)	47.4 (2.62)	-
$\boldsymbol{\phi}$ **(h)**	-3.55 (0.491)	64.9 (2.78)	-
$\boldsymbol{\alpha}$	0.123 (0.0338)	134 (5.92)	-
$\boldsymbol{slope_u}$ **(ms** μ**M^{-1})**	17 (2.57)	51.7 (4.07)	-
$\boldsymbol{ke_0}$ **(h^{-1})**	10.5 (2.4)	34.4 (46.4)	-
Additive residuals (ms)	3.72 (0.09)		

BSV and IOV are presented as the coefficient of variation, approximated by CV% = SD*100 for log-normal distributions.

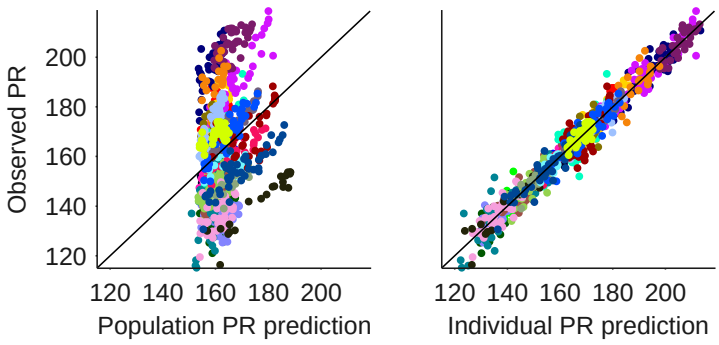

Figure 5.14 Population (left) and individual (right) model fits vs. observed PQ intervals with different colour for each subject.

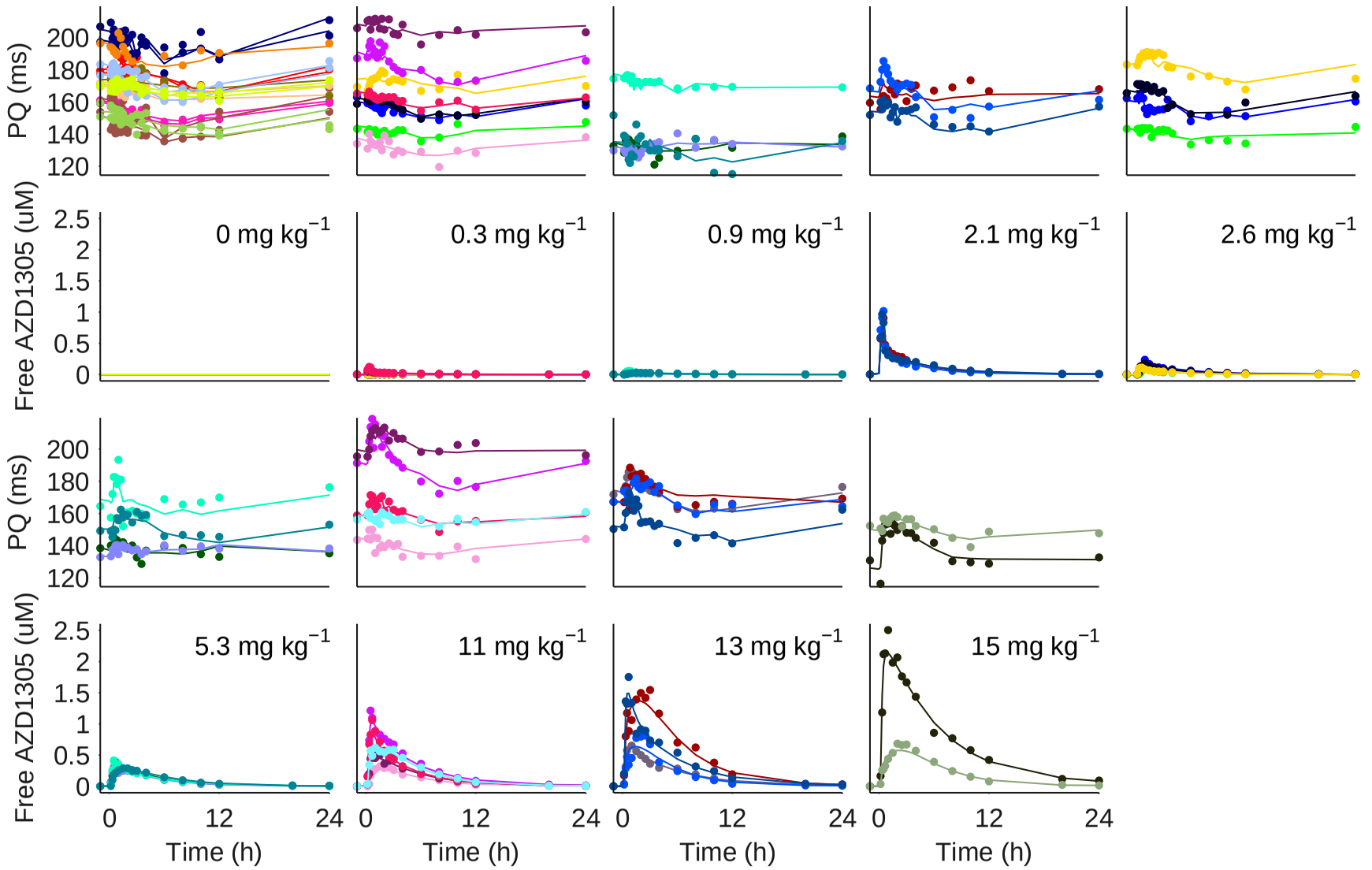

Figure 5.13 Top: PQ interval duration data (markers) and model fits (lines) for humans treated with AZD1305. Bottom: Individual PK model parameters predicting the PK in each subject were used to drive the PD response. Individual subjects are separated by colour.

5.5 Modelling of AZD8683 data

5.5.1 Acquired data

Effects of AZD8683 were available in dogs from an in-house telemetry study and in human volunteers, and the compound was administered by inhalation. Neither PR nor QRS intervals were prolonged in humans, where maximum plasma concentrations of 1.00 nM AZD8683 (geometric mean, 85 CV%) were achieved. Only dog data were therefore modelled. Maximum PQ interval prolongations in dogs were 40 ms and maximum QRS interval widenings were 3 ms (Table 5.18). Significant QRS prolongations were observed at a single time point 2 hours after C_{max}, but reported as an unlikely effect of the compound. Important side effects included AV block.

Table 5.18 Summary of the acquired AZD8683 data.

Species	**Dog**
n	4
Dose	Inhalation: 0, 0.02, 0.1, 0.25 mg kg-1
C_{max} (μM)	0.048±0.02
QRS_0 (ms)	44±3
QRS_{max} (ms)	47±4
PQ_0 (ms)	116±6
PQ_{max} (ms)	156±19
Free drug (%)	4.39

Data presented as mean±SD. QRS_0, QRS at baseline; PR_0, PR at baseline; QRS_{max}, maximal QRS; PR_{max}, maximal PR.

5.5.2 PKPD modelling in dogs

5.5.2.1 PK modelling

Two and three compartment PK models were evaluated following visual inspection of log-normalised plasma concentrations, and a three compartment model was selected as this showed improved goodness of fit to the data. A lag time was included to account for a short delay between inhalation of the dose and the initial increase of plasma concentrations. The bioavailability was observed to decrease with dose and modelled according to

$$F = 1 - \frac{DOSE}{ED_{50} + DOSE} \tag{5.8}$$

where F is the relative bioavailability, ED_{50} the dose-dependent bioavailability and DOSE is the administered (inhaled) dose in nmol. It was assumed that $F \to 0$ as $DOSE \to \infty$. As F describes the relative bioavailability, the volume of distribution

of this model represents the true volume of distribution divided by the maximum bioavailability. Absorption to the central compartment was very fast and could be approximated as instantaneous without loss of goodness of fit. The proportional part of the estimated residuals was large (>45 %) with a high degree of shrinkage for the random variables resulting in bad fits to the individual data, especially at high concentrations. A fixed proportional error of 15 % improved the fit to high concentration data and improved the estimation of individual parameters. BSV for the volume of distribution, distribution to the third compartment and rate of elimination were reduced without loss of the goodness of fit to the data. The fits to data are shown in Figure 5.15. Estimated parameters for the selected PK model are summarised in Table 5.19 and goodness of fit plots are shown in Figure 5.16.

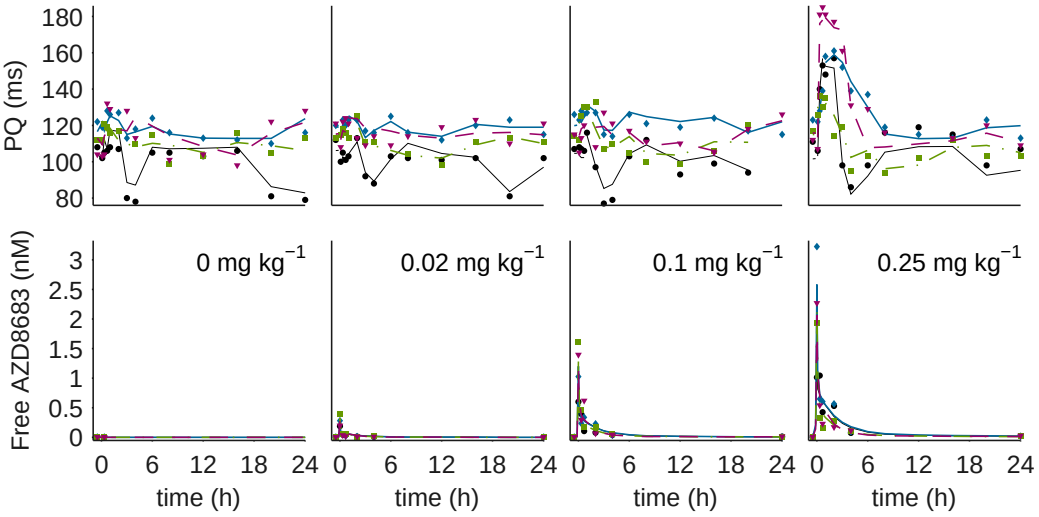

Figure 5.15 Unbound plasma concentration data (markers) and model fits (lines) for dogs treated with AZD9164.

Table 5.19 Parameter estimates for the dog AZD8683 PK model.

Parameter	Estimate (SE)	BSV % (SE)
ED_{50} (μmol)	1280 (710)	79.6 (36)
V (L kg^{-1})	2.45 (0.8)	-
k_{12} (h^{-1})	17.1 (11)	70.4 (28)
k_{21} (h^{-1})	3.59 (1.1)	55.6 (24)
k_{13} (h^{-1})	1.16 (0.002)	-
k_{31} (h^{-1})	0.064 (0.095)	-
k (h^{-1})	2.36 (0.89)	-
Additive residuals (μM)	0.695 (0.091)	
Proportional residuals	0.15 (fixed)	

BSV is presented as the coefficient of variation, approximated by CV% = SD*100 for log-normal distributions.

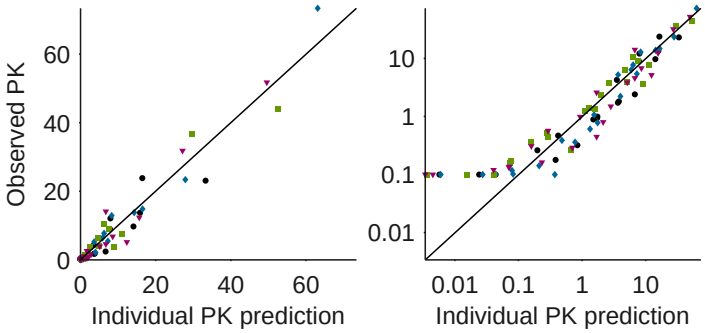

Figure 5.16 Observed data vs. individual model fits of AZD8683 concentration in linear (left) and log (right) scale with different colour/marker type for each subject. Initial horizontal points in the loglog plot are data below the limit of quantification.

5.5.2.2 PK-PQ drug effect modelling

The E_{max} model (Equation 2.2) with an effect compartment (Equation 2.5) best described PQ prolongations caused as a side effect by AZD8683. Summary statistics for a selection of tested models are provided in Table 5.20. BSV on the maximum effect did not improve the goodness of fit and was therefore removed. Although the SE of the exponent of the E_{max} model was large, this parameter was required to fit the data. The high SE was due to large variability of this value between the individual dogs. The fits to data are shown in Figure 5.17, final parameter estimates are summarised in Table 5.21 and goodness of fit plots are shown in Figure 5.18. Inclusion of both a circadian rhythm and RR correction (Equation 5.5) improved the goodness of fit to the full PQ data set and were therefore included, although circadian rhythm did not improve the goodness of fit to the vehicle data set (Section 5.3).

Table 5.20 Summary of a selection of the tested human AZD8683 PQ models.

Model	**Residuals**	**AIC**	**Relative likelihood**	**Comment**
Proportional	13.3	1755	2.89E-63	
Proportional, effect comp	10.5	1669	1.37E-44	Improved fit
Proportional, effect comp, RR corr, circ rhythm	8.37	1594	2.64E-28	Improved fit, high uncertainty BSV(A)
Proportional, effect comp, RR corr, circ rhythm, no BSV(A)	8.35	1591	1.19E-27	
E_{max}, effect comp, RR corr, circ rhythm, no BSV(A)	5.78	1467	1	Improved fit, high uncertainty BSV(E_{max})
E_{max}, effect comp, RR corr, circ rhythm, no BSV(A) or BSV(E_{max})	5.84	1468	0.607	**Selected model**

Table 5.21 Parameter estimates for the dog AZD8683 PQ model.

	Estimate (SE)	**BSV % (SE)**
$\boldsymbol{PQ_0}$ **(ms)**	109 (3)	4.53 (1.66)
$\boldsymbol{A}$ (%)	3.07 (0.61)	-
$\boldsymbol{\phi}$ **(h)**	3.30 (2.44)	139 (56)
$\boldsymbol{\alpha}$	0.194 (0.027)	21.6 (12.3)
$\boldsymbol{E_{max}}$ **(ms)**	61.0 (3.0)	-
$\boldsymbol{EC_{50}}$ **(nM)**	0.306 (0.042)	25.7 (10.0)
$\boldsymbol{n}$	6.52 (3.63)	98.7 (41.3)
$\boldsymbol{ke_0}$ **(h^{-1})**	0.632 (0.162)	48.0 (19.0)
Additive residuals (ms)	5.84 (0.30)	

BSV is presented as the coefficient of variation, approximated by CV% = SD*100 for log-normal distributions.

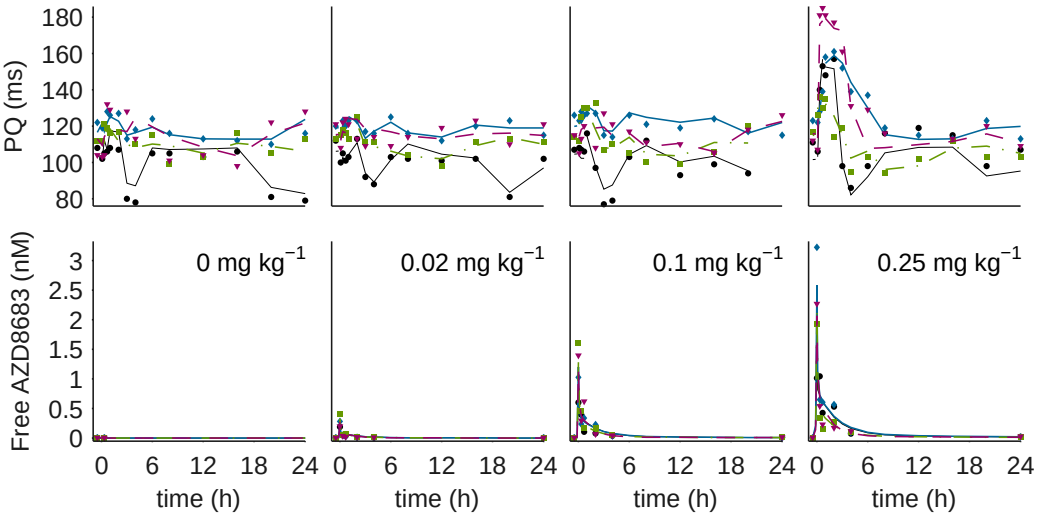

Figure 5.17 Top: PQ interval duration data (markers) and model fits (lines) for dogs treated with AZD8683. Bottom: Individual PK model parameters predicting the PK in each dog were used to drive the PD response. Individual dogs are separated by colour and marker type.

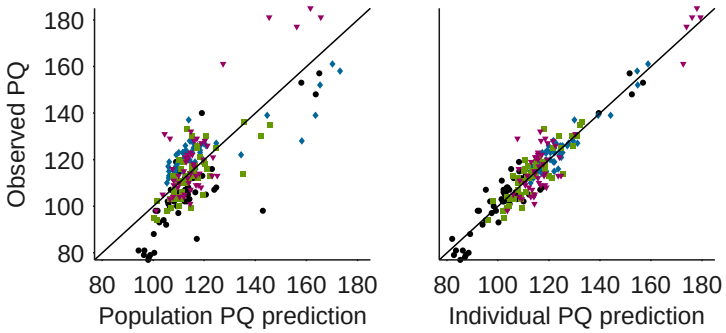

Figure 5.18 Population (left) and individual (right) model fits vs. observed PR intervals with different colour/marker type for each subject.

5.6 Modelling of AZD9164 data

5.6.1 Acquired data

Effects of AZD9164 were available in dogs from an in-house telemetry study and in human volunteers, and the compound was administered by inhalation. Neither PR nor QRS intervals were prolonged in humans, where maximum plasma concentrations of 13.2 nM AZD9164 (geometric mean, 75 CV%) were achieved. Only dog data were therefore modelled. Maximum PR interval prolongations in dogs were approximately 30 ms (Table 5.22) while no effects were observed on QRS intervals. Important side effects included AV block.

Table 5.22 Summary of the acquired AZD9164 data.

Species	**Dog**
n	6
Dose	Inhalation: 0, 0.019, 0.092, 0.220 mg kg-1
C_{max} (μM)	0.21±0.04
QRS_0 (ms)	47±5
QRS_{max} (ms)	No effect.
PR_0 (ms)	95±10
PR_{max} (ms)	124±30
Free drug (%)	12.7

Data presented as mean±SD. iv, intravenous; QRS_0, QRS at baseline; PR_0, PR at baseline; QRS_{max}, maximal QRS; PR_{max}, maximal PR. Δ QRS/PR change is provided for humans as change is from the highest dose group while baseline is from all groups.

5.6.2 PKPD modelling in dogs

5.6.2.1 PK modelling

AZD9164 exposure was only measured immediately pre- and post-dosing in the dog telemetry data set, limiting the possibility of developing a PK model using these data only as the distribution to peripheral compartments and elimination of AZD9164 are not captured in the data. Therefore, a dog tolerability inhalation study with similar study design (beagle dogs, similar inhalation duration and dose levels) was used to identify a population model of the PK profile of AZD9164. Between-subject variability in the distribution and elimination of AZD9164 was relatively small, as shown by C_{max}-normalised exposures of AZD9164 which all were within a ten-fold range (Figure 5.19). This suggests that typical parameters describing the distribution and elimination of AZD9164 can be used to predict exposure in the telemetry study, where only the exposures immediately following administration are known.

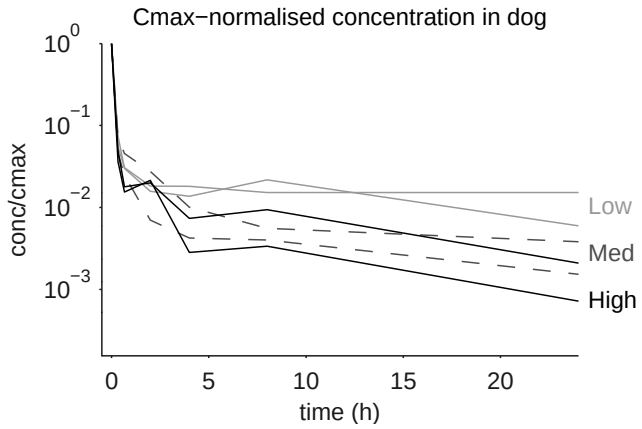

Figure 5.19 Normalised plasma concentration data over C_{max} plotted against time for the tolerability dog study of AZD9164. Data were available for 2 dogs receiving low (grey solid line), medium (dashed line) and high dose (black solid line). As the last 2 and 1 time points respectively are at the limit of quantification for the lowest dose, these points are likely to be closer to the medium and high dose than they appear in the plot.

Two and three compartment PK models were evaluated following visual inspection of log-normalised plasma concentrations, and a three compartment model was selected as this showed improved goodness of fit to the data. Absorption to the central compartment was very fast and could be assumed to be instantaneous. The proportional part of the estimated residual error was large (>30 %) resulting in poor fits to the maximal concentration data points. A fixed proportional error of 15 % improved the fits to the high concentration data. BSV was removed for all parameters except $V(/F)$ without loss of goodness of fit to the data.

For modelling exposure in the telemetry study, the distribution and elimination parameters were fixed to the values estimated in the tolerability study. To maximise the information capture from the single measured post-administration data point, a random inter-occasion variability was included for the volume of distribution. The fits to data are shown in Figure 5.20. Estimated parameters for the tolerability study PK model and the telemetry study PK model with re-parameterised volume of distribution are summarised in Table 5.23 and goodness of fit plots are shown in Figure 5.21.

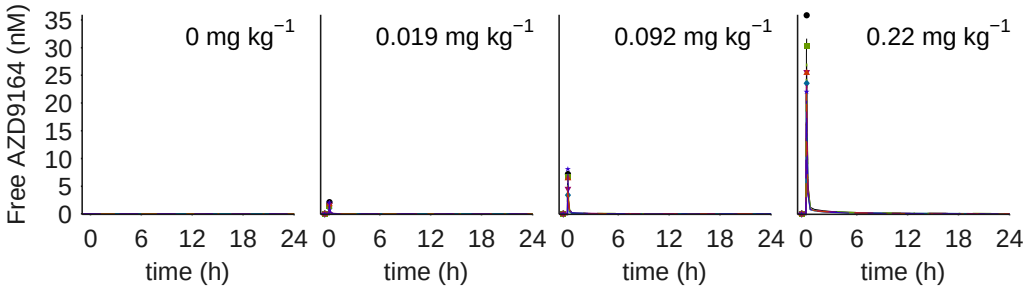

Figure 5.20 Unbound plasma concentration data (markers) and model fits (lines) for dogs treated with AZD9164.

Table 5.23 Parameter estimates for the dog AZD9164 PK models, with disposition parameter estimates generated using the PK data from a tolerability study and final volumes of distribution estimated from the PK data for the telemetry study.

	Tolerability study		**Telemetry study**	
Parameter	**Estimate (SE)**	**BSV % (SE)**	**Estimate (SE)**	**IOV % (SE)**
V **(L kg^{-1})**	2.25 (0.44)	40.7 (13)	2.3 (0.23)	40.3 (7.7)
k_{12} **(h^{-1})**	3.64 (0.75)	-	3.64 (fixed)	-
k_{21} **(h^{-1})**	0.704 (0.16)	-	0.704 (fixed)	-
k_{13} **(h^{-1})**	2.68 (0.88)	-	2.68 (fixed)	-
k_{31} **(h^{-1})**	0.135 (0.043)	-	0.135 (fixed)	-
k **(h^{-1})**	5.3 (0.42)	-	5.3 (fixed)	-
Add. res. (μM)	0.127 (0.033)		0.024 (0.016)	
Prop. res.	0.15 (fixed)		0.15 (fixed)	

BSV and IOV are presented as the coefficient of variation, approximated by CV% = SD*100 for log-normal distributions.

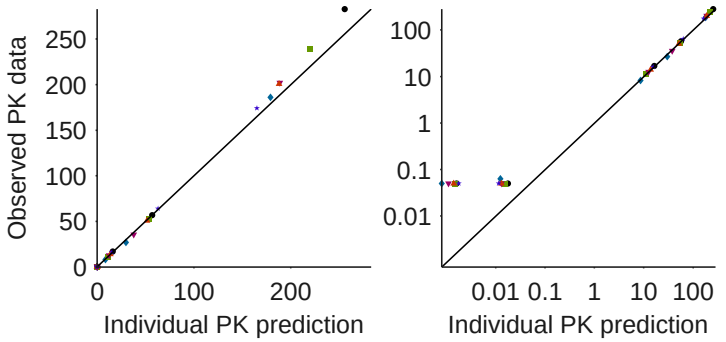

Figure 5.21 Observed data vs. individual model fits of AZD9164 concentration in linear (left) and log (right) scale with different colour/marker type for each subject. Initial horizontal points in the loglog plot are data below the limit of quantification.

5.6.2.2 PK-PR drug effect modelling

The E_{max} model (Equation 2.2) with an effect compartment (Equation 2.5) best described PR prolongations caused as a side effect by AZD9164. Summary statistics for a selection of tested models are provided in Table 5.24. BSV on the maximum effect did not improve goodness of fit and was therefore removed. Although the SE of the exponent of the E_{max} model was large, this parameter was required to fit the data. The high SE was due to large variability of this value between the individual dogs. The fits to data are shown in Figure 5.22, final parameter estimates are summarised in Table 5.25 and goodness of fit plots are shown in Figure 5.23. Similar results were obtained for modelling baseline variability between the full data set and the vehicle only data set, where inclusion of both the circadian rhythm and RR correction models improved the goodness of fits (Equation 5.5).

Table 5.24 Summary of a selection of the tested human AZD9164 PR models.

Model	**Residuals**	**AIC**	**Relative likelihood**	**Comment**
Proportional, effect comp	5.19	4674	1.6E-66	Improved fit
Proportional, effect comp, RR corr, circ rhythm	4.85	4600	1.88E-50	Improved fit
E_{max}, effect comp, RR corr, circ rhythm	4.16	4433	3.44E-14	Improved fit, high uncertainty BSV(A) and BSV(E_{max})
E_{max}, effect comp, RR corr, circ rhythm, no BSV(A) or BSV(E_{max})	3.98	4371	1	**Selected model**

Table 5.25 Parameter estimates for the dog AZD9164 PR model.

	Estimate (SE)	**BSV % (SE)**
$\boldsymbol{PR_0}$ **(ms)**	92.4 (3.3)	8.59 (2.50)
$\boldsymbol{A}$ **(%)**	2.76 (0.39)	-
$\boldsymbol{\phi}$ **(h)**	1.39 (3.47)	605 (179)
$\boldsymbol{\alpha}$	0.0688 (0.0196)	59.7 (22.9)
$\boldsymbol{E_{max}}$ **(ms)**	52.2 (1.4)	-
$\boldsymbol{EC_{50}}$ **(nM)**	3.39 (1.37)	87.5 (29.8)
$\boldsymbol{n}$	7.81 (3.07)	84.5 (29.3)
$\boldsymbol{ke_0}$ **(h^{-1})**	1.74 (1.03)	136 (43)
Additive residuals (ms)	3.98 (0.11)	

BSV and IOV are presented as the coefficient of variation, approximated by CV% = SD*100 for log-normal distributions.

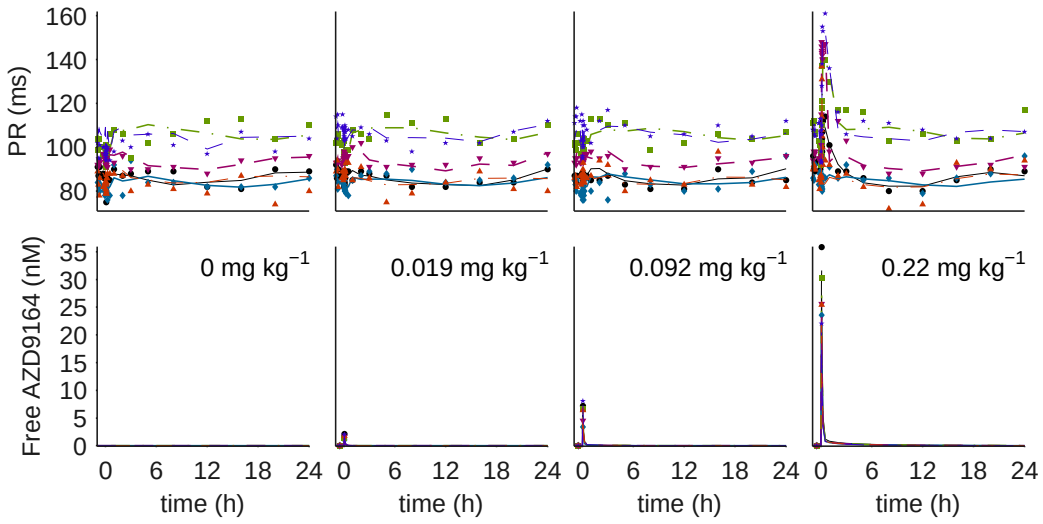

Figure 5.22 Top: PR interval duration data (markers) and model fits (lines) for dogs treated with AZD9164. Bottom: Individual PK model parameters predicting the PK in each dog were used to drive the PD response. Individual dogs are separated by colour and marker type.

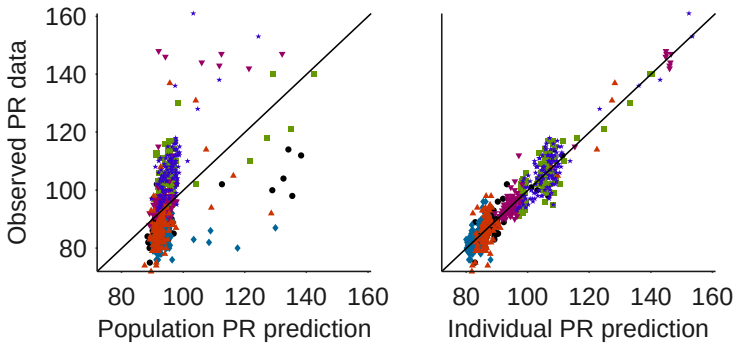

Figure 5.23 Population (left) and individual (right) model fits vs. observed PR intervals with different colour/marker type for each subject.

5.7 Modelling of flecainide data

5.7.1 Acquired data

Maximum QRS interval widenings were 6, 9 and 31 ms in guinea pigs, dogs and humans respectively and maximum PR interval prolongations were 9, 25 and 56 ms (Table 5.26). Similar exposures were acquired in guinea pigs and humans, while exposures in dogs were approximately doubled. However, as the free fraction estimated *in vitro* was smaller in dogs compared to guinea pigs and humans, the exposure of free drug may be more similar.

Table 5.26 Summary of the acquired flecainide data.

Species	Guinea pig	Dog	Human
Source of data	In-house: Single study	In-house: Single study	Literature: 16 published studies
n	4 veh + 4 treat	4	Many
Dose	iv: 0, 0.3, 1, 3 mg kg^{-1}	oral: 0, 3, 10, 20 mg kg^{-1}	iv: 1.5-2 mg kg^{-1}, 150 mg. oral: 100-600 mg
C_{max} (μM)	2.70±0.52	4.5±2.2	2.6
QRS_0 (ms)	24±2	55±5	92.5
QRS_{max} (ms)	30±4	64±11	31 (Δ)
PR_0 (ms)	55±12	97±7	160
PR_{max} (ms)	64±12	118±11	56 (Δ)
Free drug (%)	57	36.9[a]	62.1

Data presented as mean±SD. iv, intravenous; QRS_0, QRS at baseline; PR_0, PR at baseline; QRS_{max}, maximal QRS; PR_{max}, maximal PR; Δ, QRS or PR change from baseline. [a][21]

5.7.2 PKPD modelling in guinea pigs

5.7.2.1 PK modelling

Compartmental models with 1 and 2 compartments were tested following visual inspection of the log-normalised PK data and a 2 compartment model was selected to describe plasma concentrations following flecainide infusion (Figure 5.24). Estimated parameters for the selected PK model are summarised in Table 5.27 and goodness of fit plots are shown in Figure 5.25.

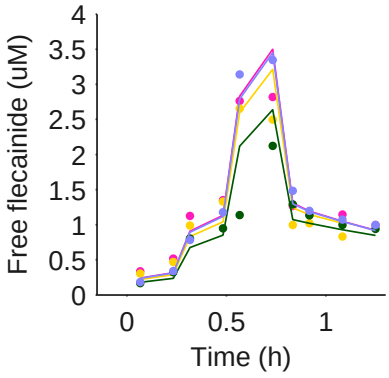

Figure 5.24 Unbound plasma concentration data (markers) and model fits (lines) for guinea pigs treated with three 15 min ascending doses of flecainide (circle) or with vehicle (black cross). Individual guinea pigs treated with flecainide are separated by colour.

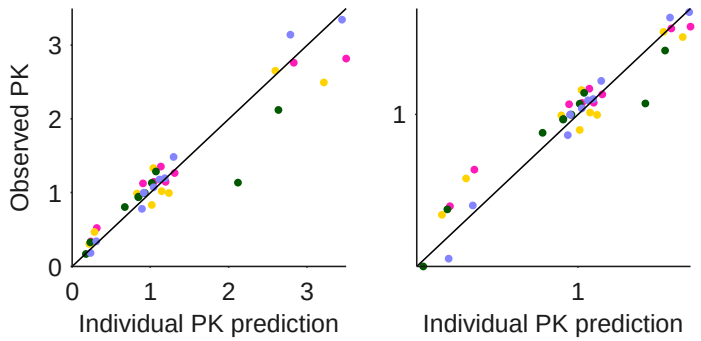

Figure 5.25 Observed data vs. individual model fits of flecainide concentration in linear (left) and log (right) scale with different colour for each animal.

Table 5.27 Parameter estimates for the guinea pig flecainide PK model.

Parameter	Estimate (SE)	BSV % (SE)
V (L kg^{-1})	0.259 (0.111)	-
k_{12} (h^{-1})	38.2 (19.4)	21.3 (9.79)
k_{21} (h^{-1})	2.7 (0.582)	-
k (h^{-1})	14.2 (6.62)	-
Additive residuals (μM)	0.0848 (0.0196)	
Proportional residuals	0.1 (fixed)	

BSV is the coefficient of variation, approximated by CV% = ω*100 for log-normal distributions.

5.7.2.2 PK-QRS drug effect modelling

Visual inspection of the PK and PD data indicated delays between plasma concentration and QRS prolongations (see Figure 5.26). This was confirmed by the PKPD modelling, as the effect compartment model (Equation 2.5) improved the goodness of fit to QRS intervals following infusions of flecainide. Summary statistics for a selection of tested models are provided in Table 5.28. The power model (Equation 2.3) best described the flecainide-induced QRS prolongations. The fits to data are shown in Figure 5.26. Estimated parameters for the selected model are summarised in Table 5.29 and goodness of fit plots are shown in Figure 5.27. The PKPD model was developed using the full data set including animals receiving vehicle and animals receiving flecainide. No correlations were observed between QRS and HR, and the RR correction model (Equation 5.4) did not improve the goodness of fit. Circadian rhythms were not evaluated due to the short experimental time (2h).

Table 5.28 Summary of a selection of the tested guinea pig flecainide QRS models.

Model	Residuals	AIC	Relative likelihood	Comment
Proportional	2.14	627.4	1.34E-54	
Proportional, effect comp	0.952	431.7	4.18E-12	Improvement
Proportional, effect comp, HR corr	0.953	435.9	5.12E-13	No improvement
Power, effect comp	0.775	383.7	0.111	Improvement, high uncertainty BSV(a)
Power, effect comp, no BSV(a)	0.776	379.3	1	**Selected model**

Table 5.29 Parameter estimates for the guinea pig flecainide QRS model.

	Estimate (SE)	BSV % (SE)
QRS_0 (ms)	21.7 (0.893)	11.6 (2.92)
a	16.9 (1.66)	-
b	2.46 (0.365)	23.4 (9.15)
ke_0 (h^{-1})	1.6 (0.111)	-
Additive residuals (ms)	0.776 (0.0495)	-

BSV is the coefficient of variation, approximated by CV% = ω*100 for log-normal distributions.

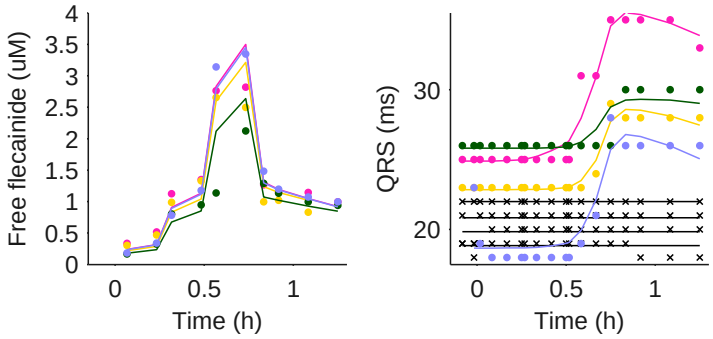

Figure 5.26 Left: Individual PK model parameters predicting the PK in each guinea pig were used to drive the PD response. Right: QRS interval duration data (markers) and model fits (lines) for guinea pigs treated with three 15 min ascending doses of flecainide (circle) or with vehicle (black cross). Individual guinea pigs treated with flecainide are separated by colour.

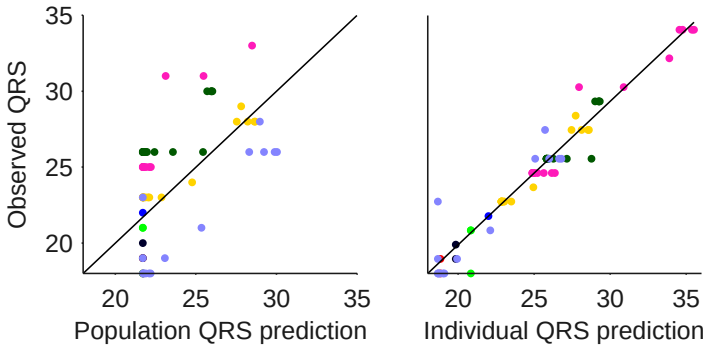

Figure 5.27 Population (left) and individual (right) model fits vs. observed QRS intervals with different colour for each animal.

5.7.2.3 PK-PR drug effect modelling

Visual inspection of the PK and PD data indicated delays between plasma concentration and PR prolongations (see Figure 5.28). This was confirmed by the PKPD modelling, as the effect compartment model (Equation 2.5) improved the goodness of fit to PR intervals following infusions of flecainide. Summary statistics for a selection of tested models are provided in Table 5.28. A power model (Equation 2.3) best described the flecainide-induced PR prolongations. The fits to data are shown in Figure 5.28. Estimated parameters of the selected model are summarised in Table 5.31 and goodness of fit plots are shown in Figure 5.29. The HR correction model (Equation 5.4) did improve the goodness of fit to PR interval data. The exponent of the PR-HR correction was assumed the same for all animals. Circadian rhythms were not evaluated due to the short experimental time (2h).

Table 5.30 Summary of a selection of the tested guinea pig flecainide PR models.

Model	**Residuals**	**AIC**	**Relative likelihood**	**Comment**
Proportional	2.43	691.8	3.1E-12	
Proportional, effect comp	2.14	664.4	0.00000276	Improvement
Proportional, effect comp, HR corr, no BSV(α)	1.94	641.7	0.235	Improvement, high uncertainty BSV(k_{e0})
Proportional, effect comp, HR corr, no BSV(α) or BSV(k_{e0})	1.95	639.8	0.607	**Selected model**
Power, effect comp, HR corr, no BSV(α)	1.87	638.8	1	No improvement

Table 5.31 Parameter estimates for the guinea pig flecainide PR model.

	Estimate (SE)	BSV % (SE)
PR_0 (ms)	57 (4.39)	21.8 (5.45)
α	0.31 (0.0575)	-
$slope_u$ (ms μM^{-1})	4.14 (1.84)	82 (31.4)
ke_0 (h^{-1})	11.9 (3.62)	-
Additive residuals (ms)	1.95 (0.124)	

BSV is the coefficient of variation, approximated by CV% = ω*100 for log-normal distributions.

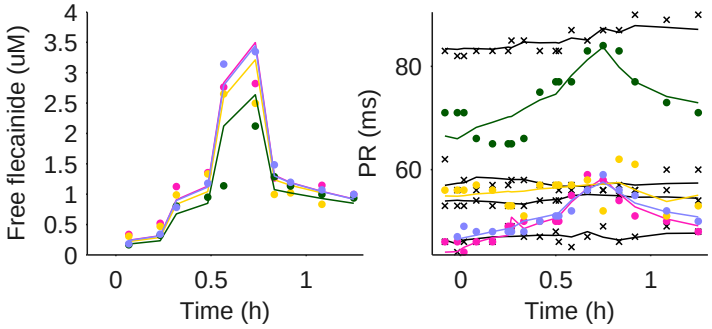

Figure 5.28 Left: Individual PK model parameters predicting the PK in each guinea pig were used to drive the PD response. Right: PR interval duration data (markers) and model fits (lines) for guinea pigs treated with three 15 min ascending doses of flecainide (circle) or with vehicle (black cross). Individual guinea pigs treated with flecainide are separated by colour.

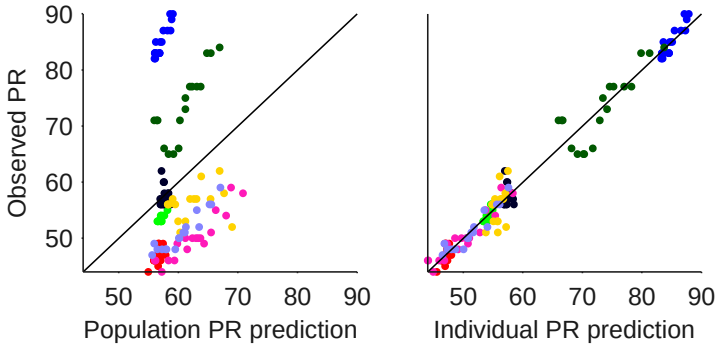

Figure 5.29 Population (left) and individual (right) model fits vs. observed PR intervals with different colour for each animal.

5.7.3 PKPD modelling in dogs

5.7.3.1 PK modelling

A one compartment model was fitted to the plasma concentrations following oral treatment with flecainide following visual inspection of the log-normalised data (Fig-

ure 5.30). A zero order absorption model improved the goodness of fit to the data compared to first order absorption, and was therefore selected. The proportional part of the estimated residual error was large (>40 %) with a high degree of shrinkage for the random variables resulting in a poor fit to individual data, especially at high concentrations. A fixed proportional error of 15 % improved the fit to the high concentration data and improved the estimation of individual parameters. BSV effects on the rate of elimination from the central compartment (k_e) could not be identified (SE >100%) and the same elimination rate was therefore assumed for all dogs. Estimated parameters of the selected PK model are summarised in Table 5.32 and goodness of fit plots are shown in Figure 5.31.

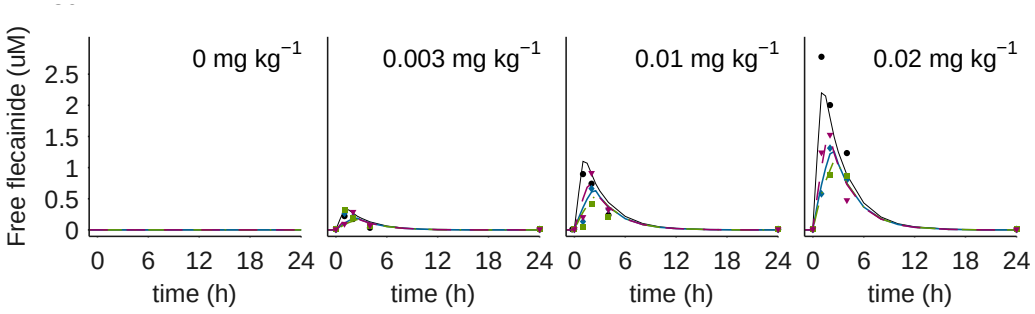

Figure 5.30 Unbound plasma concentration data (markers) and model fits (lines) for dogs treated with flecainide.

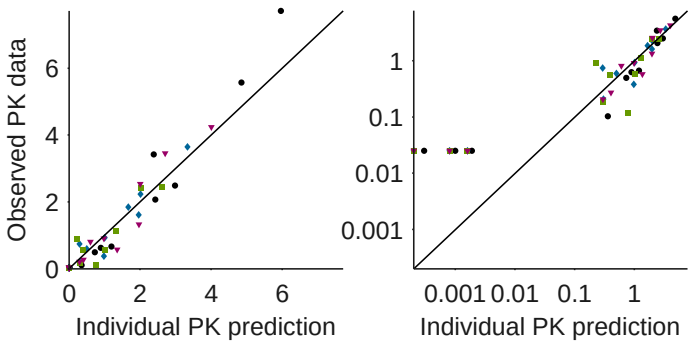

Figure 5.31 Observed data vs. individual model fits of flecainide concentration in linear (left) and log (right) scale with different colour/marker type for each animal. One animal shows highly variable PK data at low concentrations causing large errors (green squares). Initial horizontal points in the right plot are below the limit of quantification.

Table 5.32 Parameter estimates for the dog flecainide PK model.

Parameter	Estimate (SE)	BSV % (SE)
k_a (μmol h^{-1})	1.81[a] (0.42)	37.9 (16)
V (L kg^{-1})	8.1 (1.6)	21.4 (10)
k (h^{-1})	0.356 (0.091)	-
Additive residuals (μM)	0.257 (0.061)	
Proportional residuals	0.15 (fixed)	

BSV is the coefficient of variation, approximated by CV% = SD*100 for log-normal distributions. [a]Zero-order absorption.

5.7.3.2 PK-QRS drug effect modelling

A proportional direct effect model (Equation 2.4) well characterised the flecainide-induced QRS prolongations (Figure 5.32). Summary statistics for a selection of tested models are provided in Table 5.33. The direct effect model was selected despite slightly improved goodness of fit for the effect comparmtment model. As the data showed high variability and the PR data did not support the effect compartment model, it was concluded that any potential delay could not be estimated confidently. Estimated parameters for the selected model are summarised in Table 5.34 and goodness of fit plots are shown in Figure 5.33. While inclusion of RR correction (Equation 5.4) improved the goodness of fit to the vehicle only data, the constant model (Equation 5.2) equally well described the full flecainide data set and was therefore selected.

Table 5.33 Summary of a selection of the tested dog flecainide QRS models.

Model	Residuals	AIC	Relative likelihood	Comment
Proportional	2.65	1414	0.00248	**Selected model**
Proportional, RR corr	2.65	1418	0.000335	No improvement
Proportional, RR corr, circ	2.61	1420	0.000123	No improvement
Proportional, effect comp	2.58	1402	1	Improvement

Table 5.34 Parameter estimates for the dog flecainide QRS model.

	Estimate (SE)	BSV % (SE)
$\boldsymbol{QRS_0}$ **(ms)**	53.6 (1.5)	5.68 (2.03)
$\boldsymbol{slope_u}$ **(ms** μ**M^{-1})**	5.38 (0.95)	30.8 (14.3)
Additive residuals (ms)	2.65 (0.11)	

BSV is the coefficient of variation, approximated by CV% = SD*100 for log-normal distributions.

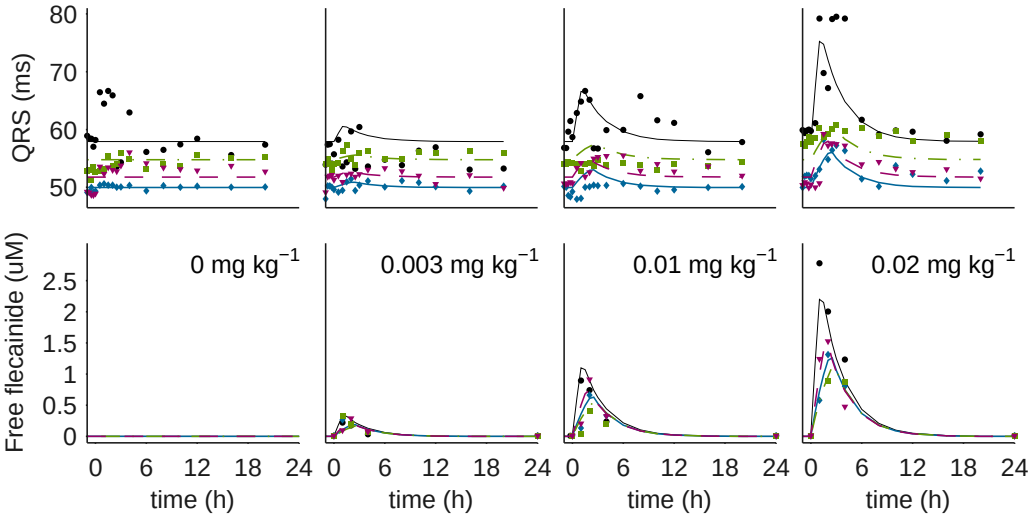

Figure 5.32 Top: QRS interval duration data (markers) and model fits (lines) for dogs treated with flecainide. Bottom: Individual PK model parameters predicting the PK in each dog were used to drive the PD response. Individual dogs are separated by colour and marker type.

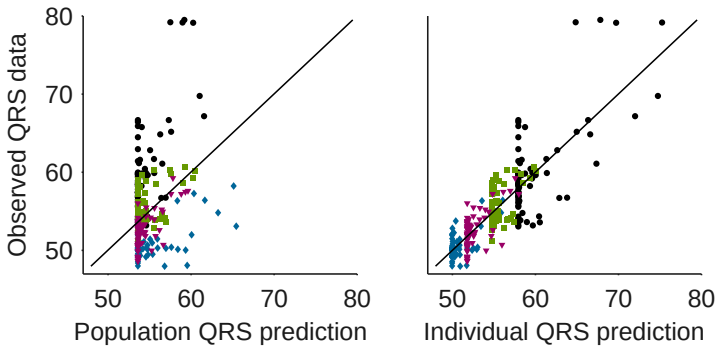

Figure 5.33 Population (left) and individual (right) model fits vs. observed QRS intervals with different colour/marker type for each animal.

5.7.3.3 PK-PR drug effect modelling

A proportional direct effect model (Equation 2.4) well characterised the flecainide-induced PR prolongations (Figure 5.34). Summary statistics for a selection of tested

models are provided in Table 5.35. Estimated parameters for the selected PR model are summarised in Table 5.36 and goodness of fit plots are shown in Figure 5.35. Inclusion of the circadian rhythm model (Equation 5.3), but not the RR correction model (Equation 5.4), improved the goodness of fits to the full flecainide data set, while both improved the goodness of fits to the vehicle data.

Table 5.35 Summary of a selection of the tested dog flecainide PR models.

Model	**Residuals**	**AIC**	**Relative likelihood**	**Comment**
Proportional	6.42	1915	3.58E-29	
Proportional, RR corr	6.27	1910	4.36E-28	
Proportional, circ rhythm	4.93	1787	0.223	Improvement, high uncertainty BSV(ϕ)
Proportional, circ rhythm, no BSV(ϕ)	4.97	1785	0.607	**Selected model**
Proportional, RR corr, circ rhythm, no BSV(ϕ)	4.87	1784	1	No improvement
Proportional, circ rhythm, effect comp, no BSV(ϕ)	4.92	1790	0.0498	No improvement

Table 5.36 Parameter estimates for the dog flecainide PR model.

	Estimate (SE)	**BSV % (SE)**
$\boldsymbol{PR_0}$ **(ms)**	95.8 (2.3)	4.76 (1.72)
$\boldsymbol{A}$ **(%)**	4.60 (1.39)	55.6 (22.8)
$\boldsymbol{\phi}$ **(h)**	0.035 (0.369)	-
$\boldsymbol{slope_u}$ **(ms** μ**M^{-1})**	11.0 (1.2)	13.3 (10.9)
Additive residuals (ms)	4.97 (0.21)	

BSV is presented as the coefficient of variation, approximated by CV% = SD*100 for log-normal distributions.

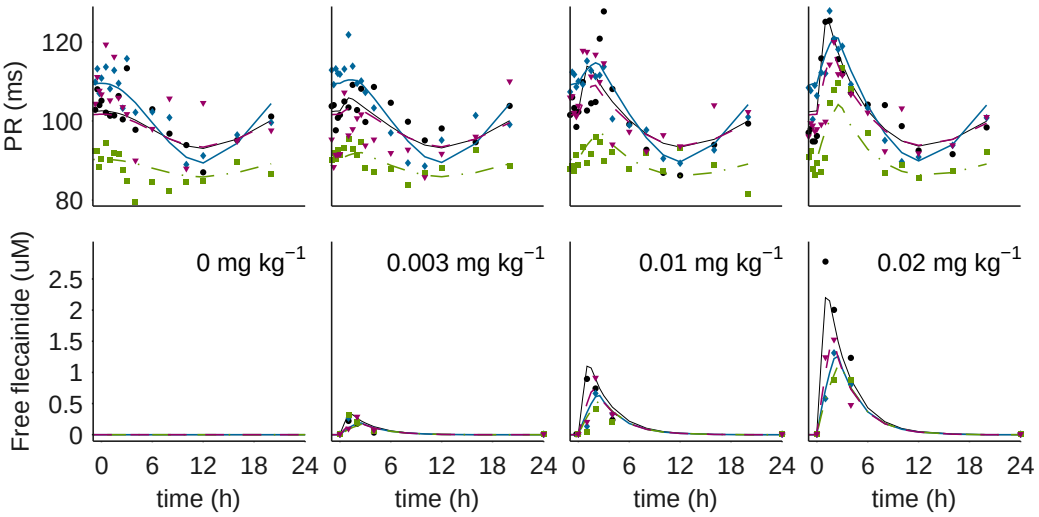

Figure 5.34 Top: PR interval duration data (markers) and model fits (lines) for dogs treated with flecainide. Bottom: Individual PK model parameters predicting the PK in each dog were used to drive the PD response. Individual dogs are separated by colour and marker type.

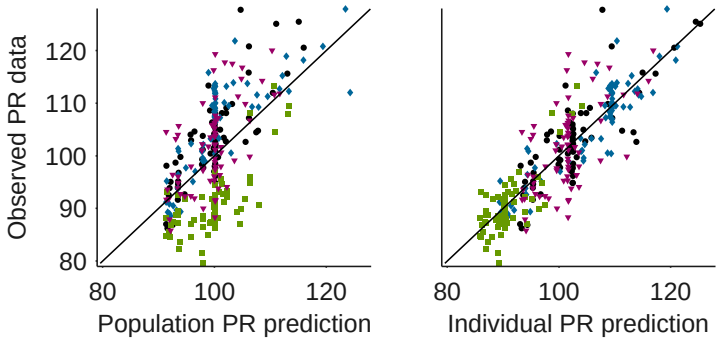

Figure 5.35 Population (left) and individual (right) model fits vs. observed PR intervals with different colour/marker type for each animal.

5.8 Modelling of quinidine data

5.8.1 Acquired data

Maximum QRS interval widenings were 5 and 18 ms in dogs and humans respectively (Table 5.37). PR was increased only at a single time point 2.5 h after dosing in the single dog dosed with 50 mg kg^{-1} quinidine. Treatment of 50 mg kg^{-1} quinidine was stopped in the remaining dogs due to adverse effects in the single 50 mg kg^{-1} dosed dog. Total exposures were doubled in dogs compared to humans, while exposures of unbound quinidine were similar due to differences in free fractions.

Table 5.37 Summary of the acquired quinidine data.

Species	**Dog**	**Human**
Source of data	In-house: Single study	Literature: 15 published studies
n	4	Many
Dose	oral: vehicle, 10, 25, 50[a] mg kg^{-1}	iv: 3.7-10 mg kg^{-1}. oral: 3 mg kg^{-1}, 100-2250 mg
C_{max} (μM)	24±12 (60)	12.3
QRS_0 (ms)	54±3 (52)	92.5
QRS_{max} (ms)	59±5 (61)	18 (Δ)
PR_0 (ms)	102±10 (95)	160
PR_{max} (ms)	n.e. (120)	-
Free drug (%)	6.18	12.2

Data presented as mean±SD. iv, intravenous; QRS_0, QRS at baseline; PR_0, PR at baseline; QRS_{max}, maximal QRS; PR_{max}, maximal PR; Δ, QRS or PR change from baseline. [a]n=1 for 50 mg dose.

5.8.2 PKPD modelling in dogs

5.8.2.1 PK modelling

A one compartment model was fitted to the quinidine exposure data following visual inspection of the log-normalised data (Figure 5.36). The bioavailability was observed to decrease with dose and this decrease was modelled according to Equation 5.8. BSV for the rate of absorption and the rate of elimination were removed as these parameters were not identifiable (SE >100%). Estimated parameters for the selected PK model are summarised in Table 5.38 and goodness of fit plots are shown in Figure 5.37.

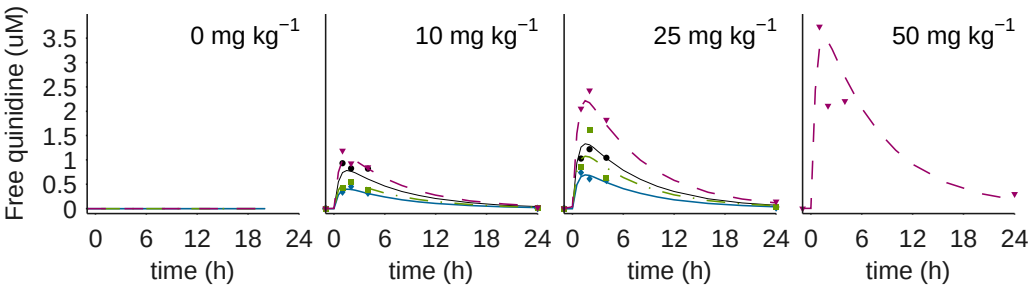

Figure 5.36 Unbound plasma concentration data (markers) and model fits (lines) for dogs treated with quinidine.

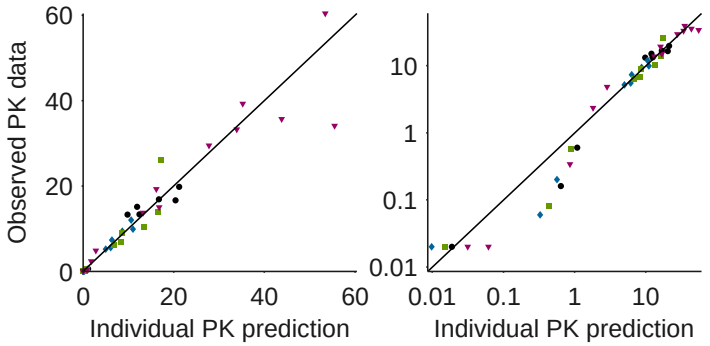

Figure 5.37 Observed data vs. individual model fits of quinidine concentration in linear (left) and log (right) scale with different colour/marker type for each animal. One animal shows highly variable PK data at low concentrations causing large errors (green squares). Initial horizontal points in th eright plot are below the limit of quantification.

Table 5.38 Parameter estimates for the dog quinidine PK model.

Parameter	Estimate (SE)	BSV % (SE)
k_a (μmol h^{-1})	1.79 (0.48)	-
ED_{50} (μmol)	124 (65)	66.1 (47)
V (L kg^{-1})	1.82 (0.43)	36.6 (17)
k (h^{-1})	0.137 (0.009)	-
Additive residuals (μM)	0.282 (0.12)	
Proportional residuals	0.207 (0.038)	

BSV is the coefficient of variation, approximated by CV% = SD*100 for log-normal distributions.

5.8.2.2 PK-QRS drug effect modelling

A proportional direct effect model (Equation 2.4) well characterised the quinidine-induced QRS prolongations (Figure 5.38). Summary statistics for a selection of tested models are provided in Table 5.39. Estimated parameters for the selected QRS model are summarised in Table 5.40 and goodness of fit plots are shown in Figure 5.39. A constant baseline model (Equation 5.2) equally well described baseline QRS variability compared to the RR correction and circadian rhythm models (Equations 5.4 and 5.3) when fitting both the vehicle only and the full data sets.

Table 5.39 Summary of a selection of the tested dog quinidine QRS models.

Model	Residuals	AIC	Relative likelihood	Comment
Proportional	2.19	830.8	0.301	High uncertainty on BSV(*slope*)
Proportional, no BSV(*slope*)	2.19	828.4	1	Selected model
Proportional, circ	2.12	831.1	0.259	No improvement
Proportional, RR corr	2.17	831.8	0.183	No improvement
Proportional, RR corr, circ	2.1	832.7	0.116	No improvement
Proportional, effect comp	2.19	834.2	0.055	Improvement

Table 5.40 Parameter estimates for the dog quinidine QRS model.

	Estimate (SE)	BSV % (SE)
$\boldsymbol{QRS_0}$ **(ms)**	53.3 (1.7)	6.25 (2.23)
$\boldsymbol{slope_u}$ **(ms** μ**M^{-1})**	3.00 (0.25)	-
Additive residuals (ms)	2.19 (0.12)	

BSV is the coefficient of variation, approximated by CV% = SD*100 for log-normal distributions.

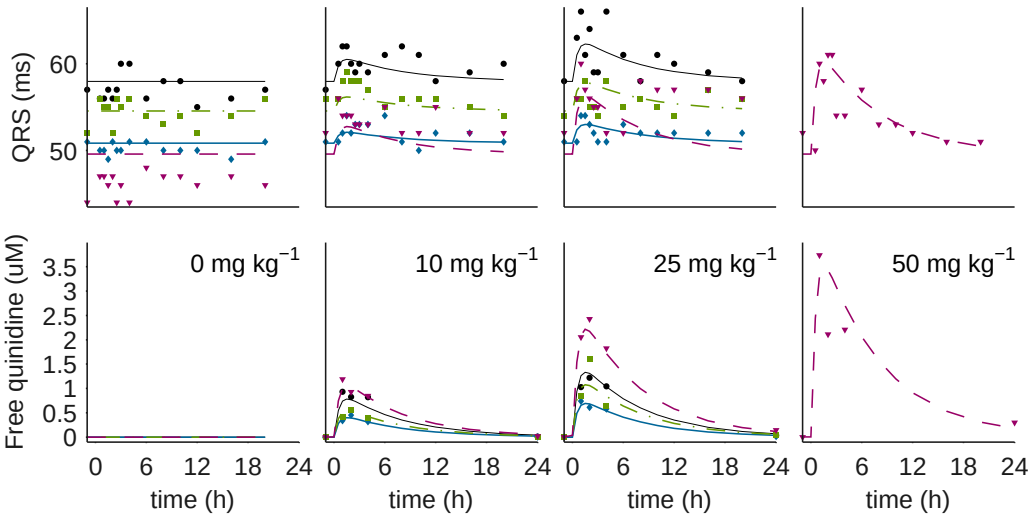

Figure 5.38 Top: QRS interval duration data (markers) and model fits (lines) for dogs treated with quinidine. Bottom: Individual PK model parameters predicting the PK in each dog were used to drive the PD response. Individual dogs are separated by colour and marker type.

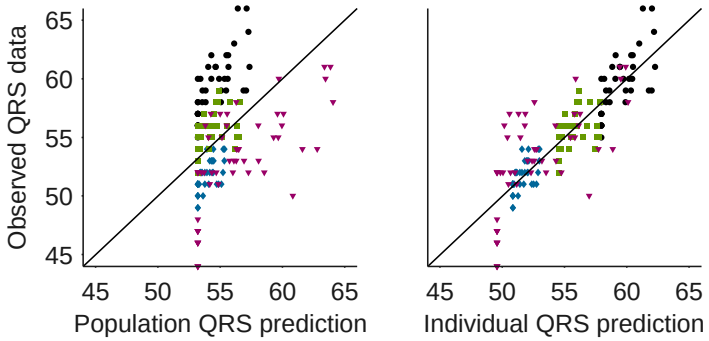

Figure 5.39 Population (left) and individual (right) model fits vs. observed QRS intervals with different colour/marker type for each dog.

5.9 Modelling of verapamil data

5.9.1 Acquired data

Maximum PR interval prolongations induced by verapamil were 16, 55 and 53 ms in guinea pigs, dogs and humans respectively (Table 5.41). No effect of verapamil was observed on QRS intervals. Exposures were doubled in guinea pigs and humans compared to dogs for both total and free drug.

Table 5.41 Summary of the acquired verapamil data.

Species	**Guinea pig**	**Dog**	**Human**
n	4 veh + 4 treat	4	16 studies
Dose	iv: vehicle, 0.1, 0.3, 1 mg kg^{-1}	oral: vehicle, 1, 5, 15 mg kg^{-1}	oral: 80-480 mg
C_{max} (μM)	1.97±0.26	0.78±0.26	1.7
QRS_0 (ms)	22±1	44±2	92.5
QRS_{max} (ms)	25±2[a] (NS)	n.e.	-
PR_0 (ms)	61±6	114±22	160
PR_{max} (ms)	77±5[a]	169±45	53 (Δ)
Free drug (%)	19.7	18.9	20.7

Data presented as mean±SD. iv, intravenous; QRS_0, QRS at baseline; PR_0, PR at baseline; QRS_{max}, maximal QRS; PR_{max}, maximal PR; Δ, QRS or PR change from baseline. [a]n=2 due to the death of 2 animals from compound-related effects.

5.9.2 PKPD modelling in guinea pigs

5.9.2.1 PK modelling

Compartmental models with 1 and 2 compartments were tested following visual inspection of the log-normalised PK data and a 2 compartment model was selected

to describe plasma concentrations following verapamil infusion (Figure 5.40). Estimated parameters for the selected PK model are summarised in Table 5.42 and goodness of fit plots are shown in Figure 5.41.

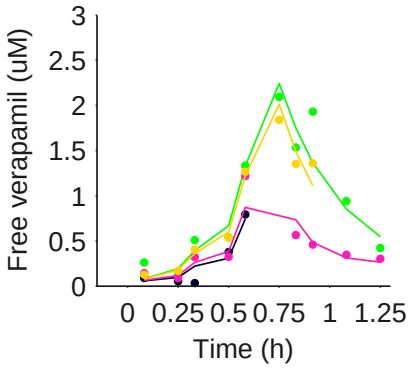

Figure 5.40 Unbound plasma concentration data (markers) and model fits (lines) for guinea pigs treated with three 15 min ascending doses of verapamil (circle) or with vehicle (black cross). Individual guinea pigs treated with verapamil are separated by colour.

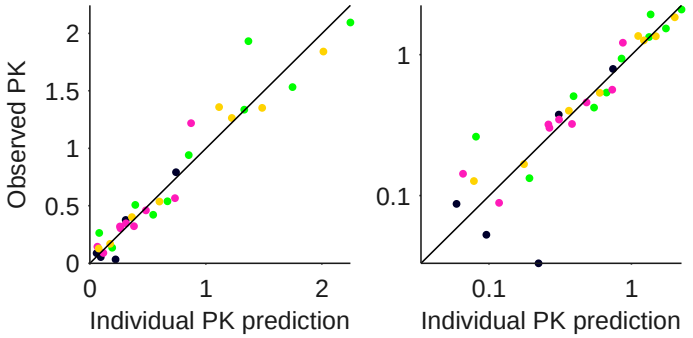

Figure 5.41 Observed data vs. individual model fits of flecainide concentration in linear (left) and log (right) scale with different colour/marker type for each animal.

Table 5.42 Parameter estimates for the guinea pig verapamil PK model.

Parameter	Estimate (SE)	BSV % (SE)
V (L kg^{-1})	0.362 (0.0415)	-
k_{12} (h^{-1})	1.94 (1.94)	145 (57)
k_{21} (h^{-1})	1.07 (0.553)	-
k (h^{-1})	2.71 (0.523)	-
Additive residuals (μM)	0.0679 (0.0203)	
Proportional residuals	0.127 (0.0465)	

BSV is the coefficient of variation, approximated by CV% = SD*100 for log-normal distributions.

5.9.2.2 PK-PR drug effect modelling

Visual inspection of the PK and PD data indicated delays between verapamil plasma concentration and PR prolongations (see Figure 5.42). This was confirmed by the PKPD modelling, as the effect compartment model (Equation 2.5) improved the goodness of fit to PR intervals following infusions of verapamil. Summary statistics for a selection of tested models are provided in Table 5.43. Verapamil-induced PR prolongations were well described by a proportional model (Equation 2.4). Estimated parameters of the selected PR model are summarised in Table 5.44 and goodness of fit plots are shown in Figure 5.43. The fits to data are shown in Figure 5.42. Inclusion of the HR correction model (Equation 5.4) did not improve the fit to PR intervals in either the vehicle only or full data set. Circadian rhythms were not evaluated due to the short experimental time (2h).

Table 5.43 Summary of a selection of the tested guinea pig verapamil PR models.

Model	**Residuals**	**AIC**	**Relative likelihood**	**Comment**
Proportional	3.96	800.8	3.32E-19	
Proportional, effect comp	2.7	717.8	0.35	Improvement, high uncertainty BSV(k_{e0})
Proportional, effect comp, no BSV(k_{e0})	2.7	715.7	1	**Selected model**
Proportional, effect comp, HR corr, no BSV(α)	2.7	719.7	0.135	No improvement
Power, effect comp, HR corr, no BSV(α)	2.66	721.3	0.0608	No improvement

Table 5.44 Parameter estimates for the guinea pig verapamil PR model.

	Estimate (SE)	**BSV % (SE)**
$\boldsymbol{PR_0}$ **(ms)**	61.6 (1.64)	7.42 (1.91)
$\boldsymbol{slope_u}$ **(ms** μ**M^{-1})**	161 (69.7)	-
$\boldsymbol{ke_0}$ **(h^{-1})**	1.07 (0.801)	86.8 (32.7)
Additive residuals (ms)	2.7 (0.171)	-

BSV is the coefficient of variation, approximated by CV% = SD*100 for log-normal distributions.

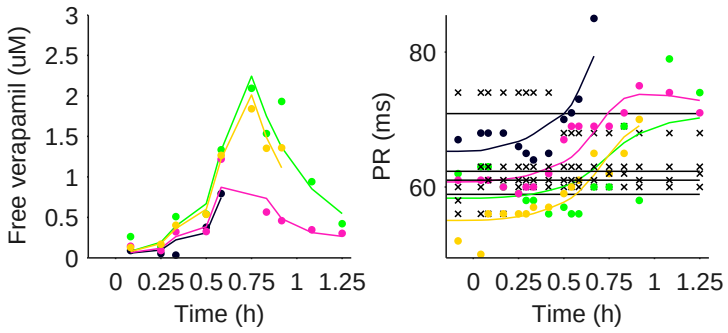

Figure 5.42 Left: Individual PK model parameters predicting the exposure in each guinea pig were used to drive the PD response. Right: PR interval duration data (markers) and model fits (lines) for guinea pigs treated with three 15 min ascending doses of verapamil (circles) or with vehicle (black cross). Individual guinea pigs treated with flecainide are separated by colour.

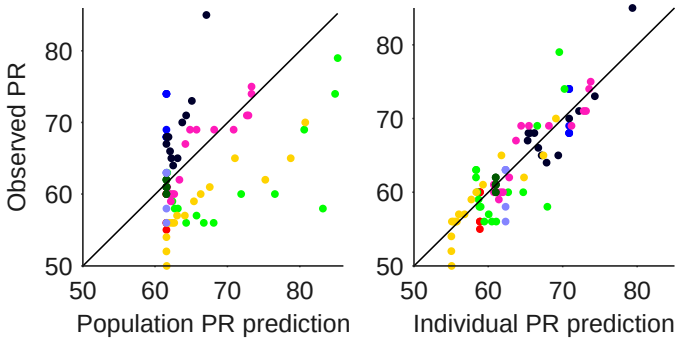

Figure 5.43 Population (left) and individual (right) model fits vs. observed PR intervals with different colour for each guinea pig.

5.9.3 PKPD modelling in dogs

5.9.3.1 PK modelling

One and two compartment models were evaluated following visual inspection of the log-normalised data and a two compartment model was selected to describe exposure following oral administration of verapamil. Exposure in one dog following 15 mg kg^{-1} verapamil was around tenfold lower than expected considering exposure following the other two doses in this dog and exposure following the 15 mg kg^{-1} dose in the other dogs. High similarity between all other data and clear effects in the PD data for this dose indicate that these data may be erroneous. The PK data for 15 mg kg^{-1} in dog 2 were therefore excluded. The PK prediction was used in the PKPD modelling step as normal. The bioavailability was observed to increase with dose. This increase was modelled according to Equation 5.7. ED_{50} could not be identified from the data as saturation was not reached, and was therefore fixed. 2 different values above the maximal tested dose were tested, namely 50 and 100 μmol. Both

resulted in accurate capture of the increased bioavailability and similar goodness of fits to the data. An ED_{50} of 100 μmol was selected based on a slightly improved performance. Furthermore, the absorption phase was not captured in the data. Fast absorption compared to elimination was assumed, and the first order rate parameter was estimated according to

$$k_{abs} = \frac{\ln C_1 - \ln C_0}{t_1 - t_0} \tag{5.9}$$

where t_0 is time of dosing and t_1 the first measured time point for the highest dose. Absorption was fixed at this value (4 h^{-1}). BSVs for the rate of distribution from the peripheral to the central compartment and the rate of elimination could not be fitted and were therefore removed. The fits to data are shown in Figure 5.44. Estimated parameters for the selected PK model are summarised in Table 5.32 and goodness of fit plots are shown in Figure 5.45.

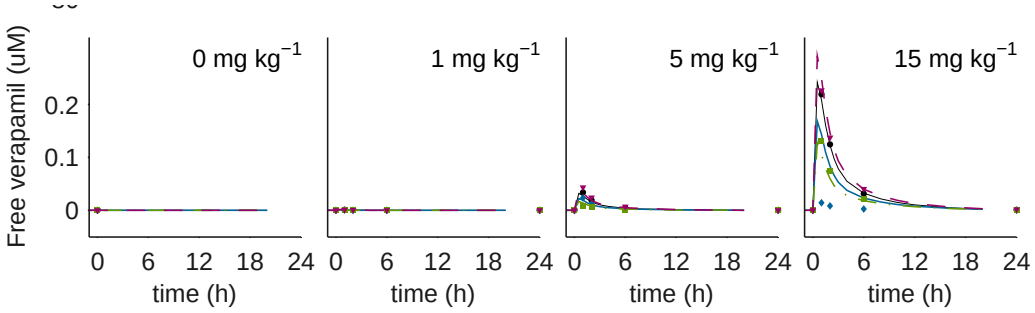

Figure 5.44 Unbound plasma concentration data (markers) and model fits (lines) for dogs treated with verapamil.

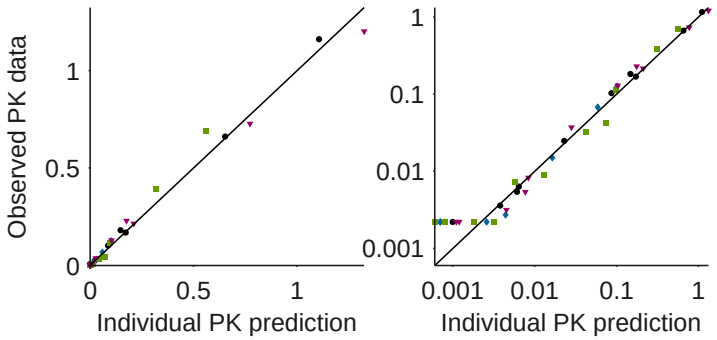

Figure 5.45 Observed data vs. individual model fits of verapamil concentration in linear (left) and log (right) scale with different colour/marker type for each animal. One animal shows highly variable PK data at low concentrations causing large errors (green squares). Initial horizontal points in the right plot are below the limit of quantification.

Table 5.45 Parameter estimates for the dog verapamil PK model.

Parameter	Estimate (SE)	BSV % (SE)
k_a (μmol h^{-1})	4 (fixed)	-
V (L kg^{-1})	100 (fixed)	-
k_{12} (h^{-1})	0.283 (0.033)	20.5 (9.8)
k_{21} (h^{-1})	0.352 (0.035)	-
k (h^{-1})	0.443 (0.029)	-
Additive residuals (μM)	0.00035 (0.00012)	
Proportional residuals	0.22 (0.038)	

BSV is coefficient of variation, approximated by CV% = SD*100 for log-normal distributions. [a]Zero-order absorption.

5.9.3.2 PK-PR drug effect modelling

The E_{max} direct effect model (Equation 2.2) well characterised the verapamil-induced PR prolongations. Summary statistics for a selection of tested models are provided in Table 5.46. The maximum effect E_{max} was assumed to be the same for all dogs. The shape factor n was fixed to 1 as this was required for successful parameter estimation. Estimated parameters for the selected model are summarised in Table 5.47 and goodness of fit plots are shown in Figure 5.47. The fits to data are shown in Figure 5.46. Inclusion of the RR correction model (Equation 5.4) but not the circadian rhythm model (Equation 5.3) improved the goodness of fits to the vehicle only and the full data sets.

Table 5.46 Summary of a selection of the tested dog verapamil PR models.

Model	Residuals	AIC	Relative likelihood	Comment
Proportional, RR corr	7.55	1924	1.04E-15	
E_{max}, RR corr	-	-	-	Parameter estimation failure
E_{max}, RR corr, no BSV(n)	6.55	1862	0.0302	Improvement
E_{max}, RR corr, no BSV(n) or BSV(E_{max})	6.83	1870	0.000553	Small drop in AIC
E_{max}, RR corr, effect comp, no BSV(n)	6.56	1855	1	Small improvement, fast k_{e0}

Table 5.47 Parameter estimates for the dog verapamil PR model.

	Estimate (SE)	BSV % (SE)
PR_0 (ms)	111 (6.13)	11 (3.91)
α	0.132 (0.0148)	-
E_{max} (ms)	105 (9.23)	-
EC_{50} (nM)	0.196 (0.0881)	83.6 (30.6)
n	1 (fixed)	-
Additive residuals (ms)	6.84 (0.298)	

BSV is presented as the coefficient of variation, approximated by CV% = SD*100 for log-normal distributions.

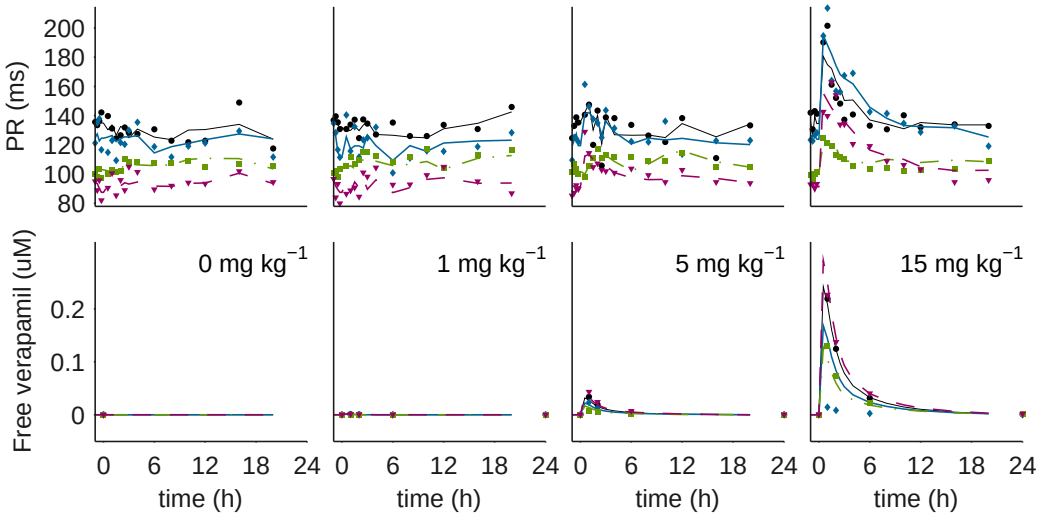

Figure 5.46 Top: PR interval duration data (markers) and model fits (lines) for dogs treated with verapamil. Bottom: Individual PK model parameters predicting the PK in each dog were used to drive the PD response. Individual dogs are separated by colour and marker type.

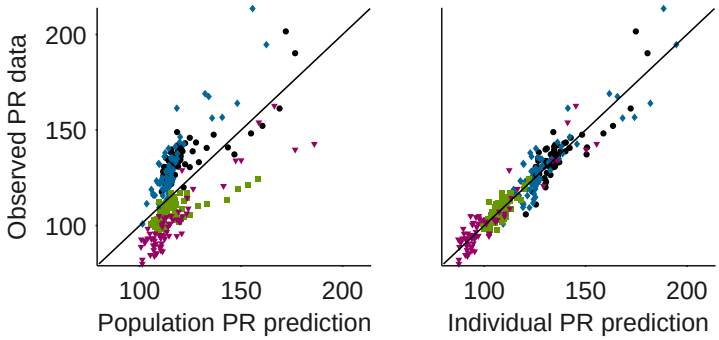

Figure 5.47 Population (left) and individual (right) model fits vs. observed PR intervals with different colour/marker type for each animal.

5.10 Discussion

This investigation presents a quantitative assessment of QRS and PR intervals in guinea pigs, dogs and humans during baseline conditions and following treatment with different compounds with CV effects.

5.10.1 Modelling drug effects on QRS interval durations

Drug-induced QRS widenings were successfully described using PKPD models with linear pharmacological effects for AZD1305, flecainide and quinidine in dogs and for AZD1305 in humans (Table 5.48). However, QRS widenings in guinea pigs following flecainide treatment were nonlinear, and better explained by a power model (Equation 2.3). Measured QRS widenings observed in dogs in the present study were lower than most E_{max} values estimated in a previous PK-QRS study of five compounds (9-16 vs. 8-57 %) [57]. Also in guinea pigs and humans, relatively small QRS widenings were seen (6 and 11 ms at the highest dose, respectively). In dogs, flecainide was most potent in terms of prolongation of QRS, followed by quinidine and AZD1305 (Figure 5.48). This is consistent with the results from hNav1.5 *in vitro* findings where flecainide, quinidine, verapamil and AZD1305 were active. Despite similar *in vitro* potency, verapamil did not prolong QRS *in vivo*. This is most likely explained by the comparatively low free drug concentrations reached in the *in vivo* study. In the current study, unbound flecainide induced QRS widening with 10 % μM^{-1} (Table 5.34). This is consistent with previous PK-QRS modelling in beagle dogs where the estimated effect was 9.1-15.9 % μM^{-1} unbound flecainide (above a threshold of 0.19 μM) at 100-200 bpm [157]. In another study, higher QRS effects of 42 % μM-1 unbound drug were observed after intravenous dosing [21]. Similar differences between oral and intravenous administration were noted for quinidine. In the current study, unbound quinidine induced QRS widening by 5.6 % μM^{-1} while higher effects of 12-35 % μM^{-1} were previously observed following intravenous administration [161, 162, 163]. However, in these studies dogs were anaesthetised or paced, which may have contributed to the observed differences as flecainide and quinidine induce rate-dependent Na^{+}-block [164, 165] causing enhanced QRS widening at increased heart-rates in dogs [157, 166] and in humans [167, 168]. In the current study adequate fits to data were accomplished without the inclusion of heart-rate dependent effects.

Table 5.48 Summary of the selected QRS drug effect models.

	AZD1305	Flecainide	Quinidine
Human	Linear	-	-
	Effect comp	-	-
Dog	Linear	Linear	Linear
	Direct	Direct	Direct
Guinea pig	-	Power	-
	-	Effect comp	-

Models refer to: Linear, Equation 2.4; Power, Equation 2.3; E_{max}, Equation 2.2; Direct, no delay; Link, Equation 2.5.

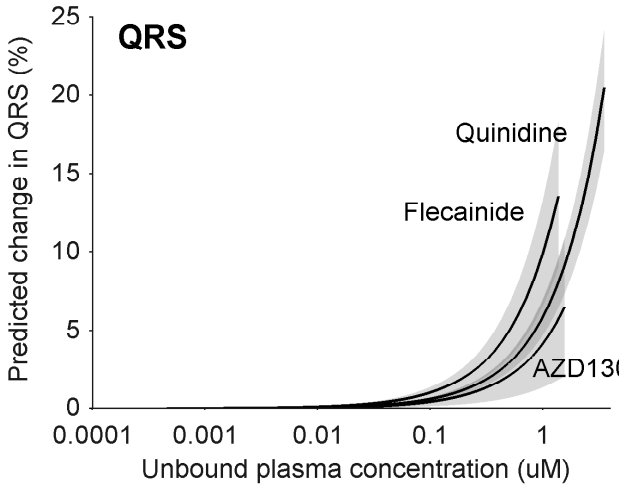

Figure 5.48 Model-predicted median and 95% confidence interval for the percent QRS interval prolongation in a typical beagle dog treated with AZD1305, flecainide or quindine.

5.10.2 Modelling drug effects on PR interval durations

Drug-induced prolongations of the PR intervals were successfully described using PKPD models with linear pharmacological effects for flecainide in guinea pigs, for AZD1305 and flecainide in dogs and for AZD1305 in humans (Table 5.49). However, a power model was required to fit PR prolongations in guinea pigs following verapamil treatment and E_{max} models could be fitted to PR prolongations induced by AZD8683, AZD9164 and verapamil in dogs. AZD1305 and flecainide induced prolongations of QRS as well as PR intervals in all tested species. AZD8683, AZD9164 and verapamil were the most potent in terms of prolongation of PR intervals in dogs (Figure 5.49), and also the most active in the hCav1.2 electrophysiology assay. However, hCav1.2 inhibition by AZD1305 and flecainide was not clearly identified in the functional assay, despite PR prolongation *in vivo*. On the contrary, all four

antiarrhythmic compounds bound to the verapamil and diltiazem binding sites of rat Cav1.2 in the radioligand binding assay. These results indicate that rat Cav1.2 radioligand assays may be more sensitive to potential PR prolongation *in vivo* compared to the automated functional hCav1.2 electrophysiology assay. Similarly, radioligand rat Cav1.2 assays have previously shown superior performance compared to functional hCav1.2 assays to predict drug-induced changes in contractility in canine myocytes [54]. Published studies of PR effects following flecainide or AZD1305 dosing in dog for comparison with the results from the current study were not identified. PR prolongations induced by the anti-arrhythmic compounds were proportional at low exposures and best captured with linear models when average maximal effects were around 20 %. E_{max} models better described compounds with average effects above 30 %. This is consistent with observations from the PKPD modelling of QRS effects. In a previous study, PR prolongations in mongrel dogs correlated to the logarithm of plasma verapamil concentrations following intravenous administration [169].

Table 5.49 Summary of the selected PR drug effect models.

	AZD1305	**AZD8683**	**AZD9164**	**Flecainide**	**Verapamil**
Human	Linear	No effect	No effect	-	-
	Effect comp	-	-	-	
Dog	Linear	E_{max}	E_{max}	Linear	E_{max}
	Direct	Effect comp	Effect comp	Direct	Direct
Guinea pig	-	-	-	Linear	Power
	-	-	-	Effect comp	-

Models refer to: Linear, Equation 2.4; Power, Equation 2.3; E_{max}, Equation 2.2; Direct, no delay; Effect compartment, Equation 2.5.

The electrophysiological side effects of the two anti-muscarinic compounds (AZD8683 and AZD9164) on the PR interval were different from the anti-arrhythmic compounds and best characterised with sigmoid E_{max} models and marked delays compared to plasma concentrations. This may reflect mechanistic differences in ion channel interactions or possibly result from the differences in the pharmacokinetics as AZD8693 and AZD9164 are inhaled drugs. AZD8683 appears to be tenfold more potent to prolong PR compared to AZD9164, while the estimated E_{max} values were similar (61.0 and 52.2 ms, respectively). PR effects above this level were measured following verapamil treatment suggesting that verapamil can induce larger PR prolongation than the two anti-muscarinic compounds. Although the E_{max} model better characterised verapamil-induced PR prolongations in dogs compared to linear or power models, the saturation level is not well captured by the data and the

estimated EC_{50} and E_{max} values are therefore correlated.

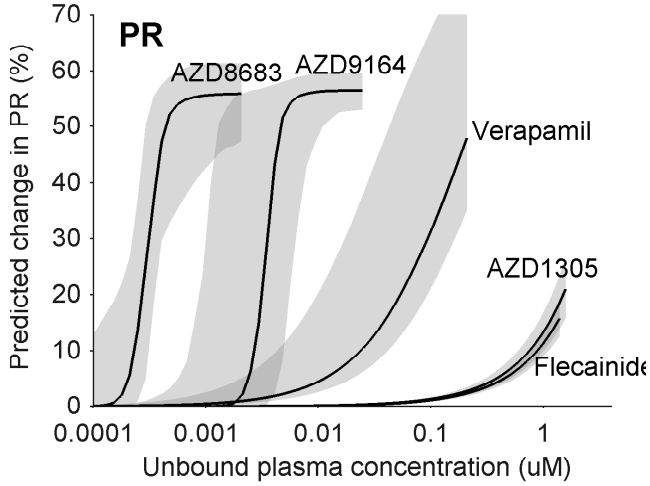

Figure 5.49 Model-predicted median and 95% confidence interval for the percent QRS (left) and PR (right) interval prolongation in a typical beagle dog treated with AZD1305, AZD8683, AZD9154, flecainide, quindine or verapamil.

5.10.3 Modelling variability of QRS and PR baselines

Baseline modelling results from the different species suggest that different baseline models may be appropriate in guinea pigs, dogs and humans as well as between QRS and PR intervals (Table 5.50). In guinea pigs, RR correction may sometimes improve fit to PR, but not to QRS data. These results are however limited by the small study sizes and few studies investigated. In dogs, analysis of both the full data sets and vehicle data only suggested that RR correction and to a lower extent circadian rhythm improved the goodness of fits to PR intervals, while RR correction marginally improved the goodness of fit to QRS data. The RR correction exponent (α) of the combined vehicle data was four times smaller for QRS compared to PR (0.04 vs. 0.16, log-normal BSV, Tables 5.2 and 5.4). Results in humans were similar, where α was 0.05 for QRS and 0.19 for PR (placebo data set; normal BSV). These results are consistent with previous results in humans, where PR intervals increase with RR in most individuals while QRS-RR relationships are close to zero and can be positive or negative [61]. Normal distribution of α in dogs was tested to allow positive and negative QRS-RR relationships and resulted in similar goodness of fits as the log-normal distribution. Linear correlations of PR and QRS intervals to RR intervals show large variability between humans [61]. This may explain the large inter-study variability observed for the typical α-values of the PR-RR correction (0-0.2, Table 5.4). Similarly, the amplitude of the circadian rhythms showed large inter-study variability, ranging from none to six percent of the point baseline (Table 5.4). Circadian variations were not included in previous PK-QRS/PR models in dogs [57, 156, 157].

Table 5.50 Summary of the suggested baseline models to describe QRS and PR interval data in guinea pigs, dogs and humans.

	QRS	PR
Human	Combined	Combined
Dog	Constant or RR correction	RR correction or Combined
Guinea pig	Constant	Constant or RR correction

Models refer to: Constant, Equation 5.2; RR correction, Equation 5.4; Combined, Equation 5.5.

Importantly, the choice of baseline model had an impact on the estimated parameter values of the drug-induced effects on PR and on the predicted drug effects. Neglecting to account for correlations with RR intervals led to predictions of smaller drug effects for four of the five compounds (AZD1305, AZD8683, flecainide and verapamil, Figure 5.50). Circadian rhythms had less impact on predicted drug effects on PR intervals. It should however be noted that the differences in predicted drug effects are within the confidence intervals for the selected models for all compounds. Similarly, inclusion of circadian rhythms was observed to have low impact on estimated sotalol effect during PK-QTc modelling [18]).

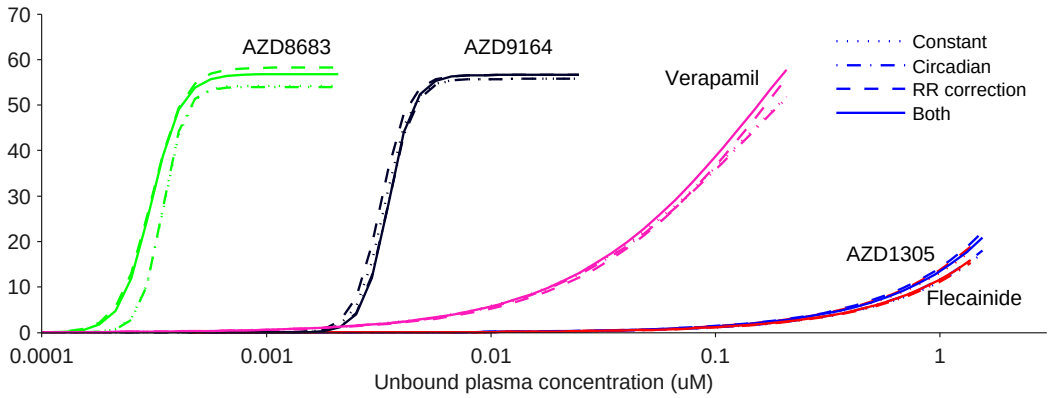

Figure 5.50 Predicted drug-induced PR prolongations by AZD1305, AZD8683, AZD9164, flecainide and verapamil assuming different baseline structures (constant, RR correction and/or circadian rhythm).

5.10.4 Time delays

Time delays were observed mainly during rapidly changing plasma kinetics (e.g. inhalation or iv infusion). Disequilibrium between plasma and effect site concentrations may therefore cause the observed delay, especially where the half-lives were

short (<30 min). Effect compartments have been utilised frequently to characterise time delays in PK-QTc models [1]. Direct PR effects were reported following intravenous infusion of verapamil to conscious dogs [169]) while published PK-PR/QRS models used both direct [57, 157] and effect compartment models [156]. Accounting for time delays resulted in considerable improvement in fitting the cardiac side effects on conduction slowing by the anti-muscarinic compounds (AZD8683 and AZD9164), with half-lives around 1 h, and QRS and PR effects in guinea pigs following iv infusion of flecainide and verapamil, with half-lives of less than 30 min. Effect compartment models also slightly improved the goodness of fit to QRS and PR prolongations in humans induced by AZD1305, although the impacts on the estimated drug effect parameters were small. Direct-effect models were selected to describe QRS and PR prolongations of all anti-arrhythmic compounds in dogs, although inclusion of effect compartments improved the goodness of the fits slightly to QRS, but not to PR prolongation induced by flecainide and AZD1305. Due to the large variability in the data it was concluded that this potential delay could not be estimated confidently. Investigating PK and PD data of higher resolution may improve the ability to distinguish between these two models.

5.10.5 Limitations

In the present study, QRS and PR intervals in six safety pharmacology studies were investigated where in-house data were available in guinea pigs, dogs and humans. Three compounds showed drug-induced QRS widenings and five caused PR prolongations. Although our current analysis demonstrates that PKPD modelling can accurately describe drug-induced QRS and PR prolongations in these species, quantifications of more compounds are needed to improve the methodology for assessing these effects in the nonclinical and clinical settings.

Most nonclinical studies in dogs that were investigated here consisted of only four animals in a cross-over study. These are typical sizes of safety pharmacology studies, but the small number of animals may reduce the accuracy of the estimated parameters. The power of PKPD analyses to detect QTc prolongations has been investigated using simulated data [18]. With four animals and three doses, QTc prolongations above 7 ms (2.8 %) were detected with reasonable power. However, this may differ for QRS and PR intervals as the power to detect drug effects depends on the variability in the data. Also, the knowledge of safe clinical margins for conduction slowing is limited, as well as the translation from pre-clinical to clinical effects. Therefore, it is difficult to assess the potential risks to humans based on the present results.

In this work we used PQ or PR intervals as recorded in the original report. However, for compounds that prolong QRS complex duration, the PQ interval may more accurately reflect atrial conduction as delays in the initial phase of ventricular

conduction (QR interval in the ECG) will prolong the PR interval. However, the relatively short prolongations of the QRS intervals (3-9 ms) compared to PR intervals (21-55 ms) indicate that any such influence on the results obtained in this study would be small.

Sequential PKPD analysis is commonly applied, as was also the case for this study. As exposure data are often limited for nonclinical studies, simultaneous analysis of PK and PD may be beneficial allowing PD data to provide information on the PK profile. Also, using PK information from separate studies with similar design can provide additional information on the PK profiles where PK data are sparse, as was done in this work for modelling AZD9164 exposure in dogs.

5.11 Summary

QRS and PR intervals have been quantified during baseline and drug-induced conditions in anaesthetised guinea pigs, conscious dogs and humans using PKPD modelling. This investigation provides a starting point for modelling QRS and PR intervals in animals and humans. The selected drug effect models will be used in Chapter 7 to investigate the translation between species, together with models describing human effects of flecainide, quinidine and verapamil described in Chapter 6.

In addition to the benefit of translational analyses, the models evaluated in this chapter may be used to improve the possibility to identify and quantify QRS and PR effects in nonclinical and clinical studies. These results show that all four anti-arrhythmic compounds display direct QRS and PR effects when orally administered. QRS and PR effects were typically proportional at low exposures (up to around 20 % prolongation). On the other hand, side effects on QRS and PR intervals during rapidly changing plasma concentrations, such as following inhalation or iv infusion, were typically delayed compared to plasma concentrations, requiring effect compartment models. Also, in these studies, the QRS and PR effects appeared to be nonlinear, requiring power or sigmoid E_{max} models to characterise the drug effects. Mechanistic explanations for this different behaviour could be of interest for further studies.

The results of these analyses can also be used to suggest models to be used to minimise baseline variability of QRS and PR. Correction to simultaneous RR intervals may improve model performance for predicting PR, but generally not QRS intervals in guinea pigs and dogs and may also have an impact on the estimated drug parameters for PR effects. In humans, RR correction improved goodness of fit to both QRS and PR intervals. Also, PR intervals follow circadian rhythms which may be captured with a cosine function, although the impacts on estimated drug effects were negligible in dogs.

PKPD models of QRS and PR intervals provide quantitative information on the pharmacological effects and can support compound selection and risk/benefit assessments through-out drug discovery and development. However, to confidently translate identified pre-clinical conduction liabilities to clinical risk, studies addressing clinical safety margins and translation from nonclinical to clinical effects are needed.

Chapter 6

Exposure-effect modelling of human QRS/PR using literature data

6.1 Introduction

To investigate the translation from nonclinical to clinical QRS and PR effects of flecainide, quinidine and verapamil, it was required to quantify the effect of these compounds in humans. These anti-arrhythmic drugs have been used over decades, and many studies of clinical effects on monitored ECGs have been published [105, 108, 122, 141]. This was utilised by performing a literature survey to find studies where both plasma concentrations and QRS/PR effects were provided (as described in Chapter 4). For the PKPD modelling of in-house data, exposure data as well as QRS and PR intervals measured over time were available from each animal/subject in the study. Such detailed data were not available for the published studies. Many published studies only provide single observations such as maximum exposure and QRS/PR effects. Therefore, it was decided to take a different approach when modelling the literature data. Pairs of exposure/effect data were collected and merged into one data set per compound and investigated interval. The QRS/PR effects of the drugs were then quantified using simple exposure-effect models. This allowed the merging of data from many studies. Thus, factors such as correction to RR intervals or circadian rhythms were not taken into account in this regression analysis. Also, individual data were not available, and the regression models were developed using average study data. The results of the modelling analyses performed in this chapter are used to investigate the *in vivo* to clinical translations of QRS and PR effects in Chapter 7. The literature study and exposure-effect modelling analyses have been published in Bergenholm et al. [**?**].

6.2 Summary of the available data

Effects of flecainide, quinidine and verapamil had been collected in a literature survey, and are summarised in Table 6.1. Detailed information of the publications are described in Chapter 4. Not all studies provided the baseline QRS or PR values. Modelling of absolute values (e.g. pre-dose and post-dose QRS and PR) would have required reductions in the data due to the missing baseline information. Instead, the change from baseline was investigated and modelled in this work. Average QRS and PR baselines were calculated using the baseline data of all healthy volunteers. These calculated baselines (92.5 ms for QRS and 160 ms for PR) were used to convert any percentage data where baseline information were missing to absolute change in ms.

Table 6.1 Summary of the acquired literature data. For details and references see Tables 4.5-4.7.

Compound	**Flecainide**	**Quinidine**	**Verapamil**
No. studies	16	15	16
Dose	iv: 1.5-2 mg kg^{-1}, 150 mg. oral: 100-600 mg	iv: 3.7-10 mg kg^{-1}. oral: 3 mg kg^{-1}, 100-2250 mg	oral: 80-480 mg
C_{max} (μM)	2.6	12.3	1.7
QRS_0 (ms)	92.5	92.5	-
ΔQRS_{max} (ms)	31	18	-
PR_0 (ms)	160	-	160
ΔPR_{max} (ms)	56	-	53
Free drug (%)	62.1	12.2	20.7

Data presented as mean±SD. iv, intravenous; QRS_0, QRS at baseline; PR_0, PR at baseline; ΔQRS, QRS change from baseline; ΔPR, PR change from baseline.

6.3 Exposure-effect modelling methods

The concentration-effect pairs collected in the literature studies were visually stratified in groups following the health status of the subjects (healthy volunteers/patients), administration route (oral/iv) and the dosing history (acute; single or first dose, chronic; following repeated dosing) to detect differences in potency between the groups.

Absolute changes in the ECG intervals were regressed over measured free concentrations in MATLAB R2013b using the built-in nonlinear model fit function *fitnlm.m*. Two drug effect models were tested, namely the proportional and the E_{max} drug effect models (Equations 2.2 and 2.4). As the ECG data were normalised to change from pre-dose value, no intercepts were included in the regression analysis. Including intercepts would have required reductions of the data sets, as data were

sometimes provided only as a change from the pre-dose value. A combined additive and proportional error model was applied (Equation 2.14). Model selection was performed considering the goodness of fit value (-2LL), visual fit to the data, residual plots, adjusted R-sqared (R^2) values and precision of and correlation between the parameter estimates.

6.4 QRS and PR effects of flecainide in humans

6.4.1 Visual inspection of the identified QRS data

QRS prolongations following flecainide treatment appear approximately proportional at lower concentrations and may saturate around 1.5 μM free flecainide (Figure 6.1). Higher and/or more frequent doses of flecainide were administered in the patient studies compared to the studies with healthy volunteers, and plasma concentrations were also higher in patients. Despite clear differences in the concentration-effect relationship between studies, no clear reason for the varying drug effects was identified.

The influence of the data point at 12 ms/1.5μM unbound flecainide [120] was investigated further during the modelling step as both QRS and PR interval prolongations were small compared to the remaining studies. No explanation for the comparatively small prolongations could be identified. In addition, QRS effects by flecainide in patients with Brugada syndrome were excluded based on increased QRS prolongation in this group compared to controls [107], as indicated in Figure 6.1.

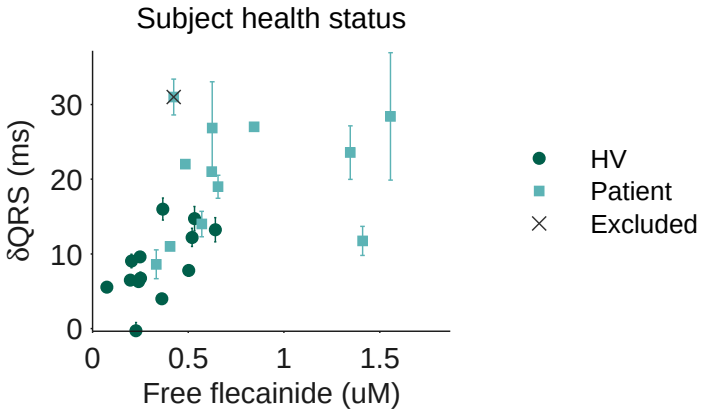

Figure 6.1 QRS widening in healthy volunteers (HV, circles) and patients (squares) induced by flecainide. Data points represent associated plasma concentration-δQRS pairs (1-8 per published study) with standard errors where available. The data point marked by a black cross was excluded prior to modelling as these Brugada syndrome patients were shown to have increased QRS prolongation compared to healthy patients [107].

Only one study was conducted at acute oral dosing in healthy volunteers similar to the dog telemetry studies [105]. No evidence was found of general differences

between healthy volunteers and patients. Visual stratification of single/repeated dosing data (acute/chronic) and iv infusion/oral administration data indicated a potentially lowered effect following chronic administration compared to acute dosing (Figure 6.2). Such lowered effects from chronic dosing may arise from tolerance development. Although no clear evidence of altered exposure-effect relationships following repeated dosing were found in the literature, the possibility of such effects was investigated in the regression analysis.

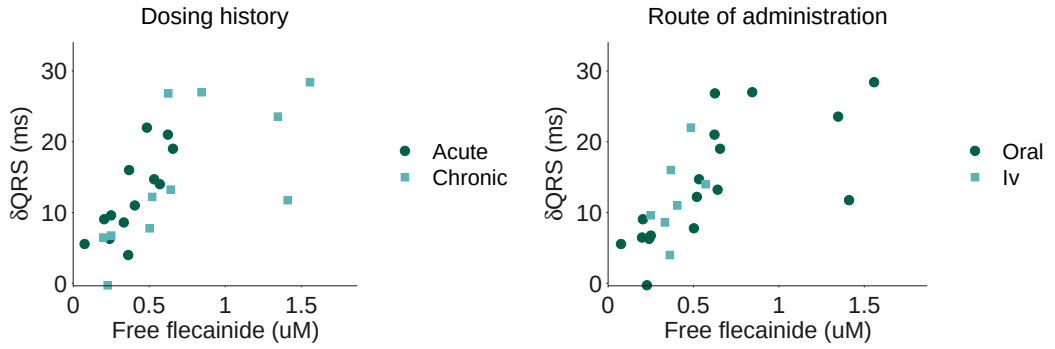

Figure 6.2 QRS widening by flecainide stratified by dosing history (left) and route of administration (right).

6.4.2 Quantification of QRS effects by flecainide in humans

Summary statistics for a selection of tested models are provided in Table 6.2. The sigmoid E_{max} model (Equation 2.2) was selected to describe QRS widenings by flecainide (Figure 6.3). The proportional model (Equation 2.4) over-predicted prolongations at higher concentrations. Also, R^2, goodness of fit value (-2LL) and residual plots were improved when applying the E_{max} models, and residual plots were further improved for the sigmoid E_{max} model. The outlier at 12 ms QRS widening/1.5 μM free flecainide was excluded from the QRS data set as this improved residual plots and visual fit to the remaining data. Exclusion of the outlier resulted in approximately 20% increase in the estimated E_{max} and EC_{50} values, while the ratio was unchanged. Including a covariate for history of dosing on the EC_{50} did not improve R^2 or the goodness of fit value and led to high uncertainty in all parameters. Estimated parameters for the selected model are summarised in Table 6.3 and residual plots are shown in Figure 6.4. High correlations were found between the estimated E_{max} and EC_{50}.

Table 6.2 Summary of a selection of the tested human flecainide QRS models.

Model	R^2	-2LL	Comment
Proportional	0.439	150	Over-predicting at high concentrations
E_{max}	0.545	144	Improved visual fit to data and residual plots
E_{max}, exclude outlier	0.656	133	Improved visual fit to data and residual plots, **selected model**
E_{max}, covariate on dosing history	0.547	143	No improvement

RMSE, root mean squared error; -2LL, -2 loglikelihood.

Table 6.3 Estimated parameter values for QRS widenings by flecainide.

Parameter	Value (SE)
E_{max} (ms)	33.7[a] (10.8)
EC_{50} (μM)	0.573[a] (0.256)
n	1.65 (0.61)

[a]Correlation E_{max}:EC_{50} = 0.977.

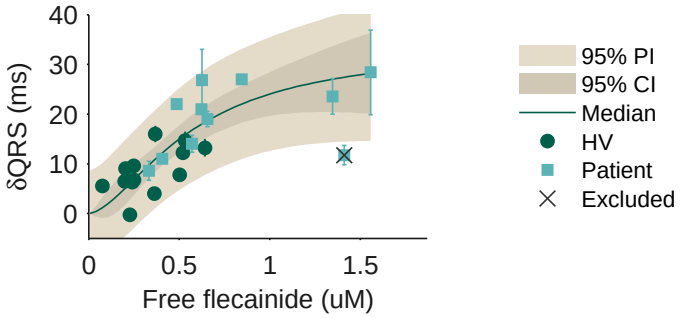

Figure 6.3 Model predictions (solid line) and observed QRS widenings in healthy volunteers (HV, circles) and patients (squares) induced by flecainide. Data points represent associated plasma concentration-δQRS pairs (1-8 per published study) with standard errors where available. Shaded areas represent the 95% confidence intervals (CI) and prediction intervals (PI). Excluded outlier is marked by a black cross.

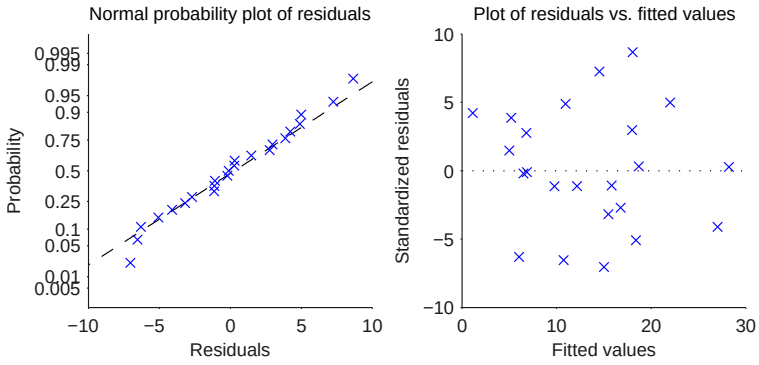

Figure 6.4 Residual plots for the selected model for QRS widenings induced by unbound flecainide.

6.4.3 Visual inspection of the identified PR data

PR prolongations show a clear concentration-dependent increase with possible saturation at higher flecainide concentrations (Figure 6.5). Higher flecainide concentrations were reached in the patient studies where higher and/or more frequent doses were generally used. The data point at 10 ms/1.5μM free flecainide [120] originates from the same study as the excluded QRS data point. This outlier was investigated further during the regression analysis as it appeared to be an outlier, potentially reducing the goodness of fit to the remaining data. Also, as this is the only observation of PQ effect rather than PR interval changes, which may contribute to the smaller effect as this excludes any potential prolongation of the QR part of the PR interval.

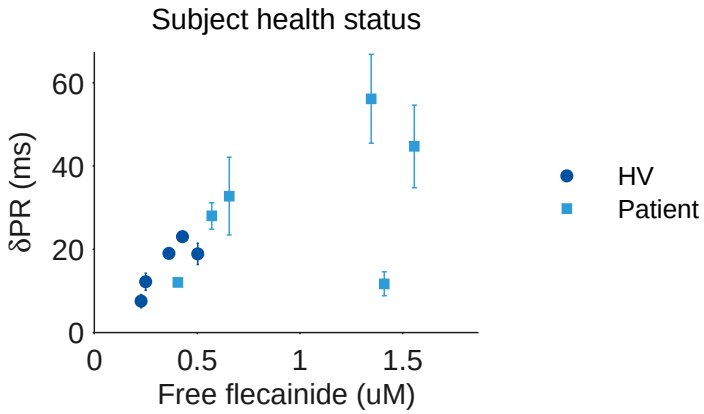

Figure 6.5 PR prolongations in healthy volunteers (circles) and patients (squares) induced by flecainide. Data points represent associated plasma concentration-δPR pairs (1-2 per published study) with standard errors where available.

Only one study was conducted at acute oral dosing in healthy volunteers similar to the dog telemetry studies [106]. No evidence was found of general differences between healthy volunteers and patients. Visual stratification of single/repeated

dosing data (acute/chronic) and iv infusion/oral administration data did not indicate any differences in the concentration-effect relationships (Figure 6.6).

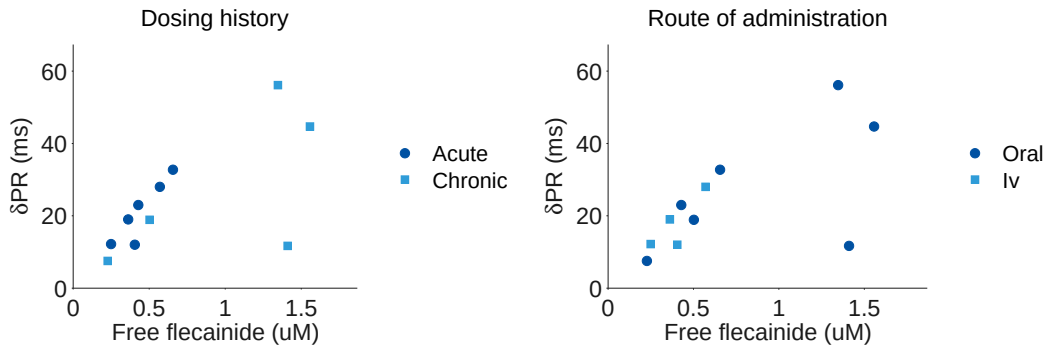

Figure 6.6 PR prolongations by flecainide stratified by dosing history (left) and route of administration (right).

6.4.4 Quantification of PR effects by flecainide in humans

Summary statistics for a selection of tested models are provided in Table 6.4. The sigmoid E_{max} model (Equation 2.2) was selected to describe PR widenings by flecainide (Figure 6.7). This model could capture the small saturation seen in the data, and the sigmoid model showed improved parameter precision. The outlier at 10 ms/1.5μM free flecainide [120] was excluded as this improved the residual plots and R^2, while the ratio of $E_{max} : EC_{50}$ remained unchanged. Estimated parameters for the selected model are summarised in Table 6.5 and residual plots are shown in Figure 6.8. High correlations were found between the estimated E_{max} and EC_{50}. A slight deviation of the normal probability plot for the residuals was observed (Figure 6.8) and deemed acceptable as this plot was improved compared to the rejected models, and the devation may be a result of the low number of data points.

Table 6.4 Summary of a selection of the tested human flecainide PR models.

Model	**R^2**	**-2LL**	**Comment**
Proportional	0.439	150	Over-predicting at high concentrations
E_{max}	0.545	144	Improved visual fit to data and residual plots
E_{max}, exclude outlier	0.656	133	Improved visual fit to data and residual plots, **selected model**
E_{max}, covariate on dosing history	0.547	143	No improvement

RMSE, root mean squared error; -2LL, -2 loglikelihood.

Table 6.5 Estimated parameter values for PR widenings by unbound flecainide.

Parameter	Value (SE)
E_{max} (ms)	68.9[a] (27.2)
EC_{50} (μM)	0.77[a] (0.43)
n	1.57 (0.51)

[a]Correlation E_{max}:EC_{50} = 0.979.

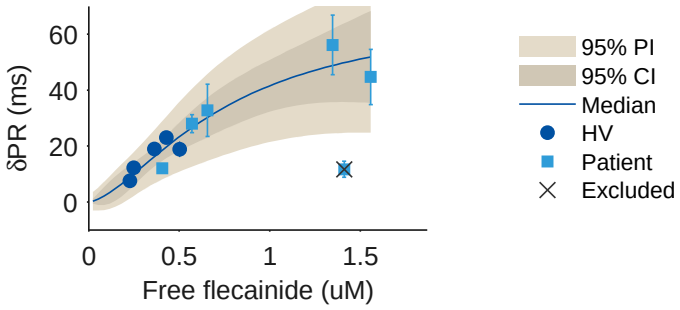

Figure 6.7 Model predictions (solid line) and observed PR prolongations in healthy volunteers (HV, circles) and patients (squares) and induced by flecainide. Data points represent associated plasma concentration-δPR pairs (1-2 per published study) with standard errors where available. Shaded areas represent the 95% confidence intervals (CI) and prediction intervals (PI). Excluded outlier is marked by a black cross.

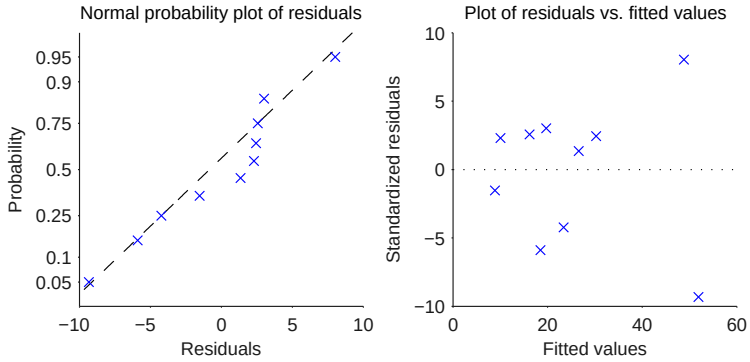

Figure 6.8 Residual plots for the selected model for PR widenings induced by flecainide.

6.5 QRS effects of quinidine in humans

6.5.1 Visual inspection of the identified QRS data

QRS widenings show a clear concentration-dependent increase with large variability at higher concentrations (Figure 6.9). The high number of studies with concentrations around 1.3-1.5 μM unbound quinidine appear to be a result of variable dosing

to reach clinically relevant concentrations in patient studies. Higher doses of quinidine were in general administered in the patient studies compared to the studies with healthy volunteers, and plasma concentrations were also higher in patients. Despite clear differences in the concentration-effect relationship between studies, no clear reason for the varying drug effects was identified. One data point of QRS shortening by quinidine was excluded (indicated in Figure 6.9) as the average QRS did not return to baseline despite concentrations below 0.1 μM [121].

Visual stratification of QRS prolongations following acute and chronic dosing and administration through the oral and iv route did not indicate any clear differences (not shown).

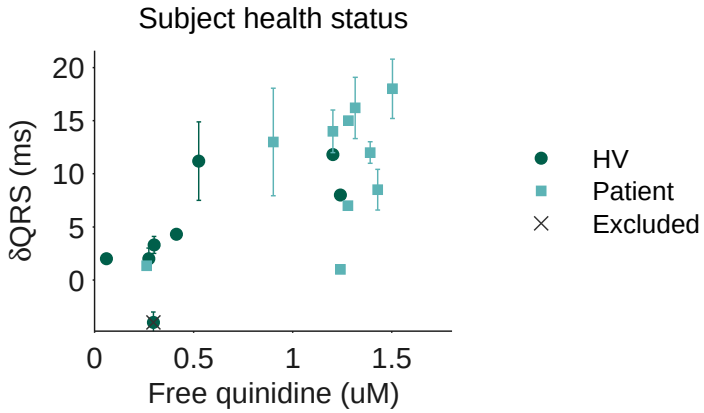

Figure 6.9 QRS widening in healthy volunteers (circles) and patients (squares) induced by quinidine. Data points represent associated plasma concentration-δQRS pairs (1-2 per published study) with standard errors where available. The data point marked by a black cross was excluded prior to modelling as the average QRS did not return to baseline despite concentrations below 0.1 μM [121].

Only three studies were conducted at acute oral dosing in healthy volunteers similar to the dog telemetry studies. No evidence was found of general differences between healthy volunteers and patients.Visual stratification of single/repeated dosing data (acute/chronic) and iv infusion/oral administration data did not indicate any differences in the concentration-effect relationships (Figure 6.10).

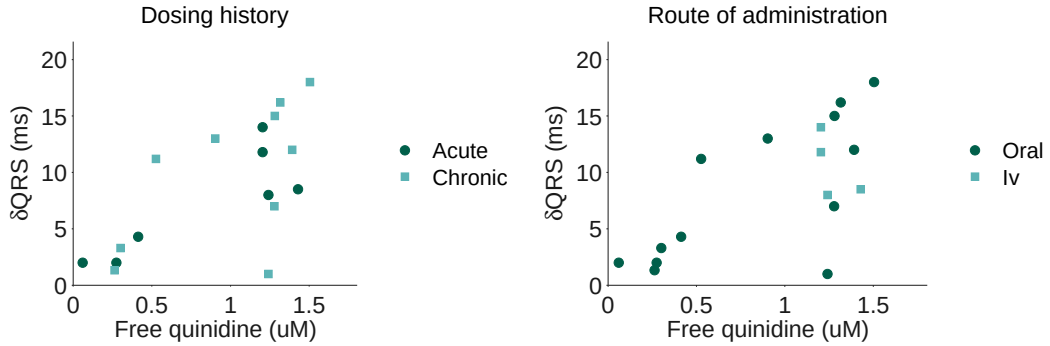

Figure 6.10 QRS widening by quinidine stratified by dosing history (left) and route of administration (right).

6.5.2 Quantification of QRS effects by quinidine in humans

Summary statistics for a selection of tested models are provided in Table 6.6. The proportional model (Equation 2.4) was selected to describe QRS widenings by quinidine (Figure 6.11) even though the E_{max} model (Equation 2.2) resulted in improved goodness of fit and R^2 value. The proportional model was selected as the sigmoid model resulted in unrealistic parameter values (E_{max}=11 ms and n =4.4) and fixing n to 1 resulted in the EC_{50} being practically unidentifiable (SE>100%). Also, although patient data are highly variable, the slope of the concentration-effect relationship was unchanged when a proportional model was fitted only to healthy volunteer data. Estimated slope of the concentration-effect relationship was 9.57±1.14 ms μM^{-1} free quinidine. Residual plots are shown in Figure 6.12.

Table 6.6 Summary of a selection of the tested human quinidine QRS models.

Model	**R^2**	**-2LL**	**Comment**
Proportional	0.614	92.1	**Selected model**
E_{max}	0.651	88.6	Unrealistic estimate of E_{max}
E_{max}, n fixed to 1	0.633	90.5	High uncertainty E_{max} and EC_{50}

RMSE, root mean squared error; -2LL, -2 loglikelihood.

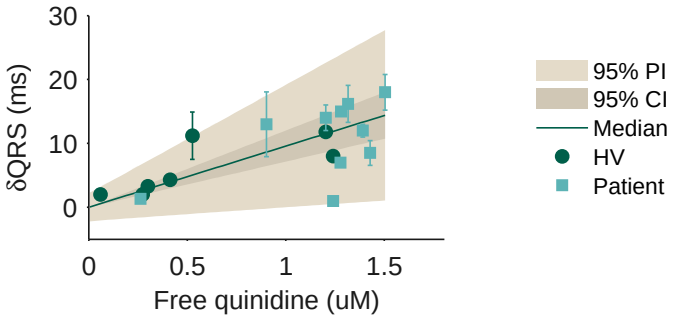

Figure 6.11 Model predictions (solid line) and observed QRS prolongations in healthy volunteers (HV, circles) and patients (squares) and induced by quinisine. Data points represent associated plasma concentration-δQRS pairs (1-2 per published study) with standard errors where available. Shaded areas represent the 95% confidence intervals (CI) and prediction intervals (PI).

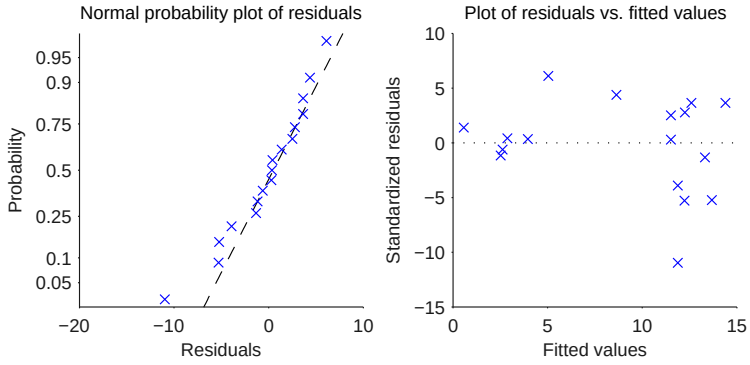

Figure 6.12 Residual plots for the selected model for QRS widenings induced by quinidine.

6.6 PR effects of verapamil in humans

6.6.1 Visual inspection of the identified PR data

PR prolongations show a clear concentration-dependent increase and saturation at higher verapamil concentrations (Figure 6.13). Higher verapamil concentrations were typically reached in the patient studies compared to the healthy voluteers. The eight patient data points clustered around 50 ms PR prolongation are from the same study, where two patient groups were treated with immediate and sustained release verapamil in two doses (240/480 mg/day) under fed and fasted conditions. The change from baseline in ms showed no dose-dependency (all between 45 and 53 ms). This suggests saturated PR prolongation at these concentrations. Two observations of PR effects conducted in patients with Crohn's syndrome were excluded as this group was found to have a reduced effect on PR compared to controls in the original study [148]. These data are indicated in Figure 6.13.

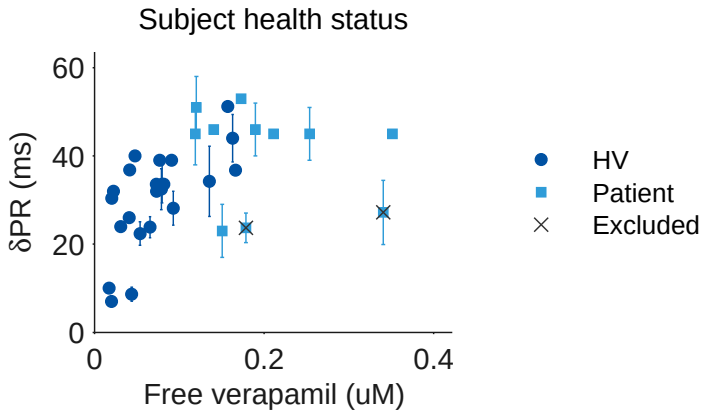

Figure 6.13 PR prolongations in healthy volunteers (circles) and patients (squares) induced by verapamil. Data points represent associated plasma concentration-δPR pairs (1-8 per published study) with standard errors where available. The data points marked by black crosses were excluded prior to modelling as verapamil induce less PR prolongation in patients with Crohn's syndrome compared to controls [148].

Of the identified studies, 11 were conducted at acute oral dosing in healthy volunteers (summarised in Table 4.7) similar to the dog telemetry studies. No evidence was found of general differences between healthy volunteers and patients. Visual stratification of the data suggests possible lower effects following chronic dosing compared to acute dosing, sustained and immediate release tablets appear to result in similar concentration-effect relationships (Figure 6.14).

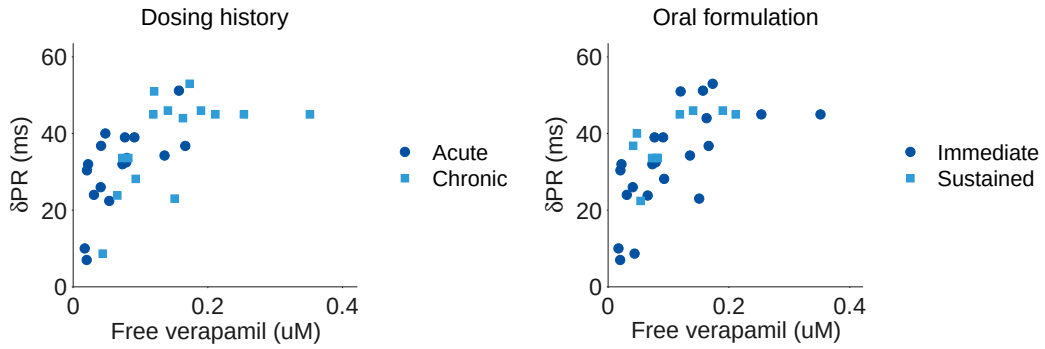

Figure 6.14 PR prolongations by verapamil stratified by dosing history (left) and route of administration (right).

6.6.2 Quantification of PR effects by verapamil in humans

Summary statistics for a selection of tested models are provided in Table 6.7. The E_{max} model (Equation 2.2) with a covariate effect of chronic dosing on EC_{50} was selected to describe PR widenings by verapamil (Figure 6.15. This covariate effect on EC_{50} was implemented according to

$$EC_{50} = EC_{50,acute} + \beta_{EC_{50,chronic}} \tag{6.1}$$

where $\beta_{EC_{50,chronic}}$ allows different EC_{50}s during acute and chronic dosing. This covariate model was selected as visual stratification of the data indicates possible differences between acute and chronic dosing in the effects at lower concentrations, with no evidence of differences in E_{max}. Inclusion of the covariate improved the residual plots, goodness of fit values and R^2 and reduced the correlations. R^2 and goodness of fit value were clearly improved when applying the E_{max} model compared to the proportional model (Equation 2.4) as effects at high concentrations were overpredicted by the proportional model. Fixing n to 1 resulted in improved model performance, indicated by smaller correlations between the parameters and similar likelihood. Estimated parameters for the selected model are summarised in Table 6.8 and residual plots are shown in Figure 6.16. Fitting only the healthy volunteer data to the E_{max} model resulted in approximately 10 % smaller E_{max} and 15 % smaller EC_{50}. As the highest concentrations reached in the healthy volunteer data set were smaller, this may be a result of missing data at fully saturated concentration levels.

Table 6.7 Summary of a selection of the tested human verapamil PR models.

Model	**R^2**	**-2LL**	**Comment**
Proportional	-0.831	286	Bad fit to data.
E_{max}	0.379	246	Improved fit, high uncertainty EC_{50} and correlations
E_{max}, n fixed to 1	0.394	246	Reduced uncertainty and correlations
E_{max}, covariate on dosing history	0.425	243	Similar E_{max} and EC_{50}. **Selected model**

RMSE, root mean squared error; -2LL, -2 loglikelihood.

Table 6.8 Estimated parameter values for PR widenings by unbound verapamil.

Parameter	**Value (SE)**
$\boldsymbol{E_{max}}$ **(ms)**	53.7[a] (7.2)
$\boldsymbol{EC_{50,acute}}$ **(μM)**	0.0371[a] (0.0144)
$\beta_{\boldsymbol{EC_{50,chronic}}}$ **(μM)**	0.0243 (0.0187)

[a]Correlation E_{max}:EC_{50} = 0.878.

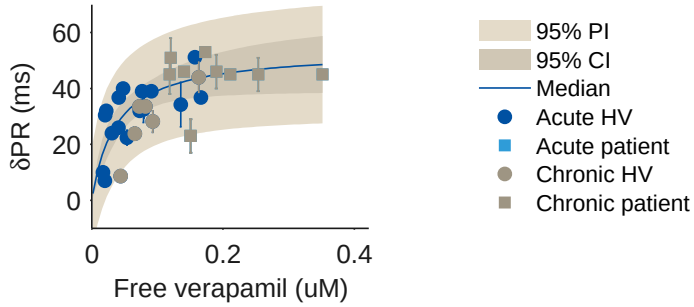

Figure 6.15 Model predictions (solid line) and observed PR prolongations in healthy volunteers (HV, circles) and patients (squares) and induced by verapamil. Data points represent associated plasma concentration-δPR pairs (1-8 per published study) with standard errors where available. Shaded areas represent the 95% confidence intervals (CI) and prediction intervals (PI).

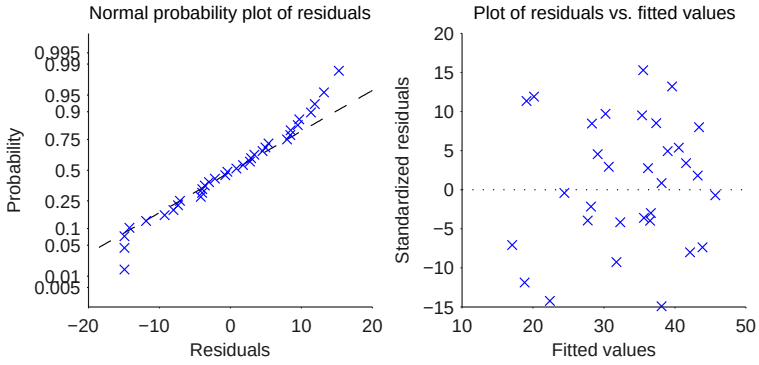

Figure 6.16 Residual plots for the selected model for PR widenings induced by verapamil.

6.7 Discussion

In this chapter, regression models were developed to describe drug-induced prolongations of QRS and PR intervals by flecainide, quinidine and verapamil in humans. Proportional and E_{max} models (Equations 2.4 and 2.2) were evaluated to describe absolute (ms) changes in QRS and PR durations using data collected in literature searches performed in Pubmed.

6.7.1 Modelling drug effects on QRS interval durations

Flecainide and quinidine induced QRS widenings in humans, with maximum widenings of 31 ms by flecainide and 18 ms by quinidine (Table 6.1). The E_{max} model (Equation 2.2) was selected to describe the flecainide data, albeit with a high correlation between E_{max} and EC_{50}. The estimated maximum effect was 34 ± 11 ms. On the other hand, the smaller effects induced by quinidine did not allow estimation of

the E_{max} model, and the proportional model (Equation 2.4) equally well described the data.

QRS widenings induced by flecainide in patients with atrial fibrillations were previously found to be 44.3 ± 18.5 ms L mg $^{-1}$ total flecainide [111], which equals 30.6 ms μM^{-1} free flecainide. Visual inspection of the final QRS model suggests that this is roughly in agreement with the predicted relationship. A smaller effect of flecainide on QRS durations was found when regressing average individual concentrations and QRS effects over 24 h in healthy volunteers [105]. In this study, average prolongations of 26-32 ms L mg $^{-1}$were estimated at steady-state dosing of 100 and 200 mg flecainide, which corresponds to approximately 18-22 ms μM^{-1} free flecainide.

QRS widenings induced by quinidine were previously analysed in a PKPD analysis, where quinidine was found to induce QRS widenings by 3.6 ms L mg^{-1} total quinidine following iv administration and 3.8 ms L mg^{-1} total quinidine following oral administration [122]. This equals approximately 1.2 ms μM^{-1} (or 10 ms μM^{-1} unbound quinidine) and is in clear agreement with the results of the current work, where the slope was 9.6 ms μM^{-1} unbound quinidine. Also, a delay was identified between plasma concentrations and QRS widening [122]. The delay was found to be short, with a half-life of around 5 min. This short half-life supports the assumption of negligible delays for the purpose of this modelling work.

6.7.2 Modelling drug effects on PR interval durations

Flecainide and verapamil induced PR prolongations in humans, with maximum prolongations of 56 ms by flecainide and 53 ms by verapamil (Table 6.1). E_{max} models could be estimated to both data sets, albeit with high correlation between E_{max} and EC_{50} for flecainide, and the maximum effects were estimated to be 69 ± 27 ms for the flecainide model and 56 ± 7 for the verapamil model (Tables 6.5 and 6.8).

Previously published models for flecainide-induced PR prolongations were not identified.

PR prolongations by orally administered verapamil were previously found to have a maximal effect of $38 \pm 13.4\%$ (61 ms assuming a baseline of 160 ms) in healthy volunteers [137], which is in agreement with the results of the current analysis. Also, the estimated EC_{50} was found to be 123 μg L^{-1} total verapamil, which corresponds to 0.055 μM free verapamil. This is comparable to the estimated EC_{50} of the current study, which was 0.041 μM free verapamil (Table 6.8).

6.7.3 Limitations

These models were developed using limited data from a large number of studies rather than detailed exposure and QRS/PR data over time from a single study. Us-

ing data from different studies conducted over decades increases variability in the data due to the development of new and improved methods for data collection during this time. Variability and uncertainty in the data would occur from differences in, for example, frequency of sampling, number of subjects and data handling. Also, several different data types were allowed, such as pairs of maximum concentrations/effects in a study or concentrations and effects measured at the same time points, which assumes that the impact of potential delays is negligible. The developed QRS and PR models would potentially have had less limitations by published high quality data of observed PK and QRS/PR measured simultaneously. Sharing of detailed data between pharmaceutical companies can thus be valuable for many different future analyses, providing new insights potentially improving drug development across companies.

6.8 Summary

QRS widenings induced by flecainide and quinidine and PR prolongations induced by flecainide and verapamil have been quantified in humans using exposure-effect modelling. This investigation was primarily conducted to quantify the drug effects in humans in order to evaluate the translation between nonclinical effects quantified in Chapter 5 and clinical effects. The translational analyses are described in Chapter 7.

Literature data from 15-16 publications for each drug were identified in an extensive survey and extracted for analysis. Detailed PKPD data were typically not available in the published material, and data sets were therefore constructed by merging pairs of concentration-effect data into one data set for each drug and endpoint. QRS widenings were best described by an E_{max} model for flecainide and a proportional model for quinidine, for which the widenings were smaller, and both models were in good agreement with previous publications. PR prolongations by flecainide and verapamil were both best described by E_{max} models, and while no published model for flecainide was identified, the verapamil model was in good agreement with previous publications.

Chapter 7

Translation from nonclinical effects to QRS/PR effects in humans

7.1 Introduction

Identifying effects on cardiac conduction slowing in nonclinical studies is vital for the progression of safe compounds into first clinical trials. Numerous investigations provide insights into the prediction of risk of prolongation of the heart-rate corrected QT (QTc) interval [9, 11, 12, 13]. However, much less is known of the nonclinical to clinical translation of conduction liabilities manifested as QRS and PR prolongations. In previous chapters, QRS and PR effects of a number of compounds were quantified in guinea pigs, dogs and humans. In this chapter, the developed QRS and PR drug effect models were used to investigate the nonclinical to clinical translation of QRS and PR effects for the anti-arrhythmic compounds AZD1305, flecainide, quinidine and verapamil.

Translations were investigated applying an empirical (top-down) translational approach, as has been successfully done for QTc [12] and used to identify nonclinical effects corresponding to 10% (appr. 10 ms) QRS widening or 10% (appr. 16 ms) PR prolongation in humans. Thresholds of 10% effect in humans were selected as such effects were deemed clinically relevant and quantifiable in clinical studies, in the absence of generally accepted thresholds for concern [15].

Furthermore, the *in vitro* to clinical translation between ion channel activity and QRS and PR interval prolongations in humans were investigated applying two different approaches. Firstly, an empirical approach was applied similar to that for the *in vivo* to clinical translation. Secondly, mechanism-based translation using an operational model [35] was investigated to identify the system parameters linking ion channel effects to clinical QRS and PR prolongations induced by AZD1305.

7.2 Methods

7.2.1 Empirical *in vitro*/*in vivo* to clinical translation

Empirical translational relationships between nonclinical and clinical effects were investigated for the anti-arrhythmic compounds AZD1305, flecainide, quinidine and verapamil, following the approach visualised in Figure 7.1.

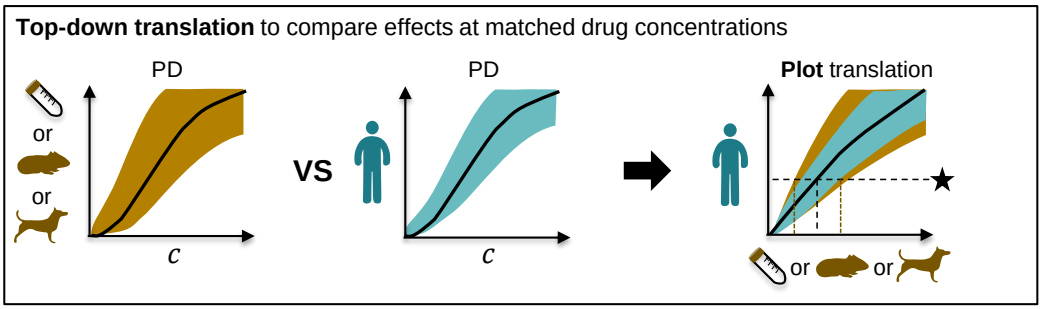

Figure 7.1 Top-down translation to empirically assess effects at matched drug concentrations were performed for AZD1305, flecainide, quinidine and verapamil. Resulting translational relationships may be used to identify approximate estimates of nonclinical effects that correspond to a clinical safety margin.

Firstly, drug effects were simulated in each species using the drug effect parameters estimated in the PKPD and exposure-effect modelling and ion channel effects were simulated using the collected *in vitro* parameters. The drug effects were simulated using the estimated models of the effect of drug in the plasma compartment (direct effect models) or the effect compartment (distributional delay models). Also, drug effects were simulated as the predicted change from baseline, thus ignoring all baseline variability or uncertainty. Change from baseline was simulated as this was the nature of the literature models for the effects of flecainide, quinidine and verapamil in humans. Three different drug effect models had been tested, including the proportional, power and E_{max} drug effect models (Equations 2.2-2.4). The final drug effect model for each drug and species was used to simulate the effects at 100 evenly spaced, matched concentrations within the supported concentration ranges. Translations were investigated at matching total and unbound concentrations, where the unbound concentration relates to the total concentration according to

$$C_u = f_u \cdot C_t \tag{7.1}$$

where C_u is the unbound (free) concentration in plasma, f_u the free fraction (1-PPB) and C_t the total concentration in plasma. This relationship was used to convert the estimated drug effect parameters of the proportional, power and E_{max} models between unbound and total effects according to

$$slope_u \cdot C_u = slope_u \cdot f_u \cdot C_t = slope_t \cdot C_t \qquad \Rightarrow \qquad slope_t = slope_u \cdot f_u \tag{7.2}$$

$$a_u \cdot C_u^{b_u} = a_u \cdot (f_u C_t)^{b_u} = a_u \cdot C_t^{b_u} f_u^{b_u} = a_t \cdot C_t^{b_t} \qquad \Rightarrow \qquad \begin{aligned} a_t &= a_u \cdot f_u^b \\ b_t &= b_u \end{aligned} \tag{7.3}$$

$$\begin{aligned} &\frac{E_{max,u} C_u^{n_u}}{EC_{50,u}^{n_u} + C_u^{n_u}} = \frac{E_{max,u} (f_u C_t)^{n_u}}{EC_{50,u}^{n_u} + (f_u C_t)^{n_u}} = \\ &\frac{E_{max,u} C_t^{n_u}}{\left(\frac{EC_{50,u}}{f_u}\right)^{n_u} + C_t^{n_u}} = \frac{E_{max,t} C_t^{n_t}}{EC_{50,t}^{n_t} + C_t^{n_t}} \end{aligned} \qquad \Rightarrow \qquad \begin{aligned} E_{max,t} &= E_{max,u} \\ EC_{50,t} &= \frac{EC_{50,u}}{f_u} \\ n_t &= n_u \end{aligned} \tag{7.4}$$

where *slope*, a and b and E_{max}, EC_{50} and n are parameters of the proportional, power and $\mathrm{E_{max}}$ models respectively, and the subscripts u and t represent parameters related to unbound and total plasma concentrations respectively. In addition, translations were investigated both in terms of millisecond and percentage change from baseline by scaling the simulated response. Uncertainty and variability in the estimated drug effects were estimated and visualised by 95% confidence and prediction intervals.

For the population PKPD models, confidence and prediction intervals for the drug effects were generated using Monte Carlo methods. Confidence intervals were constructed from the covariance matrices of the typical parameters for the PD drug effects and prediction intervals from the estimated typical parameters, between-subject variabilities and residual variabilities. 10000 randomly sampled parameter sets were simulated and sorted at each concentration, and the 2.5th and 97.5th percentiles were extracted. Non-physiological parameter values (e.g., EC_{50} below 0) were excluded. Confidence and prediction intervals for the regression models based on literature data were produced using the built-in Matlab function *predict*.

Lastly, the predicted *in vitro*, guinea pig and dog effects were plotted against the predicted human effect at matched concentrations to visualise the translations for each compound, as shown in Figure 7.1. Nonclinical effects corresponding to a 10% change in humans were extracted.

7.2.2 Semi-mechanistic *in vitro* to clinical translation

7.2.2.1 Development of an operational model to link *in vitro* and clinical AZD1305 data

In vitro and clinical AZD1305 data were combined to estimate the signal transductions from effects at the ion channel level to clinical QRS or PR prolongations using the operational model of agonism (Equation 2.10) [35] as visualised in Figure 7.2.

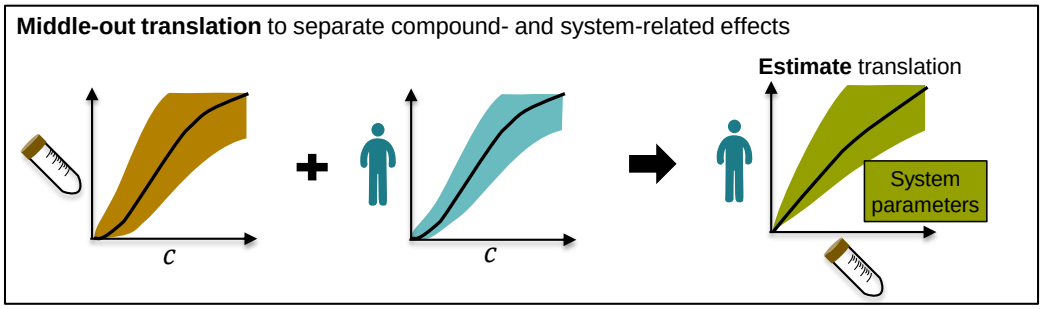

Figure 7.2 Middle-out approach combining compound potency *in vitro* with clinical data to estimate the signal transduction was performed for AZD1305. The estimated signal transduction parameters define the system and may potentially be used to predict the effects of different compounds with similar mechanisms of action.

The operational model is built by combining two functions, one linking the percentage bound/inhibited ion channel to the QRS/PR effect according to

$$\Delta ECG = \frac{E_m[RC]^n}{EC_{50}^n + [RC]^n} \tag{7.5}$$

where EC_{50} the QRS/PR prolongation at 50% bound/inhibited ion channel, E_m the maximal QRS or PR prolongations possible in the system and RC the percent bound ion channel. RC is then substituted by the second function, which links the concentration of drug to the percentage bound/inhibited ion channel according to

$$RC = \frac{R_{tot}C_u}{K_d + C_u} \tag{7.6}$$

where C_u is the predicted unbound drug concentration, K_d the concentration at 50% bound or inhibited receptor and R_{tot} the total amount of ion channels, e.g. 100%. Combining these two equations yields the operational model (Equation 2.10). However, for the hNav1.5 data, a sigmoid model better fitted the data. This model is given by

$$RC = \frac{R_{tot}C_u^\gamma}{K_d^\gamma + C_u^\gamma} \tag{7.7}$$

where γ the Hill factor of the drug-ion channel interaction. Substituting this equa-

tion in the operational model gives

$$\Delta ECG = \frac{E_m RC^n}{EC_{50}^n + RC^n} = \frac{E_m \left(\frac{R_{tot}C_u^\gamma}{K_d^\gamma + C_u^\gamma}\right)^n}{EC_{50}^n + \left(\frac{R_{tot}C_u^\gamma}{K_d^\gamma + C_u^\gamma}\right)^n} = \frac{E_m (R_{tot}C_u^\gamma)^n}{(K_d^\gamma + C_u^\gamma)^n EC_{50}^n + (R_{tot}C_u^\gamma)^n}, \tag{7.8}$$

so, if $\tau = R_{tot}/EC_{50}$, then

$$\Delta ECG = \frac{E_m (\tau C_u^\gamma)^n}{(K_d^\gamma + C_u^\gamma)^n + (\tau C_u^\gamma)^n} \tag{7.9}$$

where τ is the transducer ratio, which is the ratio of the maximum inhibited/bound ion channels to the inhibited/bound ion channels corresponding to the half-maximum response. Importantly, the reparameterisation of $\tau = R_{tot}/EC_{50}$ is required for this model to be structurally identifiable (Table 3.2). BSVs were assumed to be normally distributed for E_m to allow positive and negative effects and lognormally distributed for τ and n. As the goal was to quantify the relationship between observed *in vitro* and clinical effects, K_d and γ were fixed to the *in vitro* estimates describing hNav1.5 inhibition (QRS widening operational model) or rCav1.2 binding at the diltiazem site (PR prolongation operational model).

To estimate the parameters of the operational model using AZD1305 data, the human PK model that was developed in Chapter 5 was used to simulate individual AZD1305 exposures. In addition, the operational model was combined with the combined RR correction and circadian rhythm model (Equation 5.5 which was used to describe QRS and PR variability in humans at baseline in Chapter 5. In addition, an effect compartment model (Equation 2.5 was applied to account for the short delay between exposure and QRS and PR effect, where the distribution rate k_{e0} was assumed to be log-normally distributed.

7.2.2.2 Predicting effects of flecainide, quinidine and verapamil using the system models

The operational models estimated with AZD1305 data may be used to predict the effects of other compounds acting by the same mechanism, as the model separates compound-specific parameters (K_d and γ) from system-specific parameters (E_m, τ and n). To predict the effects of new compounds, the system-specific parameters were fixed to the estimates from the AZD1305 modelling, while the compound-specific parameters were changed to their respective *in vitro*-estimated values. By simulating these models, the effects of flecainide, quinidine and verapamil in humans were simulated and the predictions compared to the collected data from the literature study in Chapter 6. This can be viewed as a form of validation of the system-specific

parameters, as this evaluates the performance of the system model to predict new data on which it was not trained.

95% confidence intervals for the typical effects were constructed from the covariance matrices of the typical parameters for the PD drug effects, and 95% prediction intervals from the estimated typical parameters, between-subject variabilities and residual variabilities. 10000 randomly sampled parameter sets were simulated and sorted at 100 concentrations between 0 and the observed C_{max}, and the 2.5th and 97.5th percentiles were extracted.

7.2.2.3 Quantifying the translational relationship using the system models

The system parameters were used to predict QRS and PR prolongations at 0-100% inhibition/binding by simulating only the link between ion channel effect and QRS/PR effect according to

$$\Delta ECG = \frac{E_m RC^n}{(100/\tau)^n + RC^n} \tag{7.10}$$

at evenly distributed inhibition levels up to 100%. 95% confidence intervals for the typical effects were constructed from the covariance matrices of the typical parameters for the PD drug effects, and 95% prediction intervals from the estimated typical parameters, between-subject variabilities and residual variabilities. 10000 randomly sampled parameter sets were simulated and sorted at 100 concentrations between 0 and the observed C_{max}, and the 2.5th and 97.5th percentiles were extracted. The translational relationships were used to identify nonclinical effects corresponding to 10% QRS/PR prolonations in humans.

7.3 Translation to QRS widenings in humans

7.3.1 Comparison of baseline parameters between species

Models to minimise baseline variability are investigated in guinea pigs, dogs and humans in Chapter 5. In these investigations, data were pooled for each species separately, using vehicle data from two guinea pig studies and five dog studies and placebo data from one human study. A selection of baseline models were fitted to these data, namely the constant baseline model, a model incorporating correction to simulaneous RR intervals, a circadian rhythm model comprising of a single cosine function, and a combination of the two later models (Equations 5.2-5.5). Estimates for the parameters of the selected final baseline models are summarised in Table 7.1. For each species, an optimal baseline model was selected based on its relative likelihood and its complexity, where the most simple model with at least 5% relative

likelihood compared to the model with the lowest AIC value was selected (Equation 5.1).

Table 7.1 Comparison of the extracted baseline parameters of QRS intervals in guinea pigs, dogs and humans.

	Human	**Dog**		**Guinea pig**	
	Estimate	**Estimate**	**% of human**	**Estimate**	**% of dog/human**
$\boldsymbol{QRS_0}$ **(ms)**	94	47	50	22	47/23
$\boldsymbol{A}$ **(ms)**	4.8	-	-	NA	
$\boldsymbol{\alpha}$	0.046	0.038	83	-	-
Residual error (ms)	1.4	2	143	0.32	23/16

Parameter estimates from the "best" models when evaluating pooled data from two vehicle guinea pig studies, pooled data from five vehicle dog studies and placebo human data from one phase I study. The BSV of α was assumed to be lognormal in dogs and normal in humans as some humans had negative QRS-RR correlations. Assuming normally distributed α in dogs led to a similar estimate of 0.44.

Typical QRS interval point baselines were 94 ms in humans, 47 ms in dogs (50 % of human duration) and 22 ms in guinea pigs (23% of human duration). Correction to RR intervals improved goodness of fit slightly to QRS intervals in humans and dogs with estimated correction coefficient (α) values around 0.04-0.05, but were negligible when describing QRS intervals in guinea pigs. Including circadian rhythms improved the goodness of fit to human data only, with an amplitude of 1.4 ms, but did not improve the goodness of fit to QRS intervals in dogs and were not evaluated in guinea pigs as the experimental time was short compared to the period of the investigated circadian rhythm function (2 vs. 24 hours). These results suggest that simpler models are sufficient when fitting animal data compared to human data. This may be a result of different physiologies, i.e. that the circadian rhythms and correlations to RR are larger in humans, but may also be a result of less noise in the human data, allowing more detail when estimating the baselines. In fact, residual variability was larger in dogs (≈4%) compared to guinea pigs and humans (≈1.5%), most likely because dogs were allowed to move freely during the experiment, while humans were resting and the guinea pigs were anaesthetised.

7.3.2 Empirical translation of *in vivo* effects

Drug effect parameters were extracted from the final PKPD models in guinea pigs, dogs and humans (Chapter 5) and directly applied from the human exposure-effect models (Chapter 6), are summarised in Table 7.2. QRS effects of AZD1305 and quinidine were well described by proportional models in dogs and humans, as were

QRS effects by flecainide in dogs, while the effects in guinea pigs were better described by a power model and in humans by an E_{max} model (Equations in Table 7.2). Also, in humans, a short delay was identified between AZD1305 plasma concentrations and QRS widening. The collected drug effect parameters summarised in Table 7.2 were used to simulate the model-predicted drug effects in each species (Figure 7.3).

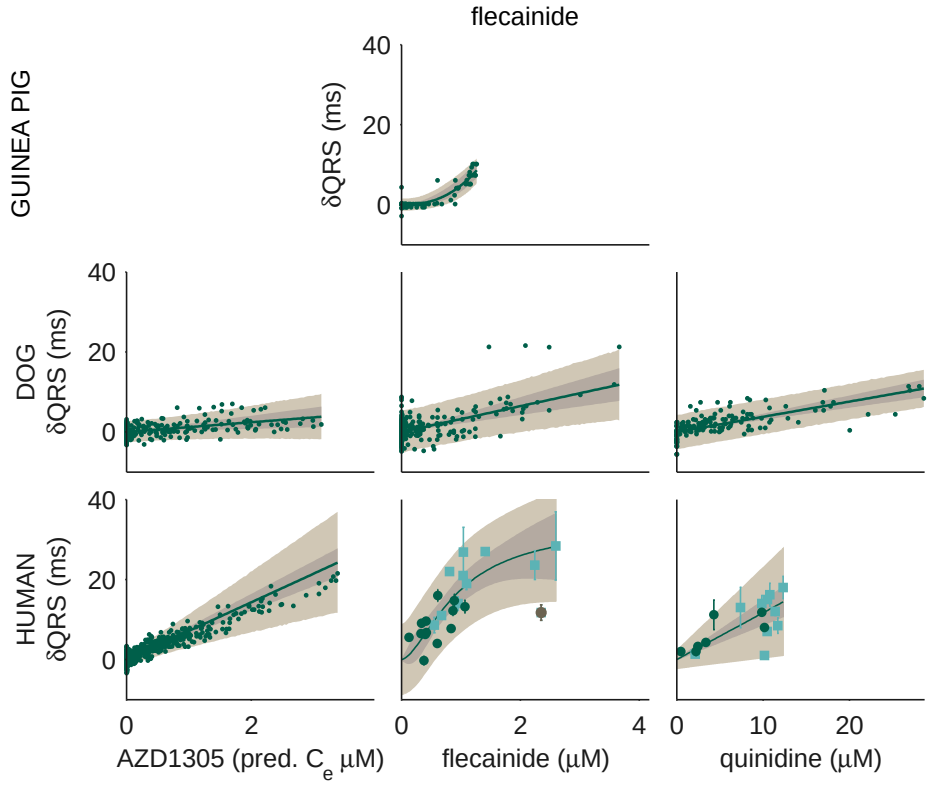

Figure 7.3 QRS prolongations in guinea pigs (top row), dogs (middle row) and humans (bottom row) induced by AZD1305 (left column), flecainide (middle row) and quinidine (right row). Data points represent individual healthy animal/human volunteer change from model-predicted QRS baseline against simulated concentrations in the plasma (dog) or effect compartment (guinea pig, AZD1305 human) (dots), or associated average exposure-ΔQRS pairs with standard errors where available in healthy volunteers (circles) and in patients (squares). The shaded areas represent the 95% confidence intervals (darker area) and prediction intervals (lighter area). Brown colours represent excluded data (human flecainide).

Simulated QRS widenings in humans were plotted against the corresponding effects at matched exposures in guinea pigs and dogs to visualise the translational relationships for each compound (Figure 7.4). 10% QRS widening in humans corresponded to 4.6% (CI range: 2.1-9.9) in guinea pig and 2.3-3.3% (CI range: 0.8-4.5) in dog at matched total concentrations. The confidence intervals for all three compounds overlapped for the dog to human translation, while only one compound was available for the guinea pig to human translation. QRS interval baselines were

Table 7.2 Summary of the selected QRS drug effect models for the antiarrhythmic compounds.

	AZD1305		**Flecainide**		**Quinidine**	
	Estimate (SE)	**BSV % (SE)**	**Estimate (SE)**	**BSV % (SE)**	**Estimate (SE)**	**BSV % (SE)**
HUMAN	$\Delta QRS = slope * C_{e,u}$		$\Delta QRS = E_{max} C_u^n / (EC_{50}^n + C_u^n)$		$\Delta QRS = slope * C_u$	
$\boldsymbol{QRS_0}$ **(ms)**	96 (1.08)	5.8 (0.838)				
slope **(ms** μ**M^{-1})**	11.4 (0.84)	26.1 (1.39)	-		9.57 (1.14)	
$\boldsymbol{E_{max}}$ **(ms)**	-	-	33.7[a] (10.8)		-	
$\boldsymbol{EC_{50}}$ **(**μ**M)**	-	-	0.573[a] (0.256)		-	
n	-	-	1.65 (0.61)		-	
$\boldsymbol{ke_0}$ **(h^{-1})**	43.1 (27.1)	203 (13.7)	-		-	
DOG	$\Delta QRS = slope * C_u$		$\Delta QRS = slope * C_u$		$\Delta QRS = slope * C_u$	
$\boldsymbol{QRS_0}$ **(ms)**	46.0 (1.4)	5.9 (2.1)	53.6 (1.5)	5.68 (2.03)	53.3 (1.7)	6.25 (2.23)
slope **(ms** μ**M^{-1})**	1.93 (0.67)	66.2 (25.2)	5.38 (0.95)	30.8 (14.3)	3.00 (0.25)	-
GUINEA PIG			$\Delta QRS = a * C_{e,u}^b$			
$\boldsymbol{QRS_0}$ **(ms)**			21.7 (0.893)	11.6 (2.92)		
slope **(ms** μ**M^{-1})**			-	-		
a			16.9 (1.66)	-		
b			2.46 (0.365)	23.4 (9.15)		
$\boldsymbol{ke_0}$ **(h^{-1})**			1.6 (0.111)	-		

All estimates are mean±SE. QRS_0, baseline; *slope*, proportional unbound drug effect; E_{max}, maximal effect; EC_{50}, unbound concentration at 50% effect; n, Hill factor; a and b, parameters of the power model; k_{e0}, rate of distribution to the effect compartment. BSV is presented as the coefficient of variation, approximated by CV% = SD*100 for log-normal distributions. [a]Correlation $E_{max} : EC_{50}$ was 0.977.

shorter in guinea pigs and dogs by approximately three quarters and half, respectively. Comparisons of absolute differences therefore further increased the translational gap. Fractions of PPB were similar between the investigated species, and similar results were therefore acquired while applying unbound and total concentrations. All *in vivo* to clinical translations are shown assuming the same PPB in each species.

7.3.3 Empirical translation of *in vitro* effects

Drug effects were simulated using the final human drug effect models and plotted against the *in vitro* effects at matched exposures to visualise the translational relationships for each compound (Figure 7.5). Nonclinical effects corresponding to 10% QRS widening in humans were extracted. QRS widening of 10% occurred at unbound concentrations corresponding to 3-7% hNav1.5 inhibition *in vitro*. This indicates that conduction liabilities may occur well below the IC_{50} of a compound, where Hill factors have a large impact. Hill factors were 0.75-1.2 for the investigated compounds. However, assuming Hill factors of 1 resulted in considerably less consistent translational relationships (2-10% hNav1.5 inhibition compared to 3-7% when Hill factors were included). Confidence intervals for AZD1305 and quinidine were overlapping, while the relationship for flecainide was steeper. Contrary to the *in vivo* to clinical translations, accounting for the free fractions of drug in plasma was vital for consistent *in vitro* to human translational relationships between the compounds.

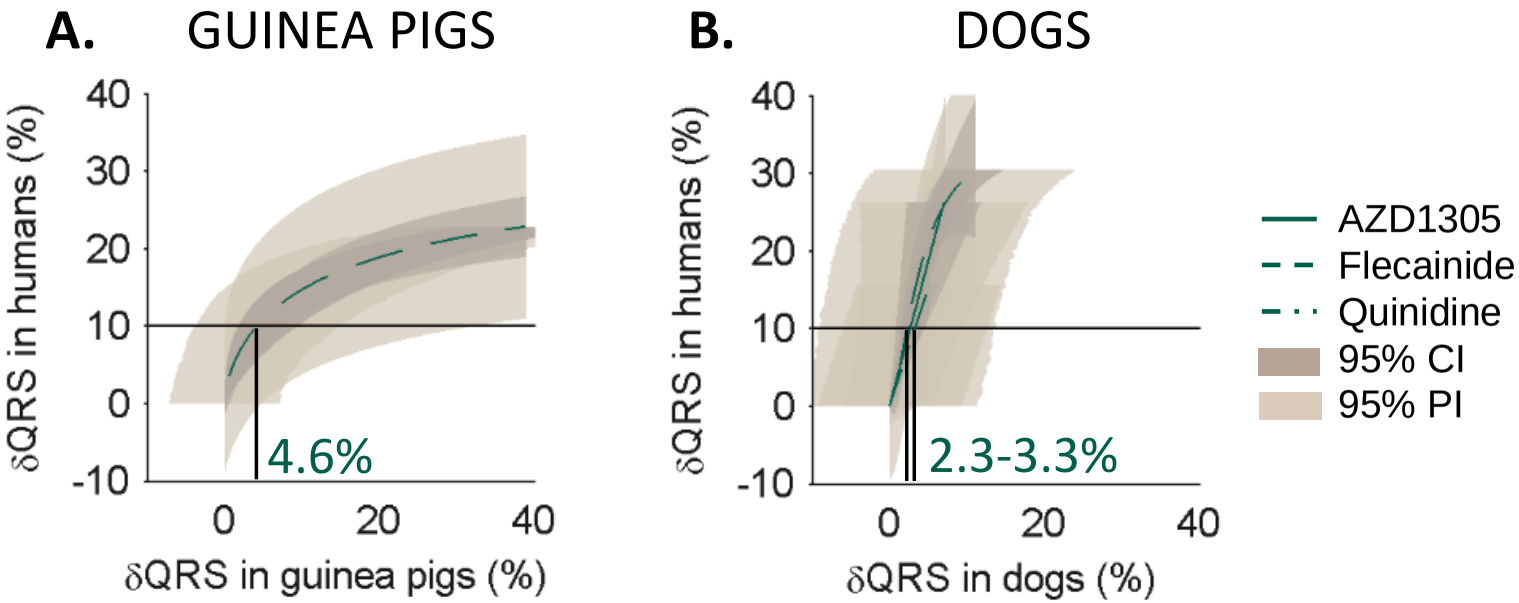

Figure 7.4 Top-down translation to QRS widenings in humans from QRS widening in A. guinea pigs and B. dogs, by AZD1305 (solid lines), flecainide (dashed lines) and quinidine (dashed-dotted lines). Effects of AZD1305 and quinidine in guinea pigs were not available.

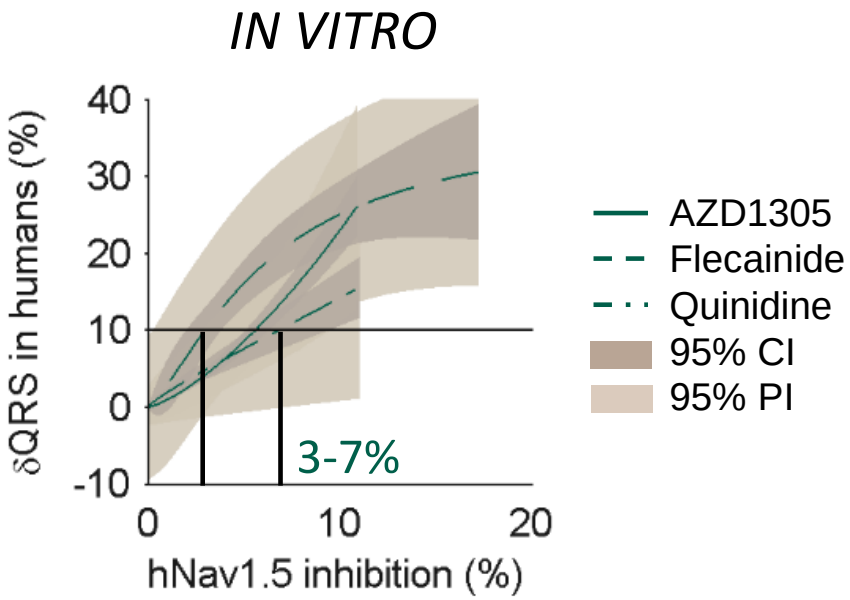

Figure 7.5 Top-down translation to QRS widenings in humans from hNav1.5 inhibition *in vitro*, by AZD1305 (solid lines), flecainide (dashed lines) and quinidine (dashed-dotted lines).

7.3.4 Semi-mechanistic translation of *in vitro* effects

The operational model (Equation 7.9) well described AZD1305-induced QRS widenings. However, as maximum QRS widenings were not reached in these data, the model was practically unidentifiable when estimating both the parameter describing the maximum QRS widening possible in the system (E_m) and the transducer ratio (τ), which control the strength of the transduction from ion channel inhibition to QRS widening. This identifiability issue led to high correlation between E_m and τ (-0.97) and was solved by fixing E_m. Different values of E_m were investigated (20-100 ms). Similar goodness of fit values and residual variabilities were achieved for E_m values between 40 and 100 ms, while the goodness of fit was worse at E_m=20 ms. To investigate the influence of the chosen E_m on the behaviour of the fitted model, simulations were conducted for optimised models with fixed E_m values between 40 and 100 ms (Figure 7.6). This showed that regardless of E_m being 40 or 100 ms, these models result in highly similar model predictions up to 20 ms (after which predictions diverge, with larger effects for increasing E_m values due to saturation at different effect levels). However, widenings above 20 ms are unlikely to occur in a safety setting (by a drug not intended to cause QRS widening), while effects in the range of 5-10 ms are likely to cause concern.

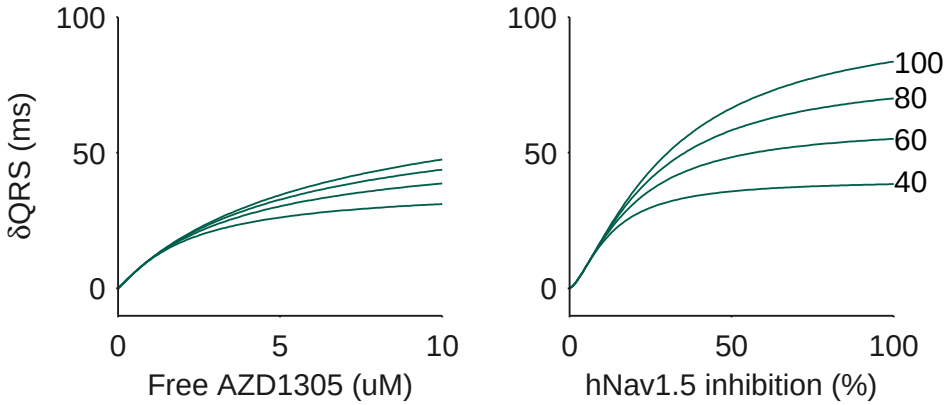

Figure 7.6 Predicted AZD1305-QRS prolongation relationship (left) and hNav1.5 inhibition-QRS widening relationship for operational models with E_m fixed at 40, 60, 80 and 100 ms (followed by estimation of the remaining parameters) show that QRS widenings up to 20 ms are predicted similarly despite the fact that E_m is varied.

An E_m of 40 ms QRS widening was selected based on the simulation results and the highest QRS widenings reached in the clinical literature data sets (31 ms). The estimated model well captured the observed drug-induced QRS widenings (Figures 7.8 and 7.7). The final estimate for τ was high (8.0 ± 0.4), suggesting an efficient signal transduction with high signal amplification (Table 7.3). The selected value of E_m influences the estimated value of τ. Baseline and effect compartment parameters were similar to the estimates for the PKPD models (Chapter 5).

Table 7.3 Parameter estimates for the human AZD1305 operational model describing baseline and drug-induced effects on QRS interval durations.

	Estimate (SE)	**BSV % (SE)**	**IOV % (SE)**
$\boldsymbol{QRS_0}$ **(ms)**	95.9 (1.08)	5.78 (0.832)	2.10 (0.32)
$\boldsymbol{\alpha}$	0.0468 (0.0077)	1340 (150)	-
$\boldsymbol{A}$ **(%)**	1.55 (0.157)	42.2 (5.79)	-
$\boldsymbol{\phi}$ **(h)**	-6.51 (0.311)	22.5 (1.37)	-
$\boldsymbol{E_m}$ **(ms)**	40 (fixed)	-	-
$\boldsymbol{\tau}$	8.00 (0.39)	8.74 (3.12)	-
$\boldsymbol{n}$	1.54 (0.10)	21.1 (2.4)	-
$\boldsymbol{ke_0}$ **(h^{-1})**	37.4 (23.7)	210 (10)	-
Additive residual (ms)	1.00 (0.02)	-	-

BSV and IOV are presented as the coefficient of variation, approximated by CV% = ω*100 for log-normal distributions.

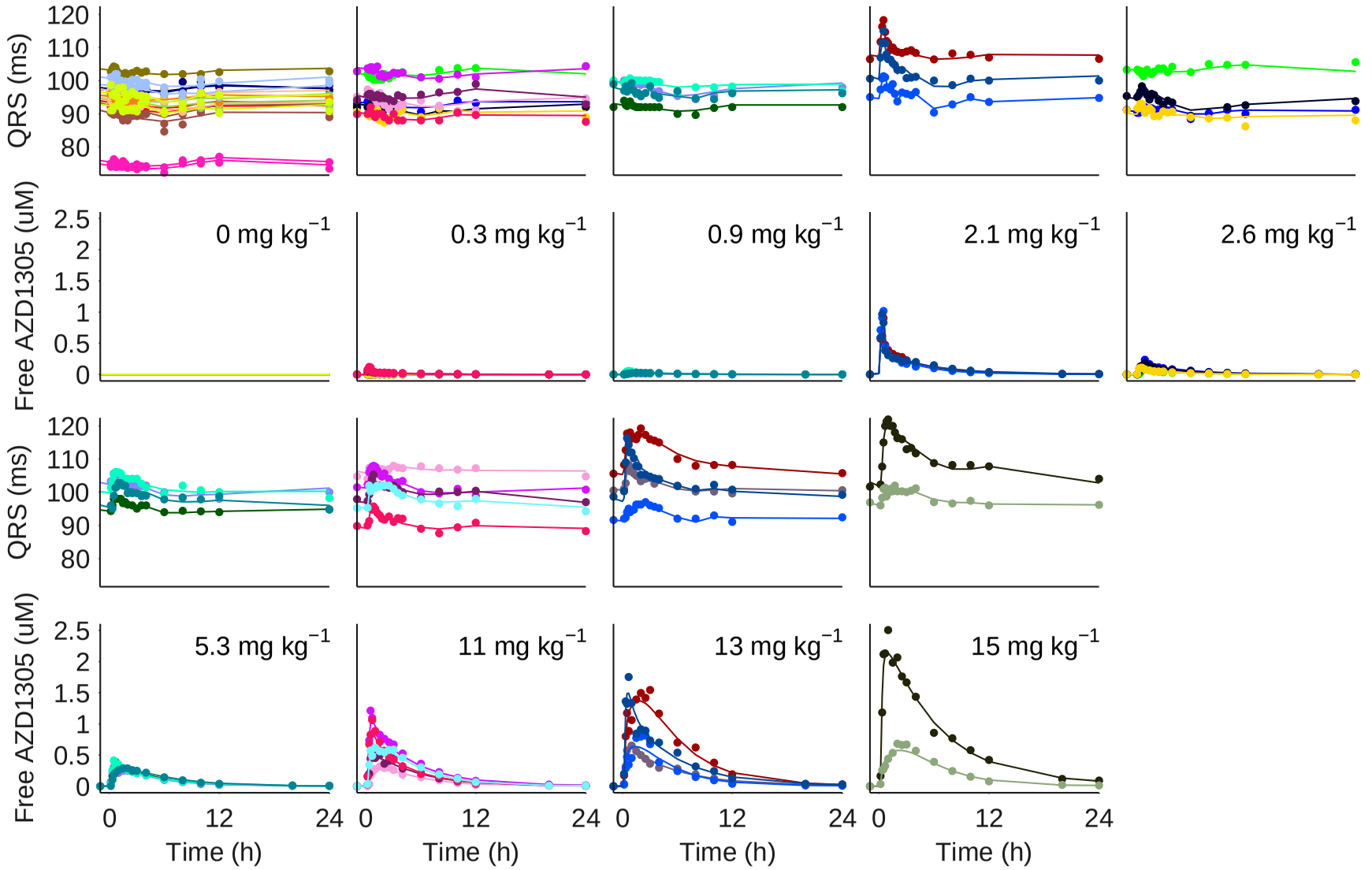

Figure 7.7 QRS interval duration and unbound plasma concentration data (markers) together with operational model fits (lines) for humans treated with AZD1305.

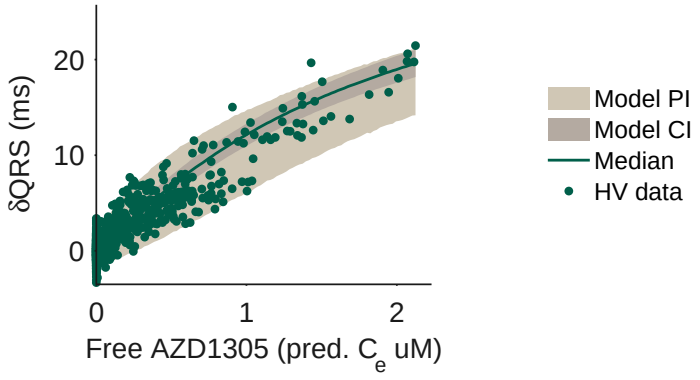

Figure 7.8 Baseline-subtracted QRS data and simulated QRS widening for the operational model.

7.3.4.1 Simulating the *in vitro* to clinical relationship

The translational relationship between inhibited hNav1.5 and QRS widening in humans was simulated and 95% confidence and prediction intervals generated (Figure 7.9). These results predict that only 5-7% inhibition of hNav1.5 is required to induce 10% QRS widening.

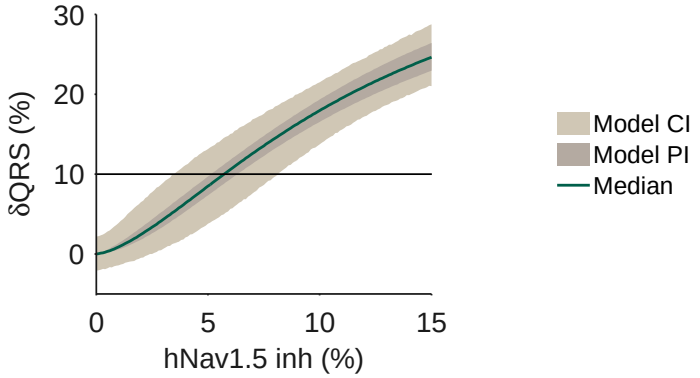

Figure 7.9 Model predicted translation between hNav1.5 inhibition *in vitro* and QRS widening in humans, highlighting the confidence interval for inhibited ion channel at 10% QRS widening.

7.3.4.2 Predicting effects of flecainide and quinidine using the estimated system parameters

The system parameters were combined with *in vitro* potency parameters for flecainide and quinidine and used to predict the QRS widening of these compounds in the measured range of unbound concentrations (Figure 7.10). QRS widenings induced by quinidine were well predicted while flecainide effects were slightly underpredicted.

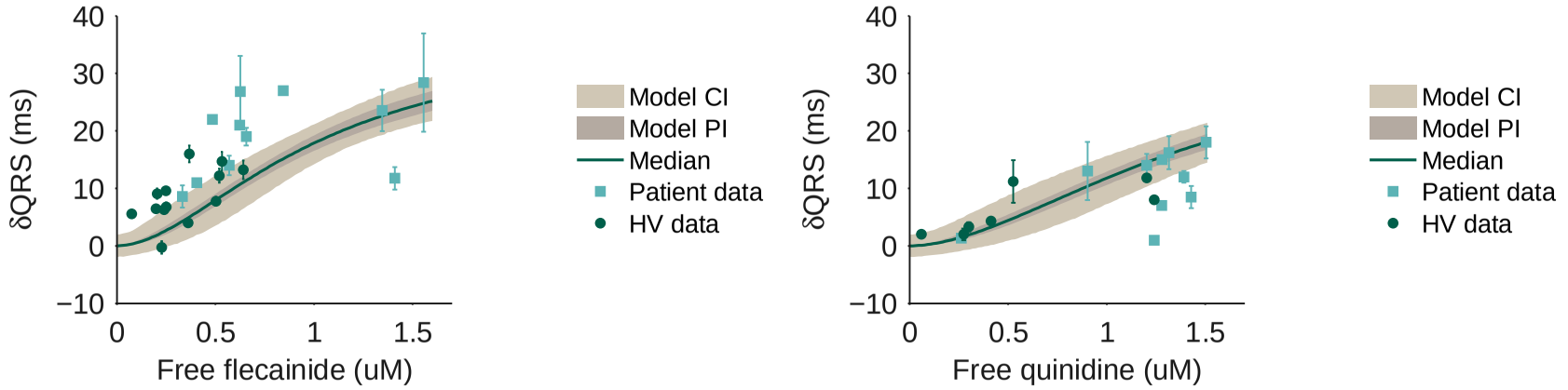

Figure 7.10 Model predicted and measured effects of flecainide and verapamil in humans. Predictions were generated using the estimated signal transduction parameters and the *in vitro* estimated potency in the hNav1.5 assay. Clinical data were collected from literature studies and represent effects in healthy volunteers (dark green) and patients (light green).

7.4 Translation to PR prolongations in humans

7.4.1 Comparison of baseline parameters between species

Models to minimise baseline variability are investigated in guinea pigs, dogs and humans in Chapter 5. In these investigations, data were pooled for each species separately, using vehicle data from two guinea pig studies and five dog studies and placebo data from one human study. A selection of baseline models were fitted to these data, namely the constant baseline model, a model incorporating correction to simulaneous RR intervals, a circadian rhythm model comprising of a single cosine function, and a combination of the two later models (Equations 5.2-5.5). Estimates for the parameters of the selected final baseline models are summarised in Table 7.4. For each species, an optimal baseline model was selected based on its relative likelihood and its complexity, where the most simple model with at least 5% relative likelihood compared to the model with the lowest AIC value was selected (Equation 5.1).

Table 7.4 Comparison of the extracted baseline parameters of PR intervals in guinea pigs, dogs and humans.

	Human	**Dog**		**Guinea pig**	
	Estimate	**Estimate**	**% of human**	**Estimate**	**% of dog/human**
$\boldsymbol{PR_0}$ **(ms)**	170[a]	103	61	62.4	61/37
$\boldsymbol{A}$ **(ms)**	4.8	1.9	136	NA	
$\boldsymbol{\alpha}$	0.19	0.16	84	0.582	306
Residual error (ms)	3.6	5.4	235	1.45	63

Parameter estimates from the "best" models when evaluating merged vehicle guinea pig (2 studies) and dog data (5 studies) respectively, and the placebo human data from the AZD1305 study. The BSV of α was assumed to be lognormal in dogs and normal in humans as some humans had negative PR-RR correlations. Assuming normally distributed α in dogs led to a similar estimate of 0.17. [a]PQ intervals.

Typical PR interval point baselines were 170 ms in humans, 103 ms in dogs (61% of human duration) and 62 ms in guinea pigs (37% of human duration). Correction to RR intervals improved the goodness of fit to PR intervals in all three species with estimated correction coefficient (α) values of 0.19, 0.16 and 0.58 in humans, dogs and guinea pigs respectively. Despite the very high α value when fitting vehicle guinea pig PR intervals, RR correction only improved estimation of RR intervals in guinea pigs in one of the two full data sets including also drug treatment data (Sections 5.7.2 and 5.9.2). Including circadian rhythms improved goodness of fit to PR intervals in humans and dogs, with amplitudes of 5 and 2 ms (3 and 2% of the estimated point baselines respectively), and were not evaluated in guinea pigs.

As for QRS intervals, residual variability was larger in dogs (≈5%) compared to guinea pigs and humans (≈2%).

7.4.2 Empirical translation of *in vivo* effects

Drug effect parameters were extracted from the final PKPD models in guinea pigs, dogs and humans (Chapter 5) and directly applied using the human exposure-effect models (Chapter 6) and are summarised in Table 7.5. PR effects of AZD1305 were well described by proportional models in dogs and humans, as were flecainide and verapamil effects in guinea pigs, while verapamil effects in dogs and humans and flecainide effects in humans were better described by E_{max} models (Equations in Table 7.5). Also, in guinea pigs and for AZD1305 treatment in humans, short delays were identified between plasma drug concentrations and PR prolongations. The collected drug effect parameters summarised in Table 7.5 were used to simulate the model-predicted drug effects in each species (Figure 7.11).

Table 7.5 Summary of the selected PR drug effect models for the antiarrhythmic compounds.

	AZD1305		**Flecainide**		**Verapamil**	
	Estimate	**BSV %**	**Estimate**	**BSV %**	**Estimate**	**BSV %**
Human	$\Delta PR = slope C_{e,u}$		$\Delta PR = E_{max} C_u^n / (EC_{50}^n + C_u^n)$		$\Delta PR = E_{max} C_u / (EC_{50} + C_u)$	
$\boldsymbol{PR_0}$ **(ms)**	160 (4)	12 (2)				
slope **(ms/μM)**	17.0 (2.6)	52 (4)	-		-	
$\boldsymbol{E_{max}}$ **(ms)**	-	-	68.9[a] (27.2)		55.9 (6.8)	
$\boldsymbol{EC_{50}}$ **(μM)**	-	-	0.77[a] (0.43)		0.041 (0.014)	
$\boldsymbol{n}$	-	-	1.57 (0.51)		1 (fixed)	
$\boldsymbol{k_{e0}}$ **(h^{-1})**	10.5 (2.4)	-	-		-	
Dog	$\Delta PR = slope C_u$		$\Delta PR = slope C_u$		$\Delta PR = E_{max} C_u / (EC_{50} + C_u)$	
$\boldsymbol{PR_0}$ **(ms)**	102 (4)	8.0 (2.9)	95.8 (2.3)	4.8 (1.7)	111 (6)	11 (4)
slope **(ms/μM)**	13.8 (1.8)	23 (10)	11.0 (1.2)	13 (11)	-	-
$\boldsymbol{E_{max}}$ **(ms)**	-	-	-	-	105 (9)	-
$\boldsymbol{EC_{50}}$ **(μM)**	-	-	-	-	0.196 (0.088)	84 (31)
Guinea pig			$\Delta PR = slope C_{e,u}$		$\Delta PR = slope C_{e,u}$	
$\boldsymbol{PR_0}$ **(ms)**			57 (4.39)	22 (5)	61.6 (1.6)	7.4 (1.9)
slope **(ms/μM)**			4.14 (1.84)	82 (31)	161 (70)	-
$\boldsymbol{k_{e0}}$ **(h^{-1})**			11.9 (3.6)	-	1.07 (0.80)	87 (33)

All estimates are mean±SE. PR_0, baseline; *slope*, proportional unbound drug effect; E_{max}, maximal effect; EC_{50}, unbound concentration at 50% effect; n, Hill factor; a and b, parameters of the power model; k_{e0}, rate of distribution to the effect compartment. BSV is presented as the coefficient of variation, approximated by CV% = SD*100 for log-normal distributions. [a]Correlation $E_{max} : EC_{50}$ was 0.979.

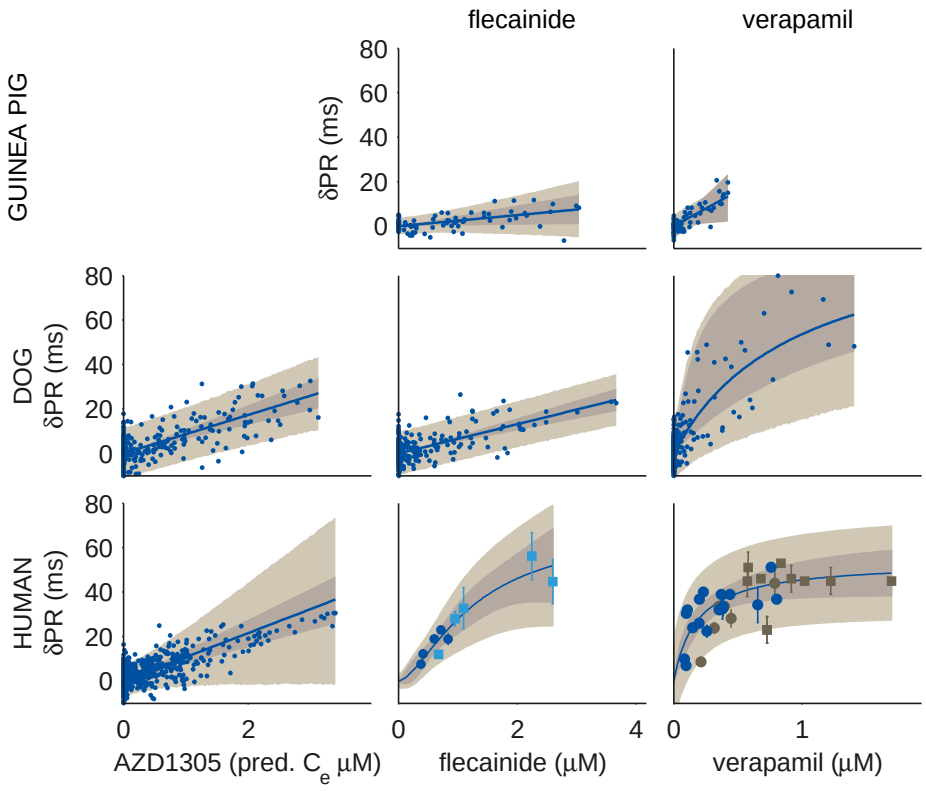

Figure 7.11 PR prolongations in guinea pigs (top row), dogs (middle row) and humans (bottom row) induced by AZD1305 (left column), flecainide (middle row) and verapamil (right row). Data points represent individual healthy animal/human volunteer change from model-predicted PR baseline against simulated concentrations in the plasma (dog) or effect compartment (guinea pig, AZD1305 human) (dots), or associated average exposure-PR pairs with standard errors where available in healthy volunteers (circles) and in patients (squares). The shaded areas represent the 95 % confidence intervals (darker area) and prediction intervals (lighter area). Brown colours represent repeated dosing data (human verapamil).

Simulated PR prolongations in humans were plotted against effects at matched exposures in guinea pigs and dogs to visualise the translational relationships for each compound (Figure 7.12). 10 % PR prolongation in humans corresponded to a 2.3-4.3 % change in guinea pigs (CI range: 0.3-7.6) and 2.4-10 % change in dogs (CI range: 1.9-28) at matched total concentrations. The confidence intervals for flecainide and verapamil overlapped in guinea pigs while the confidence intervals for AZD1305 and verapamil overlapped in dogs. The translational relationship for flecainide was steeper in dogs compared to AZD1305 and verapamil. Typical PR interval point baselines were 170 ms in humans, 103 ms in dogs (61 % of human) and 62 ms in guinea pigs (37 % of human), and absolute differences between effects in guinea pigs, dogs and humans were thus larger than relative differences. The *in vitro*-estimated plasma protein bindings (PPBs) were similar between the species, and the translational relationships are therefore shown assuming the same PPB in each species.

Similar results were acquired while applying the *in vitro* PPB estimates.

7.4.3 Empirical translation of *in vitro* effects

Drug effects were simulated using the final human drug effect models and plotted against the *in vitro* effects at matched exposures to visualise the translational relationships for each compound (Figure 7.13). Nonclinical effects corresponding to 10% PR prolongation in humans were extracted. PR prolongations of 10 % occurred at unbound concentrations corresponding to 13-21 % rCav1.2 binding at the diltiazem site *in vitro*. The *in vitro* to clinical relationship for verapamil was slightly steeper compared to those for AZD1305 and flecainide, although the confidence intervals were largely overlapping. As for QRS translations, accounting for the PPB was vital for consistent *in vitro* to human translational relationships between the compounds.

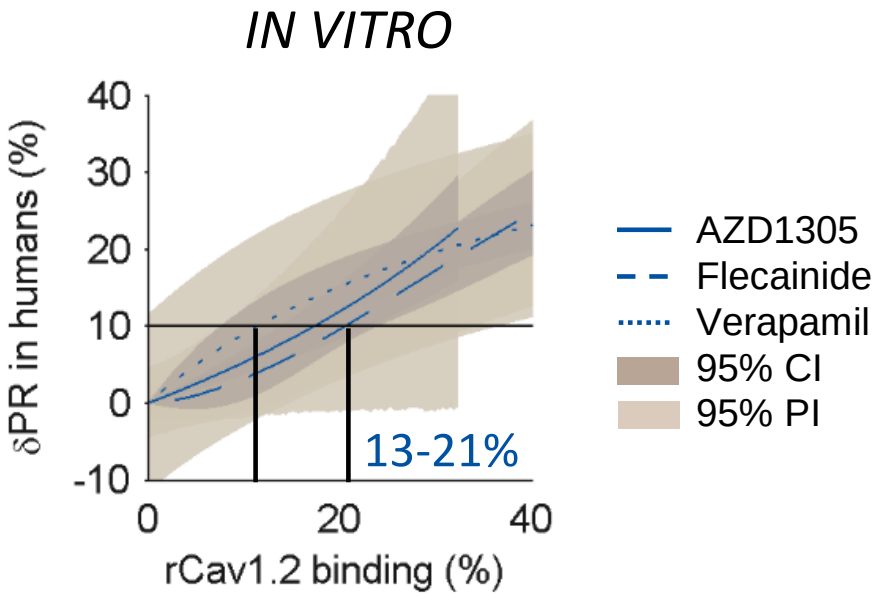

Figure 7.13 Top-down translation to PR prolongations in humans from rCav1.2 binding *in vitro* at the diltiazem site, by AZD1305 (solid lines), flecainide (dashed lines) and verapamil (dotted lines).

7.4.4 Semi-mechanistic translation of *in vitro* effects

The operational model 2.10 well described AZD1305-induced PR prolongations. However, as maximum PR prolongations were not reached in this data set, the model was practically unidentifiable when estimating both the parameter describing the maximum PR prolongation possible in the system (E_m) and the transducer ratio (τ). Similar to the QRS modelling, this identifiability issue led to high correlation

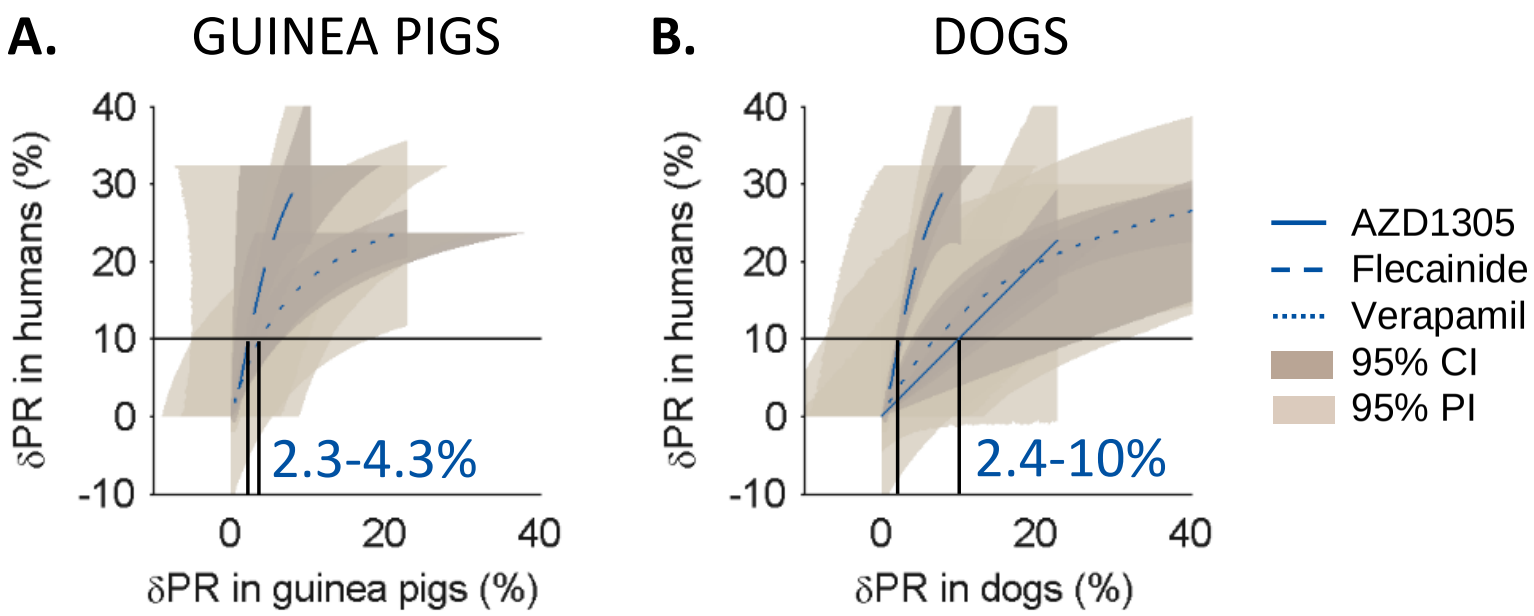

Figure 7.12 Top-down translation to PR prolongations in humans from PR prolongation in A. guinea pigs and B. dogs, by AZD1305 (solid lines), flecainide (dashed lines) and verapamil (dotted lines). Effects of AZD1305 in guinea pigs were not available.

between E_m and τ (-0.83) and was solved by fixing E_m. Different values of E_m were investigated (40-100 ms, Figure 7.14), and resulted in similar predictions up to approximately 30 ms PR prolongation regardless of E_m being 40 or 100 ms. Widenings above 30 ms are unlikely to occur in a safety setting (by a drug not intended to cause PR prolongation), where effects in the range of 10-20 ms are likely to cause concern.

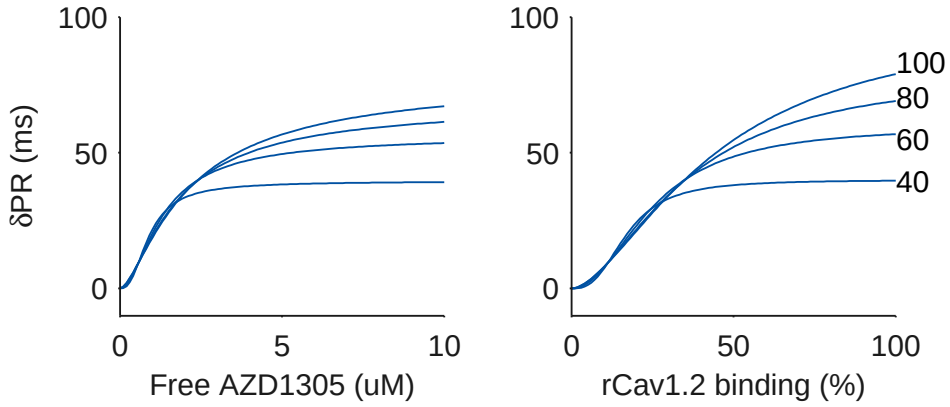

Figure 7.14 Predicted AZD1305-PR prolongation relationship (left) and rCav1.2 binding-PR prolongation relationship for operational models with E_m fixed at 40, 60, 80 and 100 ms show that small PR prolongations are predicted similarly when E_m is varied, and that predictions up to 30 ms PR prolongations are similar for E_m values above 40 ms.

An E_m of 60 ms PR prolongation was selected based on the simulation results and the highest PR prolongations reached in the clinical literature data sets (56 ms). The estimated model well captured the observed drug-induced PR prolongation although the data show large variability (Figures 7.15 and 7.16). The final estimate for the system parameter τ was lower for PR compared to QRS and with larger uncertainty (4.0 ± 0.7 vs. 8.0 ± 0.4), reflecting a less efficient signal transduction and reduced precision due to more variable data (Table 7.6). The selected value of E_m influences the estimated value of τ due to the identifiability issue previously described. Baseline and effect compartment parameters were similar to the estimated values in the PKPD models (Chapter 5).

Table 7.6 Parameter estimates for the human AZD1305 operational model describing baseline and drug-induced effects on PR interval durations.

	Estimate (SE)	BSV % (SE)	IOV % (SE)
QRS_0 (ms)	160 (3.53)	11.7 (1.59)	4.46 (0.69)
α	0.0819 (0.0211)	1340 (22.2)	-
A (%)	2.68 (0.279)	43.8 (3.68)	-
ϕ (h)	-3.09 (0.662)	107 (2.61)	-
E_m (ms)	60 (fixed)	-	-
τ	3.99 (0.69)	59.4 (1.8)	-
n	2.09 (0.22)	-	-
k_{e0} (h^{-1})	14.5 (3.9)	40.9 (43.2)	-
Additive residual (ms)	3.73 (0.09)	-	-

BSV and IOV are presented as the coefficient of variation, approximated by CV% = ω*100 for log-normal distributions.

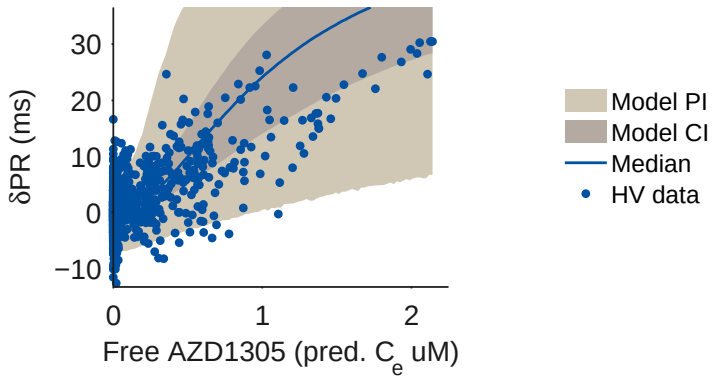

Figure 7.16 Baseline-subtracted PR data and simulated PR prolongations for the operational model.

7.4.4.1 Simulating the *in vitro* to clinical relationship

The translational relationship between bound rCav1.2 and PR prolongation in humans was simulated and 95 % confidence and prediction intervals generated (Figure 7.17). These results predict that 12-22 % binding of rCav1.2 at the diltiazem site is required to induce 10 % PR prolongation.

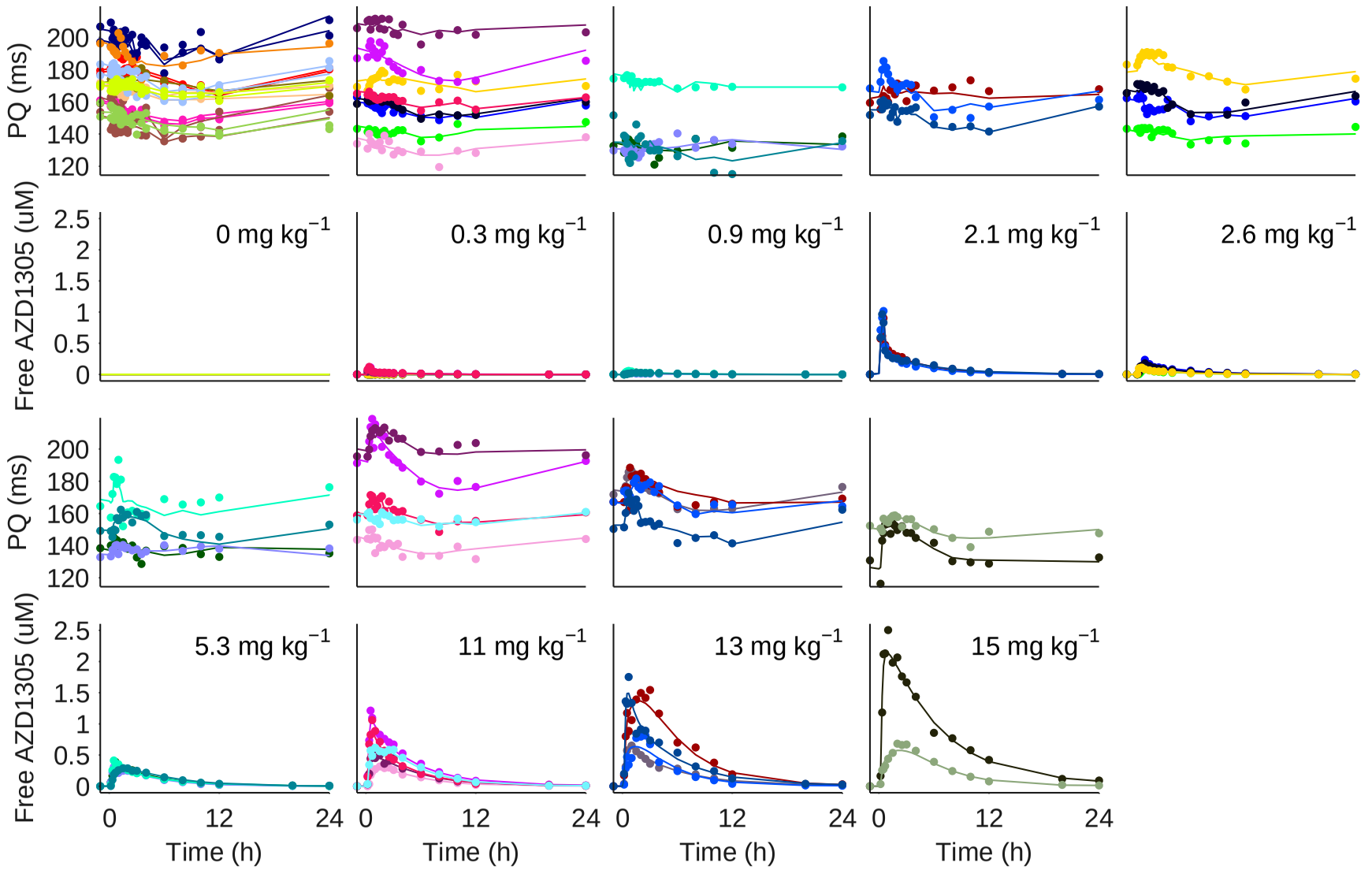

Figure 7.15 PR interval duration and unbound plasma concentration data (markers) together with operational model fits (lines) for humans treated with AZD1305.

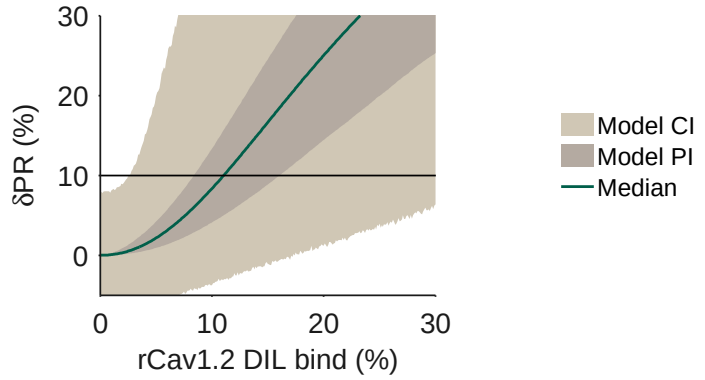

Figure 7.17 Model predicted translation between rCav1.2 binding *in vitro* and PR prolongation in humans, highlighting the confidence interval for bound rCav1.2 at 10% PR prolongation.

7.4.4.2 Predicting effects of flecainide and verapamil using the estimated system parameters

The systems parameters were combined with *in vitro* potency parameters for flecainide and verapamil and used to predict the PR prolongation of these compounds in the measured range of unbound concentrations (Figure 7.18). To account for the different potency and metabolism of the two verapamil enantiomers, the efficacy of verapamil was assumed to be mediated only by the more potent S enantiomer. The estimated K_i for verapamil of 0.044 μM was therefore corrected to account for the predicted enantiomer composition *in vivo* by

$$K_{i,invivo} = \frac{K_{i,invitro} f_{s,invitro}}{f_{s,invivo}} \tag{7.11}$$

where $K_{i,invitro}$ and $K_{i,invivo}$ are the *in vitro* and *in vivo* potencies and $f_{s,invitro}$ and $f_{s,invivo}$ the fraction of the more potent S enantiomer *in vitro* (0.5) and *in vivo* (0.18, [138]), respectively. PR prolongations induced by flecainide were slightly over-predicted while verapamil effects were well predicted by the model.

7.5 Discussion

During preclinical drug development, both *in vitro* and *in vivo* data are generated at AstraZeneca to assess potential safety risks, such as changes in QRS and PR durations. Typically, *in vitro* Cav/Nav studies are conducted during lead identification/optimisation and obtained results (IC_{50}) used, in the context with other data, to drive the chemistry and select compounds to progress into *in vivo* studies. Early *in vivo* studies (e.g. anaesthetised guinea pigs) are typically run during lead optimisation, and provide first cardiac safety information in a complete living system, including QRS/PR, to select/terminate candidate drugs from a chemical

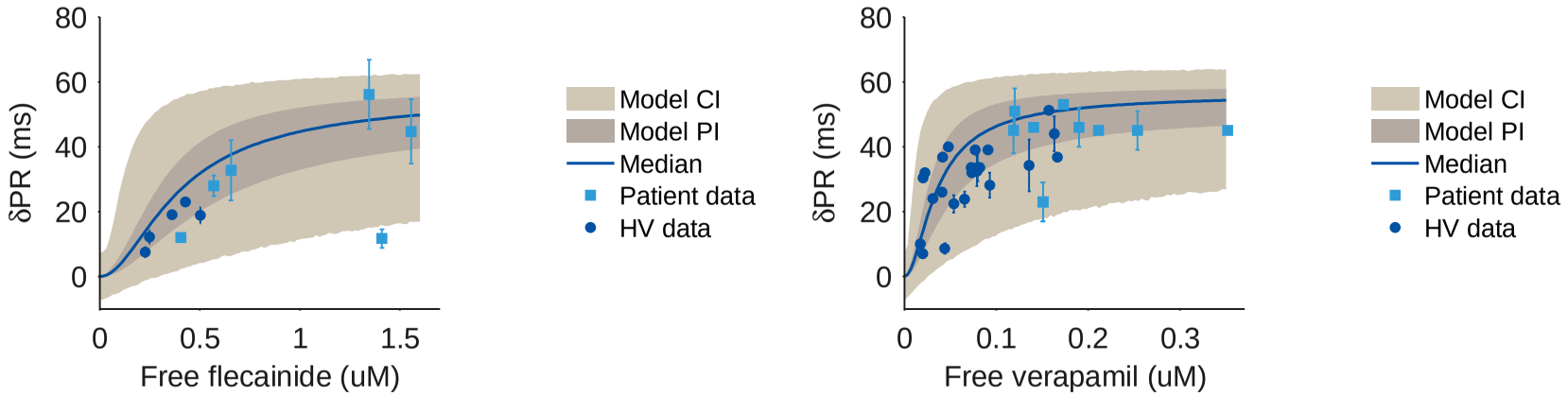

Figure 7.18 Model predicted and measured effects of flecainide and verapamil in humans. Predictions were generated using the estimated signal transduction parameters and the *in vitro* estimated potency in the rCav1.2 assay. Clinical data were collected from literature studies.

series. Prior to FTIM, ICH S7A/B guidance requires a non-rodent (typically dog) telemetry study to assess cardiovascular risk, including QRS/PR changes, as part of the pre-clinical safety package. Together, *in vitro* and *in vivo* data on cardiac conduction form part of an integrated package of evidence for the safety of a potential drug, which can be further strengthened by quantitative predictions of QRS/PR effects in humans based on nonclinical observations.

7.5.1 Small *in vitro* interactions lead to relevant QRS/PR prolongations

Translation between *in vitro* effects and QRS/PR change in humans show that relatively low hNav1.5 inhibition (3-7 %) and rCav1.2 binding (13-21 %) correlate with 10 % QRS/PR change (Figures 7.5 and 7.13). Translation using the middle-out approach resulted in similar thresholds, strengthening the confidence in the predicted relationships. Using margins to IC_{50} of 30-100-fold have been suggested both for unbound C_{max} and hERG channel inhibition [170] and for hNav1.5 [19]. However, the Hill (sigmoidicity) factors have large impact at the low inhibition levels that correlate to clinical effects. For example, 10 % inhibition occurs at concentrations 9 times lower than IC_{50} with a Hill factor of 1, but only 4 times lower with a Hill factor of 1.5. The chosen margins to IC_{50} may therefore be unnecessarily high for compounds with high Hill factors, while potentially missing compounds with small Hill factors. Concentrations corresponding to inhibitions leading to a meaningful human change may therefore provide safer margins, such as 5 % hNav1.5 inhibition and 15 % rCav1.2 binding. A limitation to using IC_{10} values rather than IC_{50} is the higher signal-to-noise ratio at these small inhibition levels, and *in vitro* effects should therefore be evaluated considering the full concentration-response curves.

In vitro to clinical translations to human QRS widenings were highly consistent, although flecainide had a steeper relationship compared to AZD1305 and quinidine (Figure 7.5). This reflects the mechanisms of action of type 1a and 1c antiarrhythmics (quinidine and flecainide, respectively), which bind to the open state of Nav1.5 [171] and dissociate to the closed states at different rates. Flecainide dissociates slower compared to quinidine (>1500 ms vs. 300-1500ms, [172], and more Nav1.5 block therefore remains at the beginning of each action potential, causing more QRS widening. As for QRS, translations of *in vitro* effects to clinical PR prolongations were relatively consistent between the investigated compounds. Verapamil had a steeper relationship, possibly resulting from AV block induced by binding to the verapamil site on Cav1.2 in addition to the diltiazem site. Also, while QRS prolongations are strongly linked to the block of a single ion channel, multiple mechanisms contribute to AZD1305-, flecainide- and verapamil-induced PR prolongations that were not taken into account in this work. For example, AZD1305

and flecainide prolong the P wave (by Nav1.5 block) and flecainide also reduces intra-cellular Ca^{2+} release [173, 174].

While the top-down *in vitro* to clinical relationships provide predictions of human effects at specific *in vitro* levels such as the predicted therapeutic C_{max}, they cannot directly be used to predict the effects for full PK curves. However, this is possible with the semi-mechanistic approach using the estimated system parameters in combination with *in vitro* (unbound) potency. Such predictions may be used to predict exposure-effect relationships as exemplified in Figures 7.10 and 7.18, or alternatively over time simulating QRS/PR effects at a predicted PK. If the true maximum prolongations possible in the systems (E_m values) are larger than the assumed values, there is a risk of under-predicting large QRS/PR effects (>20-30ms). However, such large side effects would most likely result in the discontinuation of the compound despite this under-prediction, and this limitation is therefore of small concern for the purpose of safety assessment.

7.5.2 QRS/PR effects are smaller in animals compared to humans

The translational relationships for QRS/PR effects demonstrated smaller changes at matched exposures in the nonclinical species compared to humans (Figures 7.4 and 7.12). However, across compounds, the effects were consistent, especially for QRS where low percentage changes were 3-4 times larger in humans compared to dogs. PR translations were more variable, with human changes 1-4 times larger compared to dogs. Similar relationships were found for guinea pigs, although the compound set was incomplete.

It is important to note that the levels of effects in dogs and guinea pigs that correspond to meaningful clinical changes of 10% (2-5% for QRS, 2-10% for PR) are well below the effect levels that these studies are typically powered for (guinea pig: 19/21% QRS/PR [23]. However, this power analysis is based on point-wise statistics, whereas employing a PKPD modelling approach increases sensitivity and specificity [18] as all dose levels and time points are used simultaneously. Conducting PKPD modelling of nonclinical *in vivo* data as a routine analysis is therefore recommended to improve the power to identify small QRS/PR effects. Furthermore, nonclinical effects should be evaluated well above the expected therapeutic exposure to ensure that potential side effects in cardiac conduction are developed.

7.5.3 Possible mechanisms for the reduced sensitivity in animals

Several compounds with different mechanisms of action were investigated to account for possible compound-specific differences and to achieve a broader applicability of the recommendations and translational relationships of this work. Anatomically, guinea pig and dog hearts are 300 and 6 times lighter than human hearts [175] and

have smaller specialised tissues, e.g. AV node (reviewed in [176] resulting in shorter QRS and PR intervals. Therefore, evaluating relative rather than absolute changes from baseline reduces the translational gap between guinea pigs, dogs and humans. A major assumption is that the *in vitro*, *in vivo* and clinical (unbound) plasma concentrations all are equivalent to the target tissue exposure. For these compounds, the same fractions unbound were applied as the measured PPBs were similar across species, and considered to be within the variability of the assay. However, small errors in these fractions have direct impact on the translational relationships, and high quality data for the free fractions in each species could potentially improve precision in the translational relationships. Exposures at the target sites may also differ between species due to differences in the distribution to the heart tissue and intra-cellular targets.

The reduced sensitivity of guinea pigs and dogs to conduction slowing is likely to be present at the tissue level as flecainide and quinidine reduce the depolarisation rate more in human atrial tissue compared to guinea pigs, rabbits and dogs [177]. It is not known if *in vitro* studies using guinea pig and dog Nav/Cav would indicate reduced potency compared to human Nav/Cav. Cav1.2 is multi-functional with many splice variants [178] which could potentially differ between species. Nav1.5 is highly conserved between mice, rats, pigs and humans (94-98% amino acid homology [179]), but the relative quantity of each isoform of Nav varies throughout the conduction system (reviewed in [180]) and between species [179]. Thus, conduction slowing may differ between species partly due to differences in the relative quantity of ion channel isoforms and splice variants.

7.5.4 Predicting QRS and PR prolongations in humans

The results of this work may be used to improve predictions of QRS and PR prolongations in humans using nonclinical data in combination with the translational relationships identified in this work (Figure 7.19).

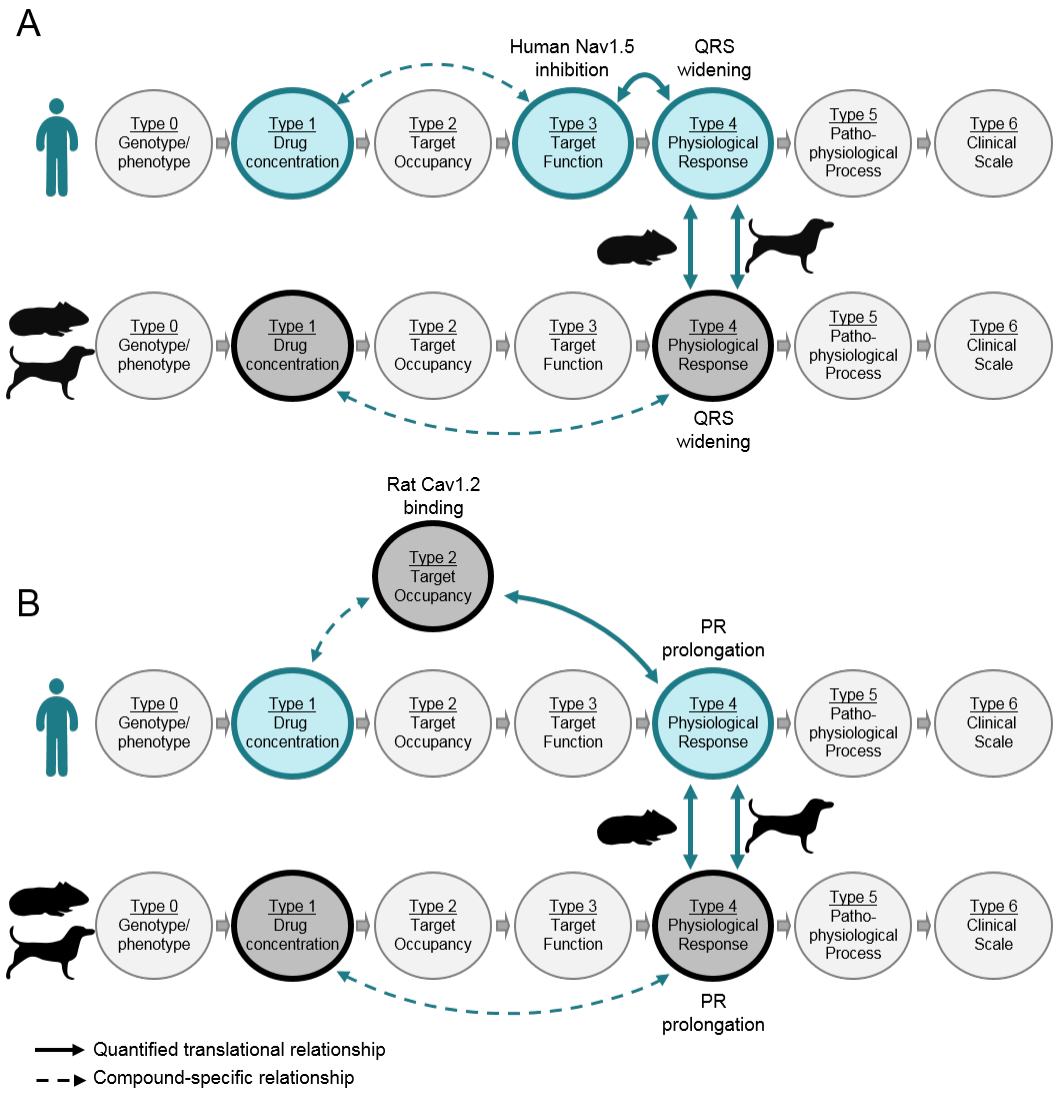

Figure 7.19 **A.** QRS widening and **B.** PR prolongations in humans may be predicted from nonclinical data using the quantitative translational relationships that have been presented in this thesis, as indicated by the arrows representing translational links in the biomarker map [32]. Dashed lines represent compound-specific relationships that can be quantified directly from nonclinical data to be used in combination with the quantitative translational relationships represented by solid lines in order to predict QRS/PR prolongations in humans.

In early *in vitro* and *in vivo* studies, nonclinical effects at exposures resulting in 10% human prolongation may be used to define a margin for acceptable levels of effects in nonclinical studies. This acceptable level is, according to these results, around 2-5% QRS/PR change in guinea pigs or dogs at expected therapeutic exposures (Figure 7.20). Similarly, acceptable *in vitro* effects were around 5% hNav1.5 inhibition and 15% rCav1.2 diltiazem binding. Further, the developed models or provided translational figures (Figures 7.4, 7.5, 7.9, 7.12, 7.13, 7.17) may be easily used to define margins related to a different human effect, such as 5 or 20 %. However, it should be emphasized that relying on *in vitro* data alone is not recommended.

As was discussed above, different mechanisms of ion channel block influences the resulting effect on conduction. For example, a quickly dissociating Nav1.5 blocker may not cause QRS widening, despite its potency *in vitro*.

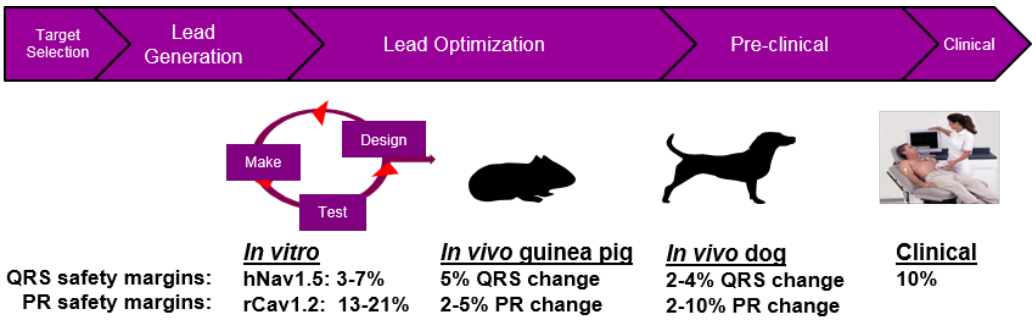

Figure 7.20 Suggested safety margins in nonclinical studies at predicted clinical therapeutic concentrations, in order to reduce risk of QRS or PR prolongations above 10%. The small *in vivo* effects emphasize the importance of sensitive methods for identifying effects in the collected data in combination with doses resulting in super-therapeutic exposures.

Before FTIM studies, a more in-depth assessment of the therapeutic dose range may be required, such as clinical simulations of PR/QRS change over time using the predicted human PK. Prior to this work, quantitative results on the translational relationships were not available in the literature, and a best guess for translating effects may have been for example equal (absolute or relative to baseline) drug effect in humans compared to animals. However, in this work, the percentage QRS/PR change was up to five times larger in humans compared to guinea pigs and dogs. Worst case QRS/PR effects in humans at the expected PK can thus be predicted by simulating not equal, but four times larger slopes than estimated slopes for dogs and guinea pig, while also accounting for baseline and protein binding differences. To include a measure of uncertainty, a best case scenario may also be predicted by a two times larger (QRS) or the same (PR) slope. Although small distributional delays may be present, QRS and PR effects are likely to be well approximated by a direct effect model for orally administered drugs. In addition, the *in vitro* system models can complete the risk assessment by predicting QRS/PR effects over time using the system parameters estimated in this work, together with *in vitro* potency, free fraction of drug in plasma and the predicted human PK. Several independent predictions of clinical effects provide additional confidence and any discordance offers a measure of the uncertainty regarding the human prediction. Therefore, a combined view applying information from *in vitro* and *in vivo* studies such as that illustrated in Figure 7.21 is vital in order to predict cardiac conduction risks before FTIM studies.

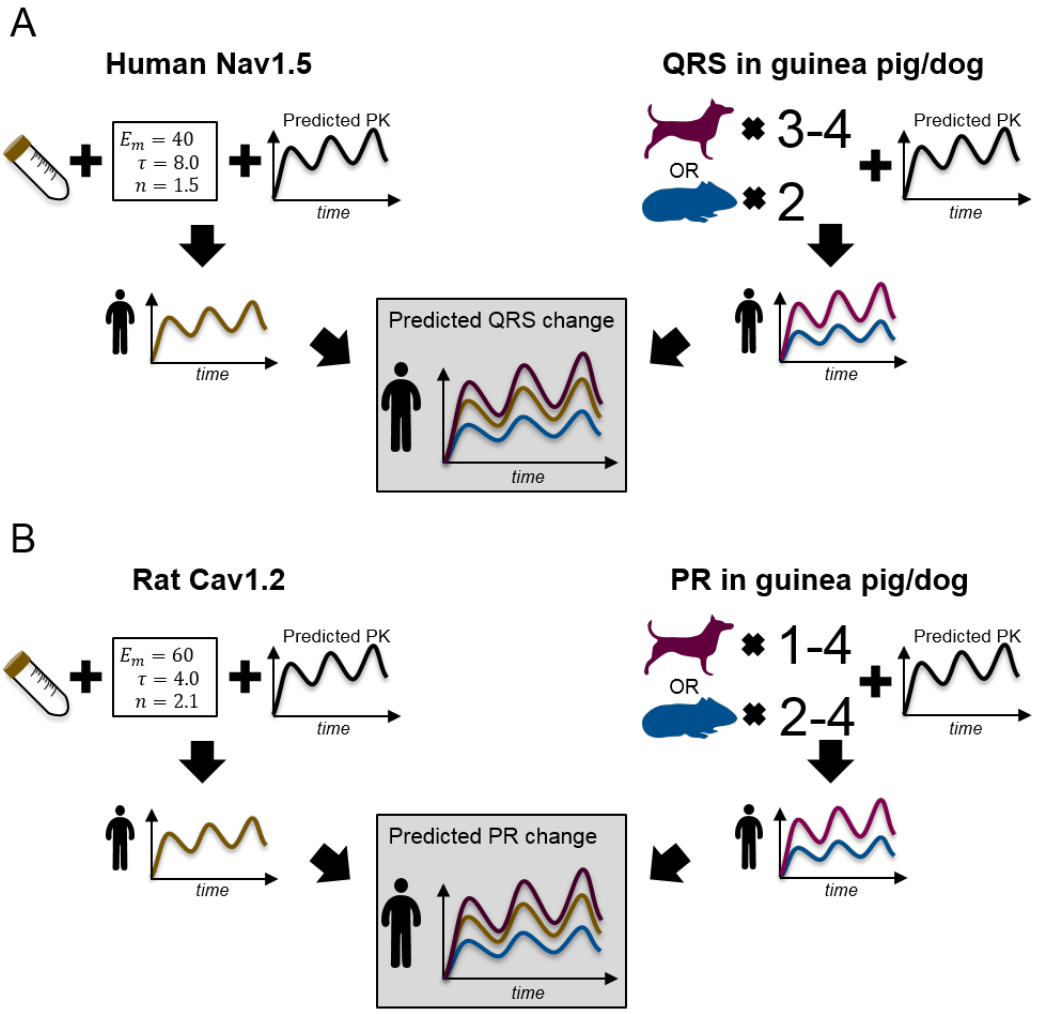

Figure 7.21 The resulting translational relationships from this thesis work can be used to generate risk assessments of **A.** QRS widening or **B.** PR prolongations in humans using nonclinical data from multiple sources, providing a combined view on the predicted risk with increased confidence compared to any single prediction.

7.6 Summary

In this chapter, two approaches to translate nonclinical effects to clinical QRS and PR interval prolongations were presented and used to investigate the translational relationships for four anti-arrhythmic compounds. This is the first quantitative assessment of non-clinical to clinical translation of QRS and PR intervals using mathematical models. The results of these analyses show that small *in vitro* interactions lead to relevant QRS/PR prolongations. These small effects should preferably be evaluated considering the full concentration-response curves as small *in vitro* effects may be difficult to measure in practice. Also, QRS/PR effects are up to four times smaller in guinea pigs and dogs compared to humans. This emphasises the importance of using sensitive techniques such as PKPD modelling to analyse routine *in*

vivo data, and also the importance of evaluating nonclinical effects well above the expected therapeutic exposure. Importantly, using data from multiple nonclinical sources to predict human effects enables multiple independent predictions, where any disagreement between the predicted effects can be viewed as an additional measure of uncertainty.

Chapter 8

Conclusions

The aim of this thesis was to increase the understanding of how drug-induced cardiac conduction slowing in humans, reflected by QRS and PR prolongations in monitored ECGs, may be predicted and mitigated using nonclinical *in vitro* and *in vivo* data. Drug-induced QRS and PR prolongations are, for indications other than cardiac arrhythmias, typically undesired and may increase CV risk [15]. Early identification of risk is therefore important for safe and efficient drug discovery and development. Predicting effects in humans based on observations in animals rely on the understanding of how sensitive animals are compared to humans. However, prior to the work performed for this thesis, no quantitative analysis of the relative effects on QRS and PR in animals and humans could be identified in the literature. In addition, no systematic investigation of M&S approaches for quantifying QRS and PR intervals in animals and humans was identified.

The first objective of this thesis was therefore to "*apply and develop models to quantify QRS and PR intervals monitored in nonclinical species and in humans at baseline conditions and during drug treatment*". This was accomplished by collecting and analysing available nonclinical (guinea pig and dog) and clinical PK and ECG data for six compounds. In Chapter 5, PKPD models were developed for QRS complex durations in guinea pigs (flecainide), dogs (AZD1305, flecainide and quinidine) and humans (AZD1305) and for PR intervals in guinea pigs (flecainide, verapamil), dogs (AZD1305, AZD8683, AZD9164, flecainide and verapamil) and humans (AZD1305). In addition, in Chapter 6, regression models assessing the concentration-effect relationships in humans using data collected in literature studies were developed for QRS widenings (flecainide and quinidine) and PR prolongations (flecainide and verapamil). AZD8683 and AZD9164 did not prolong QRS or PR in humans at the evaluated exposures.

Based on the results from these compounds, small QRS and PR effects (up to around 20%) may be modelled using proportional drug effect models, while non-linear models such as the E_{max} model may be more appropriate for larger effects.

Also, delays between plasma drug concentrations and QRS or PR effects were well described using the effect compartment model. In addition, it was shown that the choice of baseline model can influence the estimation of the drug effects. Residual unexplained variability of PR intervals was reduced by incorporating heart-rate correction and a circadian rhythm to describe baseline variability. QRS intervals required less detailed baseline models, and a constant baseline model was often sufficient. In general, the baseline models had higher influence in humans compared to dogs and least influence in guinea pigs. The results of this modelling investigation may be used to support the design of routine modelling protocols for analysing QRS and PR interval data. Such analyses may improve the sensitivity to detect small QRS/PR changes potentially missed by point-wise statistical methods, which are currently applied to analyse these data.

The second objective was to "*investigate the translation between nonclinical* in vitro *and* in vivo *effects and clinical QRS and PR prolongations*". This was accomplished by two different translational analyses, both described in Chapter 7. The first was an investigation into the relative effects of the *in vitro* and *in vivo* assays compared to the clinic, and was based on the developed models from Chapters 5 and 6. This translational investigation showed that QRS and PR changes were smaller at matched exposures in the nonclinical species compared to humans. Primarily QRS, but also PR effects, were consistent across the investigated compounds, where a 10% change in humans compared to a 2-5% QRS change and a 2-10% PR change in dogs and guinea pigs. Also the *in vitro* to clinical translation was consistent across compounds, where a 10% change in humans compared to 3-7% inhibition in the hNav1.5 assay for QRS and 13-21% binding in the rCav1.2 assay for PR. The second translational approach applied the operational model (Equation 2.10) to link the *in vitro* effects of AZD1305 to the clinical effects. Using this approach, a model describing the translational relationship was parameterised and successfully used to predict effects of quinidine, flecainide and verapamil. Also, the predicted *in vitro* effects at 10% QRS or PR prolongations were similar to those calculated from the empirical investigation (5-7% for QRS and 12-22% for PR using the 95% confidence interval).

The third objective was to "*develop a model framework to quantitatively predict QRS and PR prolongations in humans using nonclinical data that can be adopted by the pharmaceutical industry to improve safety assessment.* This relates to how the results of the translational analyses may be applied in practice to predict clinical QRS and PR effects, and is discussed in detail in Chapter 7. To reduce QRS/PR risk in early nonclinical studies, it is recommended to use the translational relationships to define margins for acceptable levels of nonclinical effects (Figure 8.1). Applying the 10% effect level as a human margin, the results of the translational work of this thesis suggest that nonclinical QRS/PR changes above around 5% are indicative of

high risk of at least 10% change in humans. Conservative nonclinical margins may be even lower, such as 2-4% QRS or PR change in guinea pigs or dogs at expected therapeutic exposures. Similarly, *in vitro* effects above 5% hNav1.5 inhibition or 15% rCav1.2 diltiazem binding indicate high risk of more than 10% QRS or PR change in humans, respectively.

The translational relationships suggested by this work may also be used to predict human effects by simulating QRS/PR changes over time. Without any translational knowledge, the best guess may be that the slope in humans is equal to that in the animal species, taking differences in baseline and protein binding into account. However, this work shows that assuming equal effects in animals and humans may lead to highly underpredicted human effects, and potentially unsafe compounds may appear safe and be progressed. Instead, the translational relationships identified in this work suggest that the human slope for QRS (as percentage change from baseline) is approximately two to four times larger compared to guinea pigs and dogs, and equal to four times larger for PR. Although these results are based on data for a limited number of compounds, they provide a current best estimate for the relative sensitivities of guinea pigs, dogs and humans to drug-induced QRS and PR interval changes. Also, compounds with different mechanisms of action were investigated to account for possible compound-specific differences and to achieve a broader applicability of the recommendations and translational relationships of this work.

Despite the relatively consistent *in vitro* to clinical translations for the investigated compounds, the influence of drug-ion channel kinetics and other mechanisms on QRS/PR prolongations highlight the importance of also evaluating drug effects *in vivo*. Improved sensitivity earlier in discovery does however reduce animal use, as potentially unsafe drugs can be discontinued at an earlier stage. Importantly, the results of the work presented in this thesis may be used to generate several independent predictions of QRS and PR effects in humans, using the observed or estimated effects *in vitro* and in guinea pigs and dogs together with the suggested translational relationships. Several independent predictions of clinical effects provides additional confidence and any discordance offers a measure of the uncertainty regarding the human prediction. Therefore, a combined view applying information from *in vitro* and *in vivo* studies is vital to predict cardiac conduction risks before FTIM studies, using the preliminary translational relationships suggested in this work to build on an integrated package of evidence of clinical QRS/PR risk.

8.1 Future work

This work provides a first attempt to quantitatively assess the nonclinical to clinical translation of QRS and PR changes, in order to identify risks in nonclinical studies and predict QRS and PR changes in humans. A limited number of compounds were

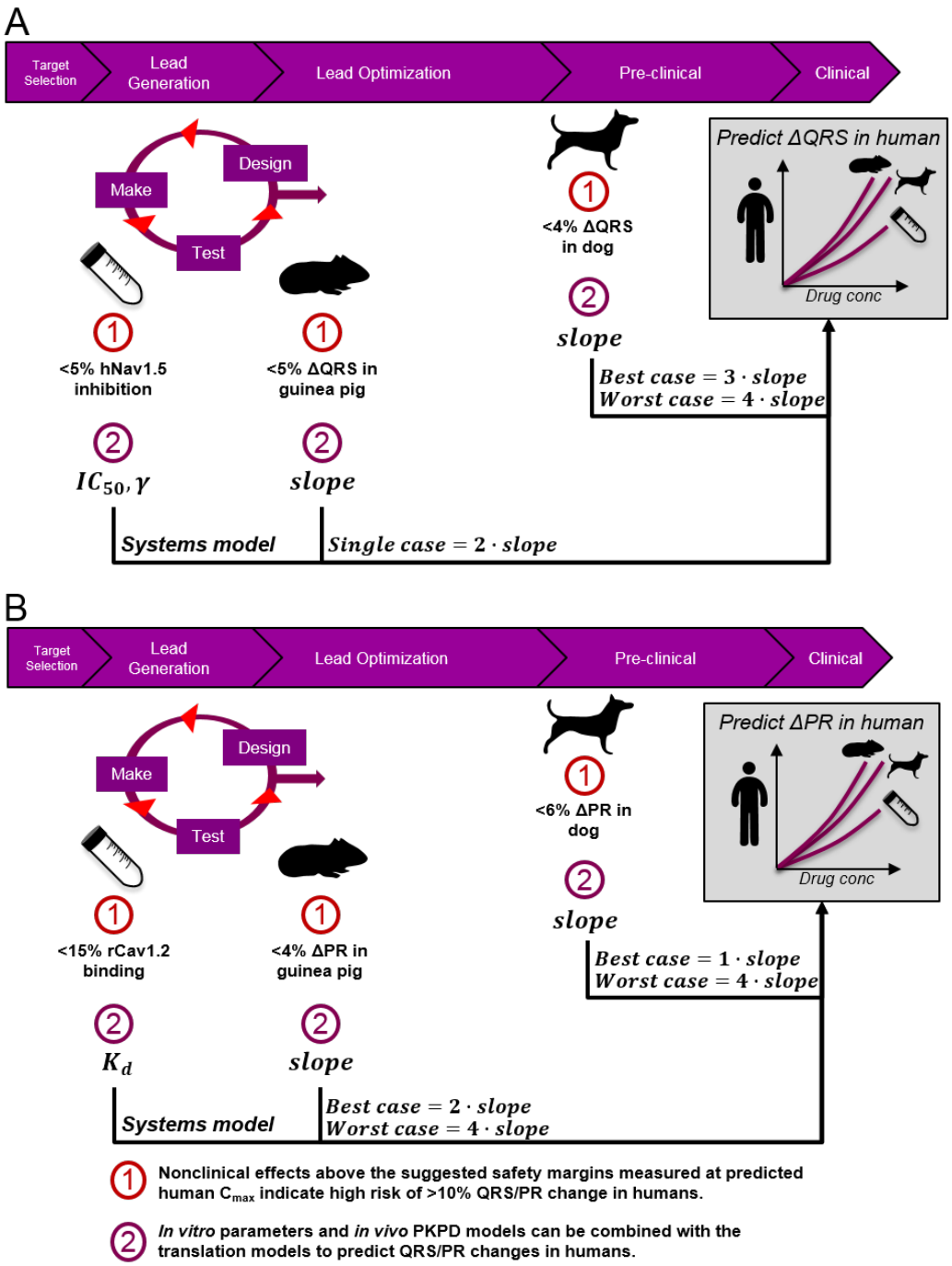

Figure 8.1 Overview of the suggested novel risk assessment processes for **A.** QRS widening and **B.** PR prolongations in drug discovery and early development. During lead generation and optimisation, the suggested safety margins for the nonclinical effects can be used to exclude compounds with high risk at the predicted human C_{max}. More thorough assessment of human risk using predicted PK profiles may be performed using the translational relationships suggested in this work together with the quantified nonclinical effects.

investigated, and analyses into the translation of additional compounds is required to improve confidence in the translation. While the full translational relationships

between *in vitro* and humans were estimated in this work, visual methods were applied to quantify the *in vivo* to clinical translations. Collating all data and estimating the parameters of the *in vivo* and clinical data simultaneously, assuming a model for the translational relationship, may further improve this quantitation.

In this work, compounds with different mechanisms of action were investigated and compared, and it was found that, despite these differences, relatively consistent translational relationships were identified. However, detailed mechanistic models may further advance these predictions as these differences may be incorporated in the model in order to predict drug effects. To date, these detailed models have largely focused on the ventricular AP, limiting the possibility of predicting effects on PR which reflect atrial depolarisation and conduction through the AV node. In such models, QRS widening is reflected by a reduced rate of depolarisation in the upstroke of the AP. Multi-level models have also been built, simulating effects at tissue or whole body level, such as the electrical activity across the torso, allowing direct comparisons with measured ECGs. While these models show great promise, and may reduce the use of animals, they must still overcome the currently missing link between drug concentrations *in vitro* and at the receptor site *in vivo*.

Prior to this study, no quantitative information was available on the relative sensitivity to drug-induced QRS/PR effects in nonclinical species and humans. Although this study is limited by the low number of investigated compounds, it provides a starting point for nonclinical assessment of conduction liabilities and predictions to humans.

Appendix A

Example model code from Monolix

```
DESCRIPTION:
Baseline with RR correction and circadian rhythm.
Proportional drug effect originating from an effect compartment.

DATA:
    path = "path_to_data_folder",
    file  ="data_file_with_PK_parameteters.csv",
    headers = {ID,OCC,ADM,X,AMT,RATE,TIME,IGNORE,X,X,X,X,X,X,X,X,X,X,Y,IGNORE},
    columnDelimiter = ","

INDIVIDUAL:
    RRref = {distribution=Normal, iiv=no},
    alpha = {distribution=Normal, iiv=yes},
    A = {distribution=logNormal, iiv=yes},
    p = {distribution=Normal, iiv=yes},
    baseline = {distribution=Normal, iiv=yes, iov=yes},
    ke = {distribution=Normal, iiv=yes},
    ke0 = {distribution=logNormal, iiv=yes},

STRUCTURAL_MODEL:
    file = "mlxt:model_file",
    path = "path_to_model_file",
    output = {E}

OBSERVATIONS:
    y1 = {type=continuous, prediction=E, error=constant}
```

```
TASKS:
    ; settings
    globalSettings={
        withVariance=no,
        settingsGraphics="path_to_graphics_settings_file",
        settingsAlgorithms="path_to_graphics_settings_file",
        resultFolder="path_to_results_folder"},
    ; workflow
    estimatePopulationParameters(
        initialValues={
            pop_RRref = 1000 [method=FIXED],
            pop_alpha = 0.02,
            pop_A = 0.015,
            pop_p = -6,
            pop_baseline = 94,
            pop_ke = 0,
            pop_ke0 = 1,
            a_y1 = 5,
            omega_alpha = 1,
            omega_A = 0.2,
            omega_p = 1.5,
            omega_baseline = 7,
            omega_ke = 1,
            omega_ke0 = 1,
            gamma_be = 1,
            } ),
    estimateFisherInformationMatrix( method={linearization} ),
    estimateIndividualParameters( method={conditionalMode} ),
    estimateLogLikelihood(method={linearization}  ),
    displayGraphics(),
```

Appendix B

Collected literature data

Table B.1 Summary of the literature flecainide, quinidine and verapamil concentration-QRS/PR data. Drug concentrations are unbound drug in μM. QRS/PR data are change from baseline in ms. Baseline levels of 92.5 ms for QRS and 160 ms for PR were used to convert published changes provided in percentage to ms where pre-dose intervals were missing.

Ref	Drug	ECG	Subjects		Dosing		Paired data	
			n	Status	Route	History	C_u (μM)	δECG (ms)
[105]	flecainide	QRS	12	HV	oral	Acute	0.240381	6.29
[105]	flecainide	QRS	12	HV	oral	Acute	0.0753	5.55
[105]	flecainide	QRS	12	HV	oral	Acute	0.532892	14.7075
[105]	flecainide	QRS	12	HV	oral	Acute	0.204179	9.065
[107]	flecainide	QRS	10	HV	iv inf	Acute	0.367811	16
[108]	flecainide	QRS	10	HV	iv inf	Acute	0.362019	4
[109]	flecainide	QRS	6	HV	iv inf	Acute	0.249069	9.6
[105]	flecainide	QRS	12	HV	oral	Chronic	0.250517	6.7525
[105]	flecainide	QRS	12	HV	oral	Chronic	0.198386	6.475
[105]	flecainide	QRS	12	HV	oral	Chronic	0.641498	13.2275
[105]	flecainide	QRS	12	HV	oral	Chronic	0.519859	12.21
[110]	flecainide	QRS	12	HV	oral	Chronic	0.227348	-0.2775
[110]	flecainide	QRS	12	HV	oral	Chronic	0.502482	7.77
[111]	flecainide	QRS	27	Patients	oral	Acute	0.622673	21
[112]	flecainide	QRS	13	Patients	oral	Acute	0.655978	19
[107]	flecainide	QRS	12	Patients	iv inf	Acute	0.424286	31
[113]	flecainide	QRS	93	Patients	iv inf	Acute	0.405461	11
[114]	flecainide	QRS	10	Patients	iv inf	Acute	0.570542	14
[115]	flecainide	QRS	11	Patients	iv inf	Acute	0.333057	8.6
[116]	flecainide	QRS	47	Patients	iv inf	Acute	0.485105	22
[117]	flecainide	QRS	9	Patients	oral	Chronic	0.625569	26.8369
[112]	flecainide	QRS	13	Patients	oral	Chronic	1.34671	23.56

Table continued from previous page

Ref	Drug	ECG	Subjects		Dosing		Paired data	
			n	Status	Route	History	C_u (μM)	δECG (ms)
[118]	flecainide	QRS	18	Patients	oral	Chronic	0.844228	27
[119]	flecainide	QRS	19	Patients	oral	Chronic	1.556681	28.4
[120]	flecainide	QRS	14	Patients	oral	Chronic	1.410426	11.7475
[106]	flecainide	PR	8	HV	oral	Acute	0.42863	23
[108]	flecainide	PR	10	HV	iv inf	Acute	0.362019	19
[109]	flecainide	PR	6	HV	iv inf	Acute	0.249069	12.2
[110]	flecainide	PR	12	HV	oral	Chronic	0.227348	7.52
[110]	flecainide	PR	12	HV	oral	Chronic	0.502482	18.88
[112]	flecainide	PR	13	Patients	oral	Acute	0.655978	32.76
[113]	flecainide	PR	93	Patients	iv inf	Acute	0.405461	12
[114]	flecainide	PR	10	Patients	iv inf	Acute	0.570542	28
[112]	flecainide	PR	13	Patients	oral	Chronic	1.34671	56.16
[119]	flecainide	PR	21	Patients	oral	Chronic	1.556681	44.7
[120]	flecainide	PR	14	Patients	oral	Chronic	1.410426	11.68
[125]	quinidine	QRS	8	HV	oral	Chronic	0.526483	11.1925
[121]	quinidine	QRS	21	HV	oral	Acute	0.274523	2
[121]	quinidine	QRS	27	HV	oral	Acute	0.297087	-4
[129]	quinidine	QRS	9	Patients	oral	Chronic	1.240995	1
[130]	quinidine	QRS	11	Patients	oral	Chronic	1.504237	18
[130]	quinidine	QRS	11	Patients	oral	Chronic	1.316207	16.2
[126]	quinidine	QRS	6	HV	oral	Chronic	0.300847	3.3
[131]	quinidine	QRS	20	Patients	oral	Chronic	1.391419	12
[127]	quinidine	QRS	20	Patients	iv inf	Acute	1.429025	8.5
[122]	quinidine	QRS	10	HV	oral	Acute	0.413665	4.3
[122]	quinidine	QRS	10	HV	iv inf	Acute	1.203389	11.8
[124]	quinidine	QRS	8	HV	iv inf	Acute	1.240995	8
[124]	quinidine	QRS	9	HV	oral	Acute	0.060169	2
[132]	quinidine	QRS	18	Patients	oral	Chronic	1.278601	7
[128]	quinidine	QRS	100	Patients	iv inf	Acute	1.203389	14
[133]	quinidine	QRS	10	Patients	oral	Chronic	0.263241	1.333333
[134]	quinidine	QRS	10	Patients	oral	Chronic	0.902542	13
[135]	quinidine	QRS	10	Patients	oral	Chronic	1.281	15
[129]	quinidine	PR	9	Patients	oral	Chronic	1.240995	2
[122]	quinidine	PR	10	HV	oral	Acute	0.413665	4.95
[122]	quinidine	PR	10	HV	iv inf	Acute	1.203389	9.92
[124]	quinidine	PR	8	HV	iv inf	Acute	1.240995	0

Table continued from previous page

Ref	Drug	ECG	Subjects		Dosing		Paired data	
			n	Status	Route	History	C_u (μM)	δECG (ms)
[139]	verapamil	PR	8	HV	oral	Acute	0.157094	51.2
[140]	verapamil	PR	6	HV	oral	Acute	0.076953	39
[141]	verapamil	PR	8	HV	oral	Acute	0.166428	36.75676
[142]	verapamil	PR	16	HV	oral	Acute	0.020491	30.4
[142]	verapamil	PR	16	HV	oral	Acute	0.022312	32
[142]	verapamil	PR	16	HV	oral	Acute	0.047811	40
[142]	verapamil	PR	16	HV	oral	Acute	0.041436	36.8
[106]	verapamil	PR	8	HV	oral	Acute	0.073311	32
[143]	verapamil	PR	9	HV	oral	Acute	0.079685	33.6
[143]	verapamil	PR	9	HV	oral	Acute	0.053731	22.4
[144]	verapamil	PR	6	HV	oral	Acute	0.020035	7
[145]	verapamil	PR	8	HV	oral	Acute	0.078866	32.48
[146]	verapamil	PR	20	HV	oral	Acute	0.017303	10
[146]	verapamil	PR	20	HV	oral	Acute	0.030963	24
[146]	verapamil	PR	20	HV	oral	Acute	0.040981	26
[147]	verapamil	PR	6	HV	oral	Acute	0.091069	39
[148]	verapamil	PR	9	HV	oral	Acute	0.135647	34.24
[149]	verapamil	PR	8	HV	oral	Chronic	0.06557	23.84
[149]	verapamil	PR	8	HV	oral	Chronic	0.043941	8.64
[150]	verapamil	PR	24	HV	oral	Chronic	0.072855	33.6
[150]	verapamil	PR	24	HV	oral	Chronic	0.081962	33.6
[151]	verapamil	PR	13	HV	oral	Chronic	0.09289	28.15385
[151]	verapamil	PR	13	HV	oral	Chronic	0.163014	44
[148]	verapamil	PR	22	Patients	oral	Acute	0.178632	23.68
[148]	verapamil	PR	14	Patients	oral	Acute	0.340598	27.2
[152]	verapamil	PR	18	Patients	oral	Chronic	0.120211	51
[152]	verapamil	PR	12	Patients	oral	Chronic	0.118845	45
[152]	verapamil	PR	18	Patients	oral	Chronic	0.253627	45
[152]	verapamil	PR	12	Patients	oral	Chronic	0.189879	46
[152]	verapamil	PR	18	Patients	oral	Chronic	0.173031	53
[152]	verapamil	PR	12	Patients	oral	Chronic	0.140702	46
[152]	verapamil	PR	18	Patients	oral	Chronic	0.351527	45
[152]	verapamil	PR	12	Patients	oral	Chronic	0.21128	45
[153]	verapamil	PR	11	Patients	oral	Chronic	0.150719	23

References

[1] T. A. Collins, L. Bergenholm, T. Abdulla, J. W. T. Yates, N. Evans, M. J. Chappell, and J. T. Mettetal, "Modeling and Simulation Approaches for Cardiovascular Function and Their Role in Safety Assessment," *CPT: pharmacometrics & systems pharmacology*, vol. 4, no. March, pp. 1–14, 2015.

[2] D. L. I. Janzen, L. Bergenholm, M. Jirstrand, J. Parkinson, J. Yates, N. D. Evans, M. J. Chappell, D. L. I. Janzén, L. Bergenholm, M. Jirstrand, J. Parkinson, J. Yates, N. D. Evans, and M. J. Chappell, "Parameter identifiability of fundamental pharmacodynamic models," *Frontiers in Physiology*, vol. 7, no. December, pp. 1–12, 2016.

[3] L. Bergenholm, T. Collins, N. D. Evans, M. J. Chappell, and J. Parkinson, "PKPD modelling of PR and QRS intervals in conscious dogs using standard safety pharmacology data," *Journal of Pharmacological and Toxicological Methods*, vol. 79, pp. 34–44, 2016.

[4] L. Bergenholm, J. Parkinson, J. Mettetal, N. D. Evans, M. J. Chappell, and T. Collins, "Predicting QRS and PR interval prolongations in humans using nonclinical data," *Under review*, 2017.

[5] H. Laverty, C. Benson, E. Cartwright, M. Cross, C. Garland, T. Hammond, C. Holloway, N. McMahon, J. Milligan, B. Park, M. Pirmohamed, C. Pollard, J. Radford, N. Roome, P. Sager, S. Singh, T. Suter, W. Suter, a. Trafford, P. Volders, R. Wallis, R. Weaver, M. York, and J. Valentin, "How can we improve our understanding of cardiovascular safety liabilities to develop safer medicines?," *British journal of pharmacology*, vol. 163, pp. 675–93, June 2011.

[6] W. Redfern, L. Ewart, T. Hammond, R. Bialecki, L. Kinter, S. Lindgreen, C. Pollard, R. Roberts, M. Rolf, and J. Valentin, "Impact and frequency of different toxicities throughout the pharmaceutical life cycle," in *The Toxicologist*, vol. 114, p. 1081, 2010.

[7] E. K. Heist and J. N. Ruskin, "Drug-induced arrhythmia," *Circulation*, vol. 122, no. 14, pp. 1426–1435, 2010.

[8] C. Van Noord, M. Eijgelsheim, and B. H. C. Stricker, "Drug- and non-drug-associated QT interval prolongation," *British Journal of Clinical Pharmacology*, vol. 70, no. 1, pp. 16–23, 2010.

[9] D. M. Jonker, L. a. Kenna, D. Leishman, R. Wallis, P. a. Milligan, and E. N. Jonsson, "A pharmacokinetic-pharmacodynamic model for the quantitative prediction of dofetilide clinical QT prolongation from human ether-a-go-go-related gene current inhibition data.," *Clinical pharmacology & therapeutics*, vol. 77, pp. 572–82, June 2005.

[10] V. Piotrovsky, "Pharmacokinetic-pharmacodynamic modeling in the data analysis and interpretation of drug-induced QT/QTc prolongation.," *The AAPS journal*, vol. 7, pp. E609–24, Jan. 2005.

[11] G. Gintant, "An evaluation of hERG current assay performance: Translating preclinical safety studies to clinical QT prolongation.," *Pharmacology & therapeutics*, vol. 129, pp. 109–19, Feb. 2011.

[12] J. Parkinson, S. a. G. Visser, P. Jarvis, C. Pollard, J.-P. Valentin, J. W. T. Yates, and L. Ewart, "Translational pharmacokinetic-pharmacodynamic modeling of QTc effects in dog and human.," *Journal of pharmacological and toxicological methods*, Apr. 2013.

[13] A. Chain, V. Dubois, M. Danhof, M. Sturkenboom, and O. Della Pasqua, "Identifying the translational gap in the evaluation of drug-induced QTc-interval prolongation.," *British journal of clinical pharmacology*, Jan. 2013.

[14] S. Polak, B. Wiśniowska, K. Fijorek, A. Glinka, and A. Mendyk, "In vitro-in vivo extrapolation of drug-induced proarrhythmia predictions at the population level.," *Drug discovery today*, vol. 19, pp. 275–81, Mar. 2014.

[15] A. Nada, G. A. Gintant, R. Kleiman, D. E. Gutstein, C. Gottfridsson, E. L. Michelson, C. Strnadova, M. Killeen, M. J. Geiger, M. L. Fiszman, L. P. Koplowitz, G. F. Carlson, I. Rodriguez, and P. T. Sager, "The evaluation and management of drug effects on cardiac conduction (PR and QRS intervals) in clinical development.," *American heart journal*, vol. 165, pp. 489–500, Apr. 2013.

[16] S. Kurl, T. H. Mäkikallio, P. Rautaharju, V. Kiviniemi, and J. a. Laukkanen, "Duration of QRS complex in resting electrocardiogram is a predictor of sudden cardiac death in men," *Circulation*, vol. 125, no. 21, pp. 2588–2594, 2012.

[17] S. Cheng, M. J. Keyes, M. G. Larson, E. L. Mccabe, C. Newton-Cheh, D. Levy, E. J. Benjamin, T. J. Wang, and R. S. Vasan, "Long-term outcomes in individuals with prolonged PR interval or first-degree atrioventricular block.," *JAMA*, vol. 301, pp. 2571–7, June 2009.

[18] V. Gotta, F. Cools, K. van Ammel, D. J. Gallacher, S. a.G. Visser, F. Sannajust, P. Morissette, M. Danhof, and P. H. van der Graaf, "Sensitivity of pharmacokinetic-pharmacodynamic analysis for detecting small magnitudes of QTc prolongation in preclinical safety testing," *Journal of Pharmacological and Toxicological Methods*, vol. 72, pp. 1–10, 2015.

[19] a. R. Harmer, J.-P. Valentin, and C. E. Pollard, "On the relationship between block of the cardiac Na+ channel and drug-induced prolongation of the QRS complex.," *British journal of pharmacology*, vol. 164, pp. 260–73, Oct. 2011.

[20] J. Cordes, C. Li, J. Dugas, R. Austin-LaFrance, I. Lightbown, M. Engwall, M. Sutton, and J. Steidl-Nichols, "Translation between in vitro inhibition of the cardiac Nav1.5 channel and pre-clinical and clinical QRS widening," *Journal of Pharmacological and Toxicological Methods*, vol. 60, no. 2, p. 221, 2009.

[21] B. M. Heath, Y. Cui, S. Worton, B. Lawton, G. Ward, E. Ballini, C. P. a. Doe, C. Ellis, B. a. Patel, and N. C. McMahon, "Translation of flecainide- and mexiletine-induced cardiac sodium channel inhibition and ventricular conduction slowing from nonclinical models to clinical.," *Journal of pharmacological and toxicological methods*, vol. 63, no. 3, pp. 258–68, 2011.

[22] C. Cros, M. Skinner, J. Moors, P. Lainee, and J. P. Valentin, "Detecting drug-induced prolongation of the QRS complex: new insights for cardiac safety assessment.," *Toxicology and applied pharmacology*, vol. 265, pp. 200–8, Dec. 2012.

[23] L. Marks, S. Borland, K. Philp, L. Ewart, P. Lainée, M. Skinner, S. Kirk, and J.-P. Valentin, "The role of the anaesthetised guinea-pig in the preclinical cardiac safety evaluation of drug candidate compounds.," *Toxicology and applied pharmacology*, vol. 263, pp. 171–183, Sept. 2012.

[24] ICH, "Guidance for Industry. S7B Nonclinical Evaluation of the Potential for Delayed Ventricular Repolarization (QT Interval Prolongation) by Human Pharmaceuticals," Tech. Rep. October, 2005.

[25] T. Bueters, B. a. Ploeger, and S. a. G. Visser, "The virtue of translational PKPD modeling in drug discovery: selecting the right clinical candidate while sparing animal lives.," *Drug discovery today*, vol. 18, pp. 853–62, Sept. 2013.

[26] J. Gabrielsson, H. Dolgos, P.-G. Gillberg, U. Bredberg, B. Benthem, and G. Duker, "Early integration of pharmacokinetic and dynamic reasoning is essential for optimal development of lead compounds: strategic considerations.," *Drug discovery today*, vol. 14, pp. 358–72, Apr. 2009.

[27] P. H. Van Der Graaf and J. Gabrielsson, "Pharmacokinetic-pharmacodynamic reasoning in drug discovery and early development.," *Future medicinal chemistry*, vol. 1, pp. 1371–4, Nov. 2009.

[28] D. R. Mould and R. N. Upton, "Basic concepts in population modeling, simulation, and model-based drug development.," *CPT: pharmacometrics & systems pharmacology*, vol. 1, p. e6, Jan. 2012.

[29] S. a. G. Visser, M. Aurell, R. D. O. Jones, V. J. a. Schuck, A.-C. Egnell, S. a. Peters, L. Brynne, J. W. T. Yates, R. Jansson-Löfmark, B. Tan, M. Cooke, S. T. Barry, A. Hughes, and U. Bredberg, "Model-based drug discovery: implementation and impact.," *Drug discovery today*, vol. 18, pp. 764–75, Aug. 2013.

[30] H. Jones and K. Rowland-Yeo, "Basic concepts in physiologically based pharmacokinetic modeling in drug discovery and development.," *CPT: pharmacometrics & systems pharmacology*, vol. 2, p. e63, Jan. 2013.

[31] M. Danhof, E. C. M. de Lange, O. E. Della Pasqua, B. a. Ploeger, and R. a. Voskuyl, "Mechanism-based pharmacokinetic-pharmacodynamic (PK-PD) modeling in translational drug research.," *Trends in pharmacological sciences*, vol. 29, pp. 186–91, Apr. 2008.

[32] M. Danhof, G. Alvan, S. G. Dahl, J. Kuhlmann, and G. Paintaud, "Mechanism-based pharmacokinetic-pharmacodynamic modeling-a new classification of biomarkers.," *Pharmaceutical research*, vol. 22, pp. 1432–7, Sept. 2005.

[33] L. B. Sheiner, D. R. Stanski, S. Vozeh, R. D. Miller, and J. Ham, "Simultaneous modeling of pharmacokinetics and pharmacodynamics: application to d-tubocurarine.," *Clinical pharmacology and therapeutics*, vol. 25, pp. 358–71, Mar. 1979.

[34] J. W. Jusko and H. C. Ko, "Physiologic indirect response models characterize diverse types of pharmacodynamic effects," *Clinical pharmacology & therapeutics*, vol. 56, no. 4, pp. 406–419, 1994.

[35] J. W. Black and P. Leff, "Operational Models of Pharmacological Agonism," *Proceedings of the Royal Society B: Biological Sciences*, vol. 220, pp. 141–162, Dec. 1983.

[36] L. B. Sheiner and S. L. Beal, "Evaluation of methods for estimating population pharmacokinetics parameters. I. Michaelis-Menten model: routine clinical pharmacokinetic data.," *Journal of pharmacokinetics and biopharmaceutics*, vol. 8, pp. 553–71, Dec. 1980.

[37] L. B. Sheiner, "The Population Approach to Pharmacokinetic Data Analysis : Rationale and Standard Data Analysis Methods The Population Approach to Pharmacokinetic Data Analysis : Rationale and Standard Data Analysis Methods," *Drug Metabolism Reviews*, vol. 15, pp. 153–171, 1884.

[38] ICON, "NONMEM."

[39] Certara, "Phoenix."

[40] Lixoft, "Monolix."

[41] MRC Biostatistics Unit, "WinBUGS."

[42] L. Gibiansky, E. Gibiansky, and R. Bauer, "Comparison of Nonmem 7.2 estimation methods and parallel processing efficiency on a target-mediated drug disposition model," *Journal of Pharmacokinetics and Pharmacodynamics*, vol. 39, no. 1, pp. 17–35, 2012.

[43] B. Delyon, M. Lavielle, and E. Moulines, "Convergence of a stochastic approximation version of the EM algorithm," *Annals of Statistics*, vol. 27, no. 1, pp. 94–128, 1999.

[44] E. Kuhn and M. Lavielle, "Maximum likelihood estimation in nonlinear mixed effects models," 2005.

[45] A. P. Dempster, A. P. Dempster, N. M. Laird, and D. B. Rubin, "Maximum likelihood from incomplete data via the EM algorithm," *Journal of the Royal Statistical Society, Series B*, vol. 39, no. 1, pp. 1—-38, 1977.

[46] H. A. I. Aike, "A New Look at the Statistical Model Identification," *IEEE Transactions on Automatic Control*, vol. 19, no. 6, pp. 716–723, 1974.

[47] A. S. Amin, H. L. Tan, and A. a. M. Wilde, "Cardiac ion channels in health and disease.," *Heart rhythm : the official journal of the Heart Rhythm Society*, vol. 7, pp. 117–26, Jan. 2010.

[48] R. McNaughton, G. Huet, and S. Shakir, "An investigation into drug products withdrawn from the EU market between 2002 and 2011 for safety reasons and the evidence used to support the decision-making.," *BMJ open*, vol. 4, no. 1, p. e004221, 2014.

[49] ICH, "Guidance for Industry. E14 Clinical Evaluation of QT/QTc Interval Prolongation and Proarrhythmic Potential for Non-Antiarrhythmic Drugs," Tech. Rep. October, 2005.

[50] ICH, "E14 Implementation Working Group ICH E14 Guideline : The Clinical Evaluation of QT / QTc Interval Prolongation and Proarrhythmic Potential for Non-Antiarrhythmic Drugs Questions & Answers (R3) Current version In order to facilitate the implementation of," vol. 41, no. December, 2015.

[51] ICH, "Guidance for Industry. S7A Safety Pharmacology Studies for Human Pharmaceuticals," Tech. Rep. July, 2001.

[52] G. Erdemli, A. M. Kim, H. Ju, C. Springer, R. C. Penland, and P. K. Hoffmann, "Cardiac Safety Implications of hNav1.5 Blockade and a Framework for Pre-Clinical Evaluation.," *Frontiers in pharmacology*, vol. 3, p. 6, Jan. 2012.

[53] X. Cao, Y. T. Lee, M. Holmqvist, Y. Lin, Y. Ni, D. Mikhailov, H. Zhang, C. Hogan, L. Zhou, Q. Lu, M. E. Digan, L. Urban, and G. Erdemli, "Cardiac ion channel safety profiling on the IonWorks Quattro automated patch clamp system.," *Assay and drug development technologies*, vol. 8, no. 6, pp. 766–780, 2010.

[54] M. J. Morton, D. Armstrong, N. Abi Gerges, M. Bridgland-Taylor, C. E. Pollard, J. Bowes, and J. P. Valentin, "Predicting changes in cardiac myocyte contractility during early drug discovery with in vitro assays," *Toxicology and Applied Pharmacology*, vol. 279, no. 2, pp. 87–94, 2014.

[55] a. R. Harmer, N. Abi-Gerges, M. J. Morton, G. F. Pullen, J. P. Valentin, and C. E. Pollard, "Validation of an in vitro contractility assay using canine ventricular myocytes," *Toxicology and Applied Pharmacology*, vol. 260, no. 2, pp. 162–172, 2012.

[56] E. M. Vaughan Williams, "The relevance of cellular to clinical electrophysiology in classifying antiarrhythmic actions.," *Journal of cardiovascular pharmacology*, vol. 20 Suppl 2, pp. S1–7, Jan. 1992.

[57] A. Caruso, N. Frances, C. Meille, A. Greiter-Wilke, A. Hillebrecht, and T. Lave, "Translational PK/PD Modeling for Cardiovascular Safety Assessment of Drug Candidates," *Journal of Pharmacological and Toxicological Methods*, vol. 70, pp. 73–85, May 2014.

[58] E. Sparve, A. L. Quartino, M. Lüttgen, K. Tunblad, A. T. Gå rdlund, J. Fälting, R. Alexander, J. Kå gström, L. Sjödin, A. Bulgak, A. Al-saffar, M. Bridgland-taylor, C. Pollard, M. D. B. Swedberg, T. Vik, and B. Paulsson, "Prediction and Modeling of Effects on the QTc Interval for Clinical Safety Margin Assessment , Based on Single-Ascending-Dose Study Data with AZD3839," no. August, pp. 469–478, 2014.

[59] H. Holzgrefe, G. Ferber, P. Champeroux, M. Gill, M. Honda, A. Greiter-Wilke, T. Baird, O. Meyer, and M. Saulnier, "Preclinical QT safety assessment: Cross-species comparisons and human translation from an industry consortium," *Journal of Pharmacological and Toxicological Methods*, vol. 69, pp. 61–101, May 2014.

[60] A. Ollerstam, A. H. Persson, S. a. G. Visser, J. M. Fredriksson, T. Forsberg, L. B. Nilsson, G. Eklund, S. J. Wiklund, J. Gabrielsson, G. Duker, and A. Al-Saffar, "A novel approach to data processing of the QT interval response in the conscious telemetered beagle dog.," *Journal of pharmacological and toxicological methods*, vol. 55, no. 1, pp. 35–48, 2006.

[61] M. Malik, K. Hnatkova, M. Sisakova, and G. Schmidt, "Subject-specific heart rate dependency of electrocardiographic QT, PQ, and QRS intervals.," *Journal of electrocardiology*, vol. 41, no. 6, pp. 491–7, 2008.

[62] R. N. Upton and D. R. Mould, "Basic concepts in population modeling, simulation, and model-based drug development: part 3-introduction to pharmacodynamic modeling methods.," *CPT: pharmacometrics & systems pharmacology*, vol. 3, p. e88, Jan. 2014.

[63] A. S. Y. Chain, K. M. Krudys, M. Danhof, and O. Della Pasqua, "Assessing the probability of drug-induced QTc-interval prolongation during clinical drug development.," *Clinical pharmacology & therapeutics*, vol. 90, pp. 867–75, Dec. 2011.

[64] S. L. Lindstedt and P. J. Schaeffer, "Use of allometry in predicting anatomical and physiological parameters of mammals.," *Laboratory animals*, vol. 36, pp. 1–19, Jan. 2002.

[65] K. H. W. J. ten Tusscher, D. Noble, P. J. Noble, and a. V. Panfilov, "A model for human ventricular tissue.," *American journal of physiology. Heart and circulatory physiology*, vol. 286, pp. H1573–89, Apr. 2004.

[66] T. O'Hara, L. Virág, A. Varró, and Y. Rudy, "Simulation of the undiseased human cardiac ventricular action potential: model formulation and experimental validation.," *PLoS computational biology*, vol. 7, p. e1002061, May 2011.

[67] T. J. Hund and Y. Rudy, "Rate dependence and regulation of action potential and calcium transient in a canine cardiac ventricular cell model.," *Circulation*, vol. 110, pp. 3168–74, Nov. 2004.

[68] D. Noble, A. Varghese, P. Kohl, and P. Noble, "Improved guinea-pig ventricular cell model incorporating a diadic space, IKr and IKs, and length- and tension-dependent processes.," *Canadian journal of cardiology*, vol. 14, pp. 123–34, Jan. 1998.

[69] M. R. Davies, H. B. Mistry, L. Hussein, C. E. Pollard, J.-P. Valentin, J. Swinton, and N. Abi-Gerges, "An in silico canine cardiac midmyocardial action potential duration model as a tool for early drug safety assessment.," *American journal of physiology. Heart and circulatory physiology*, vol. 302, pp. H1466–80, Apr. 2012.

[70] G. R. Mirams, Y. Cui, A. Sher, M. Fink, J. Cooper, B. M. Heath, N. C. McMahon, D. J. Gavaghan, and D. Noble, "Simulation of multiple ion channel block provides improved early prediction of compounds' clinical torsadogenic risk.," *Cardiovascular research*, vol. 91, pp. 53–61, July 2011.

[71] J. D. Moreno, Z. I. Zhu, P.-C. Yang, J. R. Bankston, M.-T. Jeng, C. Kang, L. Wang, J. D. Bayer, D. J. Christini, N. A. Trayanova, C. M. Ripplinger, R. S. Kass, and C. E. Clancy, "A computational model to predict the effects of class I anti-arrhythmic drugs on ventricular rhythms.," *Science translational medicine*, vol. 3, p. 98ra83, Aug. 2011.

[72] T. O'Hara and Y. Rudy, "Quantitative comparison of cardiac ventricular myocyte electrophysiology and response to drugs in human and nonhuman species.," *American journal of physiology. Heart and circulatory physiology*, vol. 302, pp. H1023–30, Mar. 2012.

[73] R. H. Clayton, O. Bernus, E. M. Cherry, H. Dierckx, F. H. Fenton, L. Mirabella, a. V. Panfilov, F. B. Sachse, G. Seemann, and H. Zhang, "Models of cardiac tissue electrophysiology: progress, challenges and open questions.," *Progress in biophysics and molecular biology*, vol. 104, pp. 22–48, Jan. 2011.

[74] T. Brennan, M. Fink, and B. Rodriguez, "Multiscale modelling of drug-induced effects on cardiac electrophysiological activity.," *European journal of pharmaceutical sciences : official journal of the European Federation for Pharmaceutical Sciences*, vol. 36, pp. 62–77, Jan. 2009.

[75] N. Zemzemi, M. O. Bernabeu, J. Saiz, J. Cooper, P. Pathmanathan, G. R. Mirams, J. Pitt-Francis, and B. Rodriguez, "Computational assessment of drug-induced effects on the electrocardiogram: from ion channel to body surface potentials.," *British journal of pharmacology*, vol. 168, pp. 718–33, Feb. 2013.

[76] M. Wilhelms, C. Rombach, E. P. Scholz, O. Dössel, and G. Seemann, "Impact of amiodarone and cisapride on simulated human ventricular electrophysiology and electrocardiograms.," *Europace : European pacing, arrhythmias, and cardiac electrophysiology : journal of the working groups on cardiac pacing, arrhythmias, and cardiac cellular electrophysiology of the European Society of Cardiology*, vol. 14 Suppl 5, pp. v90–v96, Nov. 2012.

[77] G. R. Mirams, M. R. Davies, S. J. Brough, M. H. Bridgland-Taylor, Y. Cui, D. J. Gavaghan, and N. Abi-Gerges, "Prediction of Thorough QT study results using action potential simulations based on ion channel screens," *Journal of Pharmacological and Toxicological Methods*, vol. 70, no. 3, pp. 246–254, 2014.

[78] A. Glinka and S. Polak, "The effects of six antipsychotic agents on QTc–an attempt to mimic clinical trial through simulation including variability in the population.," *Computers in biology and medicine*, vol. 47, pp. 20–6, Apr. 2014.

[79] H. Mishra, S. Polak, M. Jamei, and A. Rostami-Hodjegan, "Interaction Between Domperidone and Ketoconazole: Toward Prediction of Consequent QTc Prolongation Using Purely In Vitro Information.," *CPT: pharmacometrics & systems pharmacology*, vol. 3, p. e130, Jan. 2014.

[80] P. H. van der Graaf, "CPT: Pharmacometrics and Systems Pharmacology.," *CPT: pharmacometrics & systems pharmacology*, vol. 1, p. e8, Jan. 2012.

[81] P. Francheteau, J. L. Steimer, H. Merdjan, M. Guerret, and C. Dubray, "A mathematical model for dynamics of cardiovascular drug action: application to intravenous dihydropyridines in healthy volunteers.," *Journal of pharmacokinetics and biopharmaceutics*, vol. 21, pp. 489–514, Oct. 1993.

[82] N. Snelder, B. a. Ploeger, O. Luttringer, D. F. Rigel, R. L. Webb, D. Feldman, F. Fu, M. Beil, L. Jin, D. R. Stanski, and M. Danhof, "PKPD modelling of the interrelationship between mean arterial BP, cardiac output and total peripheral resistance in conscious rats.," *British journal of pharmacology*, vol. 169, pp. 1510–24, Aug. 2013.

[83] N. Snelder, B. a. Ploeger, O. Luttringer, D. F. Rigel, F. Fu, M. Beil, D. R. Stanski, and M. Danhof, "Drug effects on the CVS in conscious rats: separating cardiac output into heart rate and stroke volume using PKPD modelling.," *British journal of pharmacology*, vol. 171, pp. 5076–92, Nov. 2014.

[84] G. Langdon, J. D. Davis, L. M. McFadyen, M. Dewhurst, N. S. Brunton, J. K. Rawal, P. H. Van der Graaf, and N. Benson, "Translational pharmacokinetic-pharmacodynamic modelling; application to cardiovascular safety data for PF-00821385, a novel HIV agent.," *British journal of clinical pharmacology*, vol. 69, pp. 336–45, Apr. 2010.

[85] R. Bellman and K. J. Å ström, "On structural identifiability," *Mathematical Biosciences*, vol. 7, pp. 329–339, 1970.

[86] A. Raue, C. Kreutz, T. Maiwald, J. Bachmann, M. Schilling, U. Klingmuller, and J. Timmer, "Structural and practical identifiability analysis of partially observed dynamical models by exploiting the profile likelihood.," *Bioinformatics*, vol. 25, pp. 1923–1929, 2009.

[87] S. Y. A. Cheung, J. W. T. Yates, and L. Aarons, "The design and analysis of parallel experiments to produce structurally identifiable models.," *Journal of pharmacokinetics and pharmacodynamics*, vol. 40, pp. 93–100, Feb. 2013.

[88] M. J. Chappell, "Structural identifiability of models characterizing saturable binding: Comparison of pseudo-steady-state and non-pseudo-steady-state model formulations," *Mathematical Biosciences*, vol. 133, no. 1, pp. 1–20, 1996.

[89] D. E. Mager and W. J. Jusko, "General pharmacokinetic model for drugs exhibiting target-mediated drug disposition.," *Journal of pharmacokinetics and pharmacodynamics*, vol. 28, pp. 507–32, Dec. 2001.

[90] R. J. Eudy, M. M. Riggs, and M. R. Gastonguay, "A Priori Identifiability of Target-Mediated Drug Disposition Models and Approximations.," *The AAPS journal*, vol. 17, pp. 1280–1284, 2015.

[91] D. Bearup, N. D. Evans, and M. J. Chappell, "The input-output relationship approach to structural identifiability analysis.," *Computer methods and programs in biomedicine*, vol. 109, pp. 171–181, 2013.

[92] D. L. I. Janzén, M. Jirstrand, N. D. Evans, and M. J. Chappell, "Structural identifiability of mixed-effects models is dependent on the statistical sub-model." 2016.

[93] The MathWorks, "Matlab."

[94] C. E. Pollard, N. Abi Gerges, M. H. Bridgland-Taylor, A. Easter, T. G. Hammond, and J.-P. Valentin, "An introduction to QT interval prolongation and non-clinical approaches to assessing and reducing risk.," *British journal of pharmacology*, vol. 159, pp. 12–21, Jan. 2010.

[95] L. Carlsson, B. Andersson, G. Linhardt, and L. Löfberg, "Assessment of the ion channel-blocking profile of the novel combined ion channel blocker AZD1305 and its proarrhythmic potential versus dofetilide in the methoxamine-sensitized rabbit in vivo.," *Journal of cardiovascular pharmacology*, vol. 54, pp. 82–9, July 2009.

[96] L. Peletier and J. Gabrielsson, "Dynamics of target-mediated drug disposition: characteristic profiles and parameter identification.," *Journal of pharmacokinetics and pharmacodynamics*, vol. 39, pp. 429–451, 2012.

[97] B. Ploeger, H. van der Graaf, and M. Danhof., "Incorporating receptor theory in mechanism-based pharmacokinetic-pharmacodynamic (PK-PD) modeling.," *Drug metabolism and pharmacokinetics*, vol. 24, pp. 3–15, 2009.

[98] K. Sigfridsson, R. Lundqvist, and K. Ohlson, "Preformulation evaluation of AZD1305, an oxabispidine intended for oral and intravenous treatment.," *Drug development and industrial pharmacy*, vol. 38, pp. 19–31, Jan. 2012.

[99] A. Mete, K. Bowers, R. J. Bull, H. Coope, D. K. Donald, K. J. Escott, R. Ford, K. Grime, A. Mather, N. C. Ray, and V. Russell, "The design of a novel series of muscarinic receptor antagonists leading to AZD8683, a potential inhaled treatment for COPD.," *Bioorganic & medicinal chemistry letters*, vol. 23, pp. 6248–53, Dec. 2013.

[100] A. Mete, K. Bowers, E. Chevalier, D. K. Donald, H. Edwards, K. J. Escott, R. Ford, K. Grime, I. Millichip, B. Teobald, and V. Russell, "The discovery of AZD9164, a novel muscarinic M3 antagonist.," *Bioorganic & medicinal chemistry letters*, vol. 21, pp. 7440–6, Dec. 2011.

[101] A. Rónaszéki, M. Alings, K. Egstrup, Z. Gaciong, M. Hranai, C. Király, M. Sereg, W. Figatowski, P. Bondarov, S. Johansson, L. Frison, N. Edvardsson, and A. Berggren, "Pharmacological cardioversion of atrial fibrillation–a double-blind, randomized, placebo-controlled, multicentre, dose-escalation study of AZD1305 given intravenously.," *European Society of Cardiology*, vol. 13, pp. 1148–56, Aug. 2011.

[102] A. Rakhit, T. W. Guentert, N. H. G. Holford, J. Verhoeven, and S. Riegelman, "Pharmacokinetics and pharmacodynamics of quinidine and its metabolite, quinidine-N-oxide, in beagle dogs," *European journal of drug metabolism and pharmacokinetics*, vol. 9, no. 4, pp. 315–324, 1983.

[103] A. R. Harmer, N. Abi-Gerges, A. Easter, A. Woods, C. L. Lawrence, B. G. Small, J.-P. Valentin, and C. E. Pollard, "Optimisation and validation of a medium-throughput electrophysiology-based hNav1.5 assay using IonWorks.," *Journal of pharmacological and toxicological methods*, vol. 57, pp. 30–41, Jan. 2008.

[104] H. Prior, N. McMahon, J. Schofield, and J.-P. Valentin, "Non-invasive telemetric electrocardiogram assessment in conscious beagle dogs.," *Journal of pharmacological and toxicological methods*, vol. 60, no. 2, pp. 167–73, 2009.

[105] L. Tennezé, E. Tarral, N. Ducloux, and C. Funck-Brentano, "Pharmacokinetics and electrocardiographic effects of a new controlled-release form of flecainide acetate: comparison with the standard form and influence of the CYP2D6 polymorphism.," *Clinical pharmacology & therapeutics*, vol. 72, pp. 112–22, Aug. 2002.

[106] J. L. Holtzman, D. Finley, L. Mottonen, D. a. Berry, B. P. Ekholm, D. C. Kvam, R. L. McQuinn, and a. M. Miller, "The pharmacodynamic and pharmacokinetic interaction between single doses of flecainide acetate and verapamil: effects on cardiac function and drug clearance," *Clinical pharmacology & therapeutics*, vol. 46, no. 1, pp. 26–32, 1989.

[107] W. Shimizu, C. Antzelevitch, K. Suyama, T. Kurita, A. Taguchi, N. Aihara, H. Takaki, K. Sunagawa, and S. Kamakura, "Effect of sodium channel blockers on ST segment, QRS duration, and corrected QT interval in patients with Brugada syndrome.," *Journal of cardiovascular electrophysiology*, vol. 11, pp. 1320–9, Dec. 2000.

[108] A. Munafo, G. Reymond-Michel, and J. Biollaz, "Altered flecainide disposition in healthy volunteers taking quinine," *European journal of clinical pharmacology*, vol. 38, pp. 269–273, 1990.

[109] K. Muhiddin, E. Shaw, and A. Blackett, "The effect of a new antiarrhythmic agent, flecainide acetate, on systolic time intervals," *European journal of clinical pharmacology*, vol. 25, pp. 13–18, 1983.

[110] C. Funck-Brentano, L. Becquemont, H. K. Kroemer, K. Bühl, N. G. Knebel, M. Eichelbaum, and P. Jaillon, "Variable disposition kinetics and electrocardiographic effects of flecainide during repeated dosing in humans: contribution of genetic factors, dose-dependent clearance, and interaction with amiodarone.," *Clinical pharmacology and therapeutics*, vol. 55, no. 3, pp. 256–269, 1994.

[111] V. H. M. Deneer, L. Lie-A-Huen, J. H. Kingma, J. H. Proost, S. a. Gossen, A. Stuurman, G. M. M. Uytdehaag, P. H. J. M. Dunselman, and J. R. B. J. Brouwers, "Absorption kinetics and pharmacodynamics of two oral dosage forms of flecainide in patients with an episode of paroxysmal atrial fibrillation.," *European journal of clinical pharmacology*, vol. 60, pp. 693–701, Dec. 2004.

[112] G. Boriani, A. Capucci, and E. Strocchi, "Flecainide acetate: concentration-response relationships for antiarrhythmic and electrocardiographic effects.," *Journal of clinical pharmacology*, vol. 13, no. 4, pp. 211–219, 1992.

[113] J. C. Somberg, D. Tepper, H. Sacher, and J. Schwarz, "Chronic flecainide therapy selected by electrophysiology testing of intravenous flecainide.," *American heart journal*, vol. 114, no. 1 Pt 1, pp. 18–25, 1987.

[114] V. Legrand, M. Vandormael, P. Collignon, and H. E. Kulbertus, "Hemodynamic effects of a new antiarrhythmic agent, flecainide (R-818), in coronary heart disease.," *The American journal of cardiology*, vol. 51, no. 3, pp. 422–426, 1983.

[115] H. Vik-Mo, O. J. Ohm, and P. Lund-Johansen, "Electrophysiologic effects of flecainide acetate in patients with sinus nodal dysfunction.," *The American journal of cardiology*, vol. 50, no. 5, pp. 1090–1094, 1982.

[116] K. J. Hellestrand, R. S. Bexton, a. W. Nathan, R. a. Spurrell, and a. J. Camm, "Acute electrophysiological effects of flecainide acetate on cardiac conduction and refractoriness in man.," *British heart journal*, vol. 48, no. 2, pp. 140–148, 1982.

[117] R. Padrini, D. Piovan, M. Busa, M. Al-Bunni, P. Maiolino, and M. Ferrari, "Pharmacodynamic variability of flecainide assessed by QRS changes.," *Clinical pharmacology & therapeutics*, vol. 53, pp. 59–64, Jan. 1993.

[118] C. R. Webb, J. Morganroth, S. Senior, S. R. Spielman, A. M. Greenspan, and L. N. Horowitz, "Flecainide: Steady state electrophysiologic effects in patients with remote myocardial infarction and inducible sustained ventricular arrhythmia," *Journal of the American College of Cardiology*, vol. 8, pp. 214–220, July 1986.

[119] E. V. Platia, M. Estes, D. L. Heine, L. S. Griffith, H. Garan, J. N. Ruskin, and P. R. Reid, "Flecainide: electrophysiologic and antiarrhythmic properties in refractory ventricular tachycardia.," *The American journal of cardiology*, vol. 55, no. 8, pp. 956–962, 1985.

[120] T. Meinertz, M. K. Zehender, a. Geibel, N. Treese, T. Hofmann, W. Kasper, and T. Pop, "Long-term antiarrhythmic therapy with flecainide.," *The American journal of cardiology*, vol. 54, no. 1, pp. 91–96, 1984.

[121] H. El-eraky and S. H. L. Thomas, "Effects of sex on the pharmacokinetic and pharmacodynamic properties of quinidine," *Journal of clinical pharmacology*, vol. 56, pp. 198–204, 2003.

[122] N. H. Holford, P. E. Coates, T. W. Guentert, S. Riegelman, and L. B. Sheiner, "The effect of quinidine and its metabolites on the electrocardiogram and systolic time intervals: concentration–effect relationships.," *British journal of clinical pharmacology*, vol. 11, pp. 187–95, Feb. 1981.

[123] K.-M. Kaukonen, K. T. Olkkola, and P. J. Neuvonen, "Itraconazole increases plasma concentrations of quinidine," *Clinical pharmacology & therapeutics*, vol. 62, pp. 510–517, 1997.

[124] J. Karbwang, T. M. Davis, S. Looareesuwan, P. Molunto, D. Bunnag, and N. J. White, "A comparison of the pharmacokinetic and pharmacodynamic properties of quinine and quinidine in healthy Thai males.," *British journal of clinical pharmacology*, vol. 35, pp. 265–71, Mar. 1993.

[125] B. E. Bleske, P. L. Carver, T. M. Annesley, J. R. Bleske, and F. Morady, "The effect of ciprofloxacin on the pharmacokinetic and ECG parameters of quinidine.," *Journal of clinical pharmacology*, vol. 30, no. 10, pp. 911–915, 1990.

[126] B. G. Hardy, I. T. Zador, L. Golden, D. Lalka, and J. J. Schentag, "Effect of cimetidine on the pharmacokinetics and pharmacodynamics of quinidine," *American journal of cardiology*, vol. 52, pp. 172–175, 1983.

[127] D. S. Hirschfeld, C. T. Ueda, M. Rowland, and M. M. Scheinman, "Clinical and electrophysiological effects of intravenous quinidine in man.," *British heart journal*, vol. 39, no. 3, pp. 309–316, 1977.

[128] C. D. Swerdlow, J. O. Yu, E. Jacobson, S. Mann, R. a. Winkle, J. C. Griffin, D. L. Ross, and J. W. Mason, "Safety and efficacy of intravenous quinidine.," *The American journal of medicine*, vol. 75, no. 1, pp. 36–42, 1983.

[129] E.-G. V. Giardina, S. Zaim, A. L. Saroff, and M. Kirschenbaum, "lndecainide Compared with Quinidine for Chronic Stable Ventricular Arrhythmias Secondary to Coronary Artery Disease or to Cardiomyopath," *American journal of cardiology*, vol. 60, pp. 584–589, 1987.

[130] a. M. Gillis, L. B. Mitchell, D. G. Wyse, M. McDonald, and H. J. Duff, "Quinidine pharmacodynamics in patients with arrhythmia: effects of left ventricular function.," *Journal of the American College of Cardiology*, vol. 25, pp. 989–94, Apr. 1995.

[131] R. H. Heissenbuttel and J. Bigger, "The effect of oral quinidine on intraventricular conduction in man: Correlation of plasma quinidine with changes in QRS duration," *American Heart Journal*, vol. 80, pp. 453–462, Oct. 1970.

[132] M. J. Reiter, S. L. Higgins, a. G. Payne, and D. E. Mann, "Effects of quinidine versus procainamide on the QT interval.," *The American journal of cardiology*, vol. 58, no. 6, pp. 512–516, 1986.

[133] J. Turgeon, H. N. Pavlou, W. Wong, C. Funck-Brentano, and D. M. Roden, "Genetically determined steady-state interaction between encainide and quinidine in patients with arrhythmias.," *The Journal of pharmacology and experimental therapeutics*, vol. 255, no. 2, pp. 642–649, 1990.

[134] S. C. Vlay, G. I. Mallis, S. Singh, and P. F. Cohn, "Comparison of lorcainide and quinidine in the treatment of ventricular ectopy," *Chest*, vol. 86, no. 1, pp. 80–83, 1984.

[135] L. Wang, R. S. Sheldon, L. B. Mitchell, D. G. Wyse, A. M. Gillis, N. Chiamvimonvat, and H. J. Duff, "Amiloride-quinidine interaction: Adverse outcomes," *Clinical pharmacology & therapeutics*, vol. 56, no. 6, pp. 659–667, 1994.

[136] M. J. Reiter, D. G. Shand, and E. L. Pritchett, "Comparison of intravenous and oral verapamil dosing.," *Clinical pharmacology and therapeutics*, vol. 32, no. 6, pp. 711–720, 1982.

[137] H. Echizen, B. Vogelgesang, and M. Eichelbaum, "Effects of d,l-verapamil on atrioventricular conduction in relation to its stereoselective first-pass metabolism.," *Clinical pharmacology and therapeutics*, vol. 38, pp. 71–76, July 1985.

[138] H. Echizen, T. Brecht, S. Niedergesäss, B. Vogelgesang, and M. Eichelbaum, "The effect of dextro-, levo-, and racemic verapamil on atrioventricular conduction in humans," *American heart journal*, vol. 109, pp. 210–217, Feb. 1985.

[139] J. H. Ahmed, J. Godden, P. a. Meredith, and H. L. Elliott, "R-verapamil: pharmacokinetics and effects on PR interval, blood pressure and heart rate.," *British journal of clinical pharmacology*, vol. 36, no. 2, pp. 93–98, 1993.

[140] R. A. Barbarash, J. L. Bauman, J. H. Fischer, G. T. Kondos, and R. L. Batenhorst, "Near-total reduction in verapamil bioavailability by rifampin. Electrocardiographic correlates," *Chest*, vol. 94, no. 5, pp. 954–959, 1988.

[141] D. Busse, S. Templin, G. Mikus, M. Schwab, U. Hofmann, M. Eichelbaum, and K. T. Kivistö, "Cardiovascular effects of (R)- and (S)-verapamil and racemic verapamil in humans: a placebo-controlled study.," *European journal of clinical pharmacology*, vol. 62, pp. 613–9, Aug. 2006.

[142] S. Harder, P. Thürmann, M. Siewert, H. Blume, T. Huber, and N. Rietbrock, "Pharmacodynamic profile of verapamil in relation to absolute bioavailability: investigations with a conventional and a controlled-release formulation.," *Journal of cardiovascular pharmacology*, vol. 17, no. 2, pp. 207–212, 1991.

[143] T. J. Hoon, P. L. McCollam, K. J. Beckman, R. J. Hariman, and J. L. Bauman, "Impact of food on the pharmacokinetics and electrocardiographic effects of sustained release verapamil in normal subjects.," *The American journal of cardiology*, vol. 70, no. 11, pp. 1072–1076, 1992.

[144] D. N. John, S. Fort, M. J. Lewis, and D. K. Luscombe, "Pharmacokinetics and pharmacodynamics of verapamil following sublingual and oral administration to healthy volunteers.," *British journal of clinical pharmacology*, vol. 33, no. 6, pp. 623–627, 1992.

[145] P. R. Mayo, K. Skeith, A. S. Russell, and F. Jamali, "Decreased dromotropic response to verapamil despite pronounced increased drug concentration in rheumatoid arthritis," *British Journal of Clinical Pharmacology*, vol. 50, no. 6, pp. 605–613, 2000.

[146] R. G. McAllister and E. B. Kirsten, "The Pharmacology of verapamil. IV. Kinetic and dynamic effects after single intravenous and oral doses," *Clinical Pharmacology and Therapeutics*, vol. 31, pp. 418–426, Apr. 1981.

[147] D. L. D. Murdoch, G. D. G. Thomson, G. G. Thompson, G. D. G. Murray, M. M. J. Brodie, and G. T. G. McInnes, "Evaluation of potential pharmacodynamic and pharmacokinetic interactions between verapamil and propranolol in normal subjects," *British journal of clinical pharmacology*, vol. 31, pp. 323–332, Mar. 1991.

[148] F. Sanaee, J. D. Clements, A. W. G. Waugh, R. N. Fedorak, R. Lewanczuk, and F. Jamali, "Drug-disease interaction: Crohn's disease elevates verapamil plasma concentrations but reduces response to the drug proportional to disease activity," *British Journal of Clinical Pharmacology*, vol. 72, no. 5, pp. 787–797, 2011.

[149] D. Darbar, M. F. Fromm, S. Dell'Orto, R. B. Kim, H. K. Kroemer, M. Eichelbaum, and D. M. Roden, "Modulation by dietary salt of verapamil disposition in humans.," *Circulation*, vol. 98, no. 24, pp. 2702–2708, 1998.

[150] K. Dilger, K. Eckhardt, U. Hofmann, K. Kucher, G. Mikus, and M. Eichelbaum, "Chronopharmacology of intravenous and oral modified release verapamil," *British Journal of Clinical Pharmacology*, vol. 47, no. 4, pp. 413–419, 1999.

[151] Y. Jin, Y.-H. Wang, J. Miao, L. Li, R. J. Kovacs, R. Marunde, M. a. Hamman, S. Philips, J. Hilligoss, and S. D. Hall, "Cytochrome P450 3A5 genotype is associated with verapamil response in healthy subjects.," *Clinical pharmacology and therapeutics*, vol. 82, no. 5, pp. 579–585, 2007.

[152] N. T. Fuenmayor, B. M. Faggin, and L. X. Cubeddu, "Comparative efficacy, safety and pharmacokinetics of verapamil SR vs verapamil IR in hypertensive patients.," *Drugs*, vol. 44 Suppl 1, pp. 1–11, 1992.

[153] a. K. Halperin, K. M. Gross, J. F. Rogers, and L. X. Cubeddu, "Verapamil and propranolol in essential hypertension.," *Clinical pharmacology and therapeutics*, vol. 36, no. 6, pp. 750–758, 1984.

[154] M. J. Banker, T. H. Clark, and J. A. Williams, "Development and Validation of a 96-Well Equilibrium Dialysis Apparatus for Measuring Plasma Protein Binding," vol. 92, no. 5, pp. 967–974, 2003.

[155] N. P. France and O. Della Pasqua, "The role of concentration-effect relationships in the assessment of QTc interval prolongation.," *British journal of clinical pharmacology*, pp. 1–43, June 2014.

[156] A. Fleury, T. Lavé, F. Jonsson, M. Schmitt, G. Hirkaler, L. Polonchuk, and A. Breidenbach, "A pharmacokinetic-pharmacodynamic model for cardiovascular safety assessment of R1551," *Journal of Pharmacological and Toxicological Methods*, vol. 63, no. 1, pp. 123–133, 2011.

[157] J. Sällström, A. Al-Saffar, and R. Pehrson, "Pharmacokinetic-pharmacodynamic modeling of QRS-prolongation by flecainide: heart rate-dependent effects during sinus rhythm in conscious telemetered dogs.," *Journal of pharmacological and toxicological methods*, vol. 69, no. 1, pp. 24–9, 2014.

[158] K. P. Burnham and D. R. Anderson, *Model Selection and Multimodel Inference: A Practical Information-Theoretic Approach*. New York: Springer-Verlag, 2nd ed., 2002.

[159] a. S. Y. Chain, M. C. J. M. Sturkenboom, M. Danhof, O. E. D. Pasqua, and O. E. Della Pasqua, "Translational pharmacology : from animal to man and back. Establishing in vitro to clinical correlations in the evaluation of cardiovascular safety pharmacology," *Drug Discovery Today: Technologies*, vol. 10, pp. e373–e383, Sept. 2013.

[160] A. Samson, M. Lavielle, and F. Mentré, "Extension of the SAEM algorithm to left-censored data in nonlinear mixed-effects model: Application to HIV dynamics model," *Extension of the SAEM algorithm to left-censored data in nonlinear mixed-effects model: Application to HIV dynamics model*, vol. 51, pp. 1562–1574, 2006.

[161] J. D. Gallagher, "Effects of halothane and quinidine on intracardiac conduction and QTc interval in pentobarbital-anesthetized dogs.," *Anesthesia and analgesia*, vol. 75, no. 5, pp. 688–695, 1992.

[162] H. Tashibu, H. Miyazaki, K. Aoki, Y. Akie, and K. Yamamoto, "QT PRODACT : In Vivo QT Assay in Anesthetized Dog for Detecting the Potential for QT Interval Prolongation by Human Pharmaceuticals," *Journal of Pharmacological Sciences*, vol. 486, pp. 473–486, 2005.

[163] B. A. G. Wallace, R. E. Cline, W. C. Sealy, W. G. Young, and W. G. Troyer, "Electrophysiologic Effects of Quinidine: Studies Using Chronically Implanted Electrodes in Awake Dogs with and Without Cardiac Denervation," *Circulation Research*, vol. 19, pp. 960–969, Nov. 1966.

[164] T. Anno and L. M. Hondeghem, "Interactions of flecainide with guinea pig cardiac sodium channels. Importance of activation unblocking to the voltage dependence of recovery.," *Circulation research*, vol. 66, pp. 789–803, Mar. 1990.

[165] D. J. Snyders and L. M. Hondeghem, "Effects of quinidine on the sodium current of guinea pig ventricular myocytes. Evidence for a drug-associated rested state with altered kinetics.," *Circulation research*, vol. 66, no. 2, pp. 565–579, 1990.

[166] E. P. Anyukhovsky, E. A. Sosunov, S. J. Feinmark, and M. R. Rosen, "Effects of Quinidine on Repolarization in Canine Epicardium, Midmyocardium, and Endocardium : II. In Vivo Study," *Circulation*, vol. 96, pp. 4019–4026, Dec. 1997.

[167] K. Nademanee, W. G. Stevenson, J. N. Weiss, V. B. Frame, M. G. Antimisiaris, T. Suithichaiyakul, and C. M. Pruitt, "Frequency-dependent effects of quinidine on the ventricular action potential and QRS duration in humans.," *Circulation*, vol. 81, no. 3, pp. 790–796, 1990.

[168] C. Takanaka, J. K. Lee, M. Nonokawa, T. Sugiyama, and S. Yame, "Frequency dependent effects of class I antiarrhythmic agents studied in patients with implanted pacemakers.," *Pacing and clinical electrophysiology : PACE*, vol. 17, pp. 2100–5, Nov. 1994.

[169] R. G. McAllister, J. David, W. A. Bourne, and L. W. Dittert, "The pharmacology of verapamil. I. Elimination kinetics in dogs and correlation of plasma levels with effect on the electrocardiogram," *Journal of Pharmacology and Experimental Therapeutics*, vol. 202, no. 1, pp. 38–44, 1977.

[170] W. S. Redfern, L. Carlsson, A. S. Davis, W. G. Lynch, I. MacKenzie, S. Palethorpe, P. K. S. Siegl, I. Strang, A. T. Sullivan, R. Wallis, A. J. Camm,

and T. G. Hammond, "Relationships between preclinical cardiac electrophysiology, clinical QT interval prolongation and torsade de pointes for a broad range of drugs: evidence for a provisional safety margin in drug development.," *Cardiovascular research*, vol. 58, pp. 32–45, Apr. 2003.

[171] L. M. Hondeghem, "Antiarrhythmic agents: modulated receptor applications.," *Circulation*, vol. 75, no. 3, pp. 514–20, 1987.

[172] A. A. M. Wilde, "Proarrhythmia Related to Sodium Channel Blockade : Mechanisms , Monitoring , Prevention and Management," *Cardiac Electrophysiology Review*, vol. 2, no. 2, pp. 136–141, 1998.

[173] H. Watanabe, N. Chopra, D. Laver, H. S. Hwang, S. S. Davies, D. E. Roach, H. J. Duff, D. M. Roden, A. A. M. Wilde, and B. C. Knollmann, "Flecainide prevents catecholaminergic polymorphic ventricular tachycardia in mice and humans.," *Nature medicine*, vol. 15, pp. 380–3, Apr. 2009.

[174] M. L. Bannister, N. L. Thomas, M. B. Sikkel, S. Mukherjee, C. Maxwell, K. T. MacLeod, C. H. George, and A. J. Williams, "The mechanism of flecainide action in CPVT does not involve a direct effect on RyR2," *Circulation Research*, vol. 116, no. 8, pp. 1324–1335, 2015.

[175] D. R. Joseph, "The ratio between heart-weight and body-weight in various animals," *The Journal of experimental medicine*, vol. 10, pp. 521–8, July 1908.

[176] N. Abolghassem, "A concise review on the anatomy of the atrioventricular node in mammals," *Iranian Journal of Veterinary Science and Technology*, vol. 1, no. 1, pp. 1–10, 2009.

[177] Z. G. Wang, L. C. Pelletier, M. Talajic, S. Nattel, and G. Avenue, "Effects of flecainide and quinidine on human atrial action potentials. Role of rate-dependence and comparison with guinea pig, rabbit, and dog tissues.," *Circulation*, vol. 82, pp. 274–283, July 1990.

[178] F. Hofmann, V. Flockerzi, S. Kahl, and J. W. Wegener, "L-Type CaV1.2 Calcium Channels: From In Vitro Findings to In Vivo Function," *Physiological reviews*, vol. 94, no. 1, pp. 303–326, 2014.

[179] S. Blechschmidt, V. Haufe, K. Benndorf, and T. Zimmer, "Voltage-gated Na+ channel transcript patterns in the mammalian heart are species-dependent," *Progress in Biophysics and Molecular Biology*, vol. 98, no. 2-3, pp. 309–318, 2008.

[180] V. Haufe, C. Chamberland, and R. Dumaine, "The promiscuous nature of the cardiac sodium current," *Journal of Molecular and Cellular Cardiology*, vol. 42, no. 3, pp. 469–477, 2007.